DISCLAIMER:

This document does not meet the
current format guidelines of
the Graduate School at
The University of Texas at Austin.

It has been published for
informational use only.

The Dissertation Committee for Gastón Quaglia Certifies that this is the approved version of the following dissertation:

Hydro-Mechanical Characterization of Unsaturated Clays Using Centrifuge Technology

Committee:

Jorge G. Zornberg, Supervisor

Todd Caldwell

Chadi El Mohtar

D. Nicolas Espinoza

Robert B. Gilbert

Hydro-Mechanical Characterization of Unsaturated Clays Using Centrifuge Technology

by

Gastón Quaglia

Dissertation

Presented to the Faculty of the Graduate School of

The University of Texas at Austin

in Partial Fulfillment

of the Requirements

for the Degree of

Doctor of Philosophy

The University of Texas at Austin

Dedication

To Juliana

Acknowledgements

I would like to thank my advisor Dr. Jorge G. Zornberg for his advice and support throughout my years as a PhD student. Also, I would like to thank Dr. Chadi El Mothar, Dr. Todd Caldwell, Dr. David N. Espinoza, and Dr. Robert B. Gilbert for their assistance and feedback provided during my research at The University of Texas. I would like to thank my fellow graduate students, and professors at UT Austin for many discussions and experiences shared that had a positive impact on my research. In particular, I would like to thank my colleagues and friends Christian Armstrong, Calvin R. Blake, Dr. Michael Plaisted, and Dr. Marcelo Azevedo for their many thoughts and knowledge shared during these years.

Support received from the National Science Foundation under the Grant No. CMMI 1335456 and from the Argentinean Government under the Presidential Fellowship in Science and Technology (BEC.AR) is gratefully acknowledge.

To my family and friends in Argentina, thanks for your support, it was there despite the distance.

Finally, I would like to give special thanks to my wife Juliana P. Vidal, for your love and support during both the good and specially the hard times of my PhD. Thank you for being always there.

Hydro-Mechanical Characterization of Unsaturated Clays Using Centrifuge Technology

Gastón Quaglia, PhD.

The University of Texas at Austin, 2017

Supervisor: Jorge G. Zornberg

Several experimental techniques and analytical methods, with emphasis in centrifuge testing, were implemented to characterize the hydro-mechanical behavior of unsaturated clays. Particularly, experimental procedures and back-analysis methods designed to determine the Soil Water Retention Surface (SWRS) and the unsaturated hydraulic conductivity (k-function) of clays, both low and high plasticity. The goal of developing new experimental devices and non-intrusive sensors was to expressly incorporate the four key variables controlling the unsaturated flow process: moisture content, suction, volumetric strain, and hydraulic conductivity.

The hydro-mechanical behavior of unsaturated clays required the development of new equipment and sensors capable of monitoring all relevant variables, without interfering with the flow process. Two non-intrusive sensors systems were tailored to upgrade the capabilities of the centrifuge permeameter for unsaturated soils (CPUS): a water content sensor, the GTDR based on Time Domain Reflectometry, and an image-analysis tool to assess soil deformation. Both systems combined allowed continuously monitoring the changes in volume and water content in-flight. Using these tools allowed generating experimental data for the SWRS and hydraulic conductivity of clays, implementing steady state and unsteady state procedures.

Also, a new piece of workbench equipment, the ATX Cell, was developed and tested. The ATX Cell facilitates the characterization of the hydro-mechanical behavior of unsaturated clays monitoring the void ratio, matric suction, and water content. It also allows testing clays under different imposed stresses. This feature was particularly relevant when testing on expansive clays.

The hydraulic properties of an unsaturated low plasticity clay (RMA soil) were evaluated using the new devices and other standard experimental techniques. Steady state tests were implemented following "Hydrostatic" and "Imposed flow" procedures to determine the SWRS and k-function over wide range of void ratio values. It was found that destructive measurements generated volume changes that affected the reported volumetric water content and degree of saturation profiles. In order to solve this problematic, non-intrusive sensors were incorporated, improving the definition of the SWRS. Incorporating the SWRS model allowed fitting experimental data generated with standard (1.g) devices as well as with centrifuge (N.g), independently of the volume changes measured during the test. RMA SWRS was defined for a wide range of void ratio values, with samples compacted at optimum water content. Transient measurements were back-analyzed to derive the hydraulic conductivity of RMA soil. Garner's method was applied to the ATX Cell information, while Hydrus code was implemented with centrifuge data.

Experimental techniques and analytical previously tested, were implemented to characterize the hydro-mechanical behavior of unsaturated high plasticity clay, Eagle Ford. Special focus was placed in the hydraulic properties, but also the swelling of this expansive clay was measured using centrifuge technology. In this case, the inclusion of the void ratio as an additional variable is significantly relevant when interpreting the experimental data and defining the SWRS and k-function of the soil.

The ATX Cell was used to evaluate the hydro-mechanical characterization of Eagle Ford clay monitoring the void ratio and water changes through different suction stages while using different imposed stresses. It was observed that the volume changes and the proportional changes in water content depended on the initial void ratio and the stresses imposed. Moreover, a coupled behavior was identified between the swelling and the inflow rates. Also, a series of filter paper and chilled mirror hygrometer test were carried out. The experimental data generated with standard (1.g) methods incorporating the void ratio as an expressly measured variable allowed defining the SWRS.

Centrifuge tests in Eagle Ford clay showed that volume changes were observed as a result of the coupling between the imposed stresses (due to the gravitational forces) and water content changes (wetting and drying phases). Image analysis successfully detected the swelling and contraction of the soil. The volumetric water content measured with the GTDR's was found similar to the values obtained with semi-destructive measurement techniques. The inclusion of the GTDR and image analysis allowed obtaining experimental data to define the SWRS of Eagle Ford clay using centrifuge testing.

Centrifuge testing capabilities relies on its ability to increase the gravitational (up to 600g's). However, it was found that the void was reduced in a comparatively larger portion of the sample, which remained saturated despite of the higher suction imposed when testing Eagle Ford clay at 200g's. Also, longer testing times were necessary for the water to advance as a probable reduction in the hydraulic conductivity. While steady state techniques were successful implemented for low plasticity clays, this approach may become time consuming for high plasticity clays. The interpretation of transient information may become useful at determining the hydraulic conductivity.

Swelling tests performed in the centrifuge showed that volumetric water content increased rapidly during the primary swelling stage, and secondary swelling occurred

under an approximately constant degree of saturation. The image analysis tools allowed defining volume changes (and swelling) along the sample, providing additional information in the swell-stress curve.

The representation of the swelling test in the θ-e or Sr-e plane eliminated the time variable, but was found to provide a method to evaluate the expansion in a soil profile under partial wetting conditions, and showed more clearly that evaluating swelling in expansive clays is an unsaturated soil problem.

Table of Contents

List of Tables xix

List of Figures xxi

Chapter 1: Motivation, Objectives and Structure 35

1.1 Motivation of this dissertation 35

1.2 Statement of Objectives 36

1.3 Scope and Structure of this dissertation.....37

Chapter 2: Definition of Hydraulic Variables in Unsaturated Soils 40

2.1 Water flow in unsaturated soils.....40

2.1.1 Water potential.....40

2.1.2 Water flow 41

2.1.3 Water flow in a centrifuge environment 42

2.2 Hydraulic characteristics of unsaturated soils.....43

2.2.1 Soil-water potential.....43

2.2.2 Soil-water retention curve.....44

2.2.3 Unsaturated hydraulic conductivity function.....46

2.3 Hydraulic characteristic models.....47

2.3.1 Soil-water retention curve model.....47

2.3.2 k-function model.....48

2.4 Soil-Water Retention Surface (SWRS) model concept 49

Chapter 3: Rationale for the Selection of the Unsaturated Soil Testing Equipment51

3.1 Introduction.....51

3.2 Overview of standard (1.g) testing methods 52

3.2.1 SWRC determination under low suction conditions.....52

3.2.1.1 Pressure plate extractor and Hanging column test.....52

3.2.1.2 Derivation of unsaturated hydraulic conductivity based on the transient response of pressure plate test.....54

3.2.1.3 Evaporation test 56

3.2.2 SWRC determination under high suction conditions.....57
3.2.2.1 Filter paper test 57
3.2.2.2 Chilled mirror hygrometer test.....60
3.2.2.3 Comparison of methods 61
3.2.3 Opportunities for refinement of standard (1.g) test 62
3.3 Review of centrifuge testing (N.g).....63
3.3.1 Background 63
3.3.2 Centrifuge Permeameter for Unsaturated Soils – CPUS 66
3.3.2.1 Testing methodologies 66
3.3.2.2 Boundary conditions 67
3.3.2.3 Outflow system 69
3.3.3 Opportunities for improvements of the (N.g) Centrifuge testing environment 70

SECTION 1: NEW DEVELOPMENTS FOR THE HYDRO-MECHANICAL CHARACTERIZATION OF UNSATURATED SOILS 72

Chapter 4: ATX Cell: A New Device for Experimental Determination of the Soil-Water Retention Surface 73
4.1 Introduction.....73
4.2 Equipment development 74
4.2.1 Monitoring systems: weight and volume changes 77
4.3 Testing procedures 79
4.4 Typical Results.....80
4.4.1 Definition of the SWRS 80
4.4.2 Typical results from transient response 82
4.5 Summary and Conclusions 84

Chapter 5: GTDR: A New Non-Intrusive Volumetric Water Content Sensor based on Time Domain Reflectometry 86
5.1 Introduction.....86
5.2 Design process 87
5.3 Background review 90
5.3.1 Transmission line theory.....90

5.3.2 Signal interpretation 91
5.4 Equipment 93
5.4.1 Components of TDR system 93
5.4.2 Implementation in the CPUS 95
5.5 Development of non-intrusive sensor 97
5.5.1 Response of curved TDR 97
5.5.2 Influence of acrylic 100
5.5.3 Permeameter-TDR probe fusion: GTDR 102
5.5.4 GTDR Calibrations 105
5.5.4.1 Standard soil calibration using GTDR 105
5.5.4.2 Probe calibration 106
5.5.4.3 Soil calibration using GTDR's probe specific parameters 108
5.5.5 Alternative interpretation of waveforms using AWIGF 109
5.5.5.1 Probe calibration 109
5.5.5.2 Soil calibration using AWIGF 114
5.6 Summary and Conclusions 115

Chapter 6: Development of a Non-Intrusive tool to Assess Soil Displacement based on Image Analysis 118
6.1 Introduction 118
6.2 Background 119
6.3 Equipment: Camera and accessories 120
6.4 Analysis technique 123
6.4.1 Technique I: Edge detection algorithm 124
6.4.1.1 Identifying markers edges 124
6.4.1.2 Markers position 127
6.4.1.3 Clay Masking 128
6.4.1.4 Calibration 128
6.4.2 Analysis technique II: Patch 129
6.5 Analysis of typical results 131
6.6 Summary and conclusions 133

SECTION 2: HYDRAULIC CHARACTERIZATION OF UNSATURATED LOW PLASTICITY CLAYS.....135

Chapter 7: Hydraulic Characterization of Unsaturated Low Plasticity Clays Using Standard (1.g) Testing.....137

7.1 Introduction.....137

7.2 Measurements of the retention capabilities of low plasticity clays at low suction values.....137

7.2.1 ATX Cell.....137

7.2.1.1 Testing program.....138

7.2.1.2 Experimental Results.....139

7.2.2 Representative behavior of RMA soil.....141

7.2.3 Transient response.....143

7.3 Measurements of the retention capabilities of low plasticity clays at High suction values.....144

7.4 Summary and Conclusions.....147

Chapter 8: Hydro-Mechanical Characterization of Unsaturated Low Plasticity Clays Using Centrifuge (N.g) Testing.....149

8.1 Introduction.....149

8.2 Results from previous studies using RMA clay.....150

8.3 Testing program.....152

8.3.1 Testing Procedures.....153

3.2.2.4 Hydrostatic test.....153

3.2.2.5 Imposed flow test.....154

8.3.2 Measurements.....156

8.3.3 Scope of the testing program.....159

8.4 Experimental results.....159

8.4.1 Hydrostatic test: Comparison of results using semi-destructive (SD) and destructive (D) measurement techniques.....160

8.4.1.1 Dry Unit weight.....161

8.4.1.2 Gravimetric water content.....164

8.4.1.3 Volumetric water content and degree of saturation...165

8.4.2 Hydrostatic test: Results using Non-destructive (ND) measurement technique 170
8.4.2.1 Non-intrusive sensor set-up 170
8.4.2.2 Deformation measurements time response 171
8.4.2.3 Volumetric water content time response 172
8.4.2.4 Comparison of results for hydrostatic test between Non-Destructive, Semi-Destructive and Destructive measurement techniques 175
8.4.3 Transient analysis based on ND measurements from a hydrostatic test 178
8.4.4 Multistage hydrostatic test using ND measurements 181
8.4.5 Hydrostatic test: effect of the initial conditions in the mechanical response during centrifuge testing 185
8.4.5.1 Limitations to the definition of the SWRS based on the mechanical response of the soil 187
8.4.6 Summary of results for hydrostatic tests to define the SWRS 188
8.4.7 Imposed flow test: determination of the unsaturated hydraulic conductivity 191
8.5 Summary and Conclusions 195

Chapter 9: Analysis of the Hydro-Mechanical Characterization of Unsaturated Low Plasticity Clays 197
9.1 Introduction 197
9.2 Determination of the SWRS 198
9.2.1 Analytical formulation of the SWRS model 198
9.2.2 Numerical optimization 199
9.2.3 Data sets for SWRS calibration 199
9.2.4 SWRS model calibration 201
9.2.5 Performance of the predicted SWRS 207
9.3 Determination of Hydraulic conductivity from transient analysis 211
9.3.1 Analytical solution for ATX Cell transient response (1.g) 211
9.3.1.1 Analysis of transient response 211
9.3.1.2 Estimated hydraulic conductivity vs. indirect k-function 214

9.3.2 Hydraulic conductivity based on Centrifuge 216
9.3.2.1 Transient analysis model with Hydrus.....216
9.3.2.2 Hydrus model optimization.....217
9.3.2.3 Model Results 218
9.4 Summary and Conclusions 221
9.4.1 Development of SWRS.....221
9.4.2 Transient analysis.....223

SECTION 3: HYDRO-MECHANICAL CHARACTERIZATION OF UNSATURATED EXPANSIVE CLAYS.....225

Chapter 10: Hydraulic Characterization of Unsaturated Expansive Clays Using Standard (1.g) Testing.....227
10.1 Introduction.....227
10.2 Measurement of the retention capabilities of high plasticity clays at low suction values.....227
10.2.1 ATX Cell.....227
10.2.1.1 Testing program 228
10.2.1.2 Experimental Results 229
10.2.2 Transient response 232
10.3 Measurement of the retention capabilities of High plasticity clays at High suction values.....233
10.3.1 Testing program 234
10.3.2 Experimental results.....234
10.4 Summary and Conclusions 240

Chapter 11: Hydro-Mechanical Characterization of Unsaturated Expansive Clays Using Centrifuge (N.g) Tests.....243
11.1 Introduction.....243
11.2 Background 243
11.3 Testing program 245
11.3.1 Procedures and measurement techniques.....245
11.3.2 Scope of the testing program 245
11.4 Experimental results.....246

11.4.1 Hydrostatic test on expansive clays 247
11.4.1.1 Comparison of measurement techniques 247
11.4.1.2 Impact of increasing centrifuge speed 256
11.4.2 Imposed Flow test on expansive clays.....260
11.4.2.1 Comparison with low plasticity clay experimental results 264
11.5 Summary and Conclusions 264
Advantages and Disadvantages.....267

Chapter 12: Analysis of the Hydro-Mechanical Characterization of Unsaturated High Plasticity Clays.....269
12.1 Introduction.....269
12.2 Determination of the SWRS 270
12.2.1 Numerical optimization 270
12.2.2 Experimental data sets 271
12.2.3 SWRS model calibration.....272
12.2.4 Performance of the predicted SWRS 275
12.2.5 Validation of SWRS 277
12.3 Determination of Hydraulic conductivity from transient analysis.....280
12.3.1 Analytical solution for ATX Cell transient response (1.g) ..280
12.3.1.1 Analysis of transient response 281
12.3.1.2 Estimated hydraulic conductivity vs. indirect k-function 281
12.3.2 Hydraulic conductivity based on Centrifuge 283
12.4 Summary and conclusions 290

Chapter 13: Analysis of Soil Swelling using Centrifuge Technology.....293
13.1 Introduction.....293
13.2 Background review 293
13.3 Testing program 295
13.3.1 Testing procedures and measurement techniques.....295
13.3.2 Scope of the testing program 296
13.4 Experimental results.....297

13.4.1 General swelling behavior 297
13.4.2 Deformation profile and Swell-stress curve 300
13.4.3 Partial wetting analysis 302
13.5 Summary and Conclusions 307

Chapter 14: Conclusions and Recommendations 309
14.1 Introduction 309
14.2 Overall Conclusions 309
14.3 Specific Conclusions 311
14.3.1 Conclusions Section 1 311
14.3.2 Conclusions from Section 2: Hydraulic characterization of unsaturated low plasticity clays 313
14.3.3 Conclusions from Section 3: Hydro-mechanical characterization of unsaturated low plasticity clays 315
14.4 Recommendations for future work 317

APPENDICES 319

APPENDIX 1: Complementary information for the development of the GTDR sensor 320
1.1 Introduction 320
1.2 Calibrations 320
1.2.1 General calibration 320
1.2.2 Soil specific calibration for Eagle Ford Clay 321
1.2.3 Preliminary analysis of errors 324
1.2.4 Calibration of curved TDR 326
1.2.5 GTDR Calibration 328
1.3 Analysis of Wave Forms and other sources of error 329

APPENDIX 2: Analysis of Results and Construction of SWRS 332
2.1 Introduction 332
2.2 Modeling and construction of SWRS 332
2.2.1 Parameterization analysis 333

APPENDIX 3: Discussion about experimental measurements from filter paper and chilled mirror hygrometer on Eagle Ford clay.....338

3.1 Introduction.....338

3.2 Chilled mirror hygrometer test.....338

3.3 Filter Paper Test.....340

3.4 Discussion about the difference between total suction and matric suction results.....344

References.....347

Vita 354

List of Tables

Table 1: Example of Heading 7,h7 format..... **¡Error! Marcador no definido.**

Table 1. Summary of indirect soil suction measurement methods. 88

Table 2. TDR and GTDR probe parameters. Obtained with PCTDR 107

Table 3. Apparent permittivity for mixtures acrylic-liquid 113

Table 4. Prediction of Ka based on measured travel times (GTDR #7) 113

Table 5. GTDR probe parameters and mixture factors for AWIGF analysis. 114

Table 6. Testing scope for RMA soil.....139

Table 7. Scope of centrifuge tests performed using RMA soil.....159

Table 8. Constrains applied during non-linear optimization 199

Table 9. Data sets created for SWRS optimization.....200

Table 10. Fitting parameters for SWRS.....201

Table 11. Goodness of fit metrics for SWRS optimization 207

Table 13. Initial values for Hydrus model optimization.....217

Table 14. Best set of parameters and 95% confidence limits 218

Table 15. Testing scope for Eagle Ford clay 229

Table 16. Scope of centrifuge tests performed using Eagle Ford Clay 246

Table 17. Constrains applied during non-linear optimization 271

Table 18. Data sets created for SWRS optimization on Eagle Ford Clay 271

Table 19. Fitting parameters for Eagle Ford SWRS.....272

Table 20. Goodness of fit metrics for Eagle Ford clay SWRS optimization.....276

Table 21. Derived unsaturated hydraulic conductivity.....281

Table 22. Hydrus model parameters for centrifuge testing on Eagle Ford clay ..284

Table 23. Initial values for Hydrus model optimization on centrifuge testing. ...285

Table 24. Best set of parameters after model optimization 286
Table 25. Swelling tests performed using Eagle Ford clay samples.....296

List of Figures

Figure 1. (a) SWRC for different soils and (b) schematic representation using the bundle of capillary tubes model (Or et al. 2010) 46

Figure 2: Conceptual definition of SWRS: a) SWRS model indicating the drying path tests (Salager et al. 2010); and b) testing approach involving a series of samples used to define values at a single imposed suction (Salager et al. 2007). 50

Figure 3. Pressure plate extractor set up (ASTM D6836–02). 53

Figure 4. Gardners's solution applied to the measurements of ATX cell test W9 performed using RMA soil. 55

Figure 5. Hyprop test: (a) soaking, (b) installing sensors, and (c) evaporation phase. 56

Figure 6. Schematic drawing of the filter paper test set up (Tarantino et al. 2014).58

Figure 7. (a) Leong et al. (2014) calibration curves for Whatman No42, (b) Bulut and Wray (2005) calibration for Schleicher & Schuell No.589-WH. 59

Figure 8. (a) Calibrations in wetting paths for Whatman 42, and (b) single calibration equation. (Bicalho 2015).....60

Figure 9. a) WP4 Scheme (Bulut et al. 2002), and b) picture of WP4C device tray in the lab ready to place the samples.....61

Figure 10. (a) Sample in the glass container, (b) slicing, and (c) set in WP4C bin.62

Figure 11. Unsaturated hydraulic conductivity measurements performed in the centrifuge by Nimmo (1987). 64

Figure 12. Lower boundary of the centrifuge permeameter cups: a) aluminum base, and b) outflow instrumented with a pressure transducer. 68

Figure 13. Changes in voltage measured by the pressure transducer in the outflow reservoir for different imposed inflow/outflow rates (at constant speed). 69
Figure 14. Calibration curves defined for different outflow rates and centrifuge speeds. 70
Figure 15. ATX Cell base design details: a) 3D view of base, b) Cross section showing grooves, inlet, and outlet connections. c) Picture of the base. 75
Figure 16. Set-up stages in the ATX Cell including: a) sample compaction, b) sample mounted in the base, and c) base assembled with the top disc and o-ring holders. 76
Figure 17. ATX Cell aluminum cap design: a) 3D view of the cap, b) cross section, and c) piston connected to the cap. 76
Figure 18 ATX Cell ready fro testing with: a) cell mounted over the scale, b) lateral view of the piston and air connections, and c) detail of the bracket and LVDT. 78
Figure 19. Connection between ATX Cell and flushing system. 78
Figure 20. Typical results from ATX cell for a low and a high plasticity clay samples presented in two-dimensional views of the SWRS: a) θ vs ψ plane, b) e vs ψ plane and c) θ vs e plane. (CHANGE IMPROVE IMG) 81
Figure 21. Transient response of RMA and Eagle Ford clays including: a) changes in water content and b) changes in void ratio vs time. 83
Figure 22. Initial conceptual design of the GTDR: a) straight TDR next to the permeameter cup, and b) modification proposed to the TDR to be included in the walls of the acrylic permeameter. (Improve) 89

Figure 23. TDR sensor working principle (Tarantino et al. 2008b). 91
Figure 24. Waveform interpretation using TACQ (Evett, 2000b),.....92
Figure 25. Waveform in water and relevant fitting parameters from TDR100 manual 93
Figure 26. TDR components. (Change for better quality). 95
Figure 27. Datalogger CR1000, TDR100 and Multiplexer SDMX80 in the centrifuge. 96
Figure 28. Access to the TDR components located in the center of the CPUS: a) CR1000 datalogger RS-232 COM port, and b) SDMX80 Multiplexer. 96
Figure 29. Dielectric permittivity measured at several g-levels. 97
Figure 30. Evaluation of the impact of curved TDR prongs: a) manually curving TDR and b) measurements in water with the curved TDR.....98
Figure 31. Waveforms of a progressively curved TDR submerged in water 99
Figure 32. Comparison of waveforms for both, straight and curved TDR in water.100
Figure 33. Inclusion of a straight TDR in contact with acrylic. 101
Figure 34. Waveform evolution when TDR is placed in contact with acrylic and epoxy. (incorporate reference lines) 101
Figure 35. Permeameter cup design completed in solid works 102
Figure 36. GTDR assembled with soil sample showing: a) the relative position of the rods in the sample and b) the insertion of the TDR sensor heads into the cup.....103
Figure 37. Testing GTDR vs TDR in water.....104
Figure 38. Comparison of waveforms from GTDR and straight TDR in water..104
Figure 39. Comparison between TDR (straight and curved) and GTDR. 106

Figure 40. Soil Specific calibration for GTDR. 108
Figure 41. Impact of acrylic and epoxy in the travel times. 110
Figure 42. Waveform and AWIGF interpretation for: (a) air, (b) kerosene, (c) alcohol and (d) water measured with GTDR#7. 112
Figure 43. Soil-specific calibration performed on Eagle Ford clay with GTDR and AWIGF interpretation. 115
Figure 44. Camera system attached to the centrifuge bucket: a) Camera facing the soil sample, b) relative position of the mounting respect to the swinging bucket in-flight. 121
Figure 45. Inclusion of markers within the soil sample a) top view of the marker and the sample during compaction, and b) typical view of the soil sample including the markers. 122
Figure 46. Selection of local domain for image analysis in swelling tests: a) sub-region at the beginning, and b) same sub regions at the end of the tests 125
Figure 47. Image analysis interface includes: a) image to be analyze, b) selection of the analysis channel, c) histogram and binarization threshold, and c) binarized image. 126
Figure 48. Image analysis procedure: a) edge detection steps, and b) detection of upper and lower boundaries. 127
Figure 49. Procedure to calculate a calibration factor: a) Selection of reference points at known distances, b) computation of number of pixels between markers and from fix reference to obtain a calibration factor of 20.7 pix/mm. 129

Figure 50. Selection of analysis domain and rigid patches in swelling tests: a) at the beginning, and b) end of the tests. 130
Figure 51. Markers displacement: comparison between available IA techniques.132
Figure 52. ATX Cell test results in three-dimensional (ψ, θ, e) space. 140
Figure 53. Two-dimensional views of the SWRS: a) θ vs ψ plane, b) e vs ψ plane and c) θ vs e plane (Re-paste excel figure).....141
Figure 54. SWRC defined relative compaction values of 80%, 90%, and 100%.142
Figure 55. Transient response in ATX Cell test W9b for each testing stage described by: a) water content, and b) void ratio time histories. 144
Figure 56. Total suction measurements SWRC results for RMA characterization at high suction ranges and three different relative compaction values.145
Figure 57. SWRC for RMA soil defined combining measurements at low and high suction values.....146
Figure 58. Impact of the compaction water content in the slope of the SWRC for RMA soil evaluated by: a) McCartney (2007), and b) Plaisted (2014). 151
Figure 59. Effect of initial soil density on the distribution of the hydrostatic tests results performed to describe the SWRS of the RMA soil (adapted from Plaisted, 2014).....151
Figure 60. RMA unsaturated hydraulic conductivity measured by McCartney (2007). 152
Figure 61. Permeameter setup for: a) ND and SD measurements and b) D measurements.....158
Figure 62. Soil samples being sliced and measured during: a) SD and b) D measurements.....158

Figure 63. Dry unit weight profiles of Test #1 for: a) Sample A (SD) in flight and b) Sample B (D) after slicing. 162
Figure 64. External deformation measurements for Test #1.....162
Figure 65. Water content distribution of Test#1 after slicing: a) Sample A (SD) and b) Sample B (D). 165
Figure 66. Comparison of samples A and B of Test #1 using: a) volumetric water content (θ), and b) the degree of saturation (Sr) profiles. 166
Figure 67. Test#1, SWRC represented as a function of: a) θ and b) Sr. 167
Figure 68. Plane views of the SWRS from Test# 1: a) Representation of SWRC in the Sr-ψ plane, and complementary views, b) lateral view Sr-e, and c) top view e-ψ. 169
Figure 69. Scheme for Non-Destructive measurement technique indicating: a) soil layering to calculate deformation and density profiles, and b) GTDR nodes to measure the volumetric water content. 171
Figure 70. Change in height of each soil layer for Sample A during Test #1. 172
Figure 71. GTDRs time response represented by: a) apparent dielectric conductivity, and b) volumetric water content. 173
Figure 72. Reinterpretation of GTDR #Bottom waveforms using AWIGF algorithm to determine the volumetric water content. 174
Figure 73. SWRC information based on ND measurements (GTDR).....176
Figure 74. Comparison of SWRS results for Sample A of Test #1 using. ND, SD and D measurement techniques: a) Representation of SWRC in the Sr-ψ plane, and complementary views b) Sr-e, and c) e-ψ views. 177
Figure 75. Combination of ND measurements: a) water content assigned to each soil layer, and b) void ratio for each GTDR node. 178

Figure 76. Infiltration stage profiles for Sample A of Test #1 including: a) dry unit weight calculated using image analysis, b) volumetric water content estimated using GTDRs, and c) degree of saturation. 179
Figure 77. Drying stage profiles for Sample A of Test #1 including: a) dry unit weight calculated using image analysis, b) volumetric water content estimated using GTDRs, and c) degree of saturation. 180
Figure 78. Transient response in a multistage test: a) water content, and b) outflow. 181
Figure 79. Profiles at hydrostatic equilibrium for 25,50,100 and 125g's of Test #3: a) dry unit weight, b) volumetric water content, c) degree of saturation, and d) suction.(imposed) at equilibrium 183
Figure 80. SWRS plane views for multistage test: a) SWRC in Sr-ψ, b) lateral view Sr-e, and c) top view e-ψ. 184
Figure 81. Dry unit weight profiles for Test #2: a) Sample A (SD) and b) Sample B (D). 185
Figure 82. Representation of the SWRC results from Test #2. 187
Figure 83. SWRS results from centrifuge testing for RMA soil. 188
Figure 84. Plane views of the data points used to define the SWRS for RMA soil using centrifuge testing: a) SWRC in Sr-ψ, b) lateral view Sr-e, and c) top view e-ψ. 190
Figure 85. Dry unit weight profile for: a) sample A (SD), and b) sample B (D) of Test #4.....191
Figure 86. a) Measured water content, and b) derived suction profiles and fits for Test #4.....192

Figure 87. Test #4: a) suction gradient, b) gravitational and total gradients, and (c) derived unsaturated hydraulic conductivity for sample A, sample B and sample A with ND measurements (A_{GTDR}).....194
Figure 88. SWRS for Set 1. 202
Figure 89. Residuals from SWRS fitting for set 1. 202
Figure 90. SWRS for Set 2. 203
Figure 91. Residuals from SWRS fitting for set 2. 204
Figure 92. SWRS for Set 3. 205
Figure 93. Residuals from SWRS fitting for set 3. 205
Figure 94. SWRS for Set 4. 206
Figure 95. Residuals from SWRS fitting for set 4. 207
Figure 96. Comparison between surfaces for Set 1 and Set 3. 209
Figure 97. Comparison between surfaces for Set 1 and Set 3. 209
Figure 98. Comparison between surfaces for Set 2 and Set 4. 210
Figure 99. Comparison between surfaces for Set 2 and Set 4. 210
Figure 100. Analysis of inflow time response for suction reduction from 95 to 30 kPa. 213
Table 12. Derived unsaturated hydraulic conductivity 214
Figure 101. Hydraulic conductivity as function of suction for RMA soil. 215
Figure 102. Comparison between the predicted behavior in Hydrus model and the measured water contents at the three GTDR nodes during the infiltration stage of Test #1. 219
Figure 103. Water content profiles during the infiltration stage predicted in Hydrus model for Test #1. 220

Figure 104. Comparison between the derived k-function from Test #1 using Hydrus transient analysis and measurement performed in Test #4 under unsaturated steady state flow conditions, hydraulic conductivity derived from ATX cell test and VGM model k-function prediction. 221
Figure 105. Hydraulic conductivity values for Eagle Ford clay samples (Khun, 2010). 228
Figure 106. ATX Cell test results for Eagle for clay in three-dimensional (θ, ψ, e) space.....230
Figure 107. Two-dimensional views of the SWRS for Eagle Ford clay: a) θ vs ψ plane, b) θ vs e plane and c) e vs ψ plane.....231
Figure 108. Transient response in ATX Cell test EFW3a for each testing stage described by: a) water content, and b) void ratio time histories. 232
Figure 109. Experimental data from Filter Paper (total and matric suction), and WP4C test (total suction) for Eagle Ford clay samples compacted at 90% relative compaction proctor standard.....235
Figure 110. Experimental data from Filter Paper (matric suction) for Eagle Ford clay samples compacted at three different relative compactions. 236
Figure 111. Derivation of matric suction values using WP4C test results (total suction) for Eagle Ford clay samples compacted at 90% relative compaction.....237
Figure 112. Derivation of the correlation between volumetric water content and matric suction values using WP4C test results and a correction factor for Eagle Ford clay samples compacted at three relative compactions.238
Figure 113. Correlation between total suction and volumetric water content factor for Eagle Ford clay samples compacted at three relative compactions.239

Figure 114. Derivation of matric suction values using WP4C test results (total suction) for Eagle Ford clay samples compacted at dry unit weights ranging from 65% to 95% relative compaction. 240
Figure 115. Dry unit weight profiles of Test #EF1 for: a) Sample A (SD) in-flight and b) Sample B (D) after slicing. 247
Figure 116. Change in height of each soil layer for Sample A during Test #EF1.248
Figure 117. Water content distribution of Test #EF1 after slicing: a) Sample A (SD) and b) Sample B (D). 249
Figure 118. Comparison of samples A and B of Test #EF1 using: a) volumetric water content (θ), and b) the degree of saturation (Sr) profiles. 250
Figure 119. Plane views of the SWRS from Test #EF1: a) Representation of SWRC in the Sr-ψ plane, and complementary views b) lateral view Sr-e, and c) top view e-ψ. 252
Figure 120. GTDRs time response results represented by volumetric water content using: a) CSI, and b) AWIGF algorithms. 253
Figure 121. SWRC information of Test #EF1 including ND, SD (Sample A), and D (Sample B) measurements. 254
Figure 122. Plane views of the SWRS from Test #EF1: a) Representation of SWRC in the Sr-ψ plane, and complementary views b) lateral view Sr-e, and c) top view e-ψ. 255
Figure 123. Volumetric water content readings from GTDR's using AWIGF algorithm on test #EF2 for: a) Sample A, and b) Sample B. 257
258

Figure 124. Dry unit weight profiles of Test #EF2 for: a) Sample A and b) Sample B using SD measurements and comparison against average trend from #EF1. 258
Figure 125. Plane views of the SWRS including a representation in the Sr-ψ plane, and complementary top view e-ψ plane for tests: a) #EF1 and b) #EF2. 259
Figure 126. Comparison of samples A and B of imposed flow test #EF3 using: a) volumetric water content (θ), and b) the degree of saturation (Sr) profiles. 261
Figure 127. Comparison of sample profiles for test #EF3 including: a) SD and ND measurements of measured water content, and b) derived suction profiles. 262
Figure 128. Profiles derived for test #EF3: a) suction gradient, b) total gradients, and (c) derived unsaturated hydraulic conductivity for Sample A, Sample B, and ND measurements on both samples (A_G and B_G) respectively.263
Figure 129. Definition of Eagle Ford clay SWRS for data set 1. 273
Figure 130. Residuals measured between experimental data and SWRS model for set 1.....273
Figure 131. Definition of Eagle Ford clay SWRS for data set 2. 274
Figure 132. Residuals measured between experimental data and SWRS model for set 1.....274
Figure 133. Comparison of Eagle Ford SWRS obtained for Set 1 and Set 2. 277
Figure 134. Validation of SWRS model for Eagle Ford clay by comparing the equilibrium stages of test EFW2.....278

Figure 135. Validation of SWRS model for Eagle Ford clay including: a) side-view of the comparison between SWRS model and EFW2 testing stages, and b) residuals measured between tests EFW2 and model prediction. ...278
Figure 136. Comparison of SWRS model for Eagle Ford clay (Set 1) vs. results from centrifuge testing.....279
Figure 137. Evaluation of SWRS model for Eagle Ford clay (Set 1) including: a) side-view of the comparison between SWRS model and centrifuge testing, and b) residuals measured between centrifuge results and model prediction. 280
Figure 138. Hydraulic conductivity as function of suction for Eagle Ford clay including: values derived from ATX Cell tests soil, and indirect values obtained with van Genuchten-Mualem model.....282
Figure 139. Hydrus model geometry including: a) the node discretization and the location of the observation points (GTDR), and b) the geometry of the three materials.....284
Figure 140. Comparison between the predicted behavior in Hydrus for a uniform soil model and the measured water contents at GTDR #Top and #Mid nodes during the infiltration stage of Test #EF1. 287
Figure 141. Water content profiles along the sample at different times predicted by Hydrus model 1 during the infiltration stage of Test #EF1. 287
Figure 142. Comparison between the response of the Hydrus model 2 (including three soil layers) and the measured water contents at GTDR #Top and #Mid nodes during the infiltration stage of Test #EF1.....288
Figure 143. Water content profiles along the sample at different times predicted by Hydrus model 2 during the infiltration stage of Test #EF1. 289

Figure 144. Comparison between the derived k-function model using Hydrus on test #EF1 (model 2), the hydraulic conductivity measurement performed in Test #EF3 under unsaturated steady state flow conditions, and the hydraulic conductivity values derived from test #EFW3a. 290
Figure 145. Information from swelling test performed in the CPUS (Kuhn 2010): (a) swelling vs. time and (b) swelling vs. total vertical stress curve. ...294
Figure 146. Sample in swelling test: a) at the beginning, and b) end of the test. 296
Figure 147. Expansion in swelling test #ES3 expressed in terms of: a) vertical displacement and b) vertical strain. 297
Figure 148. Changes in the global variables in swelling test #ES3: a) void ratio and volumetric water content vs. time; b) void ratio and degree of saturation vs. time; and c) voltage in pressure transducer vs. time. 299
Figure 149. Top disc and markers displacement of swelling test #ES3 (Sample A).301
Figure 150. Summary of expansion at the end of the test #ES3 (Sample A): a) Swelling vs. sample height, and b) Swelling vs avg. total vertical stress per layer. 302
Figure 151. Correlation between volume change (void ratio) and: a) volumetric water content, b) degree of saturation during swelling test #ES3. 303
Figure 152. Correlation between volume change (void ratio) and: a) volumetric water content, b) degree of saturation, during swelling test #ES4. 304
Figure 153. Comparison of the experimental results for test #ES3 and #ES4 including the correlation between volume changes and: a) volumetric water content, and b) degree of saturation changes. 305

Figure 154. Comparison of the experimental results between swelling test #ES4 and ATX cell test EFW2a for Eagle Ford clay samples compacted at optimum water content and teste at 306

Chapter 1: Motivation, Objectives and Structure

1.1 MOTIVATION OF THIS DISSERTATION

The majority of structures designed by geotechnical engineers are placed on, or within unsaturated soils. However, the design of these structures more often do not account for the unsaturated condition in general or for the soil-structure response to wetting and drying processes in particular.

One relevant type of unsaturated soil is high plasticity clay, or expansive clay for short, which can undergo large volume changes in response to moisture changes. Although this effect is often not life-threatening as compared to other natural disasters, expansive soils constitute a natural hazard with an average annual damage that exceeds that caused by floods, hurricanes, earthquakes and tornados combined (Wray & Meyer 2004, Adams et al. 2008, Puppala & Cerato 2009, Rendon Herrero 2011).

While important advances have been made in understanding the physical and mechanical properties of expansive clays, our ability to physically measure the key variables (e.g. the vertical rise) responsible for such damages, remains at least limited. Because conventional "free-swell" tests require an often excessive testing time, as well as a large battery of tests to define correlation between swelling and stress, the current state of practice relies heavily on empirical correlations (e.g. between vertical rise and clay index properties).

Moreover, it can be argued that determining the vertical rise of expansive clays under full wetting conditions also bypasses other variables like the unsaturated hydraulic conductivity and moisture fluctuations that affect the soil-structure interaction.

Previous research has showed that infiltration processes and consequent swelling can be sped up using centrifuge technology, which involves imparting a controlled

gravitational gradient (Plaisted 2009, Kuhn 2010, Walker 2012, Armstrong 2014). Centrifuge technology has also been used to determine the relationships between changes in suction, water content and hydraulic conductivity of soils (Nimmo et al. 1987, Nimmo 1990, Conca and Wright 1992, McCartney 2007; Reis et al. 2011, Plaisted 2014). However, the characterization of the hydraulic properties of unsaturated expansive clays has not being fully correlated with the volume changes observed in response to imposed stresses or to changes in moisture content.

Although estimating the changes in the degree of saturation in a geotechnical project can be challenging, accounting for partial wetting and the associated volume changes is expected to lead to cost-effective solutions (Houston, 2014; Houston and Nelson, 2012). Understanding the hydro-mechanical behavior of expansive unsaturated soils is of significant importance in order to refine the design of geotechnical engineering systems.

1.2 STATEMENT OF OBJECTIVES

The overall objective of this research is to gain insight into the coupled hydro-mechanical processes affecting the behavior of clays. The approach adopted in this study includes the development of experimental techniques and analytical tools that are suitable to characterize the unsaturated behavior of clays, both low and high plasticity, with emphasis on centrifuge modeling. Specifically, the four key variables that control unsaturated flow processes and that should be explicitly taken into account are: moisture content, suction, volumetric strain, and hydraulic conductivity. The specific objectives of this work are:

- Evaluating the shortcomings and benefits of using centrifuge modeling in clays.

- Developing a suitable experimental set up that includes non-intrusive sensors to measure key variables in soils undergoing volumetric changes.
- Developing models to represent the water retention capabilities of unsaturated soils using a combination of techniques (filter paper, chilled-mirror hygrometer, pressure plate test and centrifuge methodologies).
- Providing a comparison between centrifuge (N.g) and standard (1.g) test results.
- Establishing protocols for the determination of the SWRS and the hydraulic conductivity function in expansive clays, including the testing methodology (steady or unsteady state) and analysis technique.
- Evaluating the coupled hydro-mechanical behavior of expansive soils in relation to its moisture and volume changes, in response to progressive wetting under different loading conditions.

1.3 SCOPE AND STRUCTURE OF THIS DISSERTATION

This dissertation includes fourteen chapters, which includes three introductory chapters following by technical themes that are grouped into three self-contained sections. The dissertation concludes in the fourteenth chapter with a series of general conclusions, followed by specific conclusions derived from each technical section and recommendations for future research.

This dissertation involved several experimental techniques and analytical methods to characterize the unsaturated hydraulic properties of soils, with emphasis on centrifuge modeling. In Chapter 2, the general concepts are presented about flow in unsaturated soils, developments involving centrifuge testing, and analytical models to represent the hydraulic properties of unsaturated soils. Chapter 3 presents a general overview of the experimental devices (standard -1.g- and centrifuge –N.g-) used to determine the

hydraulic properties of unsaturated soils, in order to identify the relevant equipment to be used in this research, and opportunities for improvements.

Section 1 of this dissertation (Chapters 4 to 6) focuses on the development of new equipment and sensors capable of testing the hydro-mechanical behavior of unsaturated soils. Chapter 4 includes the development of a new workbench equipment, the ATX Cell. Chapters 5 and 6 present the upgrades performed to the centrifuge permeameter for unsaturated soils (CPUS) at The University of Texas at Austin. They include: the development of a non-intrusive water content sensor, the GTDR; and the design and implementation of a non-intrusive tool to asses soil deformation based on image analysis.

Section 2 (Chapters 7 to 9) includes an evaluation of the performance of the new equipment and sensors presented in Section 1, and it also provides the results for the hydraulic characterization of unsaturated low plasticity clays. Chapter 7 includes the results from a series of standard (1.g) tests including: the ATX Cell and the chilled mirror hygrometer. Chapter 8 focuses on centrifuge (N.g) testing, including a brief examination of previous centrifuge tests results, testing procedures and measurement techniques. In addition, a series of hydraulic characterization tests on RMA soil are documented to illustrate the impact in the results of the non-intrusive techniques. Chapter 9 presents the analysis of experimental results, in particular the determination of the Soil-Water Retention Surface (SWRS) for the RMA soil, as well as the determination of the hydraulic conductivity from the transient response in the ATX Cell and centrifuge tests.

Section 3 (Chapters 10 to 13) builds upon the outcomes from Sections 1 and 2 to provide the hydro-mechanical characterization of unsaturated expansive soils. Chapter 10 includes a series of results from standard (1.g) hydraulic characterization tests. The results of centrifuge tests are presented in Chapter 11 to define the hydraulic properties of unsaturated expansive clays. Chapter 12 provides the analysis of previous results to

define the SWRS and the hydraulic conductivity function of Eagle Ford clay. Chapter 13 evaluates the coupled response of moisture changes and volumetric strain in swelling tests through the wetting process.

Finally, the overall conclusions of this research are described in Chapter 14 along with a summary of the conclusions of each section and recommendations for future work.

Chapter 2: Definition of Hydraulic Variables in Unsaturated Soils

2.1 WATER FLOW IN UNSATURATED SOILS

2.1.1 Water potential

The energy state of the soil-water is a critical variable to quantify water flow in unsaturated soils. The mechanical energy is composed of kinetic (E_K) and stored (E_S) energy. Since flow in soils is relatively slow, the kinetic energy is negligible, and flow can be attributed to differences in the stored energy. The stored energy corresponds to sources such as pressure and the relative position of the water within a gravitational field. The energy quantified in units of Joules in the SI unit system (J = N.m), corresponds to the energy stored in a system being often expressed for a unit of mass, volume or weight, as follows:

- The water potential (Φ) is defined as the hydraulic energy per unit of volume (Φ = E/V). It has units of pressure, Pascal in the SI unit system [Pa = N/m^2 = N.m / m^3].
- The hydraulic head (h) is the water potential normalized by the unit weight of the fluid. The hydraulic head is then, the energy per unit of weight ($h = \Phi/\gamma = E/V.\gamma$). It has units of length, meters (m) [m = Pa / (N/m^3) = (N.m) / (m^3) / (N/m^3)]

The water total potential in porous media (Φ_T) includes: the gravity potential, as well as the stored potential due to water pressure sources, as follows:

$$\Phi_T = \Phi_z + \Phi_P = \Phi_z + (\Phi_m + \Phi_o + \Phi_{pn}) \quad (1)$$

where, Φ_z is the gravitational potential, caused by the position of water within a gravity field, and the other three terms corresponds to pressure potential: Φ_m is the matric potential and it depends on adsorptive forces binding water to a solid matrix; Φ_o is the

osmotic potential, which depends on the concentration of a dissolved substance in the water; Φ_p is the pressure potential caused by a hydrostatic or pneumatic pressure; (Or et al. 2010). Unless a backpressure system is used, Φ_{pn} will not be included in the analysis as presented in this thesis.

2.1.2 Water flow

The first flow experiments in saturated porous media were published by Henri Darcy (1856). After completing a series of infiltration tests through sands samples, Darcy reported an empirical correlation between flow and the hydraulic gradient, known eventually as Darcy's Law, as follows:

$$q_w = Q / A = V / At = k_s i = -k_s \frac{\Delta h}{\Delta l} \qquad (2)$$

were Q is the discharge rate (Vol/time) flowing through a cross-sectional area A; q_w is the discharge velocity [m/s], and k_s is a proportionality constant between flow and hydraulic gradient known as the saturated hydraulic conductivity. The hydraulic gradient (i) is defined as the ratio $\Delta h/L$, were Δh is difference in hydraulic head between two points separated a distance L.

Darcy's law was extended in 1907 by Edgar Buckingham to the case of unsaturated soils. The main hypothesis is that the unsaturated hydraulic conductivity is a function of the water content $k(\theta)$ or total head $k(\psi)$. Flow remains proportional to the hydraulic gradient, which now includes all the terms described in (Eq.1), being expressed, in its differential form, as the Buckingham-Darcy's law, as follows:

$$q_w = -k_s\left(\theta\right)\frac{\partial h}{\partial l} = -k_s\left(\theta\right)\frac{\partial\left(h_p + h_z\right)}{\partial l} \qquad (3)$$

2.1.3 Water flow in a centrifuge environment

Flow tests in porous media performed in a centrifuge environment require proper consideration from the previously discussed definitions. While an accelerated gravitational field will increase the gravitational potential, it should not affect the other components of the total potential (e.g. matric or osmotic).

The hydraulic gradient, which is commonly defined as the change in head per unit length, can also be considered as: the change in energy per unit volume (i.e. the change in water potential) normalized by the unit weight of fluid, per unit length. The presence of an increased gravitational field should not affect the normalization done by unit weight of fluid.

For example, if a hydraulic conductivity test is performed using a difference in pressure between two points it should create a gradient component that forces flow independently of the gravitational field. Since the water potential is normalized by the unit weight of fluid ($\gamma_w = \gamma_w.g$) in a zero gravity environment that unit weight would be zero, the hydraulic head and the gradient would tend to infinity and the hydraulic conductivity to zero. In order to avoid this misrepresentation, the normalization must be done using the unit weight of fluid in the earth gravitational field (1.g). The definition of change in hydraulic head is then best represented using the following equation:

$$\Delta h_t = \Delta h_p + \Delta h_z = \frac{\Delta P}{\gamma_{w.1g}} + \frac{\Delta z\left(N.g\right)\rho_w}{\gamma_{w.1g}} \qquad (4)$$

where, $\gamma_{w.1g}$ is the unit weight of water at 1.g, and ΔP represents all the pressure sources, ρ_w is the density of water (1,000kg/m^3), and N.g is the Earth's gravitational field (9.807 m/s^2) scaled N-times.

2.2 HYDRAULIC CHARACTERISTICS OF UNSATURATED SOILS

2.2.1 Soil-water potential

In geotechnical engineering, the resultant energy from the physical and chemical soil-water interaction in unsaturated soils in named soil-water potential. This definition includes matric (Φ_m) and osmotic potential (Φ_{os}).

Matric potential is results from the physical interaction between water and the soil matrix. These interaction forces are the combined results of capillarity and the adsorptive forces. When a capillary tube is immersed into water the air-water interface inside the tube curves forming a meniscus. This meniscus results from the adhesion of water with the tube surface. According to the Young-Laplace equation a decrease in pressure occurs across the interface and the water pressure is lower than that of the air. Accordingly, water will rise inside the tube until the upward force created by the air-water-solid system reaches equilibrium with the weight of water. The height of liquid that will rise in a capillary tube (h_ψ) can be calculated, as follows:

$$h_\psi = \frac{\sigma_{aw} \cdot \cos(\gamma)}{R \cdot \rho_w \cdot g} \quad (5)$$

where R is the tube radius, σ_{aw} is the surface tension between fluids (air-water), and γ is the contact angle between the liquid (water) and solid (soil matrix). In consequence if the pore space in the soil is modeled as capillary tubes, this interface capillary forces create a

source of internal pressure in unsaturated soils, matric suction, that can be expressed with the following equation:

$$\psi_m = \rho_w \cdot g \cdot h_\psi = \frac{\sigma_{aw} \cdot \cos(\gamma)}{R} \quad (6)$$

The osmotic potential is related to the presence of solutes in the pore water. The effects of are important when: (a) there are considerable amounts of solutes in the soil and (b) there is a diffusion barrier (e.g. soil-plant root interfaces or soil water-air interfaces) (Or et al. 2010).

Since the potential is expressed in absolute pressure units they are typically referred as matric (ψ_m) and osmotic (ψ_{os}) suction. The sum of both internal sources of pressure is referred as total suction (ψ_T) defined, as follows:

$$\psi_t = \psi_m + \psi_{os} \quad (7)$$

It is important to note that total suction is not the same as total potential (1). While matric suction is relevant in all soil types, osmotic suction is primarily important in high plastic clays, due to their mineralogy or the presence of dissolved salts in the pore fluid. In addition, osmotic suction can be generally assumed to be constant for any water content, as long as the pore fluid chemistry is not modified (Tarantino et al. 2008b). Consequently, while osmotic suction may be relevant, its contribution to the hydraulic gradient is often negligible.

2.2.2 Soil-water retention curve

The soil-water retention curve (SWRC) describes the relationship between the volumetric water content (θ), or degree of saturation (S_r), and the soil-water potential at equilibrium. This function is affected by the void distribution (pore size and connectivity)

as well as the soil structure, texture and mineralogy. The SWRC is a fundamental hydraulic property; it shows a highly non-linear shape and is defined through several orders of magnitude in terms of suction. While coarse-grained (sand) materials show a rapid decrease in water content for a comparatively narrow suction range, fine-grained soils (e.g. silts and clays) show a more gradual water content reduction with increasing suction (Figure 1a).

The shape of the SWRC can be explained using a bundle of capillary tubes to represent the soil void distribution. The larger the diameter of the tubes will result in small suction, but they hold a comparatively large volume of water. On the other hand, the smaller tubes have a higher suction, but hold a small amount of water. In Figure 1b, the increasing elevation (capillary rise) corresponds to an increasing matric suction, and the volume of water stored at each elevation can be compared to the total volume of voids (volume of tubes in the model) to define the volumetric water content ($V_w/V_v = \theta$).

In coarse soils, voids are comparatively large and uniform. After a given suction value is achieved, most pores dry out losing most of its moisture. Fine-grained soils have smaller pores within a broader range in sizes. When suction increases, the water content is lost gradually. In addition, due to the tube size (pore size), a greater amount of water is held even at very high suction values. For analysis and modeling, the experimental data that defines the SWRC is fitted often by a continuous function

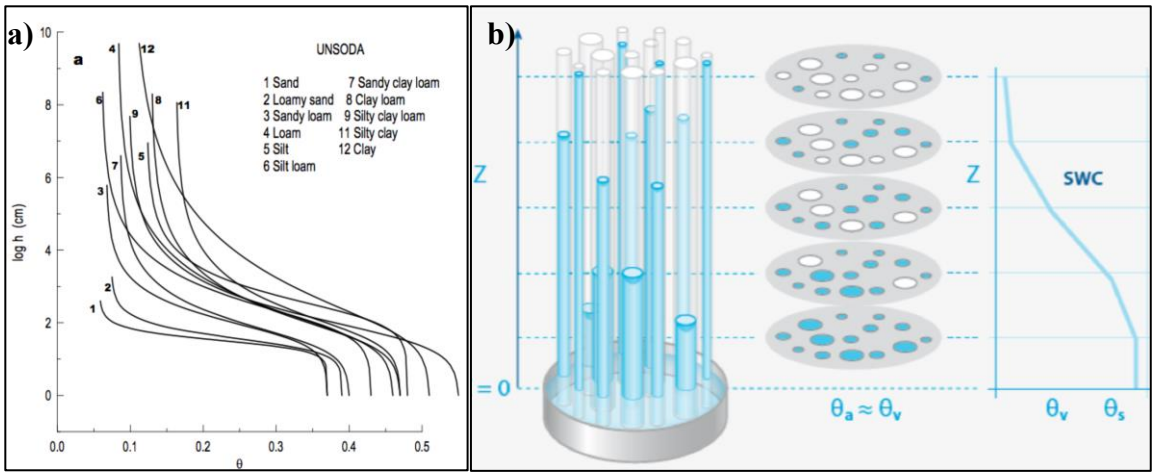

Figure 1. (a) SWRC for different soils and (b) schematic representation using the bundle of capillary tubes model (Or et al. 2010)

2.2.3 Unsaturated hydraulic conductivity function

Despite the efforts to simplify the soil matrix and void distribution, soil pores are not uniform along their length. They have an irregular geometry, and flow pathways cannot be clearly determined. Consequently, hydraulic characteristics in soils are described macroscopically as in the case for Darcy's and Buckingham-Darcy's laws.

In saturated soils all pores are filled, and this represents a condition where all the pathways for water flow are available. Starting from the saturated value (k_{sat}), the hydraulic conductivity decreases rapidly with decreasing water content (or increasing suction). As the large pores drain, the water pathways decrease, and therefore the conductivity also decreases. In fine-grained soils, with comparatively smaller pores, higher suction values are necessary to drain the stored water, and consequently the conductivity is reduced more gradually.

The relationship between the ability of water to flow through the pore space and the volume of water in those pores is represented by the unsaturated hydraulic

conductivity function. This is a highly non-linear function that can be expressed in terms of the water content k(θ) (or matric suction k(ψ)).

2.3 HYDRAULIC CHARACTERISTIC MODELS

2.3.1 Soil-water retention curve model

There are a few models that have been extensively used to represent the soil-water retention behavior of in unsaturated soils such as Brooks & Corey (1964), Van Genuchten (1980), and Fredlund and Xing (1994).

Brooks & Corey (1964), and van Genuchten (1980) SWRC models are described by the following equations:

$$\theta(\psi) = \theta_r + (\theta_s - \theta_r) \cdot \left(\frac{\psi}{\psi_{aep}} \right)^{-\lambda_{BC}} \quad (8)$$

where θ_r is the residual moisture content, θ_s is the saturated moisture content, ψ_{aep} is the air entry pressure, and λ_{BC} is a fitting parameter.

$$\theta(\psi) = \theta_r + (\theta_s - \theta_r) \cdot \left[1 + (\alpha_{VG} \cdot \psi)^{n_{VG}} \right]^{-m_{VG}} \quad (9)$$

the fitting parameters are α_{VG}, n_{VG}, and m_{VG} is typically assumed as $m_{VG} = (1\text{-}1/ n_{VG})$

The SWRC model proposed by van Genuchten (1980) has been used through all this research to analyze the experimental data. It is important to mention that due to the hysteretic behavior of the soil in wetting and drying processes, different retention curves can be obtained from different tests and initial conditions. The SWRC models are used to fit a data set independently of the initial conditions or test. Therefore, it can be argued

that θ_s does not always represent the saturated moisture content porosity, and θ_r the residual moisture content, but they can be used as additional fitting parameters.

2.3.2 k-function model

The k-function model represents the relationship between the available flow paths and the conductivity of unsaturated soils. Conceptually, the hydraulic conductivity will decrease with the decreasing water content (or increasing suction). Early approaches used this concept and presented exponential decreasing models (linear in log-space) in terms of suction. For example, (Gardner, 1958) proposed the following equation:

$$k\left(\psi\right) = k_{sat} e^{-\alpha\psi} \tag{10}$$

Due to its mathematical form Gardner's model has been very useful to solve Richard's equation analytically. However, it is more intuitive and preferable to represent the k-function in terms of the volumetric water content (or a normalized water content):

$$k\left(\theta\right) = k_{sat}\left(\Phi\right)^{\beta} = k_{sat}\left(\frac{\theta - \theta_r}{\theta_s - \theta_r}\right)^{\beta} \tag{11}$$

where Φ is the normalized water content, and b is typically between 3 and 3. 5

Later k-functions were developed based on statistical models of the pore size distribution based on the SWRC shape and their interconnectivity. One of the most common used model is the van Genutchen-Mualem model (Mualem, 1976), represented by the following equation:

$$k\left(\theta\right) = k_{sat}\sqrt{\left(\frac{\theta-\theta_r}{\theta_s-\theta_r}\right)}\left[1-\left(1-\left(\frac{\theta-\theta_r}{\theta_s-\theta_r}\right)^{\frac{1}{m_{VG}}}\right)^{m_{VG}}\right]^2 \quad (12)$$

2.4 SOIL-WATER RETENTION SURFACE (SWRS) MODEL CONCEPT

The definition of the soil-water retention surface (SWRS) (Matyas 1968, Salager et al. 2007) corresponds to an extension of the SWRC, where, the changes in the soil void ratio are taken into account and the data is presented in the space [ψ, θ, e] where ψ is the suction, θ is the volumetric water content, and "e" is the void ratio (Figure 2a).

The data necessary to define the surface can be obtained using different testing techniques, but the same considerations taken for the SWRC are valid for the SWRS for example: soil hysteresis in response to wetting or drying process; or the solely inclusion of the matric suction component in the model. Typically, a series of samples prepared at different initial densities are required to cover a wide range of the surface. The measured volume changes are used to define the void ratio on each equilibrium stage.

The testing approach used by Salager et al. (2007) included not only using samples with different initial densities, but also taking each sample from the initial "saturated" condition to a desire suction level. Once equilibrium was reached, the water content and density were measured. In this way, only one data point could be obtained for each sample.

a) **b)**

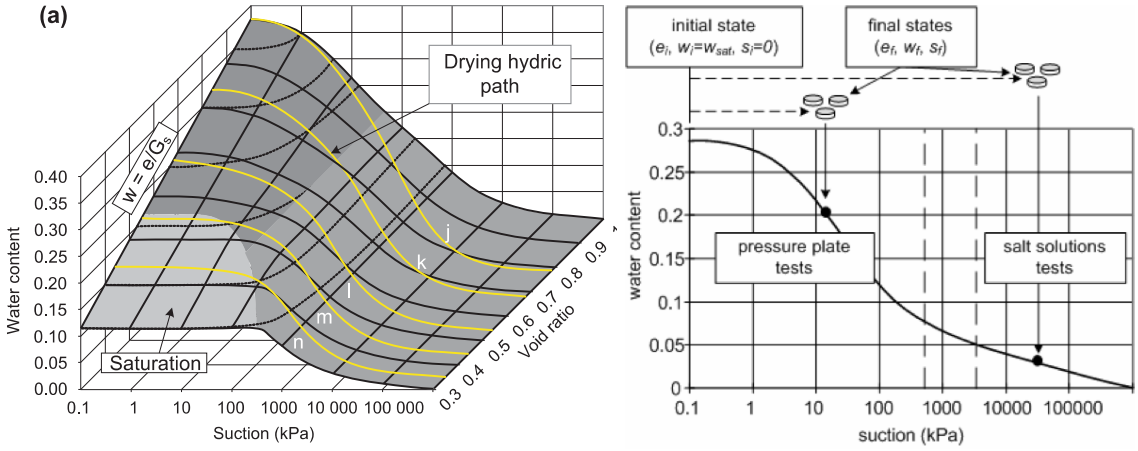

Figure 2: Conceptual definition of SWRS: a) SWRS model indicating the drying path tests (Salager et al. 2010); and b) testing approach involving a series of samples used to define values at a single imposed suction (Salager et al. 2007).

Chapter 3: Rationale for the Selection of the Unsaturated Soil Testing Equipment

3.1 INTRODUCTION

The standard equipment and methodologies used to determine the soil-water characteristics curves are documented by ASTM D6836–02. The standard tests include: Hanging column tests, Pressure plate extractor, chilled mirror hygrometer, and centrifuge test. This list can be extended to incorporate the filter paper test (ASTM D5298–10) and the Evaporation Test "Hyprop" (Schindler & Müller, 2006), which are also commonly used in practice. In general, testing approaches can be classified according to one of these frameworks:

- When determining the retention characteristics of unsaturated soils most techniques impose a suction stage or a water content value and its counterpart is measured. This process can be done in one single stage or in successive stages using the same soil sample. The selection of the method is generally related to the range of the SWRC of interest (low or high suction).
- The methodologies used to evaluate the unsaturated hydraulic conductivity typically impose either a constant hydraulic gradient or a constant flow rate, with the complementary value being measured. Depending on the behavior of these variables or on the boundary conditions with time the methods can be classified as: "steady-state" or "transient". For example, in steady methods (e.g. centrifuge), a constant flow rate is applied through time and the hydraulic gradient is measured. In transient tests (e.g. pressure plate), a suction value is imposed and the transient outflow/inflow.

A brief overview is provided here in regarding the relevant features of these tests used as routine in the determination of SWRC and K-functions. The objective of this evaluation is to highlight the benefits, shortcomings, and opportunities for improvement that can be implemented in this research. Additional details on the test equipment and analysis procedures are included in Appendix 1. A more exhaustive review of these pieces of equipment, procedures, and the theoretical interpretations used to characterize the unsaturated hydraulic conductivity in the laboratory and the field are provided by Olson and Daniel (1979), Benson & Gribb (1997), Klute (1972), Dirksen (1991), Stephens (1994), Bicalho et al. (2013), and Bulut & Mantri (2014).

3.2 OVERVIEW OF STANDARD (1.G) TESTING METHODS

In this section a review of the standard (1.g) laboratory equipment for the hydraulic characterization of unsaturated soils is presented. including: Pressure Plate Extractor, Hanging Column, Evaporation test (Hyprop), Filter Paper, and Chilled Mirror Hygrometer (ASTM D6836–02).

3.2.1 SWRC determination under low suction conditions

3.2.1.1 Pressure plate extractor and Hanging column test

The pressure plate and hanging column methods involve imposing a matric suction value and measuring the water content at an equilibrium stage. Both tests can be used in simple or multiple stages. In addition, retention curves can be measured in either drying or the wetting path.

The pressure plate extractor is a test based on the axis translation technique. Its main advantage is that it imposes at the outlet a fixed air pressure, while the water pressure is constant (and equal to atmospheric pressure). Then the capillary pressure is defined as $p_c = u_a - u_w$. After applying the air pressure, flow occurs under transient

conditions until equilibrium is reached. Thus, the water content is obtained by oven drying. This procedure can be repeated in several stages at different suction levels. The cumulative outflow is recorded to back-calculate the equilibrium water content at each stage. The range of testing goes from 10 kPa to 1500 kPa. The set up described in ASTM D6836–02 includes a collection system and an air trap (Figure 3)

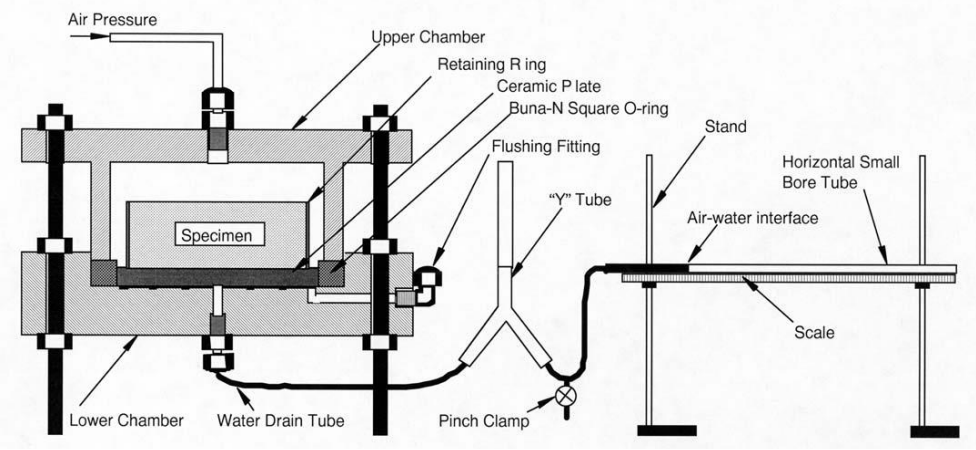

Figure 3. Pressure plate extractor set up (ASTM D6836–02).

The hanging column test is used with a similar set-up, the sample is placed into a funnel with a ceramic disc that is connected to the outflow water lines. In this case the suction is created by raising the funnel generating a negative pressure in the water that is in contact with the sample. The range of testing covers typically a range of 0 to 40 kPa.

The main difference between pressure plate and hanging column is the suction rage that can be tested. This range depends on the method used to create suction in the sample: the hanging column test is limited to a maximum suction of 100 kPa due to the cavitation of water, and pressure plate test is only limited by the air pressure provided and the air entry pressure of the ceramic disc. Pressure plate tests are typically used in the range of 0-300 kPa but can reach up to 1,500 kPa.

The results of both techniques are robust when used in one stage since the suction is well defined and the water content is calculated by oven drying the sample. Using any of these tests in multiple stages reduces the amount of work and the scatter in the results since all the measurements are performed in the same sample. However, experimental errors in the outflow system associated to evaporation, leakage, and diffused air have a direct impact in the results.

Another relevant disadvantage is that the commercially available versions of both tests do not account for any measurement of volumetric changes or provide the means to impose loads. Loads may play an important role when affecting the soil deformation in response to a wetting or drying process.

3.2.1.2 Derivation of unsaturated hydraulic conductivity based on the transient response of pressure plate test

Several analytical methods have been proposed to determine the unsaturated hydraulic conductivity using the transient outflow information from pressure plate tests. The most commonly used ones are the outflow methods where precise measurements of the transient data are required (Benson and Grib, 1977). There are four types: multi-step, one-step, multi-step direct and continuous.

Gardner (1956) developed the original multi-step outflow method. It uses the outflow data obtained from small suction increments (or decrements) that are applied to the soil in successive stages to derive the unsaturated hydraulic conductivity. The theoretical framework includes several hypothesis: 1) k (ψ) is constant in each suction step, 2) there is a negligible gravitational gradient, 3) soil is homogeneous and rigid, and 4) no impedance is created by the porous base plate. Then, the transient flow problem can be written as:

$$\frac{\partial \psi}{\partial t} = D\frac{\partial^2 \psi}{\partial t^2} \quad \text{with } k(\psi) = D\frac{\Delta\theta}{\Delta\psi} \tag{13}$$

Gardner (1956) presented a solution to Fick's second law to determine k (ψ) in terms of the outflow measured, as follows:

$$\ln\left(\frac{V_f - V_t}{V_f}\right) = \ln\left(\frac{8}{\pi^2}\right) - D \cdot t\frac{\pi^2}{4L^2} \tag{14}$$

Where V_t is the outflow at a given time, V_f, is the final outflow (for that stage), and L is the length of the specimen. The slope can be adjusted to match the outflow (left side of the equation) to calculate the diffusivity. The intercept in this equation is a fix value (ln $[8/\pi^2]$ = -0.15). When a linear fit is placed over the normalized outflow (Figure 4) the diffusivity is derived from the slope and the intercept can be compared with -0.15. If it is higher, it means that the bottom porous plate generates significant impedance.

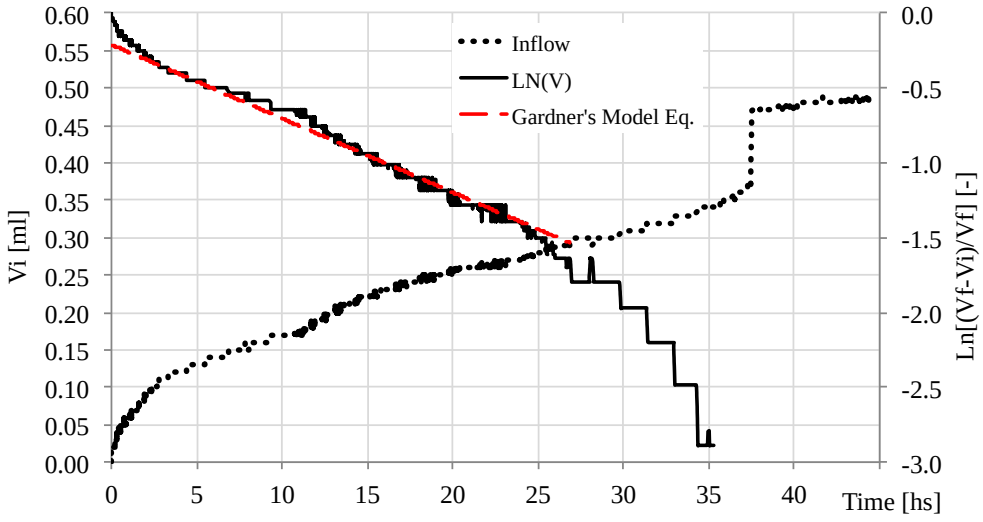

Figure 4. Gardners's solution applied to the measurements of ATX cell test W9 performed using RMA soil.

The advantage of this method is that the data can be easily obtained with the same equipment used to determine the SWRC. The main disadvantage is that it does not account explicitly for the porous plate conductivity. Porous discs have an hydraulic conductivity comparable to the soil; for example, in this research a 1-bar ceramic plates from Soil Moisture were used and their hydraulic conductivity is k_{sat}= 7.56 10^{-9} m/s.

3.2.1.3 Evaporation test

The evaporation method was developed by Wind (1968) to determine the soil water retention characteristics and unsaturated hydraulic conductivity of soils. Wind's method uses simultaneous measurements of the evaporation rate and suction values at many different heights of the soil column. Schindler (1980) prove that acceptable results could be obtained by using only two suction measurements at different depths. Schindler (1985) reported values for a great variety of soils using this method. A thorough analysis of the calculation procedure and the method limitations is presented in Wendroth (1993).

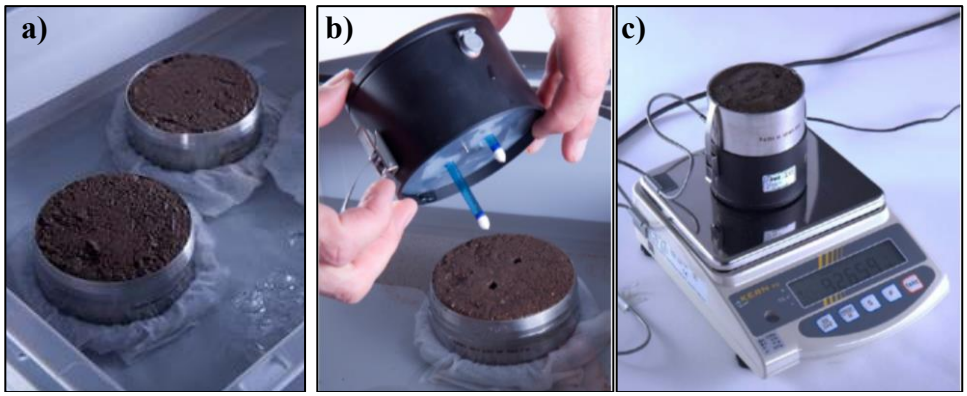

Figure 5. Hyprop test: (a) soaking, (b) installing sensors, and (c) evaporation phase.

The evaporation test is a transient test that involves simultaneous measurement of (1) the water evaporated from the upper boundary of a soil column and (2) the matric

suction at two different points within the column. Two tensiometers are installed at different heights into a soaked sample. Then, the sample is placed on a scale and soil moisture is allowed to evaporate from the upper boundary (Figure 5). The weight change is recorded with a scale and it is used to calculate the water content and the evaporation rate along the test.

Readings from the tensiometers are used to define the suction profile and the hydraulic gradient. The test is typically finished when the top tensiometer reaches cavitation (85 kPa). The sample is removed and the overall water content is measured.

This test is based on a well-defined methodology and it can provide results for both the SWRC and the k-function in a very expeditious way. However, the range of application is limited by the cavitation in the top sensor. The degree of saturation at the beginning is questionable since only imbibition from a water-bath is used. The SWRC will reproduce a scanning curve rather than the real drying branch. Like other tests described before, this set up does not account for volume change measurement or load control.

3.2.2 SWRC determination under high suction conditions

3.2.2.1 Filter paper test

Filter Paper test is an indirect and secondary method that uses a surrogate material to measure the suction from a soil sample (Tarantino et al. 2014). The soil and the filter paper are brought to equilibrium in a closed flask. Then, the gravimetric water content of the paper is measured and the suction can be inferred from the filter paper calibration curve. A detailed procedure for this test can be found in ASTM D5298-94, Houston et al. (1994), and Bulut et al. (2001).

This method allows determining matric and total suction. One filter paper is placed in contact with the soil to allow equilibration with the soil liquid phase (matric suction equilibrium). A second paper is separated from the soil allowing only moisture interchange with the vapor phase (total suction). The flask is placed inside a small container at constant temperature to facilitate the equilibrium. The equilibration time suggested is 14 days (Figure 6)

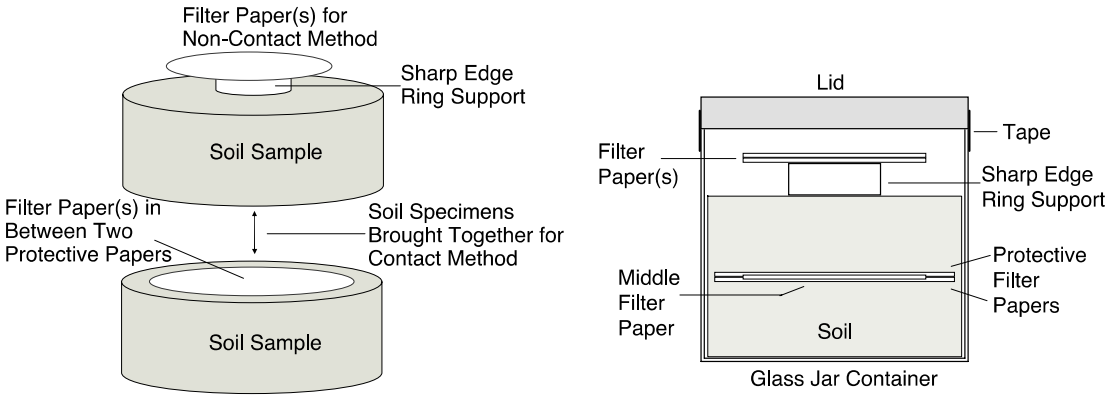

Figure 6. Schematic drawing of the filter paper test set up (Tarantino et al. 2014).

The advantages of the filter paper test are: (1) it covers a wide range of suction values (0.03 to 100 MPa), and (2) it allows determining both matric and total suction, and (3) it is relatively inexpensive. The disadvantages of this method are: (1) it requires 14 days to determine one data point, (2) each soil sample compacted at a targeted volumetric water content provides only one measurement each of the total suction and matric suction, and (3) its precision relies heavily in the testing procedure and the accuracy of the calibrations curves used.

Although Leong et al. (2002) presented two different calibration curves for both total and matric suctions (Figure 7a); Bulut et al. (2001) and Bulut & Wray (2005)

showed that only a single calibration curve is needed (Figure 7b) if it is constructed based on water vapor measurements. Walker et al. (2005) indicated that with enough equilibration time the total suction points would move towards the matric suction.

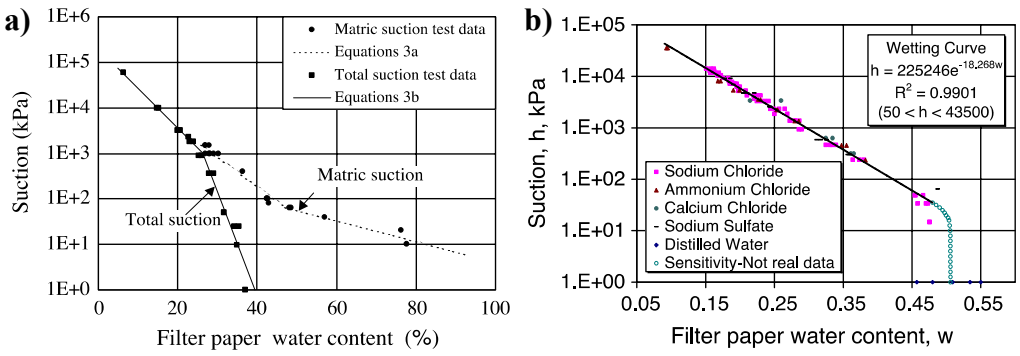

Figure 7. (a) Leong et al. (2014) calibration curves for Whatman No42, (b) Bulut and Wray (2005) calibration for Schleicher & Schuell No.589-WH.

Most calibrations are presented as bilinear functions: one part for the high range of suction (adsorbed water – total suction) and a second part for lower suctions (capillary forces – matric suction). Bicalho et al. (2015) presented a statistical comparison of many calibrations developed for the Whatman No 42 filter paper showing that: all calibrations were within an error of +/-0.25 log(kPa) from the ASTM D5298-10 curves (Figure 8a); and that a single calibration equation could be used (Figure 8b) showing a good agreement when compared to the data originally used for the current ASTM standard.

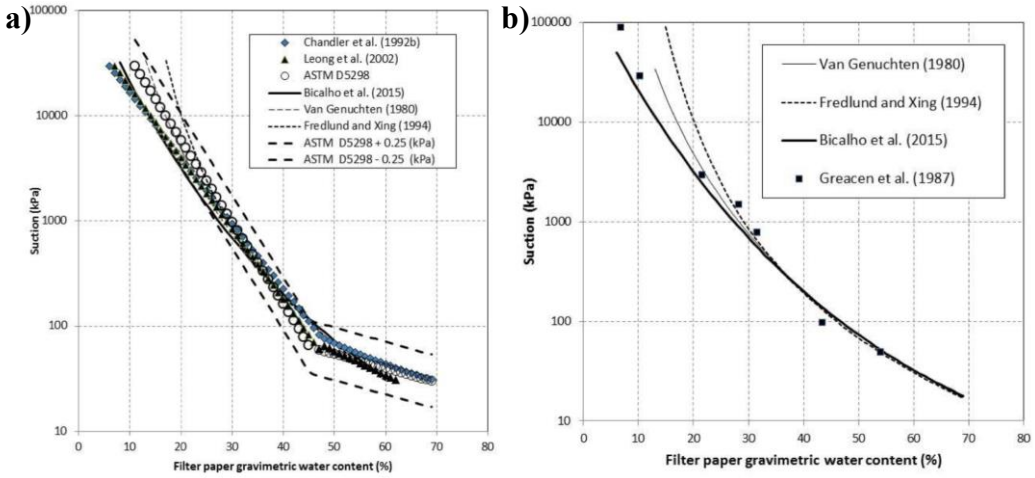

Figure 8. (a) Calibrations in wetting paths for Whatman 42, and (b) single calibration equation. (Bicalho 2015).

3.2.2.2 Chilled mirror hygrometer test

The chilled-mirror psychrometer is a primary method that measures the total suction of a soil sample. This technique can be used in the suction range of 0.10 to 5 MPa with an error of +/-0.05 MPa and between 5 to 300 MPa with an error of 1%.

The WP4C device uses the chilled mirror dew point technique to determine the vapor pressure of the air inside a closed chamber that is in equilibrium with the soil vapor phase. Kelvin's equation represents the thermodynamic equilibrium between the soil (total) suction and the air partial vapor pressure, as follows:

$$\psi_t = \left(\frac{R \cdot T}{M}\right) \ln\left(\frac{p}{p_o}\right) \qquad (15)$$

Where p is the vapor pressure of the air; p_o is the saturation vapor pressure at the sample temperature (T, in Kelvin); R is the gas constant (8.31 J/mol K); and M is the molecular mass of water.

The test procedure is explained as follows: A sample is introduced in a closed chamber; a fan speeds up the moisture equilibration between the air in the chamber and the soil vapor phase. Once equilibrium is reached, the vapor pressure (p) is determined by matching "p" with the saturation vapor pressure at a given dew point temperature. The dew point temperature is found with a mirror connected to a thermoelectric (Peltier) cooler. The dew point is detected with a laser beam and a photoelectric cell that senses the change in reflectance when condensation occurs in the mirror (Figure 9). To complete the suction measurement, the sample temperature is measured to determine p_o; an internal thermo-electrical module is used to monitor and stabilizes the block where the sample is placed. Temperature measurements for both, the sample and the mirror are critical. An error of 1C may results in an error of 8 MPa.

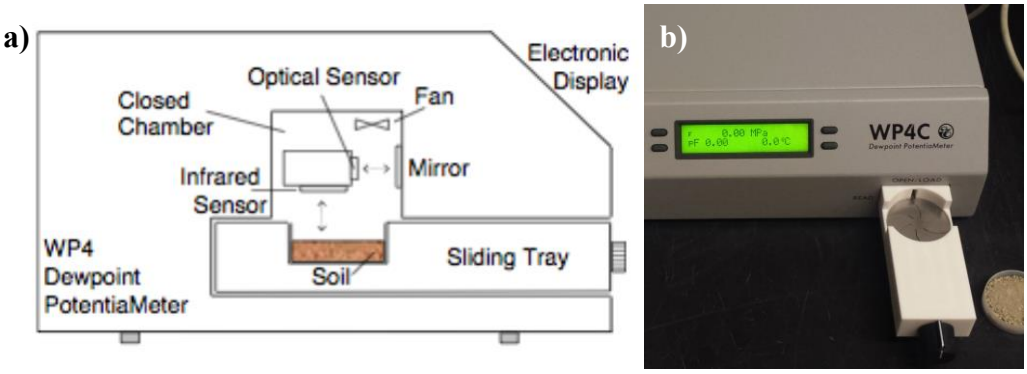

Figure 9. a) WP4 Scheme (Bulut et al. 2002), and b) picture of WP4C device tray in the lab ready to place the samples

3.2.2.3 Comparison of methods

The filter paper testing procedure was carried out in this research following the instructions and calibrations provided by the ASTM D5298-94 Samples were compacted using a displacement control frame. The filter paper used in all cases was the Whatman No 42. After the samples were removed from the glass container (Figure 10a). and the

filter papers were allowed to dry in the oven, a small fraction of the soil sample was trimmed to fit inside the cups of the WP4C. These smaller pieces were sliced with a hand-wire saw (Figure 10b). The goal was to maintain the pore structure of the sample in order to take two suction measurements from the same soil sample using two different testing techniques. The results of this procedure are presented in Chapter 10.

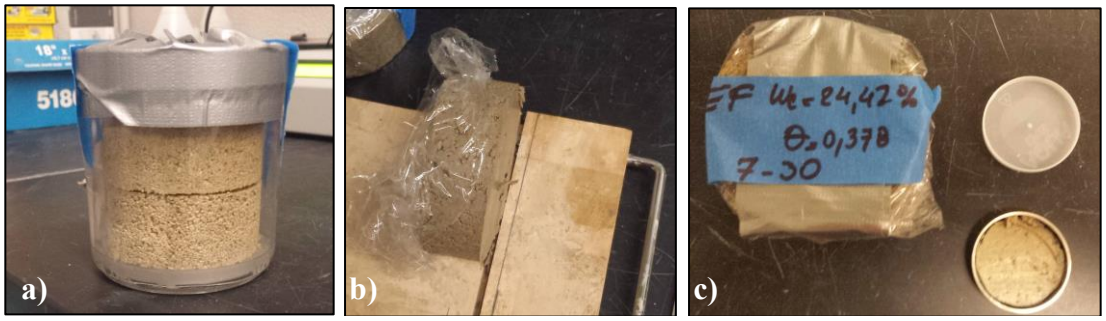

Figure 10. (a) Sample in the glass container, (b) slicing, and (c) set in WP4C bin.

3.2.3 Opportunities for refinement of standard (1.g) test

The background overview shows that it is necessary to combine different tests to cover a wide range of suction values in order to define the hydraulic properties of unsaturated soils. Also, it is fundamental to identify which component of the soil-water potential is measured in each test in order to properly combine the experimental data.

There are two main aspect that all tests have in common and can be explored: first, they do not account systematically for any volumetric changes (soil is assumed as a rigid body); second, loading conditions are not included in these tests, the possibilities of including surcharges at low suction values is limited and almost impossible in tests that assess high suction ranges. The improvement opportunities are then focused in:

- Incorporating systematic **measurements of the volumetric changes**, this time history may not be necessary in non-plastic soils, but it is mandatory in high plasticity clays;
- **Controlling the state of stresses** by adding surcharge, this could provide a way to make 1.g tests more comparable to centrifuge modeling;
- Obtaining a robust **measurement of the transient data** that can be later used to characterize the k-function.

The robustness on the suction definition, the broad testing range, and the possibility of accessing the sample make the pressure plate test a suitable candidate to incorporate all the changes listed before.

3.3 REVIEW OF CENTRIFUGE TESTING (N.G)

3.3.1 Background

Improvements in conventional testing is made to quickly determine the SWRC; however, this is not necessarily true for the k-function. In consequence, empirical correlations are mostly used to predict the unsaturated hydraulic conductivity. Centrifuge testing has proven to be one of the few methodologies used to expeditiously determine the k-function (Nimmo et al. 1987, Nimmo 1990, Conca and Wright 1992, McCartney 2007; Reis et al. 2011, Plaisted 2014).

Nimmo et al. (1987) performed tests under a steady state unsaturated flow. In their set up, flow rates were imposed using a combination of constant head reservoirs and porous disks of known saturated hydraulic conductivities. The outflow rate was measured stopping the centrifuge and weighting the reservoirs (Nimmo et al. 1992). The authors indicated that the suction gradient was negligible in comparison to the gravitational gradient in order to simplify the Hydraulic conductivity calculations (Figure 11).

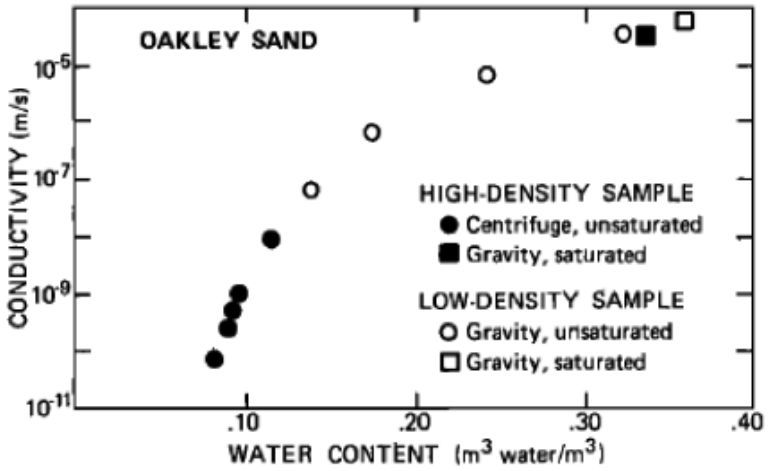

Figure 11. Unsaturated hydraulic conductivity measurements performed in the centrifuge by Nimmo (1987).

Some disadvantages of this procedure are: 1) stopping the centrifuge reduces the stresses along the sample, and it can result density in changes and moisture redistribution; 2) leakage and evaporation in the inflow/outflow reservoirs; 3) a saturated ceramic plate was used to create a zero suction lower boundary, it affected the determination of the average suction always from zero to the maximum suction imposed and drives a highly nonlinear volumetric water content distribution. After Nimmo's work, several modifications (e.g. sealed containers, combination of porous stones at the base to increase the suction at the bottom of the sample, etcetera) were introduced in order to improve the boundary conditions and in-flight measurements in small centrifuges.

Conca and Wright (1992) improved the flow imposed in the upper boundary by incorporating a flow pump to obtain an inflight unsaturated flow rate; ASTM D6527 accounts for this modification.

Reis et al. (2011) presented a modified lower boundary condition by incorporating a tall porous disc below the soil sample. Gravitational forces affect the continuous created by the base disc and the soil sample. In this way, the suction along the porous disc

increases, decreasing then the suction difference between the sample, the average suction is representative of the entire sample and the water content is reasonably constant. To determine points in the SWRC, weight measurements were made after stopping the centrifuge. They also used the transient outflow data to back-analyze the k-function. However, it is not clear if the authors accounted for any possible volume of water coming from the ceramic disc in order to calculate the soil water content in order to define the SWRC or to evaluate the transient outflow data.

Malengier et al. (2014) instrumented the buckets of a commercial small centrifuge with mini-scales in order to determine the mass of the tube containing a soil sample and the mass of the outflow chamber. They determined the SWRC and k-function by combining and smoothing the transient output. Drawbacks of this approach include: (1) calibrating the system was difficult since all elements (tubes, scales, sample) are affected by the gravitational field; (2) achieving good agreement between the range of the scale, which is dictated by the sum of masses and the maximum rotational speed, and the accuracy of the scale, as it should be able to detect small changes in weight due to the change in water content of the sample between stages.

Nimmo (1990) tested the validity of Richard's equation under low volumetric water content conditions in a centrifuge environment by monitoring the transient flow data. Moisture profiles were measured using a series of electrodes along the core-holder. For comparison, transient water content profiles were predicted by solving Richard's equation using a finite difference approach, and using soil properties measured in steady-state tests. Numerical simulation showed good agreement with the experimental data, although the authors state that their predictions for the unsaturated hydraulic conductivity could be as good as the results obtained from the characterization tests.

3.3.2 Centrifuge Permeameter for Unsaturated Soils – CPUS

McCartney & Zornberg (2005), McCartney (2007), Zornberg & McCartney (2010a), Plaisted (2014), presented several series of tests performed in the Centrifuge Permeameter for Unsaturated Soils (CPUS) that will be used in this research. The initial development included: a mechanical system with two permeameter buckets located at 0.7 m from the center and the capability of reaching 875 rpm (or 600 g); a flow rotary joint working together with a medical pump (inflow rates from 0.1 ml/min to 100 ml/min); and an in-flight data acquisition board.

3.3.2.1 Testing methodologies

McCartney (2007) run prototype tests in the centrifuge permeameter including an array of suction (HDU) and water content (TDR) sensors embedded in the soil sample to determine both the SWRC and k-function under steady state conditions.

Then, a simplified experimental testing program was conducted and interpreted using concepts from Dell'Avanzi et al. (2004) analytical solution to Richards' equation for steady-state flow. Specifically, at high g-levels the theory predicts that the suction profile will show an upper zone of a relatively constant suction and therefore a negligible gradient.

The sensor array was replaced by a single TDR probe installed within the acrylic wall of the permeameter cup to determine water content in the zone of constant suction. Values of hydraulic conductivity (k_{target}) can be determined in the upper portion of the soil sample when steady state conditions are reached. The tests involved a defined g-level and an associated infiltration rate (v_m). The unsaturated hydraulic conductivity that could be targeted with the CPUS in the configuration used in this study ranged from 10^{-5} to 10^{-11} m/s. Although one of the main hypothesis in this testing technique was that gravitational potential is the main component driving flow (like in Nimmo, 1987; and

Conca & Wright, 1992), the results obtained from fully instrumented samples (McCartney, 2007) showed that suction values in the upper portions may vary affecting the total potential.

Plaisted (2014) found that the combined action of wetting or drying of the soil sample and the use of an increased stress level modified the void ratio along the sample. Therefore, the definition of the unsaturated hydraulic properties required incorporating the void ratio as an additional variable in the interpretation.

In order to incorporate the void ratio as an additional variable all sensors were removed as they impede volumetric changes, and only destructive tests were performed. Two main sets of tests were performed using a split ring tube: "Hydrostatic" (H) and "Imposed Flow" (IF). For example, in the hydrostatic test after the sample was spun at a desired g-level an hydrostatic equilibrium was reached, the samples were removed from the centrifuge and sliced to determine the void ratio and water content [e, θ] at each slice. These values were matched to the suction value corresponding to the soil slice in order to define the correlation between the three variables [ψ, θ, e]. Also, Plaisted (2014) included the suction gradient in his calculations when determining the unsaturated hydraulic conductivity. These procedures will be further presented in detail in Chapter 8.

3.3.2.2 Boundary conditions

An upper boundary condition can involve imposing a target inflow rate or a level of ponded water using the flow rotary joint. On the other hand, the lower boundary condition of soil specimen is controlled by the interface between the soil sample and the outflow reservoir. This interface involves of a porous plate (a ceramic disc of high air entry pressure or a plastic disc) and a steel base that holds the disc and conducts the water to the reservoir.

The matric suction within the soil matrix must equilibrate the gravitational forces imposed by the centrifuge speed. In such case the suction profile increases from a reference value at the bottom, to a maximum at the top, which depends on the centrifuge acceleration (Dell'Avanzi et al. 2004). Therefore, the range of suction values that can be used to define the SWRS are limited by this boundary condition and the centrifuge speed.

In previous studies, the lower boundary condition has been addressed in different ways: McCartney (2007) used a set up involving open flow centrifugation, which does not guarantee a pressure condition at the lower boundary. During the infiltration tests a capillary barrier may form and water may accumulate until breakthrough would occur. Instrumented tests showed that the suction near the bottom was 10 to 13 kPa for RMA soil over a wire mesh. Figure 12(a) illustrates the base set up developed by Plaisted (2014), which was adapted to all the acrylic permeameter cups and was alternatively used in this research with a ceramic disc of high air entry pressure, to force a zero suction boundary condition, or with a porous plastic disc to allow free drainage.

Figure 12. Lower boundary of the centrifuge permeameter cups: a) aluminum base, and b) outflow instrumented with a pressure transducer.

3.3.2.3 Outflow system

The lower boundary condition of the soil sample can be also defined by quantifying the outflow. Figure 12(b) shows the water reservoir placed in the swinging bucket below the sample. A pressure transducer at the bottom of the reservoir was implemented to sense the hydrostatic pressure of the volume of water collected. The transducer has a range of 0 to 35 kPa, with an error +/- 0.25% of the sensor full scale. A solenoid valve allows draining it when is full. The outflow reservoir can be of different sizes in order to improve the accuracy of the outflow readings.

The accelerated gravitational field not only affects the unit weight of water, but also the internal membrane of the transducer. A calibration was performed by imposing selected inflow rates (0.1 mlh to 100 mlh) at different g-levels. A linear response between the cumulative outflow and the output voltage can be observed in Figure 13 for each rate. A power function was used to fit the change in voltage through time (slope), for different rates at a given g-level, the final calibration is shown in Figure 14.

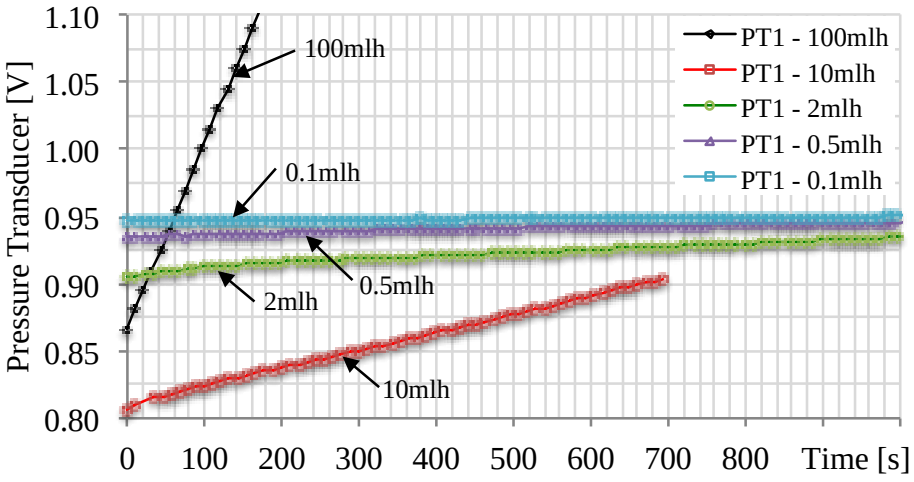

Figure 13. Changes in voltage measured by the pressure transducer in the outflow reservoir for different imposed inflow/outflow rates (at constant speed).

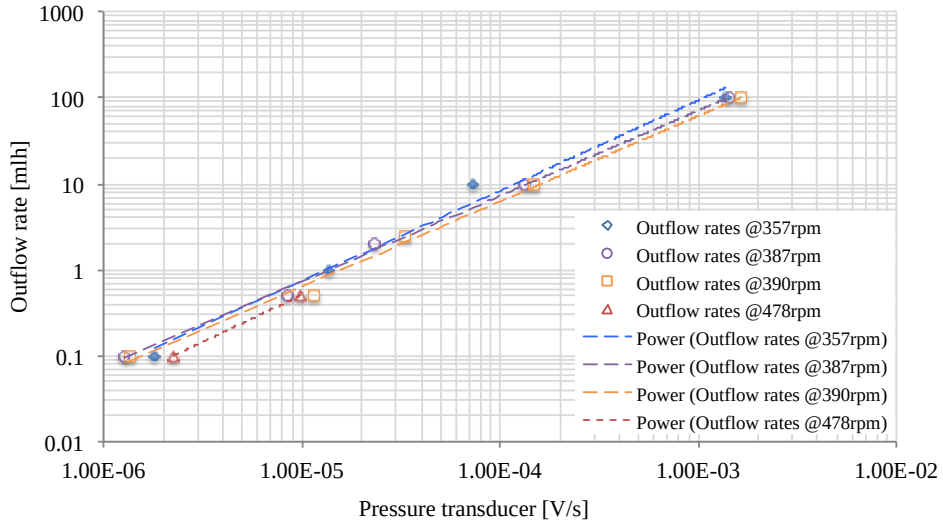

Figure 14. Calibration curves defined for different outflow rates and centrifuge speeds.

3.3.3 Opportunities for improvements of the (N.g) Centrifuge testing environment

The overview presented in this Chapter shows that centrifuge testing is an efficient methodology to determine the hydraulic properties of unsaturated soils. Yet, new tools and methods can be incorporated to the centrifuge testing technique to enhance the approach. They should focus on:

- Including **in-flight measurement** of water content and density profiles. This will allow using one sample on multiple-stage test to determine the retention capabilities and the hydraulic conductivity function while adding the void ratio as an additional variable.
- Also, the in-flight measurements could reduce the potential errors during the slicing procedure and any moisture redistribution between stopping the centrifuge and removing the soil samples.
- **Non-intrusive** measurement techniques are necessary in order to minimize any constrains imposed on soil samples that may change volume during testing. This enhancement would be certainly necessary when testing on expansive clays.

- Provide flexibility to modify the **boundary conditions**, depending on the test and soil type required. The lower boundary could be selected between suction-imposed or open flow centrifugation. On the other hand, the upper boundary could be defined by an imposed inflow rate or a desired level of ponded water.
- **Testing methodology:** the CPUS has been used to define the retention capabilities and the unsaturated hydraulic conductivity under steady-state flow conditions in low plasticity clays. High plasticity clays become unsaturated at higher suction values, and their hydraulic conductivity may be several orders of magnitude lower than the conductivity of low plasticity clays. Although steady state approaches can still be implemented, analysis of the **transient flow regime** should be evaluated as an alternative approach for these soils.

SECTION 1: NEW DEVELOPMENTS FOR THE HYDRO-MECHANICAL CHARACTERIZATION OF UNSATURATED SOILS

The objective of the research components presented in Section 1 of this dissertation is to develop new tools that are useful to characterize the hydro-mechanical behavior of unsaturated soils. The design rationale and the goals pursued for each equipment and sensor are supported by the analysis presented in Chapter 3,

The ATX Cell corresponds to the first piece of equipment developed in this research being introduced in Chapter 4. This new device is based on the pressure plate extractor technique, but it incorporates new features such as the continuous measurement of the weight and volume of the soil sample. It also has the ability to impose a vertical surcharge in order to modify the state of stresses in the soil sample.

Two non-intrusive measurement systems were also developed to enhance the capabilities of the centrifuge permeameter. The first system is a series of water content sensors based on Time Domain Reflectometry technology, which is identified herein as GTDR. A brief review of transmission line theory, the TDR equipment, as well as sensor calibration and analysis are presented in Chapter 5. Additional details about the construction, calibration, and analysis of the errors in the measurements inherent to the TDR system are described in Appendix 2.

The second non-intrusive system involved incorporation of in-flight cameras and image analysis algorithms developed to quantify the volume changes along the soil sample eliminating the restrictions imposed by contact sensors. The implementation of the in-flight cameras, control and acquisition systems, and post-processing techniques are described in Chapter 6. In addition, this non-intrusive technique allows monitoring the centrifuge test in real time.

Chapter 4: ATX Cell: A New Device for Experimental Determination of the Soil-Water Retention Surface

4.1 INTRODUCTION

The goal of this chapter is to document the development and validate the use of a new equipment capable of testing the hydro-mechanical behavior of unsaturated soils. The ATX cell incorporates features like the measurement of volumetric changes and a surcharge system to evaluate the correlation between the volumetric water content, suction and void ratio [θ, ψ, e] under different loading conditions.

The relationship between the capillary pressure (or matric suction), and water content has been traditionally represented using soil water retention curves (SWRC). Methods available to obtain this relationship include the Hanging Column Test, Pressure Extractor, Chilled Mirror Hygrometer, and Centrifuge Test (ASTM 2008). SWRC's are defined for a constant void ratio, even the most commonly used SWCC mathematical models such as Van Genuchten (1980) and Brooks and Corey (1964) do not account for changes in void ratio.

Recent work has been carried out in order to study the coupled hydro-mechanical behavior of the soil by monitoring systematically the effect of changes in suction (ψ) on the water content (θ), and the void ratio (e). In this way it has been possible to define the soil retention capabilities using a Soil-Water Retention Surface (SWRS) in the [ψ,e,w] space (Salager, 2007).

Yet, most results for the SWRS have been obtained with the same techniques and equipment used for the testing of SWCC's, where void ratio changes are not monitored during the test, but measured only at the end of each stage. Accordingly, different soil samples need to be prepared at same initial conditions and taken to different final conditions in order to generate enough experimental data.

Even though it has been possible using this approach to define a surface that correlates the three relevant variables, theoretically this is only valid if samples compacted at the same initial void ratio have the same internal structure, and that intermediate steps would not affect the soil structure and hydraulic behavior

The ATX Cell is testing device based on established techniques that allows continuous monitoring of the soil void ratio and water content during testing while different stages of suction are applied to the soil sample. The device also allows the control of the vertical total stress. The equipment is based on the pressure chamber test and allows testing soils samples within a wide range of suction levels (0.01 kPa to 1500 kPa), even for comparatively low suction values where most changes in void ratio occur and where this third variable truly affect the hydraulic response (Salager et al. 2010).

In addition, the outflow/inflow measurements obtained continuously throughout the tests facilitate the implementation of transient analysis to determine the unsaturated hydraulic conductivity of low and high plasticity clays.

4.2 EQUIPMENT DEVELOPMENT

The pressure plate extractor corresponds to a starting point to the development of the ATX Cell. The pressure extraction method is based on the axis translation technique, where the air pressure in the chamber is controlled, allowing controlling the air pressure in the pores of the sample. The new system incorporates the use of a scale to determine the changes in sample weight and, consequently, changes in the volume of water within the sample. An air piston and an LVDT sensor were included to control the surcharge and to monitor the volume changes from the top of the cell.

The ATX Cell allows testing one soil sample at the time. The base has a series of grooves that connects two diametrically opposite points for water inflow/outflow. This

allows water to be flushed through the base to remove any diffused air below the ceramic disc (Figure 15). A ceramic disc of high entry pressure is placed over the grooves and an o–ring is used to avoid pressure loses in the chamber from the bottom.

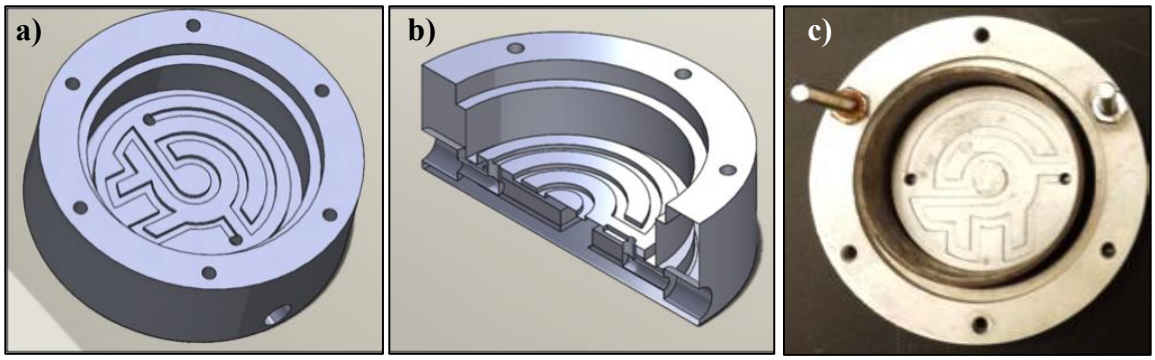

Figure 15. ATX Cell base design details: a) 3D view of base, b) Cross section showing grooves, inlet, and outlet connections. c) Picture of the base.

The soil sample is compacted into a brass ring, which is then placed inside of the base. An o-ring is used to hold the sample in position, and it seals the air pressure inside the chamber. A hard plastic porous disc of negligible weight is placed on top of the sample to facilitate good contact with the vertical rod and load distribution. The cap is then placed and tightened onto the brass ring. In addition to hold the sample, the brass ring also applies pressure over the ceramic disc and o-ring providing a good seal between the water beneath the ceramic disc and the increased air pressure above it.

Figure 16 shows there is a view of the different stages of the test: a) soil being compacted into the brass ring; b) the sample is placed into the base; and finally, c) the base is assembled including two o-ring holders to manage high air pressures.

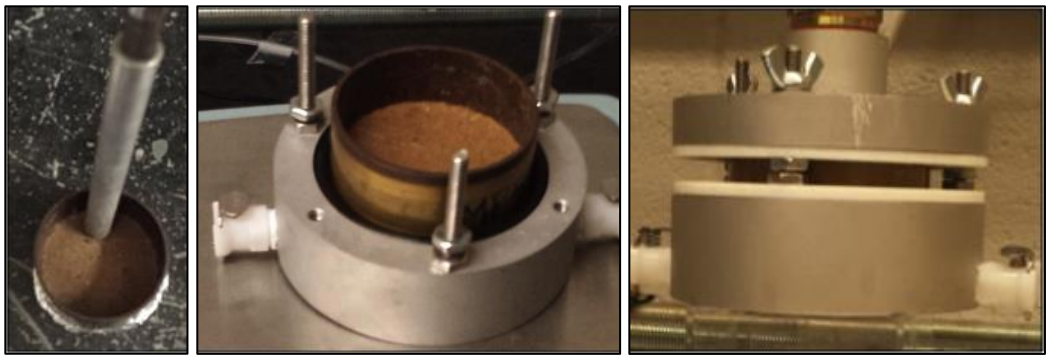

Figure 16. Set-up stages in the ATX Cell including: a) sample compaction, b) sample mounted in the base, and c) base assembled with the top disc and o-ring holders.

The cell cap includes a third o-ring used to seal the air pressure imposed at the top of the sample. It also provides a connection to the compressed air line and a central opening used to connect a double acting, double end air piston. The piston allows applying an external vertical load and monitoring the vertical displacement of the sample while maintaining the pressure inside the chamber (Figure 17). This chamber enables, the total stress to be used as an independent variable of analysis (Matyas 1968), similar to the approach used in suction controlled oedometers.

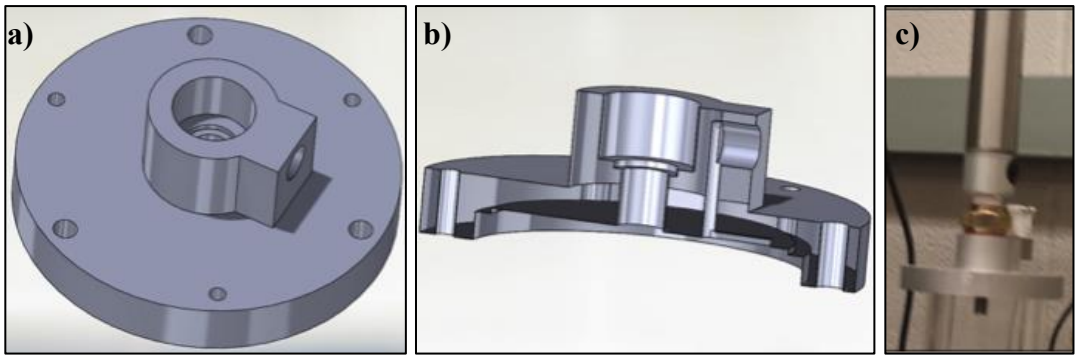

Figure 17. ATX Cell aluminum cap design: a) 3D view of the cap, b) cross section, and c) piston connected to the cap.

4.2.1 Monitoring systems: weight and volume changes

In the conventional pressure extractor set up changes in water content are calculated by measuring the inflow/outflow with a capillary tube. This method is simple and can be easily calibrated and installed. Accuracy can be improved by using comparatively thin tubes. However, measurements can be compromised by the presence of diffused air in the system, which is read as an additional outflow. Long- term readings may also be affected by evaporation and leakage

In order to avoid the problems associated with capillary tubes the new device measures the change in weight of the sample in order to obtain the change in water content. This is achieved by measuring the change in weight of the entire system, since once the whole system is saturated the only source of weight variation is the weight of the sample itself. Figure 18(a) shows the ATX cell over a precision scale (Ohaus Adventurer Pro AV3102C) with a range up to 3.10 kg and 0.01 g of precision used for weight measurements.

A flushing system was incorporated to minimize the problems associated with air diffused through the ceramic disc to the outflow system and therefore affecting its readings. It includes a flushing loop, an air trap, and a peristaltic pump that forces flow from the base through the loop to the air trap.

Figure 18(c) illustrates a bracket attached to the piston that holds an LVDT that is used to monitor vertical deflections continuously. The bracket, LVDT and all the connections have a weight that remains constant during the entire test and therefore do not affect the weight readings. In tests involving wetting paths the sample volume tends to increase with increasing water content. Since lateral displacements are constrained, changes in height correspond to the total volume change, and then the measured vertical displacements can be used to calculate changes in void ratio

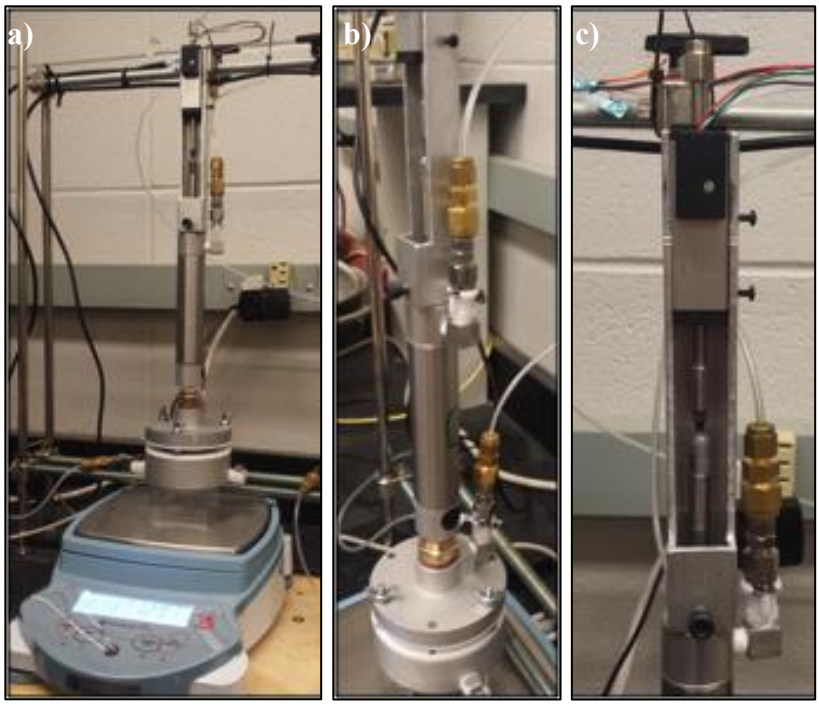

Figure 18 ATX Cell ready fro testing with: a) cell mounted over the scale, b) lateral view of the piston and air connections, and c) detail of the bracket and LVDT.

In addition, very flexible tubing is used for all air and water connections in order to avoid affecting the weight readings (Figure 19). In this set up the capillary tubes, are installed together with the scale in order to provide a source of water for the sample, to keep a redundancy of the measurements.

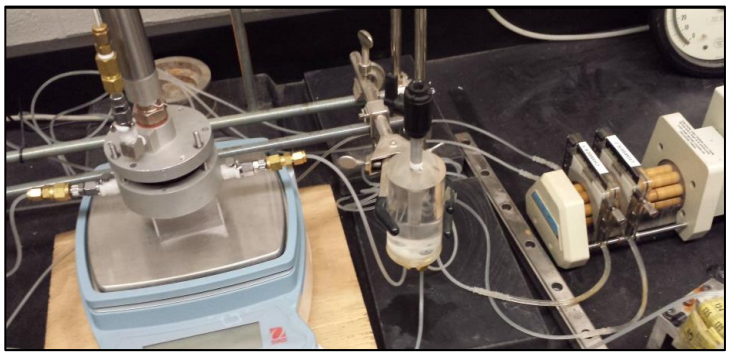

Figure 19. Connection between ATX Cell and flushing system.

4.3 TESTING PROCEDURES

The testing procedure carried out in the ATX Cell developed in this research, involved multiple steps decreasing the suction (air pressure) gradually in each one of the stages. The equilibrium points were obtained from the same sample and therefore from the same initial soil structure that changes with the changes in moisture.

After the air pressure is reduced at each stage, the equalization process begins and the sample can incorporate water until reaching equilibrium. The flushing system should be kept running at all times. Each stage is run until no change in water content is observed. Once equilibrium is reached at the end of the last stage, the chamber is disassembled to record the final sample weight and height of the sample, and gravimetric water content is measured by oven drying the sample.

The ATX Cell is assembled as follows: 1) water is placed in the base and flushed with the pump to remove air bubbles; 2) the intermediate o-ring and brass ring with the sample are placed in the base; 3) a plastic disc is placed over the sample; 4) the top cap is placed and tightened; 5) the piston rod is carefully handed down until it barely touches the upper disc; 6) the chamber placed over the scale; 7) the LVDT is set on the bracket; 8) air lines are connected to the chamber and piston; 9) DAQ system is initiated; 10) air pressure is applied into the chamber and to the piston; 11) tubes on the sides of the base are connected and water exchange begins.

The main limitation of this procedure is that under no vertical loads only wetting path tests could be obtained. When the water content increases, the volume can increase as well and volumetric change involves vertical displacements. Typically, hanging column and pressure plate tests are performed starting with a saturated condition drying the sample progressively increasing the air pressure (matric suction). Since the matric suction is an isotropic stress, expected volume changes should be isotropic as well.

Strictly, not only vertical measurements, but also radial measurements would be needed to account for the volume change in drying path tests.

4.4 TYPICAL RESULTS

4.4.1 Definition of the SWRS

The ATX Cell allows evaluating the hydro-mechanical behavior of the soil using a single soil sample. The soil-water retention surface (SWRS) can be defined testing several samples compacted at different initial void ratio values. Still, it should be emphasized that the results will only reproduce a portion of the SWRS.

In this section the results from two tests one in a low plasticity clay (RMA soil), and other in a high plasticity clay (Eagle Ford) are presented together in order to illustrate the typical output obtained when using the ATX Cell. RMA soil sample was compacted at optimum gravimetric water content (12%) and maximum dry unit weight (proctor standard); Eagle Ford clay sample was compacted at the optimum gravimetric water content (24%) and maximum dry unit weight (proctor standard). Additional details about the soil properties and results will be presented for both clays in Chapters 7 and 10.

The results for multistage tests were obtained measuring the matric suction (ψ), volumetric water content (θ) and void ratio (e) at the end of each stage. Using this information, it is possible to define a representation of the hydro mechanical path of the soil test in the [θ, ψ, e] space. Figure 20 illustrates three plan views of this space in order to observe the correlation between each pair of variables

Figure 20(a) shows a typical representation of the SWRC (e.g. [ψ, θ] plane). This SWRC would typically be reported as the retention capabilities corresponding to the initial void ratio of the sample. Typically for the range of suction tested (lower than 100 kPa) a greater reduction of the water content could be expected for the low plasticity clay

in comparison to the expansive clay. However, as it will be shown in Chapter 7, no plateau could be identified for RMA soil that indicates an air entry pressure value for RMA soil samples compacted at maximum dry unit weight. As for the expansive clay the sample increases its water content through the whole suction range.

Figure 20(b) illustrates the correlation between the void ratio and water content. It can be observed that for low plasticity clays the void ratio remains almost constant during the test. However, as expected for expansive clays, the sample volume increases rapidly with the increasing water content.

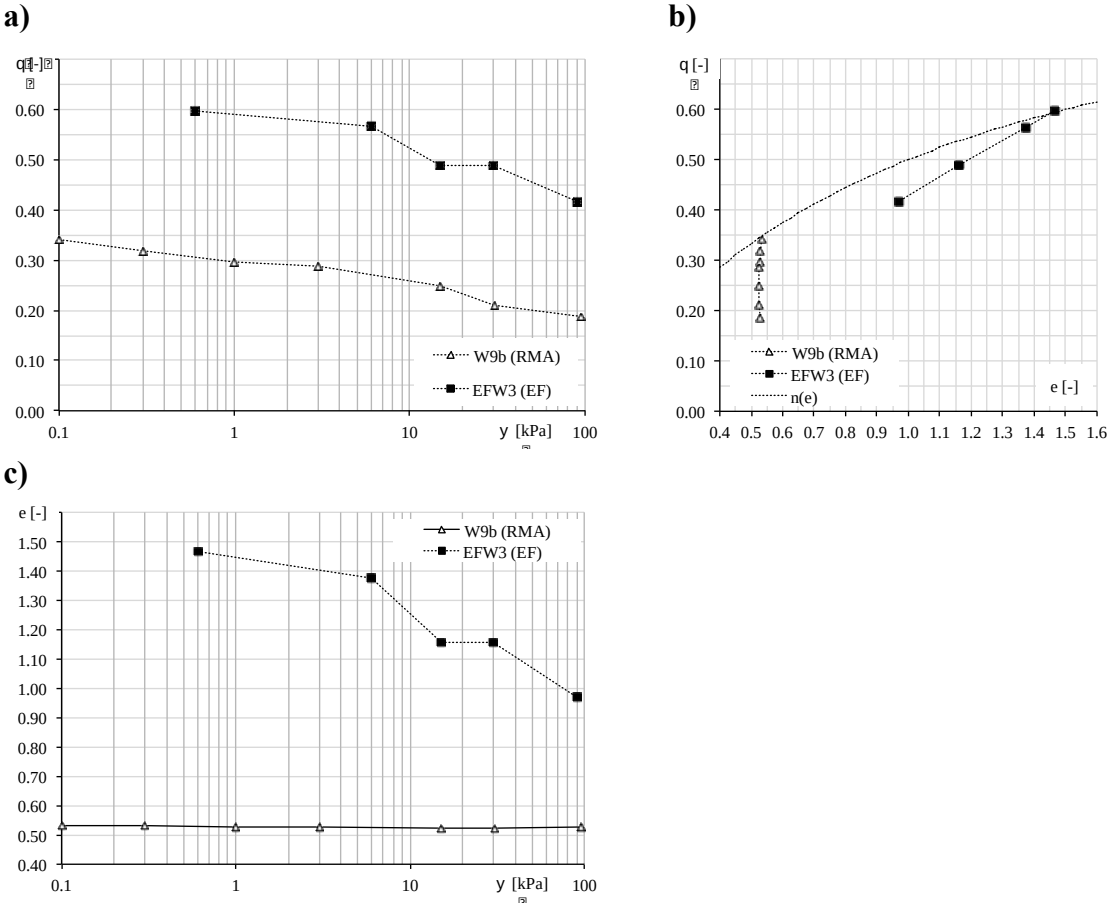

Figure 20. Typical results from ATX cell for a low and a high plasticity clay samples presented in two-dimensional views of the SWRS: a) θ vs ψ plane, b) e vs ψ plane and c) θ vs e plane. (CHANGE IMPROVE IMG)

Figure 20(c) shows the correlation between the volume changes and the imposed suction. As it was observed previously the void ratio in the low plasticity clay remains constant through all the test stages. The behavior of low plasticity clays in this test correlate well with the hypothesis of constant void ratio used to evaluate the soil SWRC. However, the expansive clay sample changes its volume and the experimental data presented in Figure 20(a) no longer belongs to a plane curve (at constant void ratio), but to a series of SWRC models obtained at different void ratio values. In the approach proposed in this research, the experimental data points belongs to a SWRS that represent the retention capabilities of each soil, and these surfaces can be defined independently of the volume changes observed in any specific test.

The initial compaction conditions (void ratio and water content) as well as the magnitude of the applied normal load affect the results modifying the increase in water content and volume changes. In this case, both tests were run using a surcharge of 1 kPa to allow the contact of the piston with the top of the soil sample.

4.4.2 Typical results from transient response

Transient data corresponding to the change in weight of the samples (water inflow) was collected for both samples during all testing stages. The transient response of each sample can be represented by its change in weight (or water content) and changes in volume as a result of the water inflow forced by a reduction in the air pore pressure.

The ATX Cell allows the continuous monitoring of the sample weight and height throughout each testing stage. The implementation of the scale and a DAQ system has some additional features in comparison to the use of capillary tubes. It is easier to increase the number of data points to show the transient response, and the advective-diffusive phenomenon can be seen more clearly.

Figure 21(a) illustrates the changes in water content of two samples that were at hydrostatic equilibrium under an imposed matric suction of 90 kPa, and a reduction in the air pressure set the new equilibrium suction at 30 kPa. First, it can be observed that the total changes in water content are completely different for both samples. The total increase in water content is the amount used to calculate the [θ, ψ, e] values for the new imposed stage. Second, due to the difference in the unsaturated hydraulic conductivity reaching it required less than 2 days for the RMA sample to reach equilibrium, while more than 13 days were necessary for the expansive clay.

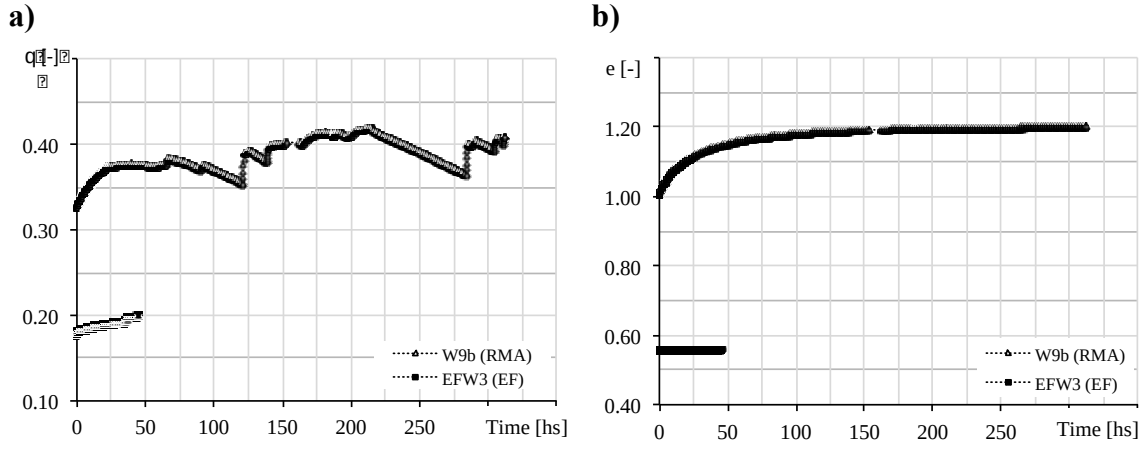

Figure 21. Transient response of RMA and Eagle Ford clays including: a) changes in water content and b) changes in void ratio vs time.

In general, the increase in water content for both soil samples presented in Figure 21(a) show that the flow velocity reduces with time as internal pressure difference between the air pore and the capillary suction decreases. Equilibrium is typically assumed when no more change in water content is observed.

Even though it possible to minimize the sources of evaporation and leakage, the flushing system must be used periodically. The drops observed in the water content data in Figure 12 correspond to air bubbles that build-up inside the chamber, the scale

readings increases rapidly when the air is released. Air bubbles can be observed in the air trap at the same time.

Figure 21(b) illustrates the volume changes vs time represented by the change in void ratio. In this case, no volume changes were observed for RMA soil, but a large change is observed for the expansive clay. In particular it can be observed that for the expansive clay, the transient response in the volume changes follow a similar shape than the water content changes. However, in the case of the sample volume the artifact of the air bubble does not affect the measurements. This information will be used in Chapter 9 and Chapter 12 to derive the unsaturated hydraulic conductivity of RMA and Eagle Ford clay soils.

4.5 SUMMARY AND CONCLUSIONS

A new pressure chamber was developed with the objective of obtaining continuous measurement of void ratio, matric suction, and water content along wetting paths. This allows the determination of the soil-water retention surface (SWRS) of approach a soil. Evolution of the results from tests conducted using two clays showed that:

- The implementation of a scale to measure the sample weight allowed a better quantification of the advective- diffusive transport phenomenon, and it minimized the errors associated to leakage and evaporation.
- The use of an air piston enabled applying a vertical normal stress and monitoring the continuous volumetric changes in the sample along with the changes in water content.
- The new device not only was able to follow the hydro-mechanical path of the soil sample, but it also allowed defining several experimental data points of the soil-water retention characteristics of the soil using a single soil sample.

- For low plasticity clays tested with the ATX Cell, no volume changes were observed for suction values ranging from 0.01 kPa to 100 kPa.
- The experimental data generated in single test to describe the water-retention properties of low plasticity soil could be represented by plane curve models (SWRC).
- For expansive clays, the void ratio was found to increase with decreasing suction and increasing water content.
- The experimental data generated in a single test to describe the water retention properties of expansive clays can not be represented using a curve at a constant void ratio. The SWRS could provide a better tool to fit the testing results.
- The time history of the water content and volume changes was measured from a single sample over a wide range of suction values. This transient information could be used to determine the unsaturated hydraulic conductivity.
- It was observed that for the expansive clay, the transient response in the volume changes followed a similar shape than the water content changes.
- It should be noted that the procedure proposed for the new device involves only testing soil samples in wetting paths to correctly determine the volume changes based on the sample height.

Chapter 5: GTDR: A New Non-Intrusive Volumetric Water Content Sensor based on Time Domain Reflectometry

5.1 INTRODUCTION

The development of non-intrusive sensors was an important objective of the research presented in this dissertation. The objective of this research component is to provide all the details about the design, construction, calibration and implementation of the volumetric water content sensors GTDR based on Time Domain Reflectometry (TDR) technology.

TDR has been reported as a reliable and highly accurate technique for the determination of the volumetric water content of soils (Jones 2002, Robinson et. al 2003, Tarantino 2008b). The potential of this methodology comes from the capability of the TDR technology to determine accurately the apparent dielectric conductivity of soils (K_a), and from the strong correlation between this dielectric property and the soil volumetric water content θ_v (Topp et al. 1980). Also, TDR has proven to be a successful ground-based sensor for point measurements, and has been reported to cover a wide sampling-range in the laboratory and the field (Vereecken, 2008).

When compared to other sensors, the implementation of TDR technology requires a deeper understanding of soil dielectric properties and transmission line theory. The physical principles of the propagation velocity of an electromagnetic wave in porous materials and the TDR analysis technique are discussed in this chapter.

TDR systems include: a pulse generator, data loggers for automation, control and storage of the data, multiplexers to manage measurements from multiple probes, and a transmission line that can include a sensor in contact with the porous media. The GTDR sensor (a combination of regular TDR sensor adapted to the permeameter cup) was

created to provide measurements of the soil volumetric water content without interfering with the soil deformation or the water flux in the centrifuge environment.

The development of the non-intrusive sensor detailed in this chapter includes specifically: a design analysis, probe calibration and soil-specific calibration, and the inclusion of an alternative algorithm for waveform interpretation. Additional details from the calibration results and other topics such as the analysis of non-uniform water content distributions are included in Appendix 1.

5.2 DESIGN PROCESS

The design of a non-intrusive sensor aimed at determining the suction or volumetric water content (VWC) of unsaturated soils needed to incorporate several requirements:

- Minimize the interaction with the soil sample in a way that it does not constrain the volume changes or causes additional deformations.
- Measure a broad range of VWC and/or suction provided that both low and high plasticity clays can be tested with the same set up.
- Measurements are somehow localized in order to define several data points of a VWC profile along the soil sample.
- Adapt it to the centrifuge environment. This means not being affected by increased gravitational fields and being contained in the permeameter acrylic cup of 100 mm (outer diameter)

One of the main difficulties in the design process was the selection of the appropriate technology used to measure either the volumetric water content or suction, while providing a fast enough response, minimizing the interaction with the soil, and being flexible to adapt to the centrifuge permeameter

The use of suction sensors was discarded because most techniques for suction measurement are unable to work under a wide range of suction values. Besides, most of them use surrogate materials that need time to reach equilibrium with the soil. To illustrate these limitations a summary of the suction sensors available in the market is presented in Table 1 (Tarantino 2008b).

Table 1. Summary of indirect soil suction measurement methods.

Category	Method	Suction	Suction range (kPa)	Equilibrium time	Source/manufacturer
Primary	TP[a]	Total	300–7000	1 h	Wescor: www.wescor.com Campbell Scientific: www.campbellsci.com
	TrP[a]	Total	100–10,000	1 h	Soil Mechanics Instrumentation: Australia
	CMP[a]	Total	500–30,000 (or higher)	10 min	Decagon Devices: www.decagon.com
Secondary	FPM[a]	Total/Matric	50–30,000 (or higher)	5–14 days	Whatman: www.whatman.com Schleicher & Schuell: www.schleicher-schuell.com
Tertiary	TCS[a]	Matric	1–1,500	Hours to days	Campbell Scientific: www.campbellsci.com GCTS: www.gcts.com
	ECS[a]	Matric	50–1,500	6–50 h	Soil Moisture Equipment: www.soilmoisture.com

[a] TP, thermocouple psychrometer; TrP, transistor psychrometer; CMP, chilled-mirror psychrometer; FPM, filter paper method; TCS, thermal conductivity sensor; ECS, electrical conductivity sensor

Water content sensors based in the response of electrical properties were considered as a feasible option. Techniques to measure either bulk resistivity or surface resistivity measurements were evaluated. Both techniques minimize the contact with the soil, can provide fast measurements, and in the case of bulk resistivity a vast volume of soil can be sampled. However, the calibration resolution is poor at high water contents, and in the case of surface resistivity they suffer a great impact from the soil-sensor contact (McCarter 1984, Munoz-Castelblanco et al. 2012).

Time Domain Reflectometry (TDR) technology was found to be a more reliable technology. It has been reported to be essentially independent of soil type (Topp et al. 1980) and it shows a good response for a broad range of water contents.

However, typical set ups require the TDR probe to be fully embedded within the porous material. McCartney (2007) implemented a TDR probe partially embedded in the wall of the acrylic permeameter cup to determine the average water content in the upper third of the sample. The VWC profile was assumed to be constant, and only one average value was measured. Yet, this example showed TDR to be a promising solution.

In summary, suction sensors were abandoned and the approach selected was to measure the VWC profile using TDR technology. Figure 22(a) shows a straight TDR next to the acrylic permeameter, and Figure 22(b) shows the concept of the solution proposed, that involves curving the TDR prongs and placing them inside the walls of the acrylic permeameter.

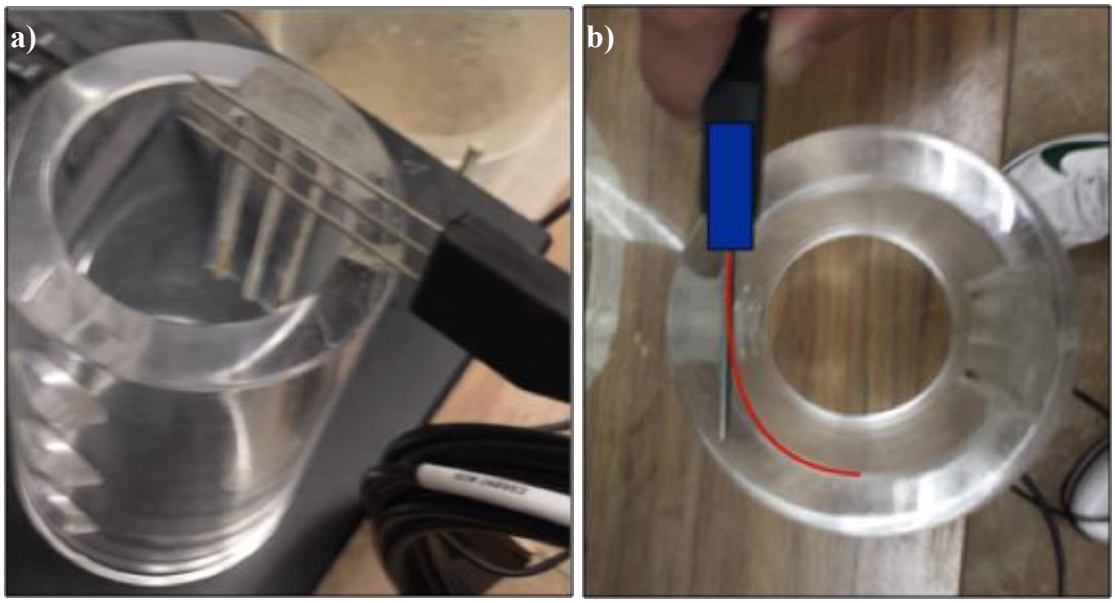

Figure 22. Initial conceptual design of the GTDR: a) straight TDR next to the permeameter cup, and b) modification proposed to the TDR to be included in the walls of the acrylic permeameter. (Improve)

5.3 BACKGROUND REVIEW

5.3.1 Transmission line theory

The TDR technique requires the determination of the soil apparent dielectric permittivity. This value is obtained from the analysis of the propagation velocity of an electromagnetic wave in a porous media.

The propagation velocity of an electromagnetic wave (V_p) along a probe embedded in soil can be obtained by measuring the time it takes the wave to travel along a transmission line of a known length. The apparent dielectric permittivity (K_a) of the porous material can be related to the propagation velocity using the following equations:

$$V_p = 2L/\Delta t \quad (16)$$

where Vp is the propagation velocity of the wave, L is the real length of the probe□□□Δt is the time that takes an electromagnetic wave to travel along a probe (down and back)

$$K_a = \left(c/V_p\right)^2 = \left(c \cdot \Delta t/2L\right)^2 \quad (17)$$

where Ka is the apparent dielectric permittivity, and c is the speed of light in vacuum:

$$K_a = \left(c/V_p\right)^2 = \left(c\frac{t_C - t_B}{2L_{BC}}\right)^2 = \left(L_a/L\right)^2 \quad (18)$$

where t_B and t_C corresponds to the initial and final time that it takes the wave to travel along the probe of length (L_{BC}), and La is indicated as the apparent length of the probe.

The working principle is briefly illustrated by Tarantino et al. (2008b) as follows: The TDR generates a fast rise step pulse that is detected by the oscilloscope (point A, t =

t_A). The signal travels through the transmission line until it enters to the probe (point B); here the porous media has different impedance, the travel velocity changes and this generates a first reflection ($U_{r,1}$). This reflection is in counter-phase with the original signal and therefore a drop in voltage is detected at time t = t_B. Part of the signal continues traveling along the probe ($U_{t,1}$) until it hits the end and it is fully reflected (point C, open circuit). The reflection is in phase with the original signal. When $U_{t,1}$ reaches point B, part of the energy is transmitted ($U_{t,2}$), and part is reflected ($U_{r,2}$). The fully reflected wave is detected at time t = t_C. Since it is in-phase, a sudden increase in the voltage will be detected. All this process is recorded, digitalized, and further analyzed.

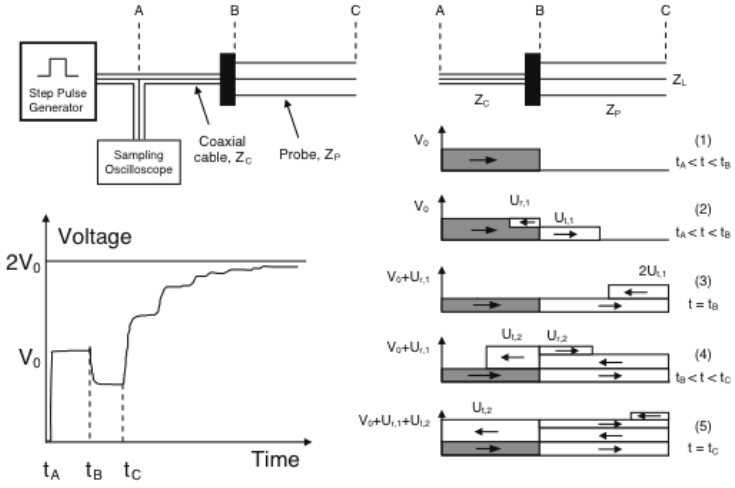

Figure 23. TDR sensor working principle (Tarantino et al. 2008b).

5.3.2 Signal interpretation

The actual value of the apparent permittivity (Ka) is dictated by the detection of the reflection times (t_B and $t_{C,}$) and probe longitude. When the amplitude of the electromagnetic wave and its reflections are recorded, this continuous signal is transformed in a series of data points that need to be interpreted. Since both reflection

times are not fully distinguishable points, they are obtained interpreting key features of the digitalized signal.

Several authors have presented different interpretation methodologies: Topp et al. (1982), Baker and Allamaras (1990), and Heimovaara (1993). Evett (2000) presented TACQ one of the firsts completely automated *"Computer Program for Automatic Time Domain Reflectometry Measurements"*.

The advent of fully controlled systems reduced the need to focus on signal interpretation. Different sensors companies have developed their own firmware for waveform interpretation: Acclima-AWGIF (Schwartz et al. 2014) and Campbell Scientific-PCTDR (CSI, 2015). Figure 24 shows the main parameters and features analyzed by TACQ. The reflection times will be indicated as t_1 and t_2 following the nomenclature of the algorithms implemented in this research

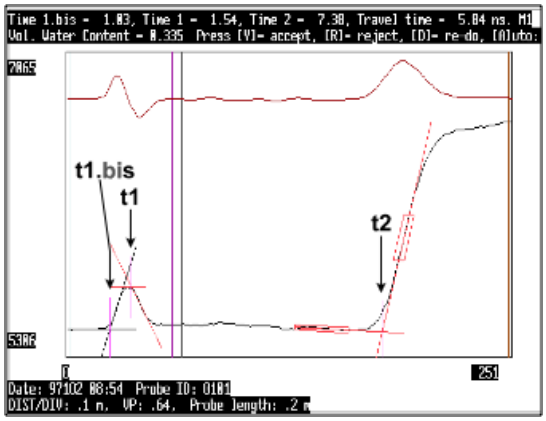

Figure 24. Waveform interpretation using TACQ (Evett, 2000b),

Although the algorithms were built on the same basic concepts, they may track different features resulting in slightly different travel times. In this research, Campbell Scientific equipment was used and most calibrations were performed using their

algorithms. However, AWIGF was later explored as an alternative method to interpret waveforms, if they were available, for cases where the scatter in the CSI results was significant.

5.4 EQUIPMENT

5.4.1 Components of TDR system

The TDR equipment used in this research was obtained entirely from Campbell Scientific (CS, http://www.campbellsci.com). The components of the TDR system and their specific function are indicated as follows:

TDR100 unit: It is used as a for-pulse generator with a fast time rise output of 250 mV (at 50 ohm in the line); the operating frequency is located around 6.25 GHz. The signal can be digitalized using a variable number of points (20 to 2048) and several waveforms can be stacked together to minimize the noise in the signal. CS recommends to stack four consecutive signals and to use 256 data points to describe the waveforms.

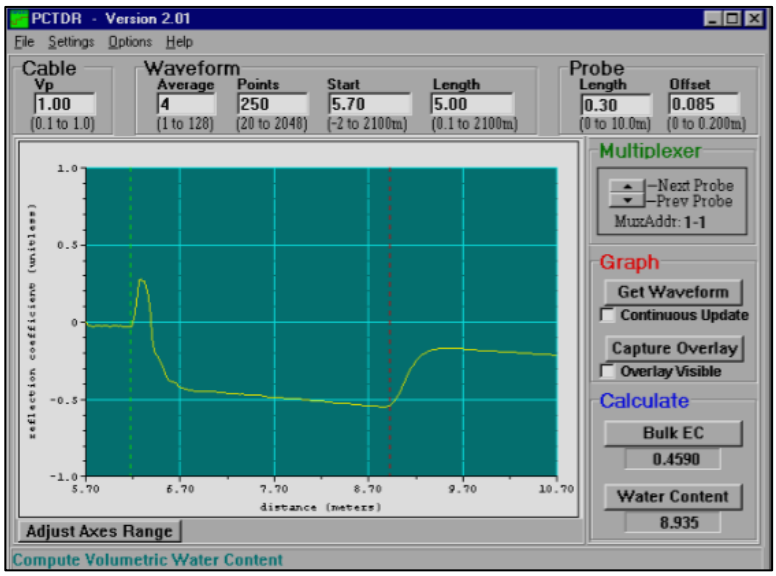

Figure 25. Waveform in water and relevant fitting parameters from TDR100 manual

Figure 25 shows a digitalized signal obtained using CS software PC-TDR. A higher number of signals or data points do not mean a better output. It was found that increasing the number of data points generated high scatter in the initial time (t_B). These values must be evaluated all together with the selected algorithm.

In order to incorporate several probes and automatic measurements a CR1000 datalogger and a multiplexer SDMX80 were incorporated in addition to the TDR100 unit. Figure 26 shows all the components connected together outside the centrifuge during the calibration tests.

The CR1000 is in charge of the communication with the TDR100 and the multiplexer. The CR1000 is controlled with a user-defined script that indicates: time between measurements, which channels to use from the multiplexer, the fitting parameters for each channel, type of information to be saved (e.g. dielectric permittivity, VWC, waveforms and/ or its first derivative, etcetera). Each multiplexer can handle up to eight probes. If more probes are required three levels of multiplexers can be created to incorporate up to 256 probes.

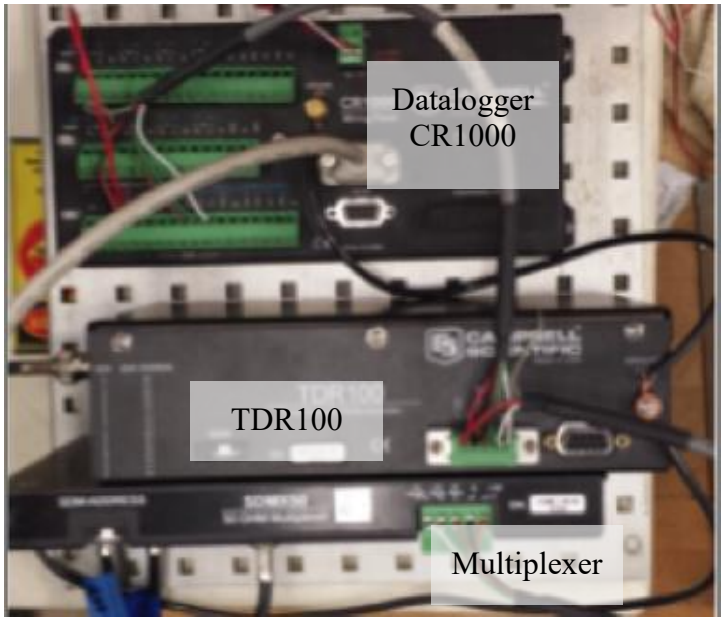

Figure 26. TDR components. (Change for better quality).

5.4.2 Implementation in the CPUS

A TDR system was available in earlier configurations of the CPUS (McCartney 2006b). It used a Mini-Trase system from Soil Moisture, with a cable tester (6050X) and a 16-channel multiplexer (6021C16). The cable tester was controlled through the slip ring stack. However, it was later removed. The TDR set up presented in Figure 26 was incorporated instead. The equipment was located in the center of the permeameter table to reduce the influence of the accelerated gravitational field.

Figure 27 shows the allocation of the TDR equipment inside the centrifuge permeameter. The TDR100 that is the most sensitive component remains in the center. Figure 28(a) shows the lateral view to access the multiplexer and Figure 28(b) the opposite lateral view with direct access to the datalogger.

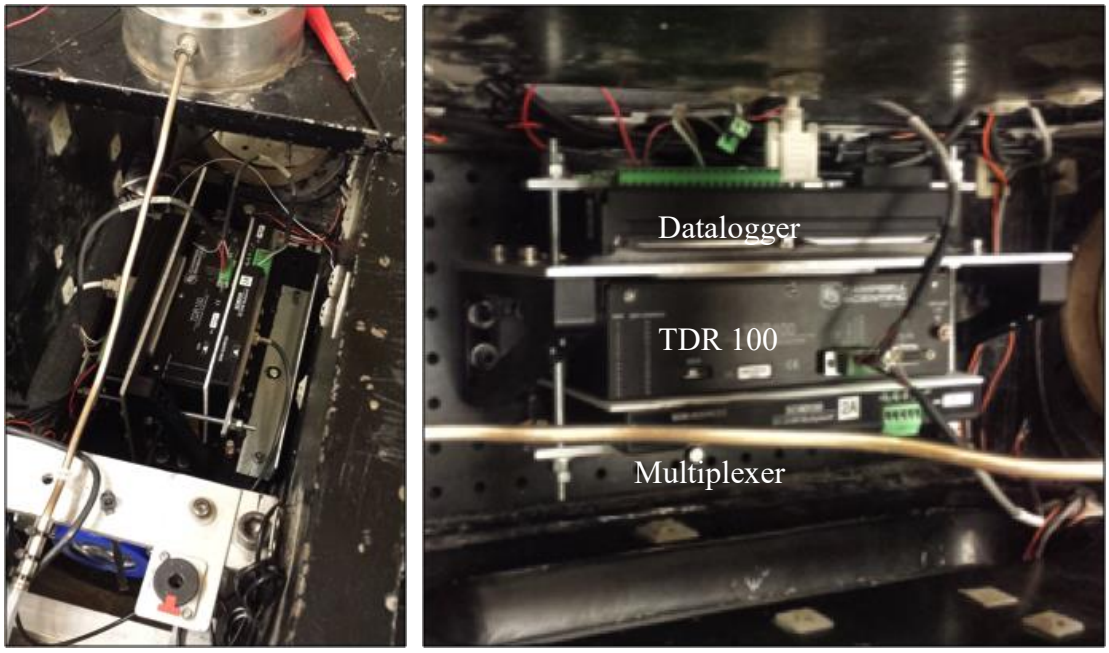

Figure 27. Datalogger CR1000, TDR100 and Multiplexer SDMX80 in the centrifuge.

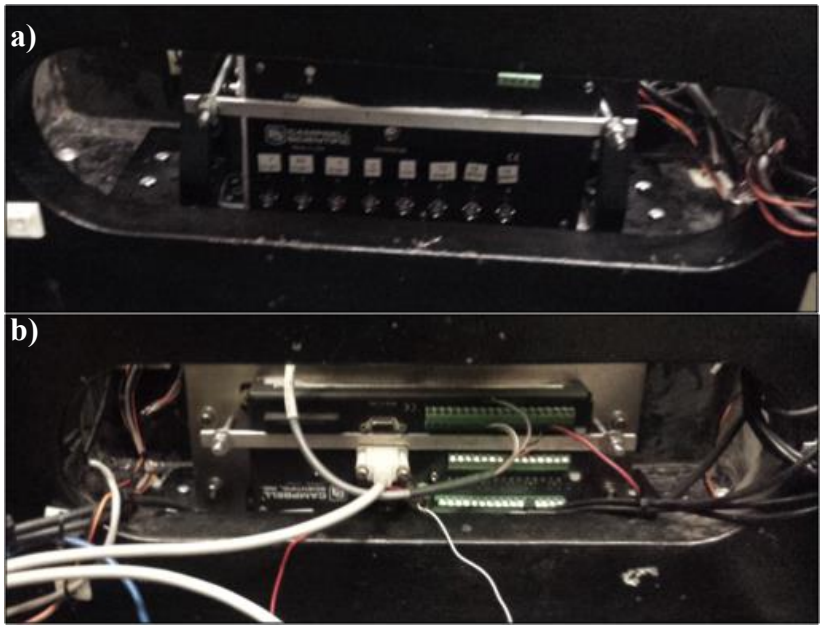

Figure 28. Access to the TDR components located in the center of the CPUS: a) CR1000 datalogger RS-232 COM port, and b) SDMX80 Multiplexer.

At the University of Florida, Xu et al. (2003) showed a good response of Campbell's equipment using a similar set up. They found that voltage signals were independent of the g-level used up to 50 g's. The authors also reported a 20% reduction in the signal when using multiplexed systems.

Even though no influence should be expected in the TDR as result of increased gravitational fields, a series of measurements were conducted at different rotational speeds (equivalent to 50g, and 100g) to confirm this hypothesis. Figure 29 shows that the scatter in the measurements is independent of the g-level used.

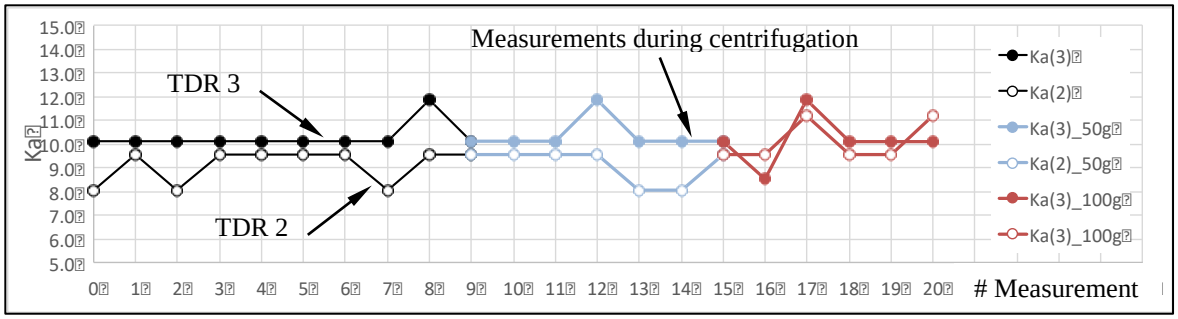

Figure 29. Dielectric permittivity measured at several g-levels.

5.5 Development of non-intrusive sensor

The conceptual solution was implemented incorporating A CS645 TDR sensor into an acrylic permeameter tube. The three rods should be curved and incorporated in the walls of the acrylic permeameter while still maintaining contact with the soil. The progressive steps in the design and construction of the sensor are detailed in this section.

5.5.1 Response of curved TDR

A CS645 probe was curved progressively in order to assess the impact of this deformation over the TDR measurements. Five different curvature radii (CR) were

implemented from 28 cm to 3.5 cm (Figure 30a). The smallest one corresponds to the inner diameter of the centrifuge permeameter cup.

Each time the TDR was bended to a new curvature radius a measurement was taken placing the probe in water (Figure 30b). Figure 31 illustrates the waveforms acquired. All curves were similar and produced almost the same dielectric value.

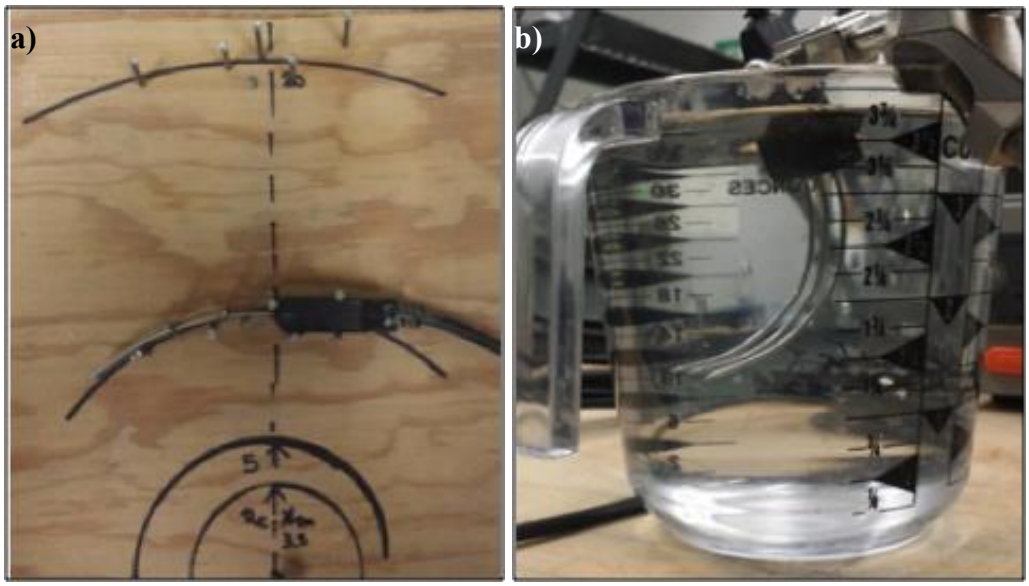

Figure 30. Evaluation of the impact of curved TDR prongs: a) manually curving TDR and b) measurements in water with the curved TDR.

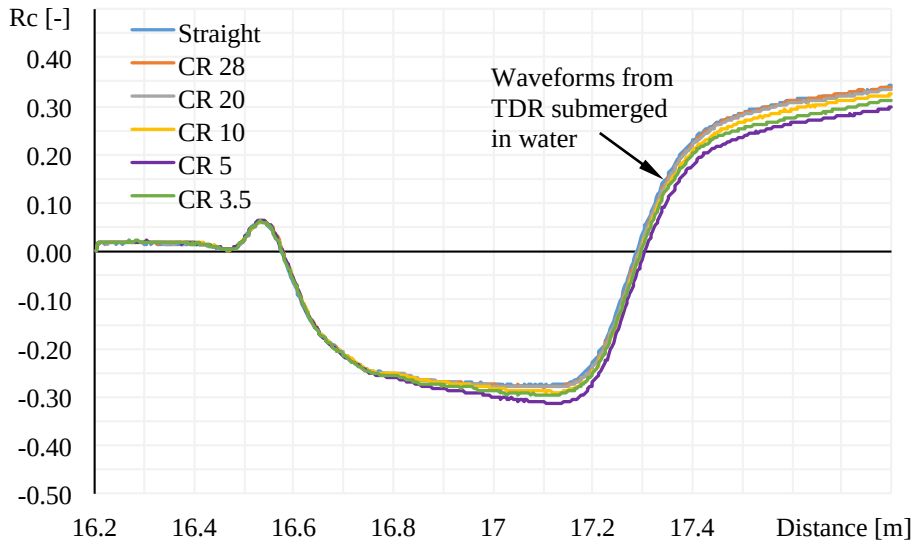

Figure 31. Waveforms of a progressively curved TDR submerged in water

Figure 32 shows a comparison between waveforms and the derivatives recorded from a measurement in water using a straight TDR and a fully curved TDR. It can be observed that the features of both waveforms remain similar, and therefore the measurements were not influenced by the curvature of the prongs. In order to confirm that these results were valid when measuring the travel time in a porous media, a soil-specific calibration was carried out on Eagle Ford clay using one straight TDR and one curved TDR. The results of this calibration are included in Appendix 1.

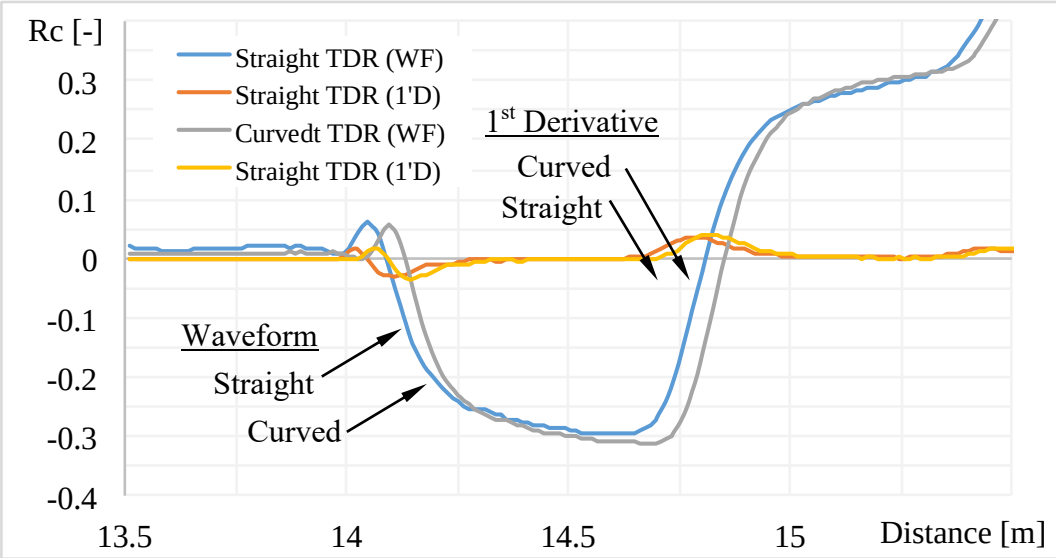

Figure 32. Comparison of waveforms for both, straight and curved TDR in water.

5.5.2 Influence of acrylic

It was observed that the interaction of the TDR sensor with the acrylic has a considerable impact in the travel time. Three different configurations were used to evaluate the influence of the acrylic and the epoxy used in the construction of the GTDR: a) straight CS645 TDR, b) TDR was placed in contact with a piece of acrylic, c) epoxy was added around the rods to secure the sensor. Figure 33 shows a straight TDR placed in contact with an acrylic block including the grooves and epoxy to simulate the construction procedure.

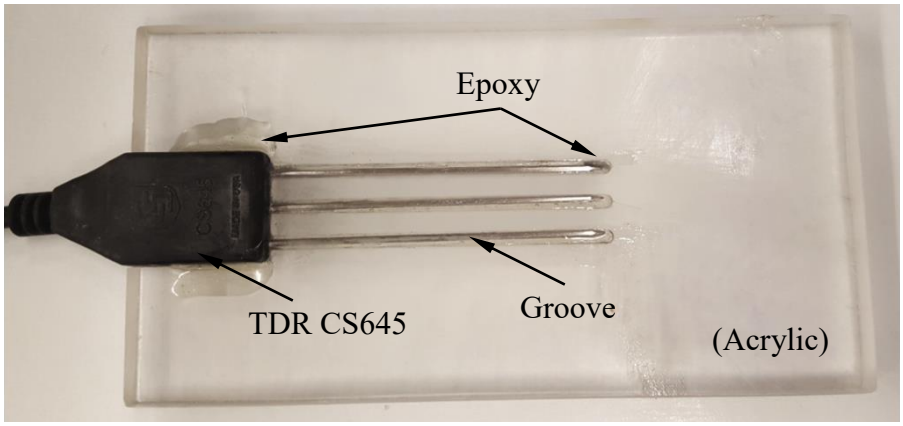

Figure 33. Inclusion of a straight TDR in contact with acrylic.

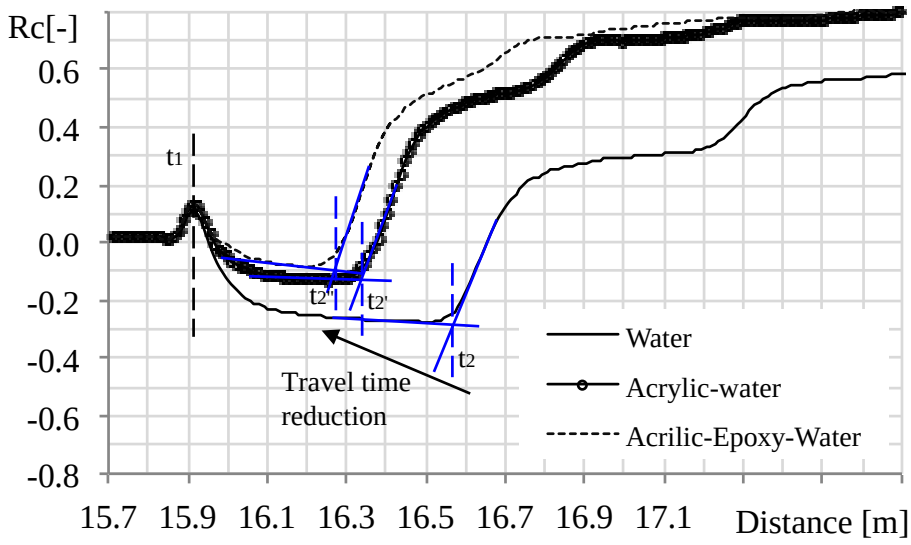

Figure 34. Waveform evolution when TDR is placed in contact with acrylic and epoxy. (incorporate reference lines)

Figure 34 illustrates the waveforms measured in water using the three different configurations detailed before. The inclusion of the acrylic and the epoxy does not modify the first reflection of the waveforms (t_1), but it reduces the time of the second reflection (t_2). In consequence the travel time is reduced showing a lower the apparent permittivity from the same measurement in water.

5.5.3 Permeameter-TDR probe fusion: GTDR

Figure 35 shows the design of the acrylic permeameter cup where the TDR sensors were incorporated. In this design part of the probe head was placed into the tube and the rods enter the tube tangential to the inner diameter, continuing their way into three grooves. In order to seal the cup and fix the probes in place, a two-component clear epoxy was used. The three rods are partially embedded in acrylic and partially in contact with the soil, and as it was shown before this configuration will have an impact over the sensor performance.

The combination of the acrylic permeameter cup and the standard sensors curved and attached to the cup are referred in this research as GTDR. Figure 36 shows an image of the final design of these permeameter cups after several prototypes were completed.

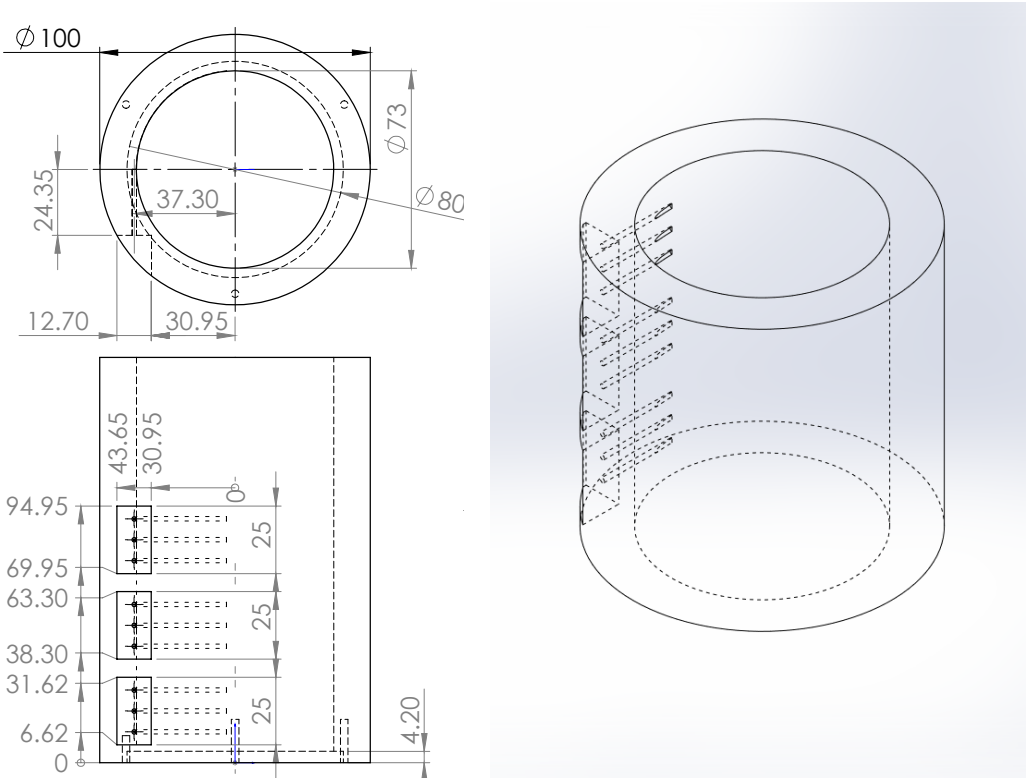

Figure 35. Permeameter cup design completed in solid works

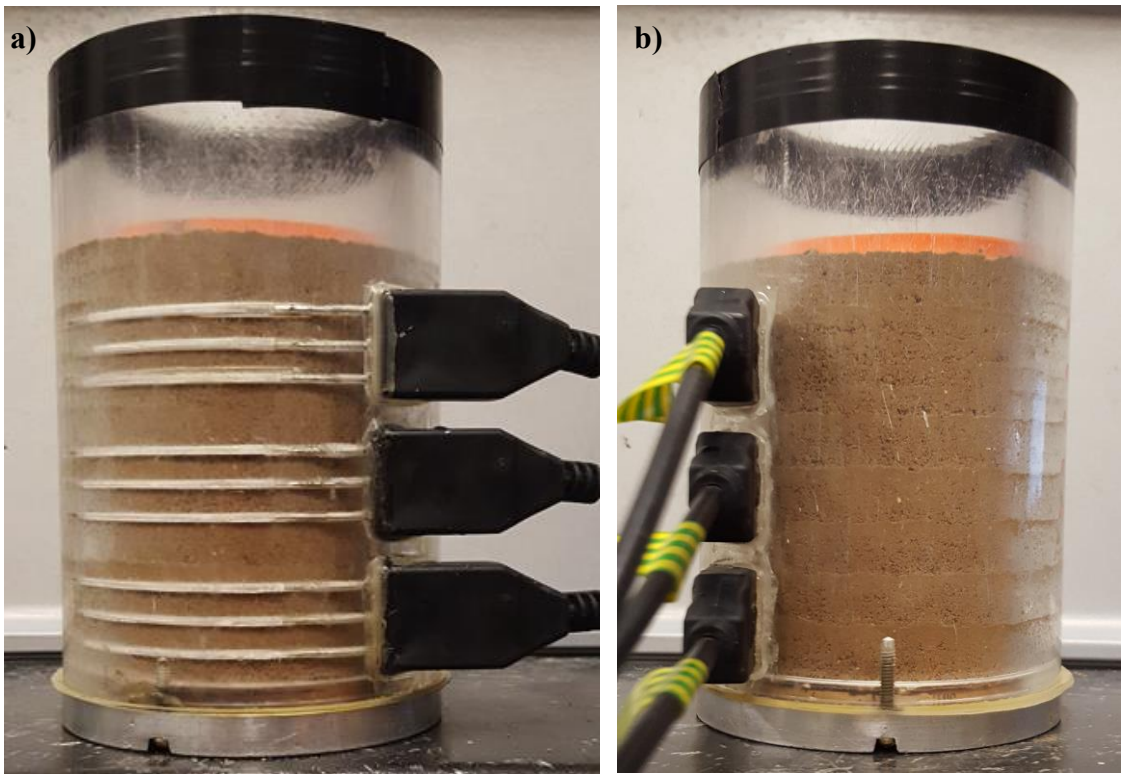

Figure 36. GTDR assembled with soil sample showing: a) the relative position of the rods in the sample and b) the insertion of the TDR sensor heads into the cup.

In order to confirm the previous analyses waveforms in water were acquired using the GTDR and a straight TDR (Figure 37). Figure 38 shows a comparison between the waveforms recorded with PC-TDR. The waveforms for the TDR and the GTDR are different, but the main features remain (first and second rebound points) remain visible.

The apparent dielectric conductivity in water dropped from $K_{a,water}$ = 85 (straight TDR) to $K_{a,water}$ = 27 (GTDR). The first consequence that could be derived from these results is a change in the range of measurements values that the GTDR sensor could provide when testing in soil. While a TDR is expected to return K_a values between 4 and 85, the GTDR would have a range between 4 and 27.

Figure 37. Testing GTDR vs TDR in water.

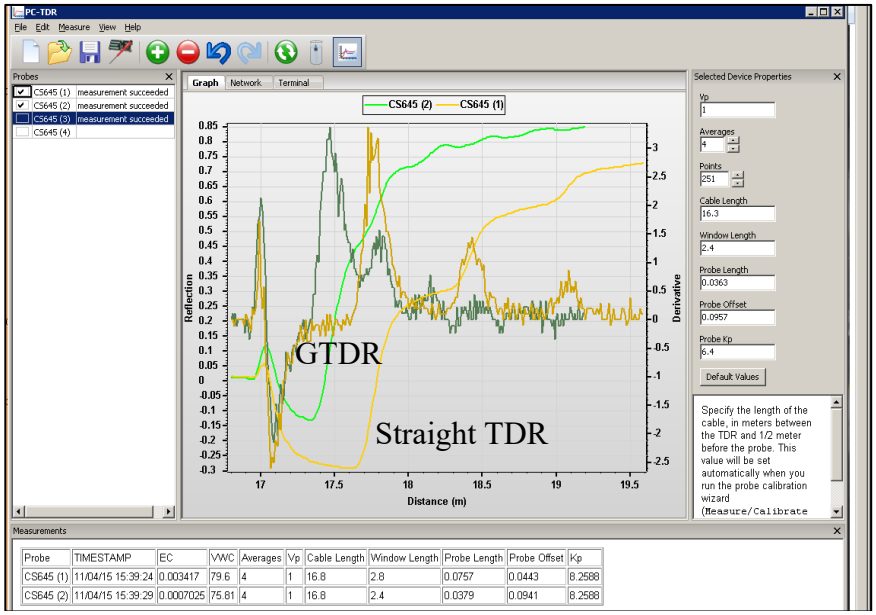

Figure 38. Comparison of waveforms from GTDR and straight TDR in water.

In order to evaluate the correlation between the apparent dielectric permittivity values obtained with the GTDR and the volumetric water content of the soil a calibration was carried out compacting Eagle Ford clay samples inside the GTDR. Additional details about this calibration are included in Appendix 1.

5.5.4 GTDR Calibrations

Soil-specific calibrations were performed as part of this study using the CS645 probes using samples of Eagle Ford Clay in order to compare a soil-specific calibration with Topp's universal equation. Also, the impact of curving the TDR was evaluated repeating the calibration. In both a large soil column was used to avoid the influence of the acrylic and standard parameters provided from Campbell Scientific were used the results of these calibrations are summarized in Appendix 1.

The following sections provide the main results from the calibrations performed using the GTDR and the alternative approaches used to define the correlation between the apparent dielectric permittivity (Ka) and the volumetric water content of the soil. Additional details and partial results of these calibrations are included in Appendix 1.

5.5.4.1 Standard soil calibration using GTDR

A soil specific calibration was carried out compacting soil samples water contents from Eagle Ford clay at different inside the acrylic permeameter with the GTDR. Figure 39 shows a comparison between the results obtained for previous calibrations where no acrylic was presented and the results obtained with the GTDR.

It can be observed that although the range of values for the apparent dielectric permittivity measured with the GTDR was reduced for the same range of water contents the results still showed a clear correlation between the dielectric property of the soil and the water content. These results were obtained using the same default parameters provided from CSI that were used for the straight TDR.

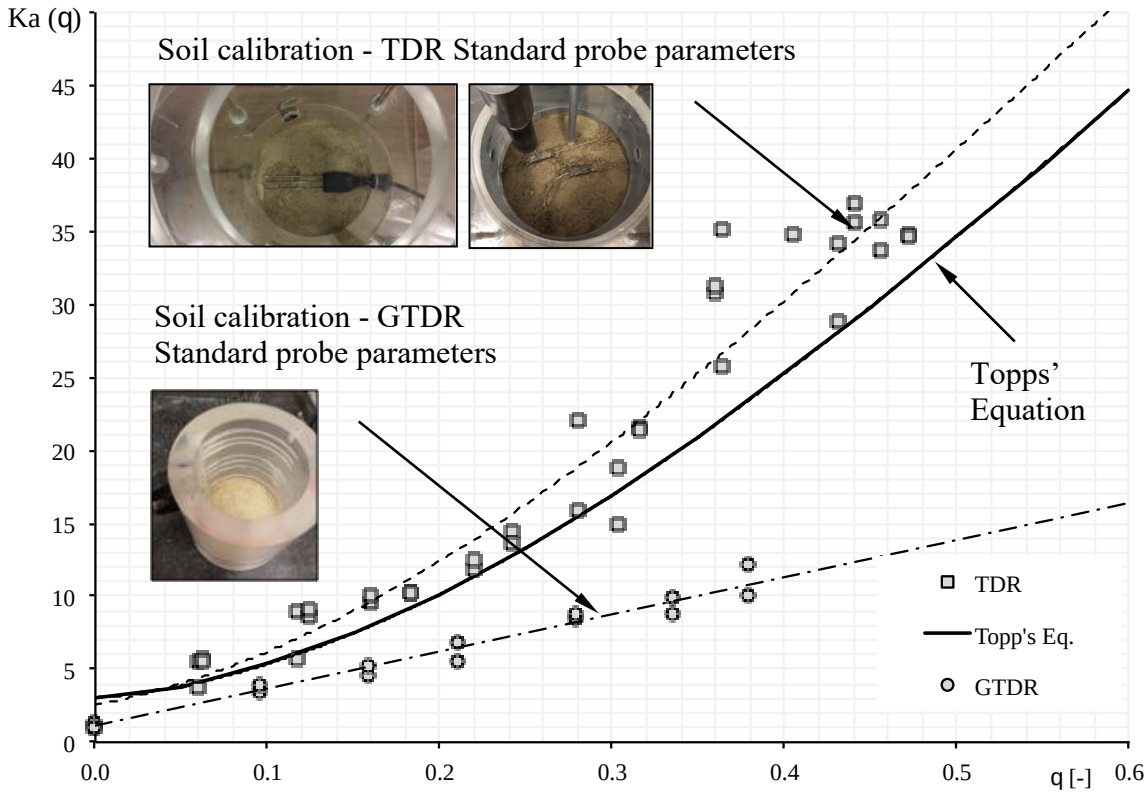

Figure 39. Comparison between TDR (straight and curved) and GTDR.

5.5.4.2 Probe calibration

After all previous calibrations were completed the interaction with the engineers from Campbell Scientific lead to a different procedure. This procedure incorporated a new (beta) version of the PC-TDR software in order to perform a calibration of the GTDR to obtain the offset length, the probe length, the cable length, and the window length that should be used with each probe

This probe calibration is a two-point calibration and requires measuring the dielectric permittivity in air and water. It is important to notice that this calibration takes two travel times and modifies the probe parameters in order to fit the pre-established dielectric permittivity values of air and water (1 and 79 respectively). This calibration

does not take into account the presence of the acrylic, but indirectly accounts for it modifying the probe settings. This procedure was carried out for all the GTDR and one straight TDR. The calibration results of the probe-fitting parameters for each sensor are presented in Table 2.

Table 2. TDR and GTDR probe parameters. Obtained with PCTDR

Probe	Cup	Cable Length	Window Length	Probe Length	Offset Length
		[m]	[m]	[m]	[m]
GTDR#2	1	16.8	2.4	0.0379	0.0941
GTDR#3	1	16.3	2.4	0.0363	0.0957
GTDR#6	2	1.9	2.3	0.0247	0.1379
GTDR#7	3	3.3	1.2	0.0254	0.1313
GTDR#8	3	3.3	1.2	0.0233	0.1322
GTDR#9	3	3.15	1.2	0.0251	0.1266
GTDR#13	3	2.2	0.8	0.029	0.1112
GTDR#10	4	2.2	1.0	0.0301	0.1020
GTDR#11	4	2.3	1.0	0.0267	0.1332
GTDR#12	4	2.2	1.0	0.0297	0.1042
TDR CS645	-	variable	1.6	0.075	0.035

The probe-fitting parameters for the regular TDR are slightly different from those recommended for the CS645 sensor. However, parameters obtained for the GTDR are significantly different. These new probe-fitting parameters for the GTDR are no longer physically meaningful. They are only fitting parameters influenced by the size of the probe, but selected to match the expected Ka value (in air and water).

5.5.4.3 Soil calibration using GTDR's probe specific parameters

A new soil calibration was performed using the GTDR with the new set of fitting parameters obtained with PC-TDR. Figure 40 shows the result of this new correlation between Ka and the VWC in comparison to the previous calibrations. The results obtained in this case almost matched Topp's universal equation.

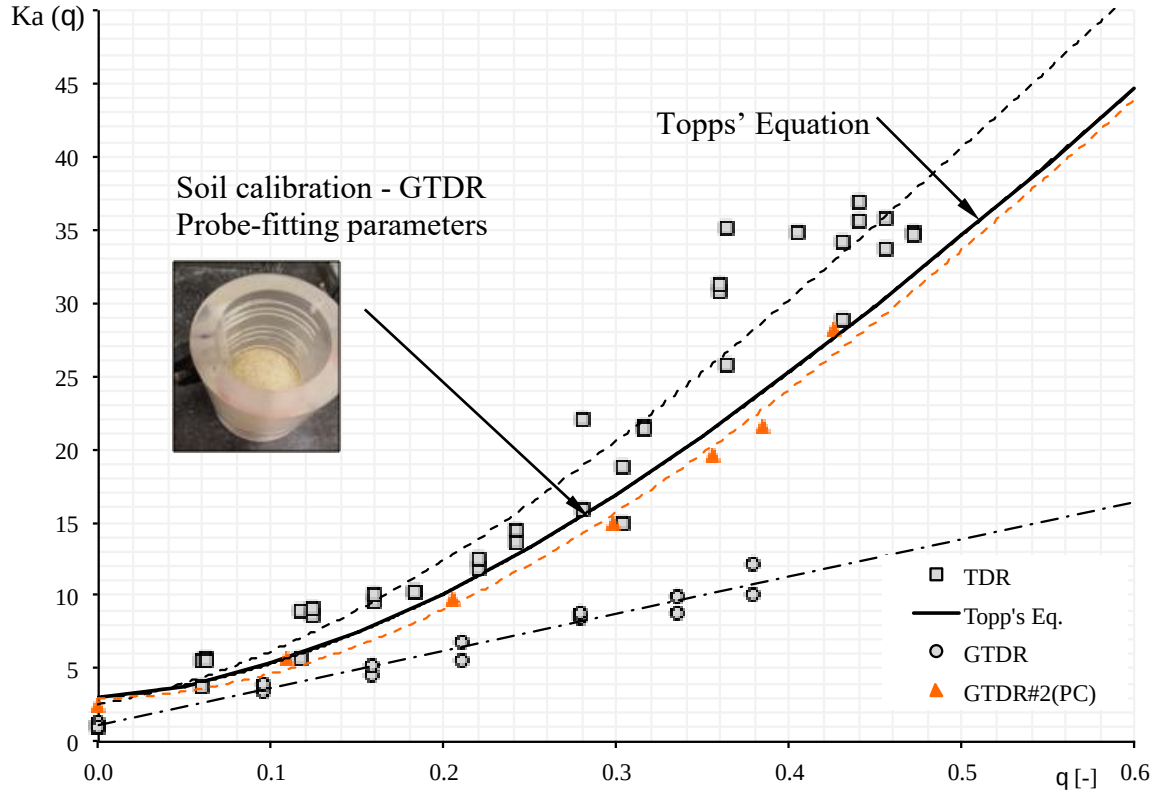

Figure 40. Soil Specific calibration for GTDR.

Two different outcomes should be indicated from the results showed in Figure 40:

- The extension of the Ka measurements over a greater range (3-81) is only due to the new fitting parameters selected to transform the travel times into Ka values between 4 and 85.

- The sensors are still measuring acrylic on half of the volume instead the VWC of the soil and therefore their accuracy remains reduced in comparison to regular TDR fully embedded in soil.
- After building any new GTDR, only a set of "fitting parameters" are required and they can be used in conjunction with Topp's equation. A Soil-probe-permeameter calibration like the one presented in Figure 39 could not be necessary any more.

5.5.5 Alternative interpretation of waveforms using AWIGF

In this research Campbell Scientific software was implemented as the standard procedure for the analysis of waveforms. However, in several occasions it did not perform correctly and results presented a large scatter.

AWIGF (adaptive waveform interpretation with Gaussian filtering) algorithm (Schwartz et al. 2014) was selected as an alternative methodology for the re-interpretation of the waveforms to obtain a VWC value in addition to the one reported by CSI. This procedure was implemented all the times that waveforms were available.

5.5.5.1 Probe calibration

In order to use the AWIGF algorithm, a probe calibration was performed. Similar to the two-point calibration performed with PC-TDR, in this case the waveforms for four different liquids of known permittivity (in air, kerosene, alcohol and water) were recorded. Then the best probe-fitting parameters were obtained by matching the measured travel times with the known permittivity values.

Figure 41 shows a comparison of the waveforms measured with the straight TDR placed in acrylic from Figure 33 immersed in different liquids. It can be observed that the influence of the acrylic and the epoxy for each mixture can be relevant to interpret the travel times. In those cases where the acrylic permittivity is lower than the liquid

permittivity (brine, water, alcohol) the travel time is reduced; while for air and kerosene the travel time it is extended.

The presence of the acrylic was explicitly incorporated in this calibration using a power-mix model. In such case the fitting parameters were adjusted to match the permittivity of the mixture.

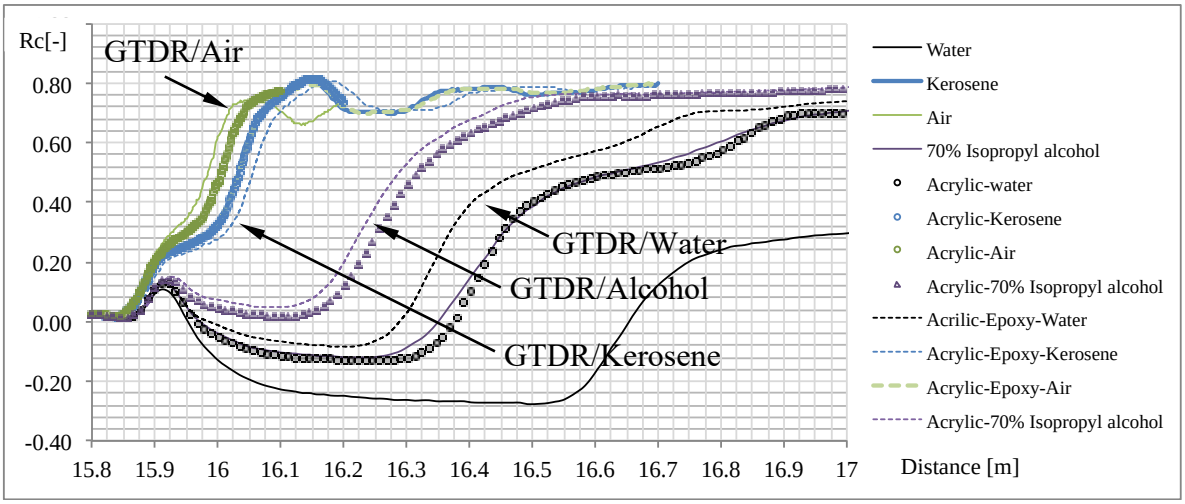

Figure 41. Impact of acrylic and epoxy in the travel times.

AWIGF has an automated selection of $t_{1.bis}$ and t_2, but the parameters t_c (correction time) and L_e (length of the probe) must be indicated in order to determine the travel time (t_t) and the permittivity (Schwartz et al. 2014). Since t_c and L_e are the unknown probe-fitting parameters an iterative process was required for this calibration. The calibration was completed as follows (names keep the original nomenclature of the code):

A first estimate for t_c was indicated in order for AWIGF to correctly detect t_1 and t_2. Since t_c depends mainly on the characteristics of the equipment it could be constrained manually within a short range.

Waveforms recorded for each acrylic-liquid mixture were interpreted using AWIGF in order to obtain $t_{1.bis}$ and t_2. The travel time and the apparent permittivity were calculated using the following equations:

$$t_t = t_2 - t_1 = t_2 - \left(t_{1.bis} - t_c\right) \quad (19)$$

where t_t is the travel time, $t_{1.bis}$ corresponds to the time related to the separation of the outer braid from the coaxial cable with the probe rods, t_1 the time when the pulse exits the handle and enters the soil, t_c is a correction time to obtain t_1 form $t_{1.bis}$, t_2 the time when the pulse reaches the ends of the probe rods.

$$K_{a.eff} = \left(c \cdot t_t / 2 \cdot L_e\right)^2 \quad (20)$$

A power-law mixing model was implemented to take into account the permittivity of the mixture acrylic-liquid for each case. For calibration purposes, only the real part of the permittivity was used. In such case the apparent dielectric permittivity of the mixture (Ka_acrylic-liquid) can be calculated as:

$$K_{a.eff} = \left[f \cdot \left(K_{a.liquid}\right)^{\alpha} + \left(1 - f\right) \cdot \left(K_{a.acrylic}\right)^{\alpha}\right]^{(1/\alpha)} \quad (21)$$

Where α is the mixing model exponent is assumed equal to 0.5, and tc, Le, and f left as unknowns. Measurements must be performed in at least three mixtures to obtain three travel times to solve this problem with three unknowns.

Figure 42 shows an example of the waveform analyzed using AWIGF for four different mixtures. In this case measurements in air, kerosene, alcohol and water were placed inside the permeameter cup with the GTDR.

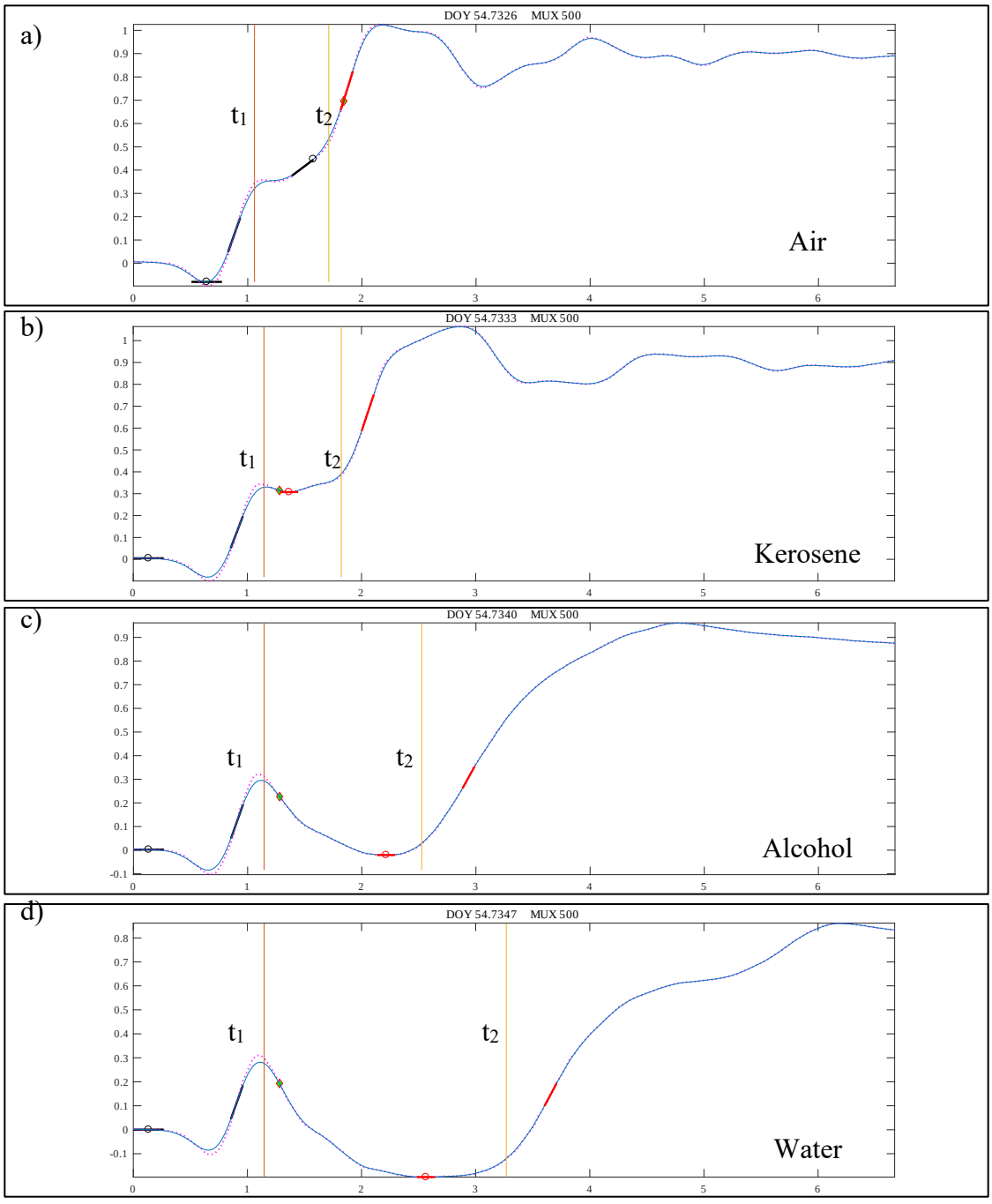

Figure 42. Waveform and AWIGF interpretation for: (a) air, (b) kerosene, (c) alcohol and (d) water measured with GTDR#7.

AWIGF determines $t_{1.bis}$ and t_2 based on the shape of the waveform, and calculates t_1 based on the first estimation of t_c. AWIGF displays t_1 and t_2 as vertical lines (Figure 42). Using the values of $t_{1.bis}$ and t_2 for all the mixtures, the three variables are determined (using excel solver) finding the best comparison between the measured (or predicted) apparent dielectric permittivity obtained from the waveform analysis and the permittivity of the mixture (Keff). In this procedure, f is used to calculate Keff (Table 3) and tc and Le are used to calculate the predicted apparent permittivity values (Ka-predict) (Table 4).

In this case, for GTDR#7 the values obtained were f=0.475, tc=0.37 and Le=0.0534. Table 5 summarizes the probe-fitting parameters obtained for all the GTDR used in this research, as well as the parameter "f" that indicates the level of interaction in the mixture between the acrylic and the liquid.

Table 3. Apparent permittivity for mixtures acrylic-liquid

Liquid	α	f	Ka.acrylic	Ka.liquid	Ka.eff
[-]	[-]	[-]	[-]	[-]	[-]
Air	0.5	0.475	6.0	1.0	3.1
Kerosene	0.5	0.475	6.0	1.8	3.7
Alcohol	0.5	0.475	6.0	19.0	11.3
Water	0.5	0.475	6.0	78.0	30.3

Table 4. Prediction of Ka based on measured travel times (GTDR #7)

Liquid	t1.bis	tc	t1	t2	tt	L	Ka.predic
[-]	[-]	[-]	[-]	[-]	[-]	[-]	[-]
Air	3.080	0.370	3.450	4.039	0.588	0.0534	2.73
Kerosene	3.096	0.370	3.466	4.138	0.672	0.0534	3.57
Alcohol	3.093	0.370	3.463	4.724	1.260	0.0534	12.5
Water	3.062	0.370	3.431	5.362	1.930	0.0534	29.4

Table 5. GTDR probe parameters and mixture factors for AWIGF analysis.

Probe	Cup	tc [m]	Le [m]	f [-]	a [-]
GTDR#2	1	0.40	0.0547	0.569	0.5
GTDR#3	1	0.40	0.0547	0.569	0.5
GTDR#6	2	0.40	0.0519	0.493	0.5
GTDR#7	3	0.37	0.0534	0.475	0.5
GTDR#8	3	0.35	0.0489	0.465	0.5
GTDR#9	3	0.33	0.0501	0.489	0.5
GTDR#13	3	0.30	0.0590	0.481	0.5
GTDR#10	4	0.28	0.0548	0.491	0.5
GTDR#11	4	0.30	0.0555	0.468	0.5
GTDR#12	4	0.28	0.0569	0.523	0.5

5.5.5.2 Soil calibration using AWIGF

The waveforms obtained in previous calibrations were reinterpreted using AWIGF and the new set of parameters. The results presented in Figure 43 are similar to those first obtained with PCTDR; the range of apparent dielectric permittivity is now restricted to values between 3 and 30, that correspond to the air and water mixtures with the acrylic. The best fitting for this data is obtained with a third degree polynomial function, in the same way than the previous calibrations and Topp's universal equation.

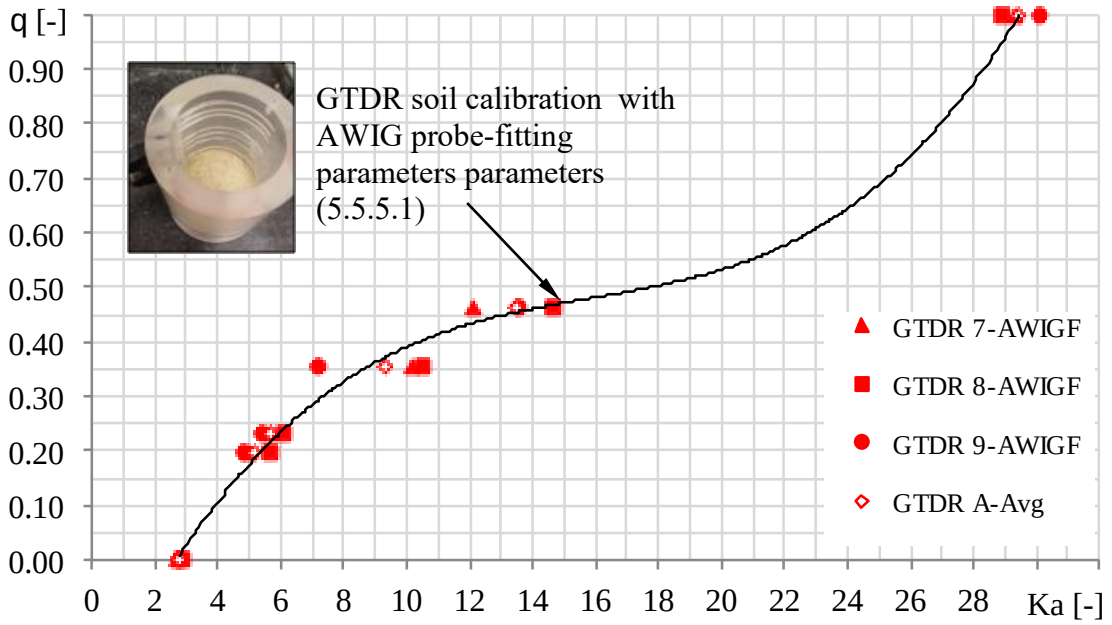

Figure 43. Soil-specific calibration performed on Eagle Ford clay with GTDR and AWIGF interpretation.

5.6 Summary and Conclusions

This Chapter presents the development of a Non-Intrusive volumetric water content sensor based on time domain reflectometry. Specifically, the GTDR sensor was developed as a solution to define the soil water content profile during centrifuge testing without interfering with moisture-induced soil deformations.

Transmission line theory, and relevant hardware and software components of the TDR system were assessed to evaluate their impact on the measurements. Its reliability and the strong empirical correlation of the soil dielectric permittivity (Ka) with the soil VWC were important attributes towards its selection in this study for development of a non-intrusive sensor. The construction of the GTDR consisted of a regular 3-rod sensor embedded in the acrylic tube wall was successful, the conclusions of this work are:

- Curving the TDR probes was found not to affect the travel times through the rods. However, the presence of the acrylic was found to directly impact on the waveforms modifying the travel time.
- Probe calibrations performed with PC-TDR software from Campbell Scientific was found to simplify the development bypassing the presence of the acrylic and forcing the probe-fitting parameters to fit air and water dielectric permittivity.
- The inclusion of probe-fitting parameters for each GTDR resulted in a measured correlation between the apparent dielectric permittivity and the volumetric water content similar to Topp's universal equation.
- Further GTDR were constructed without requiring soil specific calibrations for each sensor. Only probe-fitting parameters calibrations were necessary to use the sensors with the already established soil calibrations or with Topp's universal equation.
- Although not strictly necessary, soil-specific calibrations were found to be useful to determine a more specific correlation between the apparent dielectric permittivity and the VWC of the soil.
    - Campbell Scientific software was found not to perform correctly at analyzing waveforms on every occasion. The AWIGF algorithm (Scwartz et al. 2013) was found to be a reliable alternative to analyze the recorded waveforms in order to determine the VWC of soils.
- The implementation of AWIGF code required a specific probe-calibration to determine the probe-fitting parameters. The presence of the acrylic was expressly incorporated using a mixture-law. Measurements had to be performed in at least three liquids (liquid-acrylic mixtures) to obtain the GTDR fitting parameters.

- In order to determine the VWC of soils using AWIGF a soil-specific calibration was required to determine the apparent dielectric conductivity of the soil at different water contents using the probe-fitting parameters derived for AWIGF.
- TDR equipment was placed into the centrifuge and no influence of the increased g-level was noticed in the measurements.

Chapter 6: Development of a Non-Intrusive tool to Assess Soil Displacement based on Image Analysis

6.1 INTRODUCTION

In centrifuge tests, instrumentation was incorporated to measure soil conditions such as water content and suction. However, currently available sensors are often of sizes comparable to those of the model itself, possibly impacting the soil response. The expansive nature of highly plastic clays imposes restrictions on the use of sensors during the infiltration process. Consequently, it was necessary to develop non-intrusive displacement measurement techniques in a centrifuge testing environment.

While grids and markers along with conventional photography have been used in studies involving geotechnical models to evaluate their mechanical behavior; the affordability of digital cameras that can be used in non-conventional environments, such as centrifuges, gives the opportunity to create a non-contact tool that can provide deformation measurements of high-precision as well as to gain insight and information from the flow processes and soil response.

The objective of this Chapter is to document the development of a non-intrusive sensor based on image analysis technique that allows tracking displacements to quantify the soil deformation. Unlike other displacement instruments, this approach can deliver information without interfering with the hydro-mechanical response of the soil during the testing. In addition, the ability of retrieving images of the full sample in-flight is expected to provide visual insight in processes like changes in the soil structure.

The scope of this chapter includes a description of the in-flight equipment and the two analysis techniques named “Edge Detection” and “Patch Tracking.” The centrifuge buckets were equipped with GoPro cameras and short focal length lenses that remain

fixed in relation to the samples. In addition, LED lights were placed inside the centrifuge to provide uniform diffusive lighting condition.

In the infiltration columns tested in the centrifuge the soil deformation and water flow are both one-dimensional, and in the vertical direction. “Edge detection” is a simplified approach that benefits from these simplifications and incorporates markers into the soil to evaluate the displacements. In this way, simple and fast calculations can be performed.

On the other hand, “Patch tracking” is based on template matching technique and remains as a robust methodology, but it relies on complex matching schemes that require longer computation times, and concrete features that remain constant throughout the test.

Results showed a good performance of the system and a comparison with measurements from reference rulers and from data collected using LVDTs placed at the top.

6.2 BACKGROUND

The centrifuge permeameter (CPUS) at the University of Texas at Austin was built with some multimedia capabilities: a CCTV system that is transferred through the slip-ring stack (Zornberg & McCartney 2003) and a window in the lid that allows visual inspection of the test using a strobe light that. The light matches the rotational frequency of the centrifuge, as a result and a “quasi-static” image is obtained. Yet, both systems were designed to qualitatively track the progress of the test and not to perform measurements.

In order to enhance the centrifuge capabilities, cameras are needed inside the centrifuge permeameter to provide high quality images that can be subsequently analyzed. The drawbacks of this option are an increased gravitational field that affects the

internal mechanisms of the cameras (like the mechanic shutter) and the lack of physical space to place the camera and the short focus distance.

Measurements of soil displacements using image analysis have been developed through different methodologies. In particular, image particle velocimetry (PIV) is a template (patch) matching technique (Adrian 1991) that has been widely used and it has derived in proprietary and open source codes such as GeoPIV-RG (White et al. 2003), from the University of Western Australia (http://www.geopivrg.com). Indeed, PIV has been used to obtain displacement fields in centrifuge models (Stainer & White 2013).

However, some disadvantages of this method make it less appealing for this study. First, the "patch" must remain undisturbed. It works satisfactorily with coarse grain soils, like sands, but it does not apply effectively for fine grain soil like clays that undergo volume changes when their water content changes. Second, it is time consuming. It requires comparing a selected sub-image against every new picture to define the best match. A coarse search can be followed by a posterior refinement, but this method can be misleading by wrong local minima.

Motion detection through edge detection has also been widely used in both image and video. This technique requires that specific features like markers are present to be detected, but in comparison the mathematical procedures for edge detection and filtering are much simpler and therefore less time-machine consuming.

6.3 EQUIPMENT: CAMERA AND ACCESSORIES

The cameras selected for this study are two 4-Megapixel GoPro Hero 4. They have an electronic shutter, are small enough to be attached next to the buckets and they have a wireless network that allows controlling and collecting the pictures through Wi-Fi,

eliminating the requirement of an internal memory. In addition, a Lab View interface was developed to control the cameras remotely through the wireless network.

Figure 44(a) shows the camera facing the bucket where the sample will be located. A mountable lens was incorporated to obtain clear pictures within a short focal range and to reduce the fish eye effect. The minimum distance to an object can be located is 90 mm to obtain a sharp image that can be properly analyzed. The camera and the lens are located inside a lightweight casing created using 3D printing specially designed for these elements. The casing then is attached to a structure composed of threaded that can be used to adjust the position of the camera relative to the soil sample. (Figure 44b).

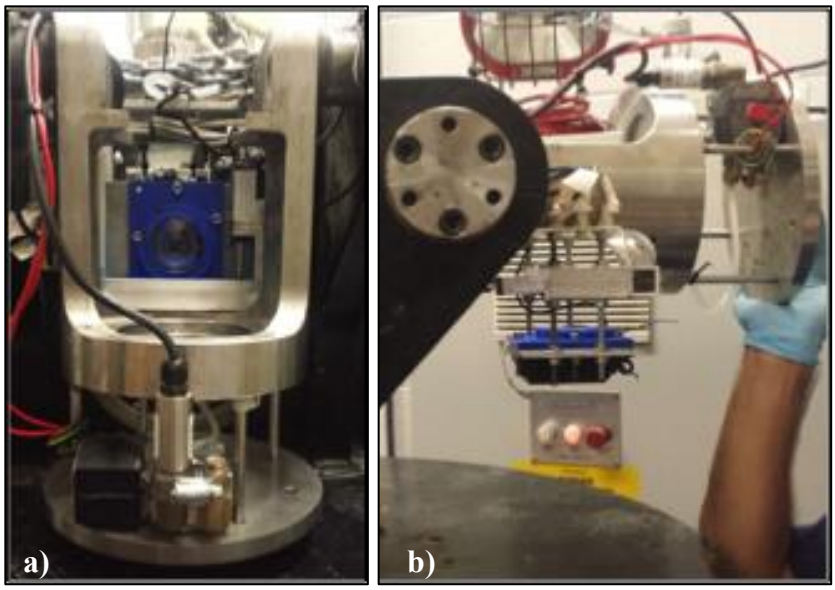

Figure 44. Camera system attached to the centrifuge bucket: a) Camera facing the soil sample, b) relative position of the mounting respect to the swinging bucket in-flight.

LED lights were incorporated inside the centrifuge drum at several locations to obtain a uniform and diffuse lighting condition. The CCTV benefits from this improvement and video can be recorded at any stage of the test.

To describe the deformation profile along the sample, different types of markers were evaluated throughout the project. Two types of markers were considered: a) plastic 3D-printed markers, which had the advantage of combining different colors within a small size, and b) aluminum markers covered with spray paint that were bigger and were less affected by clay masking. Figure 45(a) shows a top view of the sample during the compaction stage. The markers were fabricated of a length similar to the diameter of the permeameter tube to be located across the sample and to quantify the average displacement of the sample, minimizing side effects. A typical view of the soil sample with the markers is presented in Figure 45(b).

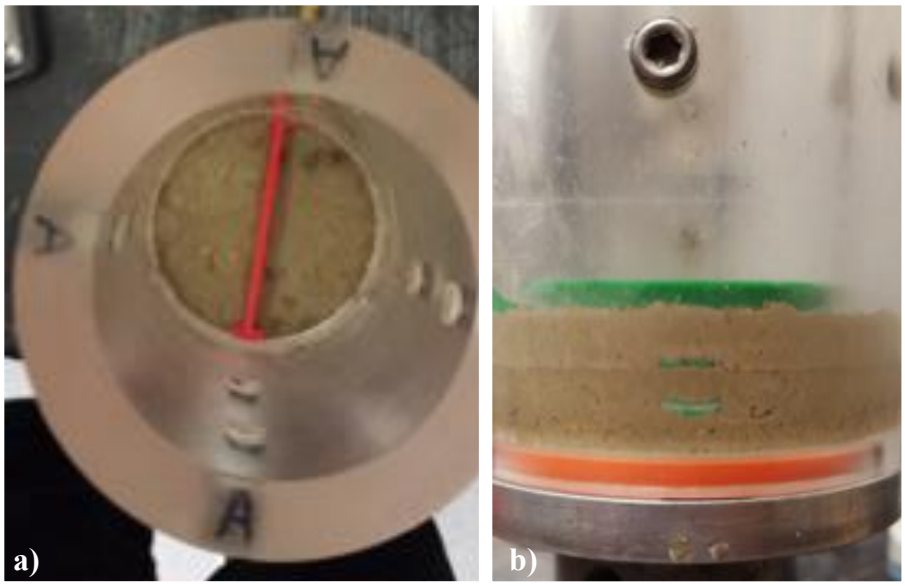

Figure 45. Inclusion of markers within the soil sample a) top view of the marker and the sample during compaction, and b) typical view of the soil sample including the markers.

6.4 ANALYSIS TECHNIQUE

The objective of this section is to present the concepts and assumptions as well as the procedures used as part of the image-analysis (IA) code developed to provide continuous measurements of the soil displacement during hydraulic characterization tests.

The IA code was written in MATLAB, which capitalized on the capabilities of the Image Processing Toolbox. The toolbox includes subroutines such as Canny's edge detection algorithm, binarization through histogram analysis, and morphological operators. The concept was to benefit from the physical features of the test to simplify the analysis without compromising the robustness and accuracy of the tool.

Two main groups of algorithms were developed as part of this study, "Edge detection" and "Patch tracking" (Blake et al. 2017). The "Edge detection" code was developed to rapidly detect and compute the displacement of rigid bodies included in the soil to ultimate define a soil deformation profile.

The second group of algorithms, "Patch tracking" code is a template matching technique will be mostly used to obtain the displacement of subsidiary objects that expose any possible rigid movements of the camera system. Although it requires additional computational time, it can also be used to track the markers displacement.

While IA is independently of the soil type, the post-processing may require an additional step when dealing with expansive clays. Due to their volume change in response to water, expansive clays can partially cover the edges of the marker observed through the permeameter wall. During the post-processing it is required that the user observes this incident and consequently selects the edge that better represent the displacement of the marker. Eventually a patch analysis can be performed. In addition, features such as the size of the marker throughout the test can be computed to quantify the impact of the edge masking.

6.4.1 Technique I: Edge detection algorithm

Physically, the displacement of each marker represents the integration of strains along the soil column that is located below the marker. While the comparatively high stresses that can develop due to centrifugation may induce soil compression and downward movement of the markers, the infiltration of water into high plasticity clays will induce swelling and the markers to move upwards. The movements are always 1-dimensional, along the flow direction.

For edge detection, the markers contours are analyzed to determine their upper and lower boundaries. The differences in the position of these boundaries for successive images taken at different times define the movement (in pixels). The displacements of the markers can be calculated in millimeters using a calibration factor (mm/pix).

Finally, the relative movement between the acrylic tube and the camera is measured by tracking a fiduciary point (a fix rigid feature) in the tube that is not being deformed. Any displacement detected in the fiduciary point should be added to the displacement of the markers. The relative displacement between two consecutive markers allows determination of the strain within the soil.

6.4.1.1 Identifying markers edges

Analyses are performed in local domains to reduce the amount of information and to enhance the contrast between the regions of interest. The local domains are sub-regions of the picture defined in the vicinity of each marker. The local domain must cover the area where the marker moves throughout the test. These domains can be easily defined comparing the first and last picture of the test (Figure 46a).

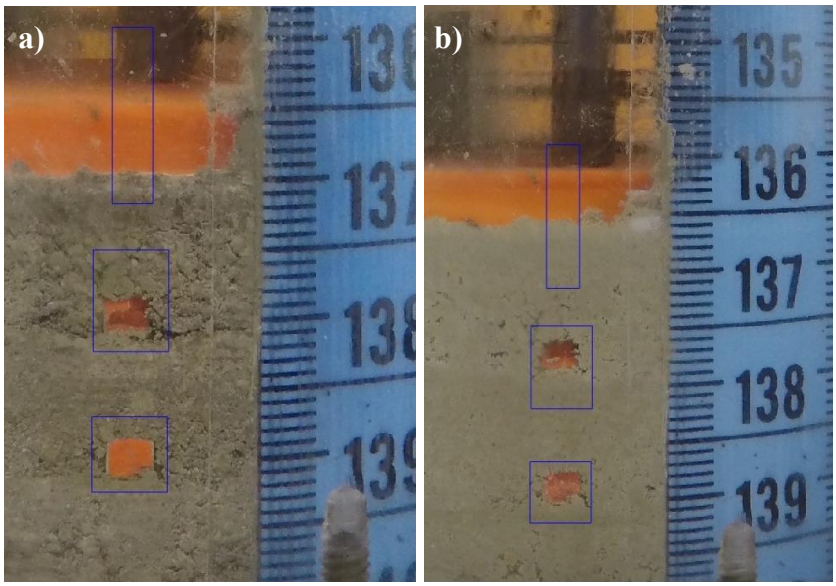

Figure 46. Selection of local domain for image analysis in swelling tests: a) sub-region at the beginning, and b) same sub regions at the end of the tests

The sample image in Figure 47(a) is analyzed using the image-analysis algorithm interface. Images are inspected in both the RGB and the YUV spaces. Each channel (R, G, B and Y, U, V) are inspected separately (selecting the desired channel in Figure 47b) to find an image that provides a distinctive contrast between the background and the markers (Figure 47c).

The images that provide a high contrast between the marker and the soil are typically represented by a bimodal histogram of the pixel distribution. In such case, most of the information in the image belongs to either the marker or the background colors. Figure 47(d) shows the threshold selected in the histogram to binarize the image. In general, this process has a low sensitivity to small variations in the threshold value.

After the binarization is completed, morphological operators (Open-Close routine) are conducted to eliminate small imperfections from the binarization process (Figure 47e). The window-size for these operators is indicated in Figure 47(b).

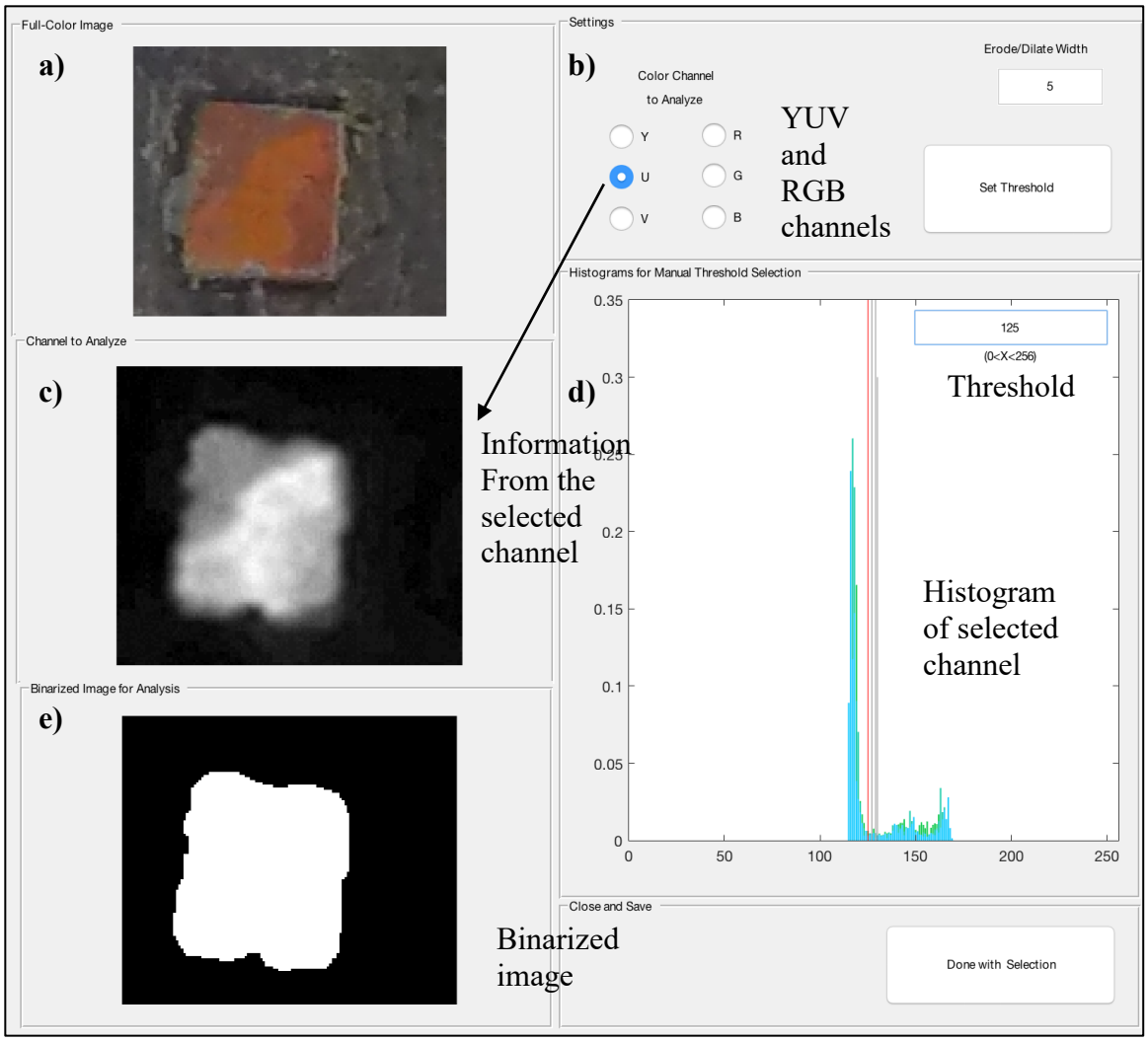

Figure 47. Image analysis interface includes: a) image to be analyze, b) selection of the analysis channel, c) histogram and binarization threshold, and c) binarized image.

Canny (1986) edge detection algorithm is implemented from MATLAB's library to obtain the contour of the binary images. The position of both edges will be determined based on the markers contour from the binarized image.

The shape (square) and color (orange) of the markers used in this research were chosen to minimize the intrusion on the soil and to provide a clear image of the object to

be tracked. For example, channel "U" was found to be the best option for clays samples with orange markers. Only one set of parameters (analysis channel, threshold value, and window-size) is selected to analyze all the pictures of the same test.

6.4.1.2 Markers position

Figure 48(a) summarizes all the edge detection steps in Figure 47. Figure 48(b) shows the defined contours (from the binary image) overlapped to the initial image to visually evaluate the success of this process.

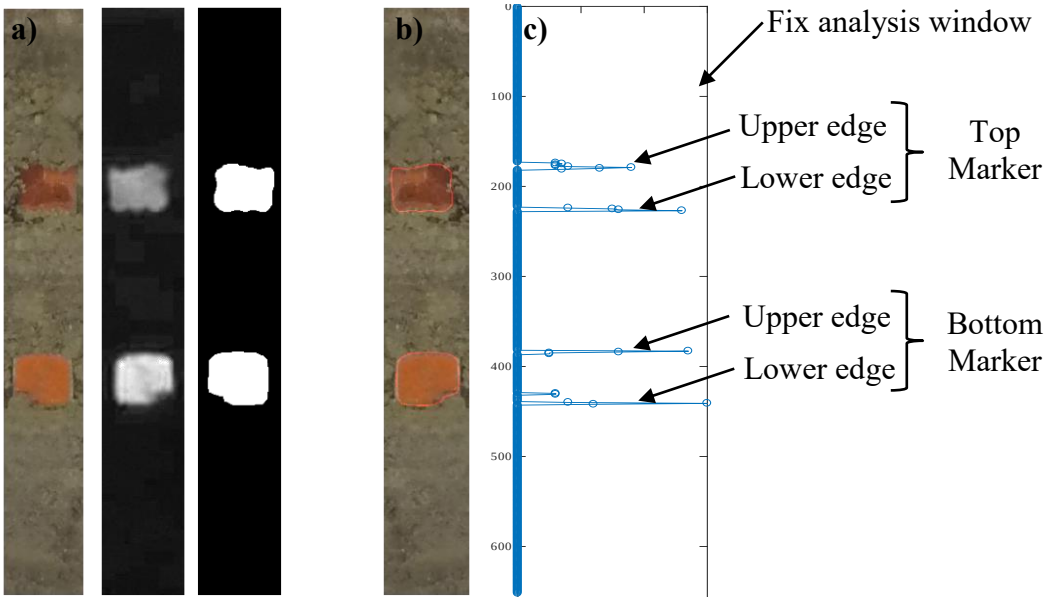

Figure 48. Image analysis procedure: a) edge detection steps, and b) detection of upper and lower boundaries.

The position of the markers is computed analyzing only the contour images to detect the position of the upper and lower boundaries of the markers. The procedure is performed as follows: 1) A summation of the number of pixels on each row of Figure 48(b); 2) values lower than 4 are converted into zero to eliminate the presence of those rows containing the lateral edges or minor features along the top and bottom edges; 3) the

number of pixels along each row are presented in Figure 48(b); 5) two peaks are detected indicating the upper and lower boundaries of each marker. 6) The position where the highest summation was found is indicated as the position of the marker boundary. Conceptually, this criterion matches what a user will target as a marker edge under a naked eye selection process.

The last component needed to define the actual displacement of the markers is the rigid movement between the camera and the sample tube. It is calculated using a fiduciary feature that does not deform during testing. The edge detection approach can be used to analyze a rigid edge from the permeameter cup.

6.4.1.3 Clay Masking

The markers edges were found to often become blurred or partially covered by the clay, especially in the case of expansive clays after water infiltration. This edge-masking effect can result in errors when determining the boundaries of the markers

In this study, careful observation of the markers was conducted to select which of both edges would be more representative of the marker movement. Also, to evaluate this phenomenon, the average height of the markers can be calculated computing the distance between the edges along the test. If the markers height reduces progressively during the test this mean masking occurs and the position of the marker boundary is being affected.

Typically, masking occurred from top to bottom due to the infiltration and it affected the upper boundary mainly. This error could be used later to correct the boundary position.

6.4.1.4 Calibration

Calibration was conducted using a measure tape placed inside the permeameter cup in the same plane than the markers. Figure 49 shows the main steps of this procedure:

First the position of each pixel was computed for each millimeter mark in the measure tape (Figure 49a). The distance in pixels was computed between successive marks, and between a fix reference point and the marks. Using this number and the known distance in millimeters a calibration factor of 20.7 pix/mm was obtained on average (Figure 49b). This number also express that the maximum resolution of the system is 0.0483 mm. Using this calibration factor the movements in pixels calculated in previous steps are transformed into displacements in millimeters.

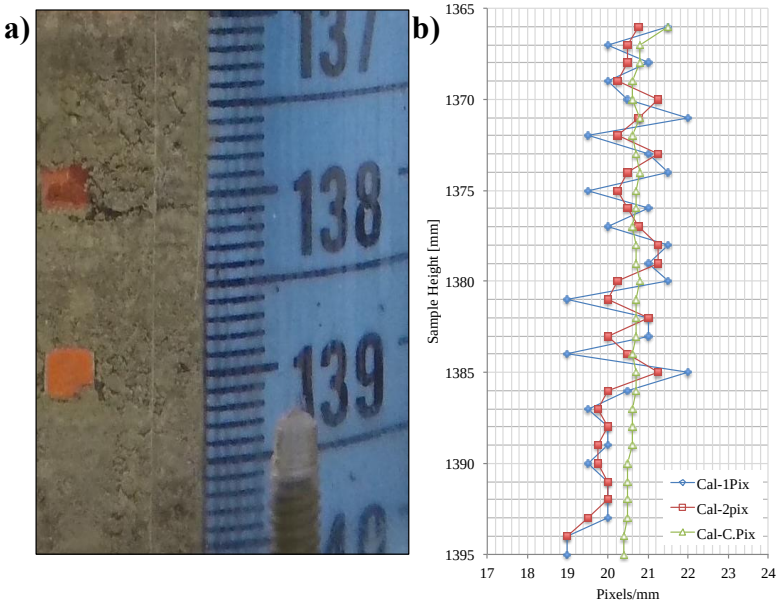

Figure 49. Procedure to calculate a calibration factor: a) Selection of reference points at known distances, b) computation of number of pixels between markers and from fix reference to obtain a calibration factor of 20.7 pix/mm.

6.4.2 Analysis technique II: Patch

The procedure described in this section is based on Digital Image Correlations, such as PIV technique. Specifically, an initial "patch" (a sub-image of j-by-k pixels) is selected, including the feature we want to track (e.g. the marker). A template-matching scheme is used to compare the reference patch with the successive test images.

For every new image, a search with a jxk sub-window is performed within a predetermined fix-size searching window. At each position, the sub-window assumes temporarily the value of the pixels that is enclosing. Then a comparison is performed with the original patch. The numerical value of each pixel on each of the channel (RGB) is compared between the temporary subset and the original patch. The summation of the numerical difference for each channel and for each pixel is calculated as the "error" in the agreement for every position. The new position of the patch corresponds to the sub-window with the lowest error. If no changes in the soil particles or the light intensity were expected, the error should be zero for a perfect match. The movement of the marker is defined as the movement of the whole patch through each consecutive picture. Rigid displacements should also be added to the computed markers displacements.

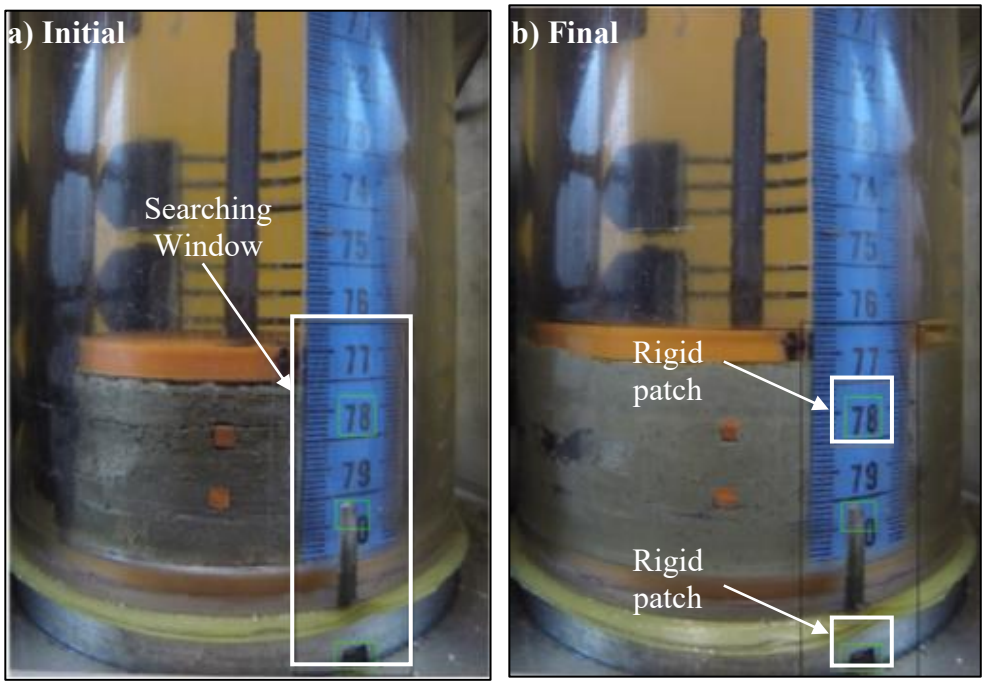

Figure 50. Selection of analysis domain and rigid patches in swelling tests: a) at the beginning, and b) end of the tests.

Figure 50 shows the rigid patches selected and the analysis window where the template-matching algorithm will look for the best match of the selected patches through all the pictures in the test. This technique is particularly helpful to define the rigid movements of the permeameter cup since the system is tracking the displacement of a rigid patch, e.g. grove in the base, a perforation in the acrylic or the numbers of the measuring tape.

6.5 ANALYSIS OF TYPICAL RESULTS

In order to illustrate the capabilities of the algorithms the analysis from a set of pictures from the unsaturated expansion test presented. Figure 51 shows the displacements of each rigid body, two markers, and one top plate calculated using both algorithms (edge detection –ED- and patch matching –PM-). These values represent the deformation of all the soil located below the selected marker. Ideally, both the upper and lower boundary measurements should be equal. However, the effect of the clay masking can create a difference between them.

After this analysis is completed, the user decides which boundary is deemed as less affected by the clay and will provide an accurate measurement of the displacements. This step has been taken into account and only one of the boundaries is used for the comparison between algorithms. The deformation measured with an LVDT from the top of the sample is also included in Figure 51 for comparison purposes. For the test shown in Figure 50, cameras went off during 8 hours of testing and a blank in data points can be appreciated.

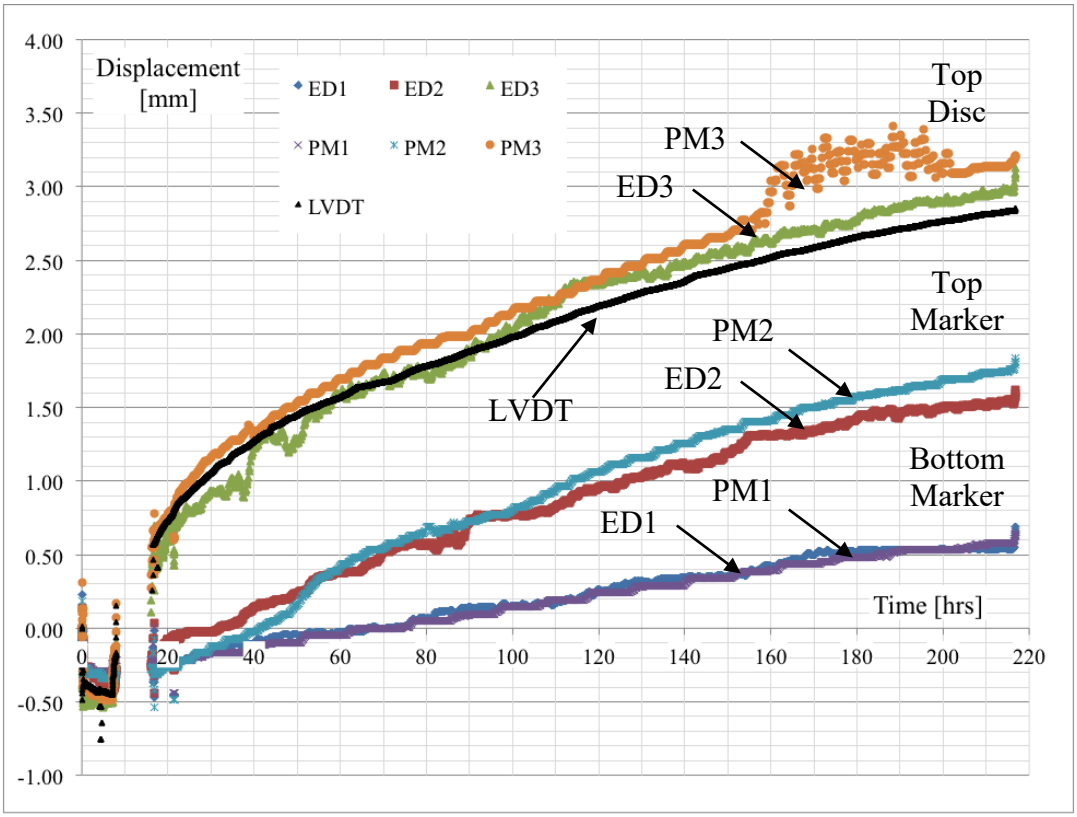

Figure 51. Markers displacement: comparison between available IA techniques.

Both techniques represent accurately the progress of swelling during a centrifuge test, a compression phase during the first ten hours was observed and then an expansion process that continues for about 9 days. As expected, the results show that the higher the markers position in the column the greater the expansion measured.

When compared the two series obtained for each marker (ED_i and PM_i) in Figure 51, a good agreement was found with a maximum difference of 0.2 mm for a range of displacements between 1.0 to 3.50 mm considering the three markers.

In general, the patch analysis shown in Figure 51 predicted a higher displacement, and a good comparison was obtained between the LVDT readings and the image analysis ED results for the top disc. Not only in the final result, but also the trend over the test.

6.6 SUMMARY AND CONCLUSIONS

The objective of the research component presented in this chapter was to develop a non-intrusive sensor based on image analysis technique that allows tracking displacements to quantify the soil deformation during centrifuge testing. The implementation of GoPro cameras in the permeameter buckets, with the addition of mountable lenses and LED lights provided the means to obtain clear pictures within a narrow range that can be used for analysis. Additionally, the multimedia capabilities were enhanced allowing the CCTV set up to provide a real time oversight of the test. The following conclusions can be drawn from this research component:

- Two different image analysis codes were developed to detect the movement of rigid bodies that exposes soil deformation. Similar results were obtained when using both methods to analyze the same data.
- While the "patch" technique is more robust because it tracks several features included in the patch, it was found to require a larger computational time.
- A patch constituted of only soil particles could not be used for clays, particularly for expansive clays that would change their appearance upon wetting.
- Both procedures were designed to be applied in local regions in order to minimize the amount of the data to be handled at each step.
- Edge detection algorithm requires a user interaction to define the analysis parameters (searching window, channel, threshold) and to observe which edge of the rigid body is better preserved during the test.
- Edge detection technique showed the best agreement with the contact displacement sensor.

- Only a third of the computing time was necessary to obtain the displacements of the markers using the edge detection algorithm in comparison with the patch technique. This comparison was performed evaluating each marker individually.
- Despite of clay masking, the edges could be successfully detected. The results from a typical expansion test showed a good comparison between the displacements obtained with the edge detection and patch algorithms, with a maximum difference of 0.2 mm for displacements between 1.0 to 3.50 mm.
- The patch technique was found to be particularly useful at determining rigid movement of the permeameter cup, since the template remains unaltered.

SECTION 2: HYDRAULIC CHARACTERIZATION OF UNSATURATED LOW PLASTICITY CLAYS

An important objective of the research components presented in Section 2 of this dissertation is to evaluate the performance of the newly developed equipment and sensors presented in Section 1. An additional key objective was to describe the hydraulic properties of unsaturated low plasticity clays. In order to accomplish these goals a series of testing procedures and measurement techniques were developed. The Rocky Mountain Arsenal (RMA) soil used in previous studies (McCartney 2007, Plaisted 2014) was also selected as baseline material in this research. Moreover, volume changes measured in this low plasticity clay can be attributed to the applied loads and measuring techniques. Also, the hydraulic properties of this material have already been tested exhaustively in previous studies.

Section 2 includes three chapters, with Chapter 7 presenting the results from a series of standard (1.g) tests, including tests conducted using the ATX Cell (low suction), filter paper technique and chilled mirror hygrometer test (high suction).

Chapter 8 focuses on centrifuge (N.g) testing. It includes a brief evaluation of previous results obtained for RMA soil as well as a description of the testing procedures and measurement techniques that can be implemented in the CPUS. Subsequently, the results from a series of hydraulic characterization tests on RMA soil are presented to illustrate the impact of the non-intrusive techniques, as well as to generate a data set that is consistent with the developments presented in this research.

Finally, Chapter 9 includes further analyses of the experimental results presented in Chapters 6 and 7. This Chapter initially presents the determination of the Soil-Water Retention Surface (SWRS) for the RMA soil. This involves, assessment of the proposed

analytical model, and a comparison of the SWRS that can be obtained using different experimental data sets. These data sets included standard (1.g) test results, centrifuge (N.g) test results, or a combination of both. Also, the degree of agreement between the SWRS and the experimental data is evaluated on each case. Chapter 9 subsequently documents the back analysis of the transient response of the ATX Cell test and the infiltration process in centrifuge testing. These procedures were conducted to present an alternative tool set to obtain the unsaturated hydraulic conductivity properties of the RMA soil.

Chapter 7: Hydraulic Characterization of Unsaturated Low Plasticity Clays Using Standard (1.g) Testing

7.1 INTRODUCTION

In this Chapter the characterization of the unsaturated hydraulic properties of the Rocky Mountain Arsenal (RMA) soil is obtained using standard (1.g) laboratory tests. Tests were conducted to cover a broad range of suction values by combining results from the ATX Cell and chilled mirror hygrometer (WP4C) tests. In order to maintain consistency with the overall objective of this research, the void ratio (e) is adopted as an additional variable.

The objectives of the research presented in this Chapter are: a) assess the quality of the data generated for the determination of the Soil-Water Retention Surface for the RMA soil; b) present the results in a manner that facilitates comparison with centrifuge test results; c) measure changes in the void ratio in cases where the soil samples are subjected to progressive wetting; and d) evaluate the performance of the newly developed ATX cell.

7.2 MEASUREMENTS OF THE RETENTION CAPABILITIES OF LOW PLASTICITY CLAYS AT LOW SUCTION VALUES

7.2.1 ATX Cell

The ATX Cell presented in Chapter 4 of this dissertation allows the determination of the hydro-mechanical behavior of the soil over a broad suction range using a single soil sample. Following the previously discussed testing procedure the magnitude of the variables that describe the soil at equilibrium under unsaturated conditions can be determined. The final goal is to use the measured discrete data points to define the continuous representation of the Soil-Water Retention Surface (SWRS). This is achieved by testing a soil using a range of different initial unit weights. However, it should be

emphasized that the ATX Cell will generate data to define only a portion of the SWRS. Specifically, the current testing set up can only operate for suction values ranging from 0.1 to 500 kPa. This corresponds to the entire range of the hanging column test and part of the suction range of the pressure plate.

7.2.1.1 Testing program

A testing program was conducted as part of this research using soil from a batch of a low plasticity Clay (CL) obtained from the Rocky Mountain Arsenal (RMA) alternative cover. This soil classifies as clay although its fine-grained fraction is 50.5% without particles above sieve #4. The Atterberg's limits are LL=32, PL=12 and specific gravity is Gs=2.77. The maximum dry unit weight ($\gamma_{d.max}$) is 18 kN/m^3 using the standard proctor compaction effort, and its optimum water content is w_{opt}=14.5%. The saturated hydraulic conductivity for the range of unit weights tested in this research component conditions is approximately 8.5 10^{-7} m/sec.

Soil samples were prepared using a target moisture equal to the optimum water content and several unit weights to cover a wide range of void ratio values. A summary of the characteristics for the initial conditions of the soil samples is presented in Table 6. Samples were initially subjected to a sitting load that imparts a uniform pressure of about 1 kPa. The change in void ratio, also reported in Table 6, due to the application of the vertical load was comparatively small.

Table 6. Testing scope for RMA soil

Test	RC_t	w_c	γ_d	e
[#]	[%]	[%]	[kN/m^3]	[-]
W3	80	14.5	14.50	0.878
W4	80	14.5	14.22	0.883
W5	80	14.5	14.40	0.887
W6	80	14.5	14.29	0.901
W7a	90	13.0	16.19	0.679
W7b	90	13.0	16.50	0.647
W8a	90	13.0	16.11	0.687
W8b	90	13.0	16.74	0.623
W9a	100	13.0	17.45	0.557
W9b	100	13.0	17.65	0.539

7.2.1.2 Experimental Results

Experimental results were obtained from multistage ATX Cell tests. The data used to generate the SWRS is collected when equilibrium has been reached at the end of the various stages. Each testing stage involved imposing a target matric suction (ψ) value. The data obtained in each test includes: the volumetric water content (θ), unit weight (γ) and void ratio (e). Using this data, it is possible to define a three-dimensional representation of the hydro-mechanical path of each test in the (ψ, θ, e) space.

Figure 52 shows the results of the tests listed in Table 6, presented in the (θ, ψ, e) space. This representation provides insight on the impact of the unit weight over the retention capabilities of the RMA soil, and on the representation of the experimental data when the void ratio is included as an additional variable and the SWRS is used as a fitting tool.

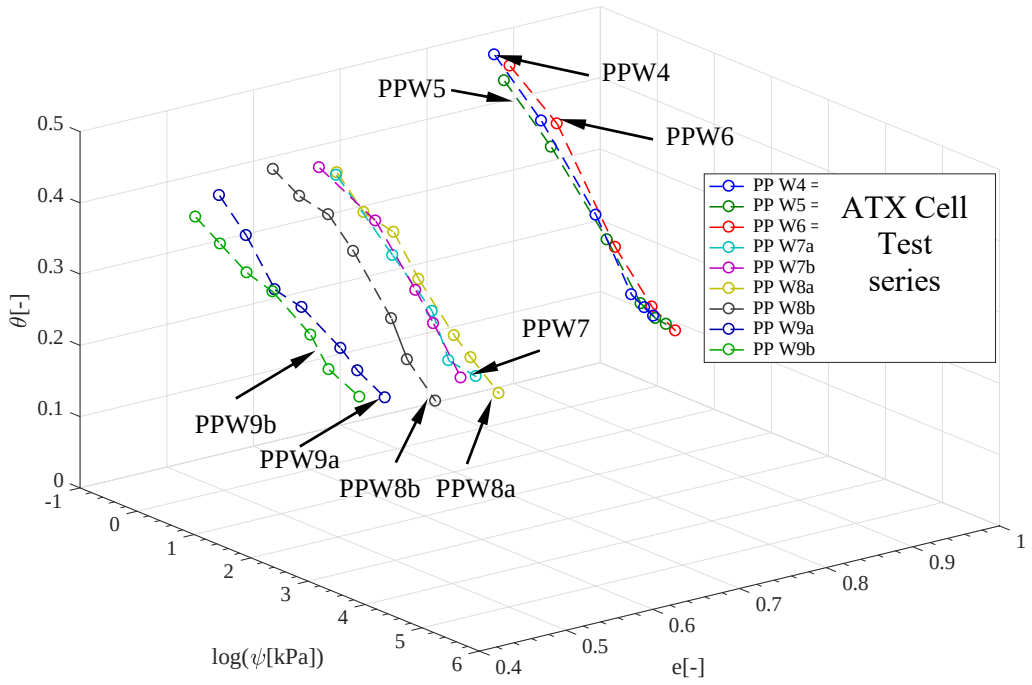

Figure 52. ATX Cell test results in three-dimensional (ψ, θ, e) space.

Three two-dimensional views of the same experimental data are shown in Figure 53 to illustrate the relationship among the variables. Figure 53(a) shows a typical representation of the SWRC as presented in the θ-ψ plane. It can be observed that all tests follow a similar trend. They show comparatively small changes in volumetric water content for matric suction values above 30 kPa, with the most significant changes arriving in lower suction range. Also, no plateau was reached on water content values at comparatively low suctions. Consequently, no suction value could be identified as the air entry pressure. A very low suction (0.1 kPa) was required to fully saturate the samples, as observed in Figure 53(b) where samples in the last stage are typically at a volumetric water content equal or near the porosity value.

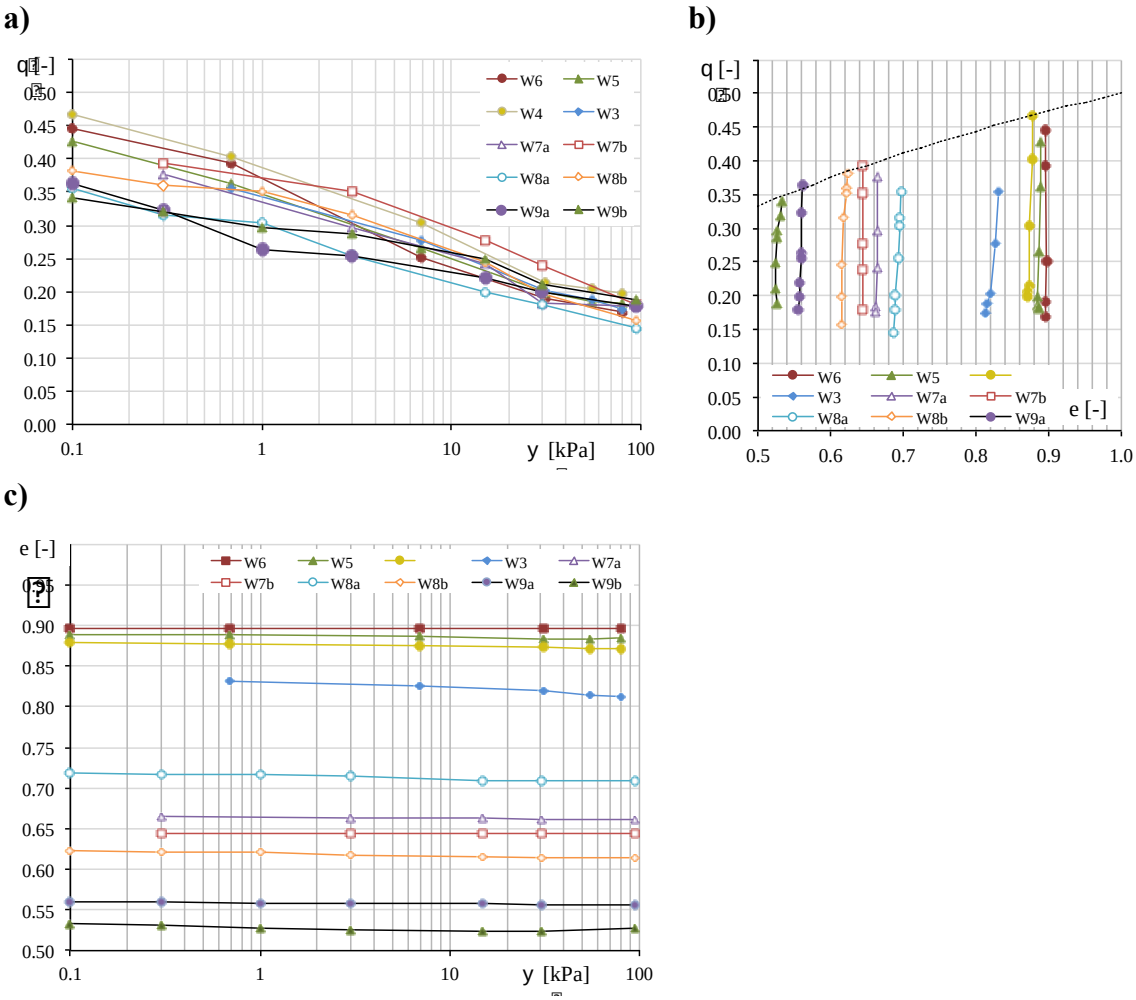

Figure 53. Two-dimensional views of the SWRS: a) θ vs ψ plane, b) e vs ψ plane and c) θ vs e plane (Re-paste excel figure)

Although Figure 53(c) shows that the changes in void ratio were negligible. The goal was also to monitor the three variables to define the complete hydro-mechanical path of the soil. As expected for this soil, the results from one of the tests could be deemed as representative of the tests conducted at the indicated void ratios.

7.2.2 Representative behavior of RMA soil

Figure 54 shows three curves that represent the behavior of the retention capabilities at relative compaction values of 80%, 90%, and 100% compiled to facilitate

the data analysis. As previously indicated, no plateau or inflection point can be noticed in any of these curves. The use of a larger logarithmic suction scale does change the previous observation of the same data presented in Figure 53(a). The results in Figure 54 also reveal that the water content near saturation increases with the increasing void ratio (and porosity) values.

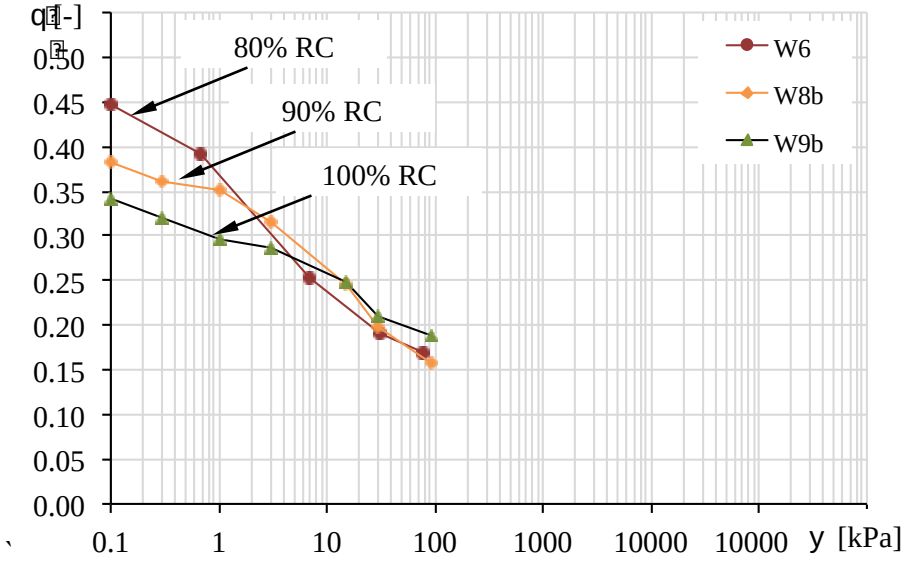

Figure 54. SWRC defined relative compaction values of 80%, 90%, and 100%.

Another relevant feature identified in Figure 54 is that the difference in density between samples results in a somewhat marked impact on the slope of the curves. Samples compacted at high density (i.e. low void ratio) are comparatively flat, they show a small increase in the water content through a large range of suction values tested. While for samples compacted at low density (i.e. high void ratio) the increase in the water content is much larger for the same range of suction values tested.

SWRC models such as van-Genuchten (1980) was used to define different curves for this data in order to understand the behavior of the fitting parameters and their

evolution with the void ratio. These analyses will be later discussed in Chapter 9 and Appendix 2. These results provide a preliminary insight in the behavior of the Soil-Water retention surface (SWRS). While the parameter representing the saturated volumetric water content increases with the increasing void ratio, the residual water content remains almost constant through the range of void ratio values tested.

7.2.3 Transient response

Every testing stage involving changing the air pressure to impose a new equilibrium condition (i.e. fixing the matric suction) results in a transient response where the soil sample changes in water content and in volume. As explained in Chapter 4, the ATX Cell allows measuring the changes in total weight and in height of the soil sample. Using the transient information from the tests, the relevant variables (e.g. volumetric water content or the void ratio) values can be defined as a function of time.

This transient process occurs every time for each test when the suction is changed. In this case a total of five or six stages were imposed to obtain the SWRS data points. Figure 55 illustrates the successive time responses for sample test W9b. The data includes monitoring of the sample changes in weight as the water flow into the pores. The changes in the volumetric water content with time are shown Figure 55(a). The results show that the flow velocity tends to decrease with time as the water meniscus in the soil pores equilibrates with the imposed air pressure. The new equilibrium point was typically defined after no additional changes in water content were recorded.

In addition, the time history of volume changes can be represented evaluating the void ratio time history. Volume change information is collected continuously during the ATX Cell tests, results are shown in Figure 55(b). In this case since the changes in the

void ratio were negligible, and volume changes were not considered to define equilibrium.

As indicated previously in Chapter 4, the main difference between the volumetric water content and the void ratio time histories is that, the measurement of the total weight is affected by the potential presence of air bubbles and sudden increments can be recorded, while the sample height is not affected by the air in the lines and the results are somewhat more continuous. This transient data will be used later in Chapter 8 to derive the unsaturated hydraulic conductivity.

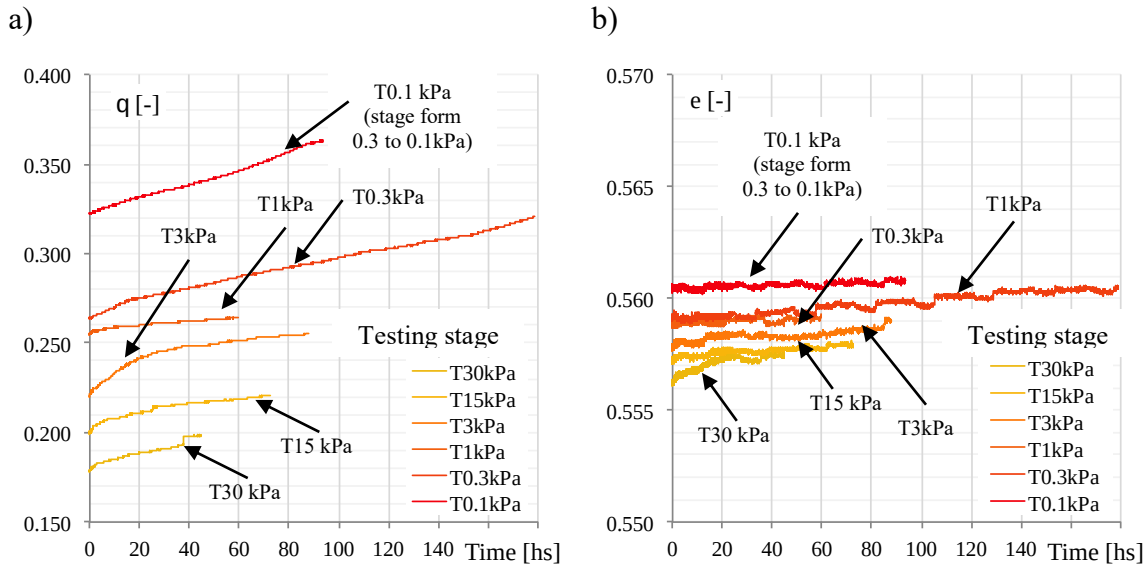

Figure 55. Transient response in ATX Cell test W9b for each testing stage described by: a) water content, and b) void ratio time histories.

7.3 MEASUREMENTS OF THE RETENTION CAPABILITIES OF LOW PLASTICITY CLAYS AT HIGH SUCTION VALUES

In order to supplement the characterization of the unsaturated hydraulic properties of the RMA soil, soil samples were also tested using the WP4C (chilled mirror hygrometer, ASTM D6836-02(2008)). This test allows determining the total suction of

soil samples over a wide range of water contents. The results obtained for three series of tests involving samples compacted at three different densities corresponding to relative compaction values of 80%, 90%, and 100% are presented in Figure 56.

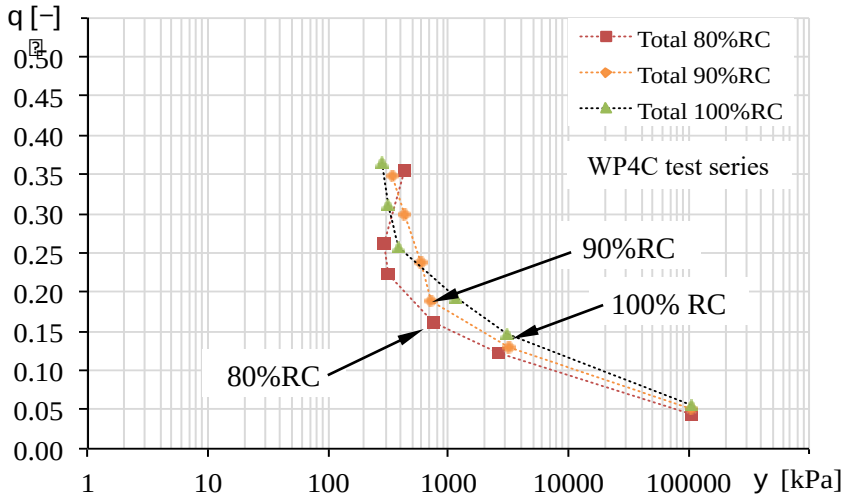

Figure 56. Total suction measurements SWRC results for RMA characterization at high suction ranges and three different relative compaction values.

It can be observed that for higher water contents, approximately between 0.25 and 0.35, the measured total suction values are essentially constant. This trend indicates that although the matric suction decreases with the increasing water content, the osmotic component may correspond to the most relevant component of the total suction.

It could be inferred that for the densities and water contents tested, the RMA soil has an osmotic suction ranging from 300 to 1,000 kPa. If the osmotic suction is subtracted from the total suction measurement, the remaining value corresponds to the matric suction, which can be compared directly with the results obtained from the ATX Cell.

A simplified analysis was performed assuming a constant value for the osmotic suction. Figure 57 shows the total suction results measured with the WP4C, the predicted matric suction values and the measured results obtained performed with the ATX Cell. An osmotic suction value of 600 kPa was found to be the best estimate for all the series. Although the osmotic suction component may vary with the void ratio the differences in the present analysis were found relatively small.

Due to the scatter in the total suction measurements obtained for samples tested using WP4C at comparatively high water contents, some of the predicted matric suction results were negative and were ignored from these test series. Yet, a reasonable agreement with the matric suction values obtained from the ATX Cell can be observed. It should be emphasized that only measurement of the same type of suction (e.g. matric suction) should be used to define a representative SWRS.

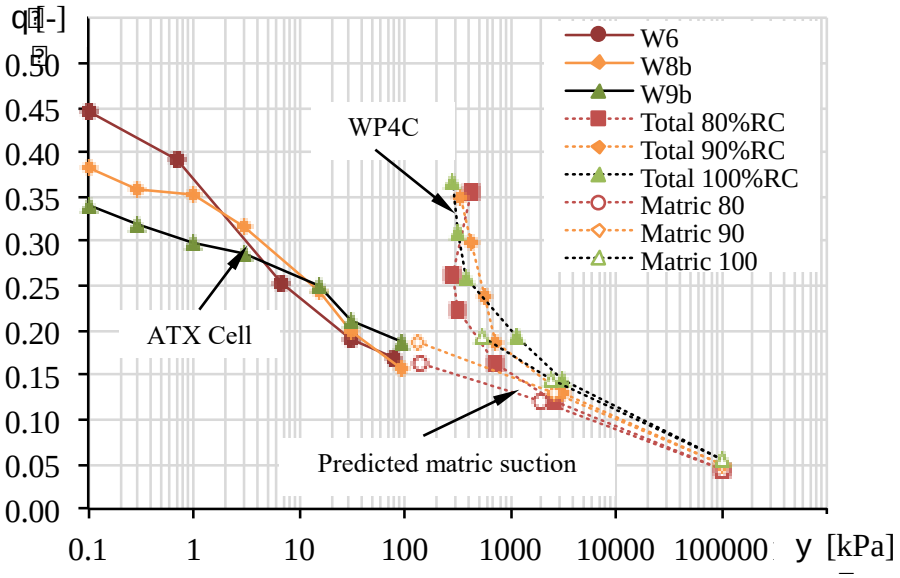

Figure 57. SWRC for RMA soil defined combining measurements at low and high suction values.

7.4 SUMMARY AND CONCLUSIONS

Characterization of the unsaturated hydraulic properties of a low plasticity clay, the Rocky Mountain Arsenal (RMA) soil, was successfully achieved after implementing standard (1.g) laboratory tests. The information compiled to define the SWRS includes a comparatively wide range of matric suction values, ranging between 0.1 kPa to 100 MPa, and three targeted dry densities.

In order to combine the results from multiple tests all the experimental data was expressed in terms of the same suction component (matric suction). Based on the results obtained in the research component presented in this chapter, the following conclusions can be drawn:

- The ATX Cell was found to facilitate the hydro-mechanical characterization of a low plasticity clay, RMA soil, providing continuous measurement of void ratio, matric suction, and water content.
- Although the changes in void ratio were negligible for RMA soil, the testing protocols adopted were found to lead to consistent results, The goal of monitoring the three variables was achieved for a range of void ratio values from 0.50 to 0.95.
- The initial density of the soil was found to affect the slope of the hydro-mechanical path of the soil samples describing the correlation between the water content and matric suction.
- In particular, for low plasticity clays the path of each sample was described at a relatively constant void ratio. The generated experimental data could be interpreted using SWRC models.
- The change in water content and void ratio, were continuously measured during ATX Cell tests, and resulted in suitable experimental data to derive the unsaturated hydraulic conductivity.

- While the volumetric water content defined using weight measurements required accounting for the effect of the entrapped air, the void ratio could be defined using direct measurements of the sample height and did not require any further interpretation.
- WP4C tests were found to provide an expeditious determination of the total suction vs. soil moisture relationship of the soil for suction values ranging from 300 kPa to 100 MPa. For water content values between 0.20 and 0.35, the total suction was found to become essentially constant for the soil evaluated in this study.
- The combination of the ATX Cell and WP4C results allowed the determination of the osmotic suction, which for the RMA soil was approximately 600 kPa. It should be emphasized that in order to define a representative SWRC or SWRS only measurement of the same type of suction (e.g. matric suction) should be used.

Chapter 8: Hydro-Mechanical Characterization of Unsaturated Low Plasticity Clays Using Centrifuge (N.g) Testing

8.1 INTRODUCTION

The centrifuge permeameter for unsaturated soils (CPUS) has been previously used to characterize the hydraulic properties of low plasticity clays (McCartney, 2007; Plaisted, 2014). However, as previously described in Chapter 2, a number of simplifications regarding in-flight volume changes had been adopted.

In this research component, a series of tests was carried out in the centrifuge in order to relax some of these simplifications and to alternative procedures based on the experimental developments presented in Section 1 of this study. In particular, the goals of the research presented in this chapter are:

- Review the results from previous research involving RMA soil to identify the range of unsaturated hydraulic properties that could be measured using centrifuge testing.
- Propose modifications to the testing methodology in order to incorporate the non-intrusive sensors presented in Chapters 5 and 6
- Evaluate the time response of the in-flight, non-intrusive sensors as well as their accuracy in comparison to other measurement techniques.
- Compare the volumetric water content and void ratio profiles obtained with different measurement techniques (e.g. destructive, semi-destructive and non-destructive) from the same centrifuge test.
- Gain insight into the characterization of the unsaturated hydraulic properties of RMA soil using centrifuge technology.

8.2 RESULTS FROM PREVIOUS STUDIES USING RMA CLAY

The results from McCartney (2007) and Plaisted (2014) research constitute a robust initial resource to evaluate the range of values that can be obtained when studying the unsaturated hydraulic properties of soils using centrifuge testing. In particular, under the testing methodologies and measurement techniques presented in these studies it could be inferred that:

- For the condition of hydrostatic equilibrium, the water content values measured at a given suction level, was independent of the g-level.
- The suction imposed at a given height in the soil sample depends on the rotational speed and the imposed boundary condition. The highest suction value that could be imposed is 500 kPa (assuming 0 kPa at the lower boundary). However, the highest suction value registered was 90 kPa, at 100 g's.
- Different pore structure lead to differences in the unsaturated hydraulic characteristics of the soil. For example, the results in Figure 58 reveal differences in the slope of the successive SWRC depending on the compaction water content. It can be inferred that, even at the same density, higher water contents result in smaller macro pores (a disperse structure) and in consequence a flatter SWRC.
- The stresses imposed by the increased gravitational field could modify the density across the soil sample. Under hydrostatic equilibrium conditions, the lower soil layers are under low imposed suction values and high stresses. In consequence, the ability of generating experimental data at low suction values and high void ratio values may be limited. For example, the results in Figure 59 show that when samples are compacted under a low initial void ratio (high density) the samples remain dense after testing, however samples compacted at medium to lose conditions (high void ratio) will experience compression.

- The lower the initial void ratio (at compaction), the smaller the changes in void ratio expected during centrifugation. For RMA soil Mc Cartney(2007) reported the results using samples compacted at an initial void ratio of 0.54 (porosity 0.35), while Plaisted (2014) reported results using samples with initial void ratio ranging from 0.6 to 1.

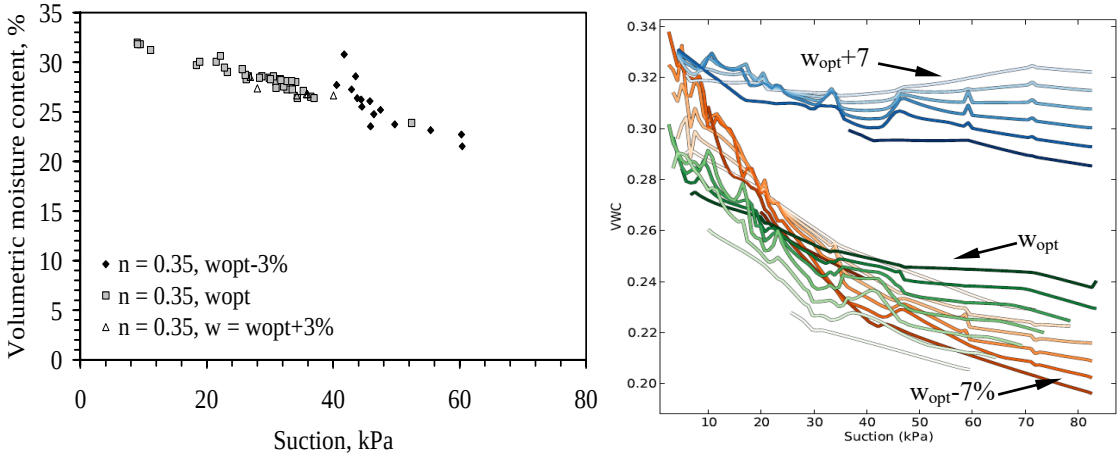

Figure 58. Impact of the compaction water content in the slope of the SWRC for RMA soil evaluated by: a) McCartney (2007), and b) Plaisted (2014).

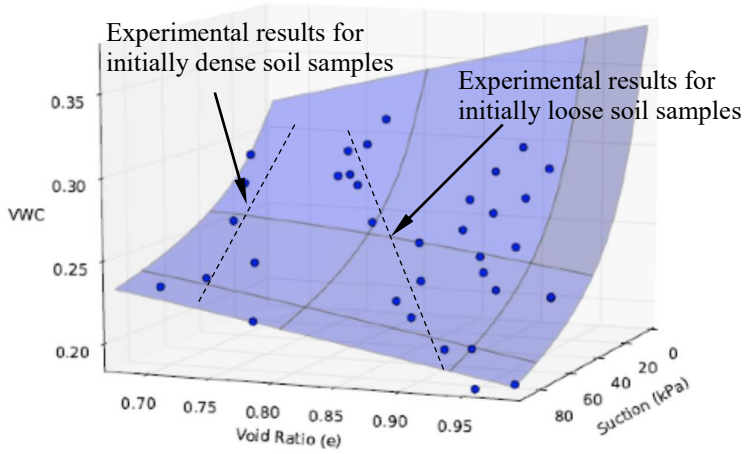

Figure 59. Effect of initial soil density on the distribution of the hydrostatic tests results performed to describe the SWRS of the RMA soil (adapted from Plaisted, 2014).

- The targeted hydraulic conductivity measured at a given suction level was independent of the g-level.
- Figure 60 shows the unsaturated hydraulic conductivity values obtained by McCartney (2007) using steady state centrifuge testing. The unsaturated hydraulic conductivity of the RMA soil was found to range from $1x10^{-7}$ m/s to $1x10^{-10}$ m/s for the compaction conditions and the suction range considered in this study.
- The results show that the hydraulic conductivity can be orders of magnitude smaller for a given suction value (or water content) when compacted at the same density, but wet of optimum (Figure 60).

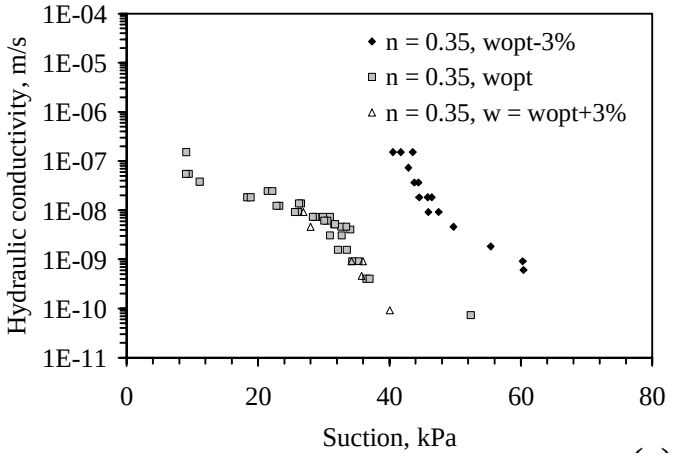

Figure 60. RMA unsaturated hydraulic conductivity measured by McCartney (2007).

8.3 TESTING PROGRAM

A specific testing program was conducted in this study to achieve the goals previously listed. An important focus was placed in assessing the response of sensors and the impact of the measurement techniques. The testing protocols were adapted from those reported as "Hydrostatic" and "Imposed Flow" tests by Plaisted (2014), conducted to determine the SWRS and the k-function respectively of the RMA soil.

A relevant difference with previous tests is that different measurement techniques were used in this research to identify the volumetric water content and the density profile on a given soil sample. As a result, different data sets were obtained using the same sample at a given stage. Additionally, the inclusion of non-destructive measurement techniques allowed conducting multiple stages tests.

8.3.1 Testing Procedures

3.2.2.4 Hydrostatic test

The hydrostatic (H) tests were used to determine the soil SWRS. They involve two main stages: soaking and drying. During the soaking stage the samples, spun at a selected speed, are saturated using a comparatively high constant inflow rate. The inflow rate is selected to be approximately equal to the product of the saturated hydraulic conductivity and the imposed gravitational gradient. This condition is maintained until reaching steady state condition, which is verified by achieving a constant outflow rate and constant water content values in the sensors placed along the permeameters. For example, for RMA soil the inflow adopted for tests at 100g's was 40 mlh, and at least 1 hour was necessary to achieve steady state.

During the subsequent drying stage, water inflow is stopped and the samples dry out to an imposed rotational speed. The drainage process is monitored, with the transient response being captured by the water content sensors. When a steady state condition is achieved (i.e. no flux and a steady water content profile) the soil samples are considered to have reached hydrostatic equilibrium. This means that the inner forces interaction forces between the soil particles and the water meniscus (suction) match forces the mass forces imposed by the external gravitational field. Assuming that the base of the sample

used as datum is held at zero suction (Plaisted, 2014), the imposed suction profile is described by the following equation:

$$\psi(z) = \frac{1}{2}\rho_w \omega^2 \left(r_o^2 - \left(r_o - z \right)^2 \right) \quad (22)$$

where ψ is the matric potential [M/L/T^2, Pa], z_m [L, m] is the position in the sample from the base of the specimen (toward the central axis of rotation), r_o is the radius at the base of the sample, ρ_w is the bulk density of water [M/L^3, kg/m^3], and ω is the angular velocity [rad/T, 1/s].

After equilibrium is achieved the water content (θ) and the void ratio (e) profiles are determined along the sample using a specific measurement technique. The values obtained are used to establish their relationship with the known suction (ψ) profile. The testing program conducted as part of this research incorporates the use of new measurement techniques. The measurement procedures are detailed in section 8.3.2.

Because non-destructive measurements are used in the approach developed in this study, the drying process can be repeated using different angular velocities. The soil sample is spun at a selected rotational velocity, hydrostatic equilibrium is achieved and the volumetric water content and the void ratio along the sample are determined. After completing this stage, the velocity is increased and the drying process begins again. The sample is spun until a new equilibrium state is achieved. This procedure is named multi-stage hydrostatic test and it allows determining multiple data points in the SWRS, at increasing suction values using the same soil sample.

3.2.2.5 Imposed flow test

The imposed flow (IF) tests were conducted to measure unsaturated hydraulic conductivity of the soil. In this test, a comparatively low infiltration rate is imposed under

a constant rotational velocity until achieving steady state flow (i.e. when a constant outflow rate and constant water content values are obtained from each sensor). Since the inflow rate is known and the gradient is measured, the hydraulic conductivity can be directly derived. The Darcy-Buckingham law for one-dimensional flow in the centrifuge can be written as function of the rotational speed and the pressure sources (McCartney, 2007; Plaisted 2014), as follows:

$$v = -k(\psi)\left(\frac{\omega^2}{g_1}\left(r_o - z\right) - \frac{1}{\rho_w g_1}\frac{d\psi}{dz}\right) \quad (23)$$

where v is the flux velocity [L/T, m/s], k is the hydraulic conductivity [L/T, m/s], ψ is the matric suction [M/L/T^2, Pa], ρ_w is the bulk density of water [M/L^3, kg/m^3], ω is the angular velocity [rad/T, 1/s], and g is the gravitational acceleration [L/T^2, 9.81 m/s^2].

Zornberg & McCartney (2010) proposed a procedure based on theoretical interpretations for cases when the suction gradient under steady state flow conditions is negligible in the upper section of the sample. In this way, imposing a rotational speed and inflow rate was sufficient to target a hydraulic conductivity value. In addition, a TDR was placed in the upper section of the sample in order to associate the imposed discharge value and unsaturated hydraulic conductivity to the measured water content.

Plaisted (2014) showed that the suction gradient might not be negligible across the soil sample. The suction across the sample was determined and the suction gradient was explicitly incorporated to calculate the unsaturated hydraulic conductivity. The suction profile was found to be dependent on both the water content and the void ratio profiles. A post-processing procedure was necessary to determine the suction profile as a function of the water content and void ratio, which were experimentally determined by using destructive tests.

The innovative features incorporated in the testing program conducted in this study included the determination of the void ratio and the volumetric water content profile in-flight (non-destructive). In order to calculate the hydraulic conductivity incorporating the total gradient, also a post-processing procedure was followed to determine the matric suction profile.

8.3.2 Measurements

In the two testing procedures described in section 8.3.1, it is necessary to determine the volumetric water content (θ) and the void ratio (e) profiles. They are used along with the imposed suction profile (ψ) in the hydrostatic tests (8.3.1.1) to determine the soil water retention surface (SWRS). In the imposed flow test once the water content and the void ratio are determined, the suction is calculated at each slice using the SWRS. Using this information, the suction gradient and the hydraulic conductivity can be calculated.

The measurement techniques implemented to measure these values may have a direct impact on the results. Three different measurement techniques were utilized in this research to determine the void ratio and water content profile: Destructive (D), Semi-destructive (SD), and Non-destructive (ND). In each one of these measurement techniques the data was collected as follows:

- Destructive (D): The permeameter tube holds an inner split-ring. After a target condition is achieved (e.g. steady state) the soil samples are removed from the centrifuge and sliced. The height of each ring is measured with a caliper, and the gravimetric water content and dry soil mass are measured by oven drying. The volumetric water content and the void ratio are then calculated using the measured results.

- Semi-destructive (SD): In this case the thickness of each layer is measured in-flight using the non-intrusive image analysis tool described in Chapter 6. The relative displacement between the markers is used to determine the change in height of each layer. The void ratio is calculated by considering that the soil dry mass remains constant in each sub-layer. After a target condition is achieved (e.g. steady state) the sample is removed from the centrifuge and the soil column is sliced at the position of each marker. The gravimetric water content is measured by oven drying. The volumetric water content is then calculated using the measured results.
- Non-Destructive (ND): Both the void ratio and the volumetric water content profiles are determined in-flight. The thickness of each layer is measured using the image analysis tool described in Chapter 6, and this information is used to calculate the void ratio profile. The volumetric water content profile is measured with the GTDR sensors described in Chapter 5.

A clear permeameter was developed to visualize the markers. Figure 61(a) illustrates the clean permeameter instrumented with three GTDRs. This permeameter setup was used for "SD" and "ND" measurements. Figure 61(b) shows the permeameter with the split rings. This permeameter setup was used for "D" measurements.

In order to report the results, the soil layers in tests conducted using the SD and ND measurement techniques were delimited by the markers at the end of the test. On the other hand, the soil layers reported using D measurements were delimited by the fix height of the split rings. Figure 62 illustrates the permeameter setup and the slicing procedure for the different measurement techniques.

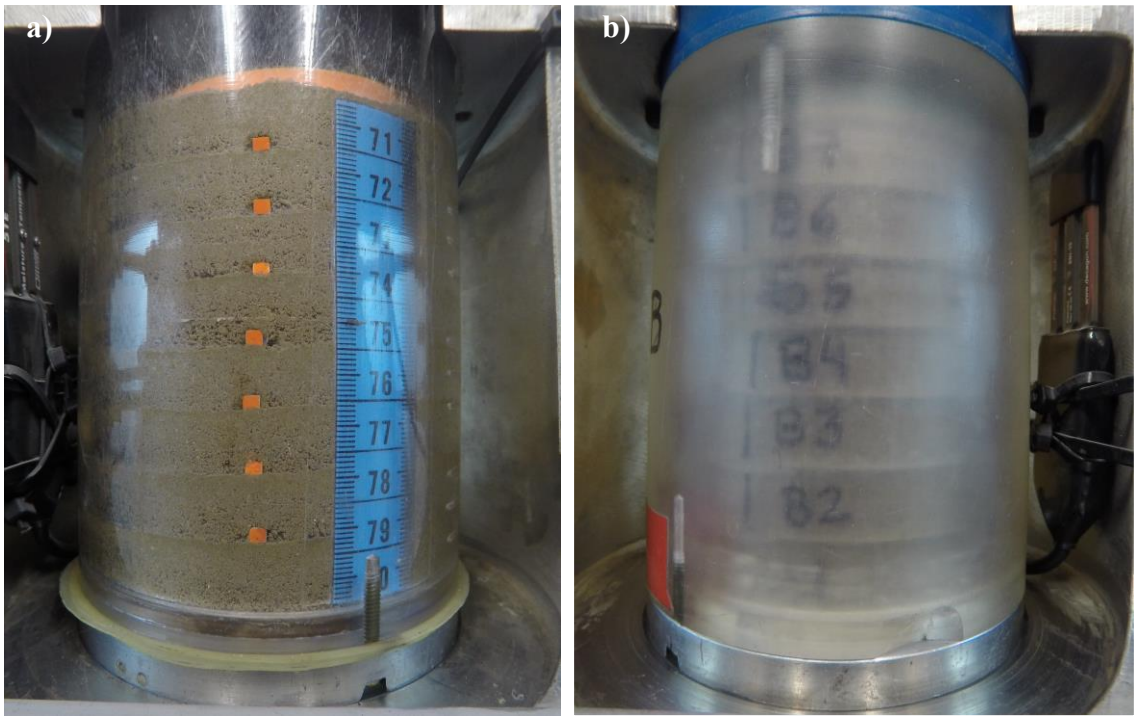

Figure 61. Permeameter setup for: a) ND and SD measurements and b) D measurements.

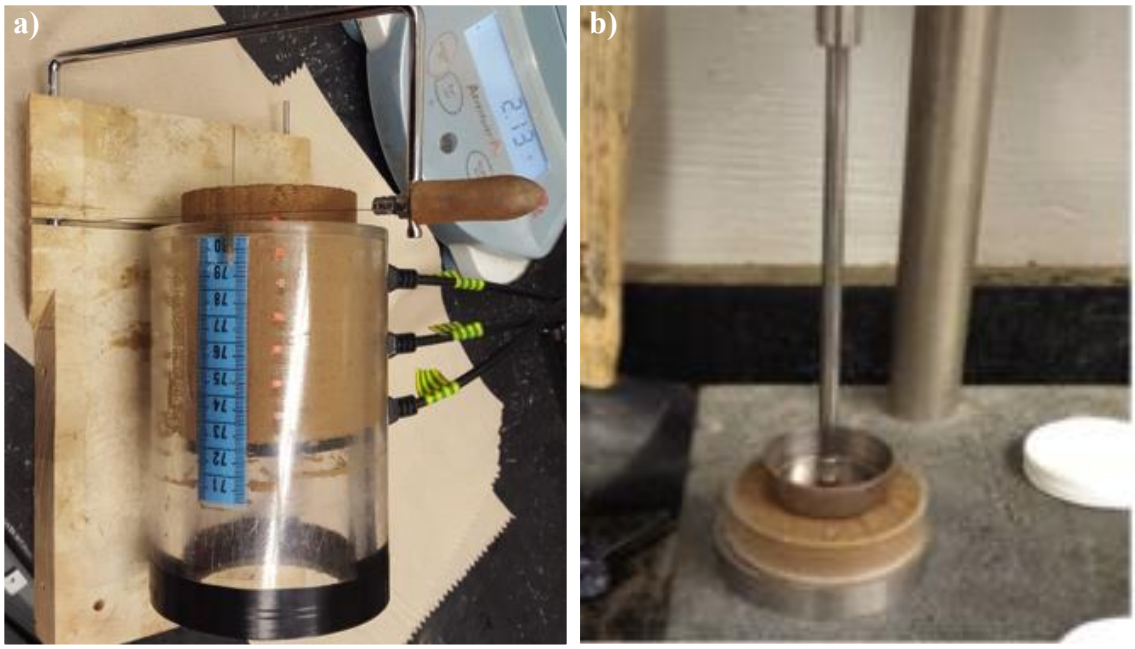

Figure 62. Soil samples being sliced and measured during: a) SD and b) D measurements.

8.3.3 Scope of the testing program

The scope of the testing program includes hydrostatic (H) tests conducted to determine the SWRS, as well as imposed flow (IF) tests, conducted to measure the unsaturated hydraulic conductivity. A series of test was performed which involved different initial densities and rotational speeds to characterize the unsaturated hydraulic properties of RMA soil. An important additional objective was to evaluate the new testing procedures and compare the different measurement techniques.

A summary of the test series conducted in this research component, including the initial soil conditions, drying stages and measurement techniques is provided in Table 7. The centrifuge equipment (CPUS) described in section 3.3.2 has two testing buckets. The soil samples placed on these buckets are identified as Sample A and Sample B, independently of the permeameter set up and the measurement technique used on each tess.

Table 7. Scope of centrifuge tests performed using RMA soil

Test	Date	Initial RC	Initial w_c	Test Type	Testing Stages	Equivalent g-level	Measurement technique	
[#]	[-]	[%]	[%]	[-]	[#]	[N]	Sample A	Sample B
1	12/15/16	90	15.0	H	1	90	ND/SD	D
2	12/19/16	80	15.0	H	1	90	ND/SD	D
3	2/6/17	90	14.7	H	MS	25/50/ 100/125	ND/SD	D
4	2/14/17	90	14.7	IF	1	100	ND/SD	D
5	12/15/16	90	14.7	H	1	25	ND/SD	ND/SD
6	12/15/16	90	14.7	H	1	50	ND/SD	ND/SD

8.4 EXPERIMENTAL RESULTS

The results from the Hydrostatic and Imposed flow tests are presented in this section. The results are grouped and presented according to the test type and the

measurement technique. These results complement those presented in Chapter 7 for the characterization of the unsaturated hydraulic properties of RMA soil.

During centrifuge testing the soil samples undergo changes in both volume and degree of saturation in response to the increased gravitational forces. The initial soil density and water content (as compacted) have a direct impact on the coupled hydro-mechanical response of the soil structure.

Samples were prepared at different initial density and tested at different rotational speed to investigate the soil-water retention capabilities of the RMA soil, as well as to examine the mechanical response of the soil samples during centrifuge testing. Hydrostatic tests were carried out to define the SWRS in one stage and multiple stage modes. The unsaturated hydraulic conductivity was measured using imposed flow test under steady state conditions.

The combinations of testing procedures and sample initial conditions indicated in the testing scope were selected to isolate the impact in the final results of the main factors intervening such as, the soil mechanical response, measurement technique, and sensor response. The analysis of the experimental results is structured following the same reasoning. Each sub-section provides additional insight on a specific testing factor.

8.4.1 Hydrostatic test: Comparison of results using semi-destructive (SD) and destructive (D) measurement techniques

The Hydrostatic tests were conducted in order to obtain data to define the SWRS. In this section a comparison of the results using SD and D measurement techniques is provided. In both, the SD and D measurement techniques the volumetric water content is obtained as the product of the dry unit weight and gravimetric water content. In this section an analysis of the results from Test #1, listed in Table 7 (90% RC, 90 g) is presented in detail to compare the results obtained using these measurements techniques.

8.4.1.1 Dry Unit weight

For both SD and D measuring techniques only a single set of [e, θ, ψ] results can be obtained along the sample height after the drainage stage in the test is completed. Figure 63 illustrates the dry unit weight density profiles obtained using Semi-Destructive (Sample A) and Destructive (Sample B) measurements techniques. The point measurements correspond to the values measured at each layer, non-destructively for sample A and destructively for sample B.

Figure 63(a) shows that the unit weight of Sample A remains almost constant from the beginning to the end of the test. These measurements were performed in-flight with a non-intrusive system. On the other hand, Figure 63(b) shows that despite testing very similar soil samples, the final unit weight in all layers of Sample B is lower than the initial (as compacted) unit weight. In this case the measurements were performed destructively after the centrifuge was stopped and the sample removed from the buckets.

In order to provide an additional insight, the overall volumetric behavior of the soil samples was also monitored using an LVDT on top of the soil samples. Figure 64 illustrates the displacements measured at the top of the soil sample during all the testing stages. This is a typical behavior of the soil samples during one-stage hydrostatic test. There is an initial compression during the centrifuge spin up caused by the increased gravitational field. It is followed by an additional compression during the wetting and drying stages caused by the increment in the soil unit weight, and finally, there is a decompression of the soil samples when the centrifuge stops.

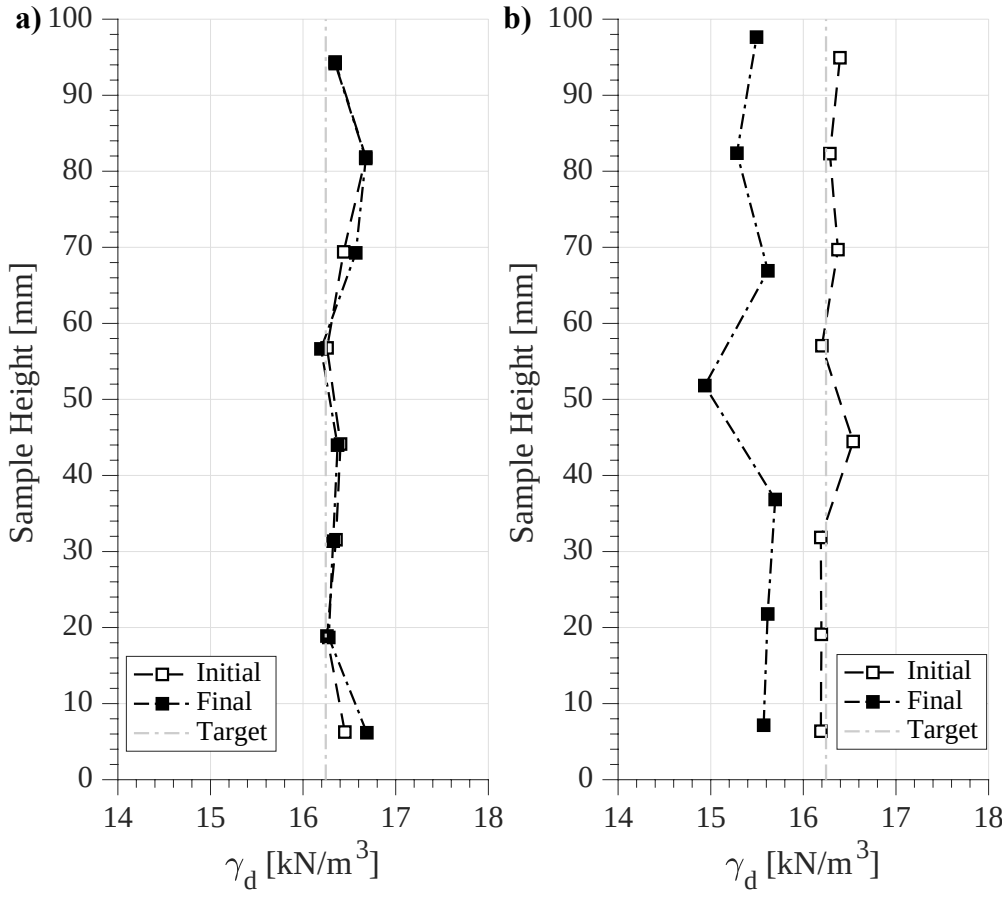

Figure 63. Dry unit weight profiles of Test #1 for: a) Sample A (SD) in flight and b) Sample B (D) after slicing.

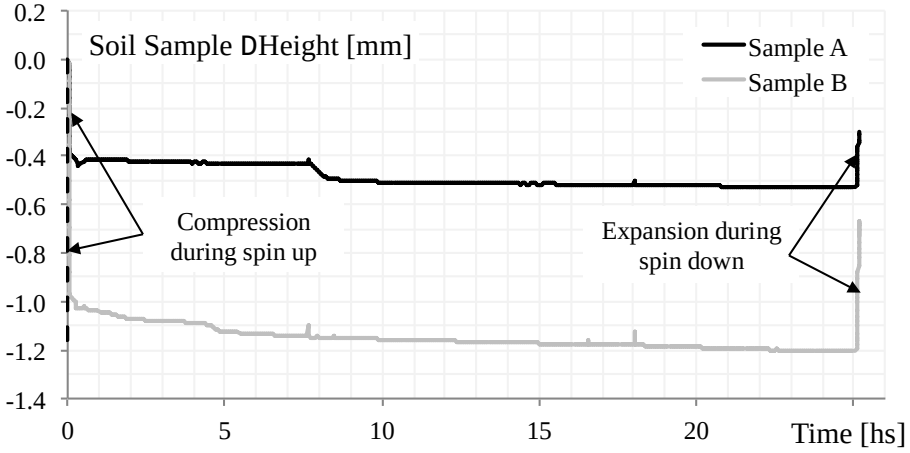

Figure 64. External deformation measurements for Test #1.

This information was used to calculate the average dry unit weight of each sample and can be compared with the results previously showed in Figure 63. In sample A, the top displacement measured in-flight corresponds to a compression of -0.5% based on the LVDT. This value had a good agreement with a -0.2% measured with the image analysis (IA) technique. In this case, the average dry unit weight results in an estimated range of 16.4 to16.5 kN/m^3. After the centrifuge was stopped, and the sample was removed a rebound of 0.15% was measured with caliper in the workbench. The dry average unit weight is 16.38 kN/m^3, almost identical to the initial value.

In sample B, the displacement measured with the LVDT showed a maximum compression of about -1.2% in-flight and a rebound measured in the workbench of 0.3%. These values correspond to dry unit weights of 16.2 and 16.0 kN/m^3, and cannot reproduce the lower density measured using the slicing procedure.

However, the total height of the sample is calculated using the sum of the height of all the slices, a rebound of about 4% is obtained. The corresponding average dry unit weight is 15.4 kN/m^3. This result matches (on average) the density profile in Figure 63b.

It can be observed that, for Test#1 both samples show essentially elastic behavior for this initial unit weight and moisture at compaction and the loads applied through centrifugation. Changes in the overall dry unit weight with the inflight IA tool agree with the measurements obtained using the external LVDT. Even after the centrifuge stops, and the imposed stresses are removed, the rebound measured in the workbench was not substantial to modify the dry unit weight.

However, the destructive measurement technique used in Sample B to determine the soil layers height and calculate the sample dry unit weight profile influenced the actual results. The slicing procedure induced an additional rebound that reduces the dry

unit weight of each layer. Accordingly, the cumulative rebound of all the layers results in a total height that differs with the external measurement performed outside the centrifuge.

The results obtained from Test #1 show that the most relevant factor creating the decompression was the slicing of the soil sample between the rings, and not the removal of the imposed stresses during centrifugation. In addition, it indicates that the soil dry unit weight is underestimated when this destructive measurement technique is used.

8.4.1.2 Gravimetric water content

The gravimetric water content is measured, in both the SD and D measurement techniques, slicing the soil samples after the centrifuge stops. The values obtained for both samples in Test #1 are presented in Figure 65. As expected, the gravimetric water content profiles in both soil samples are very similar. The profile shows a distribution with essentially constant gravimetric water content in the upper half of the soil sample.

Stopping the centrifuge and slicing the soil samples may take between 20 to 40 minutes. A source of error that could be identified in this procedure is assuming that after reducing the gravitational forces the water migration between layers is negligible.

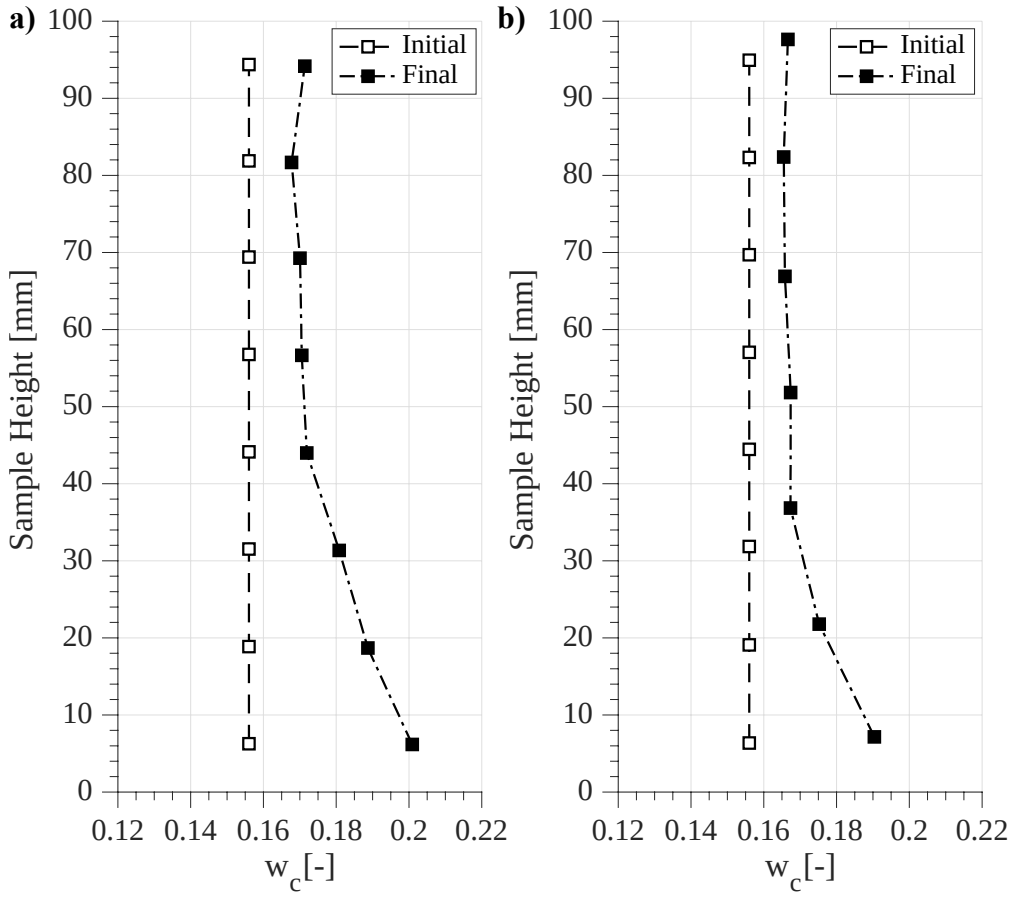

Figure 65. Water content distribution of Test#1 after slicing: a) Sample A (SD) and b) Sample B (D).

8.4.1.3 Volumetric water content and degree of saturation

The results of Figure 63 (density) and Figure 65 (gravimetric water content) are used to define the volumetric water content (θ) and the degree of saturation (Sr) profiles (Figure 66) at equilibrium. Although the gravimetric water content profiles are essentially identical, the volumetric water content and saturation (Sr) profiles in sample B are lower than in Sample A as a result of the lower unit weight.

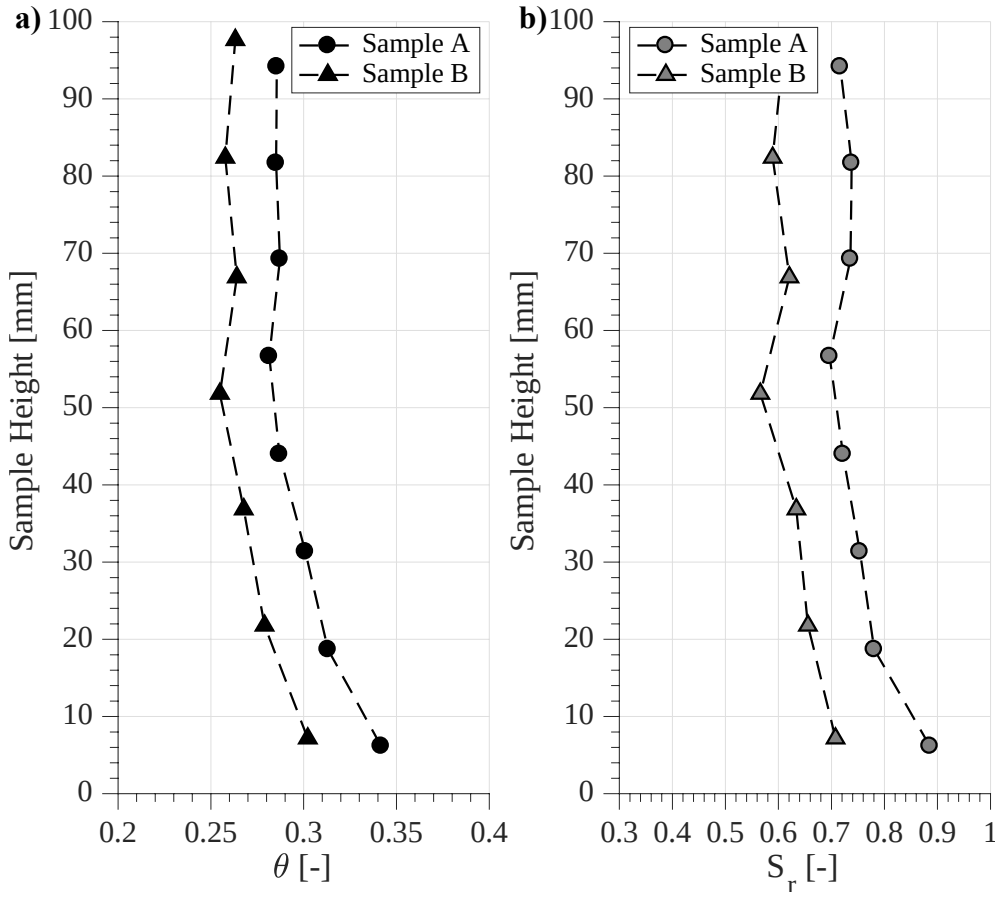

Figure 66. Comparison of samples A and B of Test #1 using: a) volumetric water content (θ), and b) the degree of saturation (Sr) profiles.

The results presented in Figure 66 for each soil layer are combined with the suction profile at hydrostatic equilibrium described by the equation (22). This information could be used to provide typical representations of the SWRC of the soil.

Figure 67 shows the correlation for both samples of Test #1 between the water content vs. suction and degree of saturation vs. suction. The results show in both planes an offset between Sample A and Sample B. In this case, the offset between each set of curves could be attributed to the difference in the density of the soil samples.

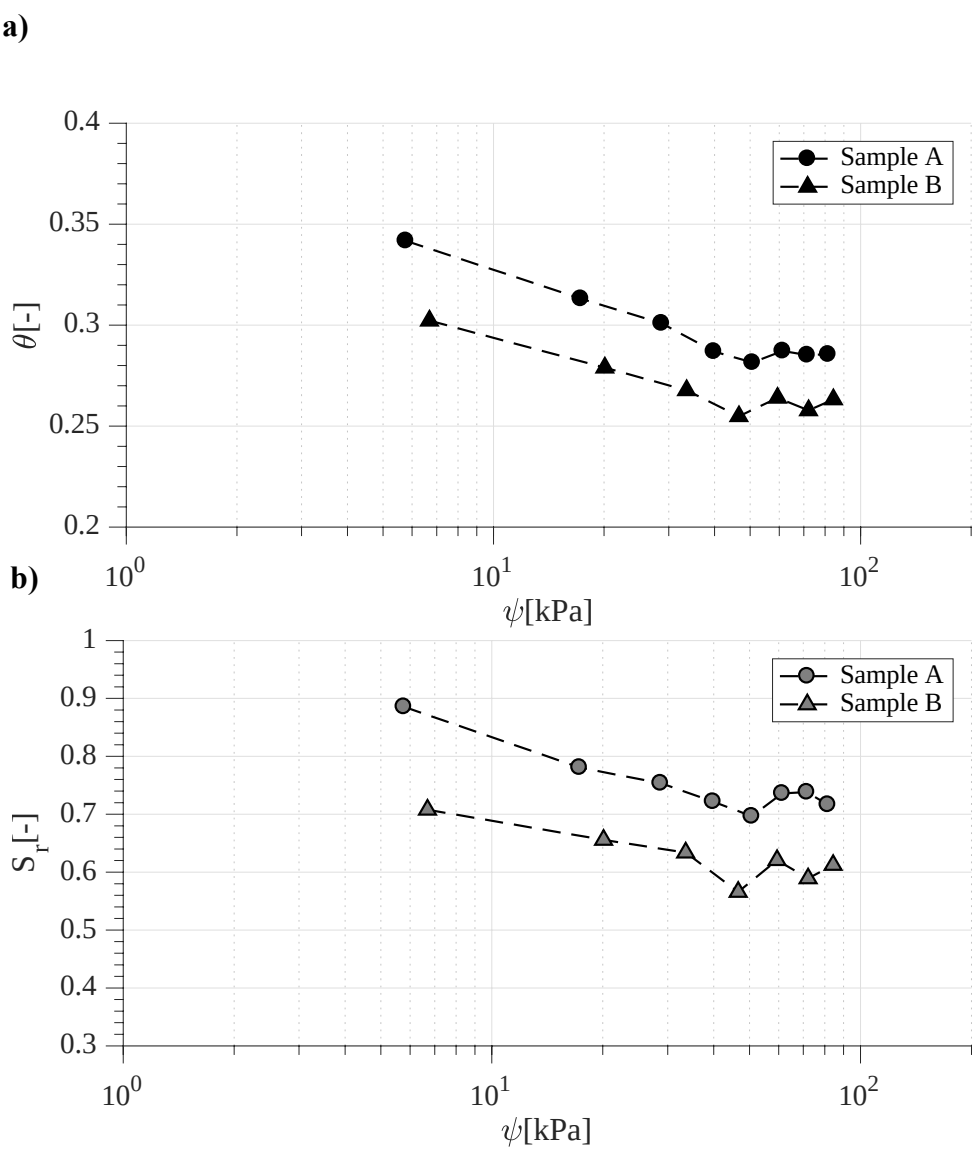

Figure 67. Test#1, SWRC represented as a function of: a) θ and b) Sr.

Incorporating the void ratio as a third variable provides a better understanding of the results of hydraulic characterization tests. The data is represented in the [S_r, e, ψ] space to define the SWRS. This figure now concentrates all the information available and the impact of the soil sample density in the results is explicitly included.

Figure 68 shows the three plane views of the SWRS. Figure 68(a) provides the same information as Figure 67, but is now complemented by two additional planes.

Figure 68(b) provides the correlation between the degree of saturation vs. void ratio. The difference in density created by the slicing procedure is now clearly observed as an offset in the void ratio. In consequence, this increase in volume of the soil sample reduces the corresponding degree of saturation. Figure 68(c) shows the relation between the void ratio vs. suction values, this image also indicates that the offset in void ratio does not depend of the suction value imposed by the centrifuge environment, and it is related to the measuring technique selected.

Moreover, using the information provided by the SWRS (Figure 68) it is possible to back-calculate the values in Figure 63 (unit weight) and Figure 65 (gravimetric water content). This is not possible if only the information in Figure 67 is available.

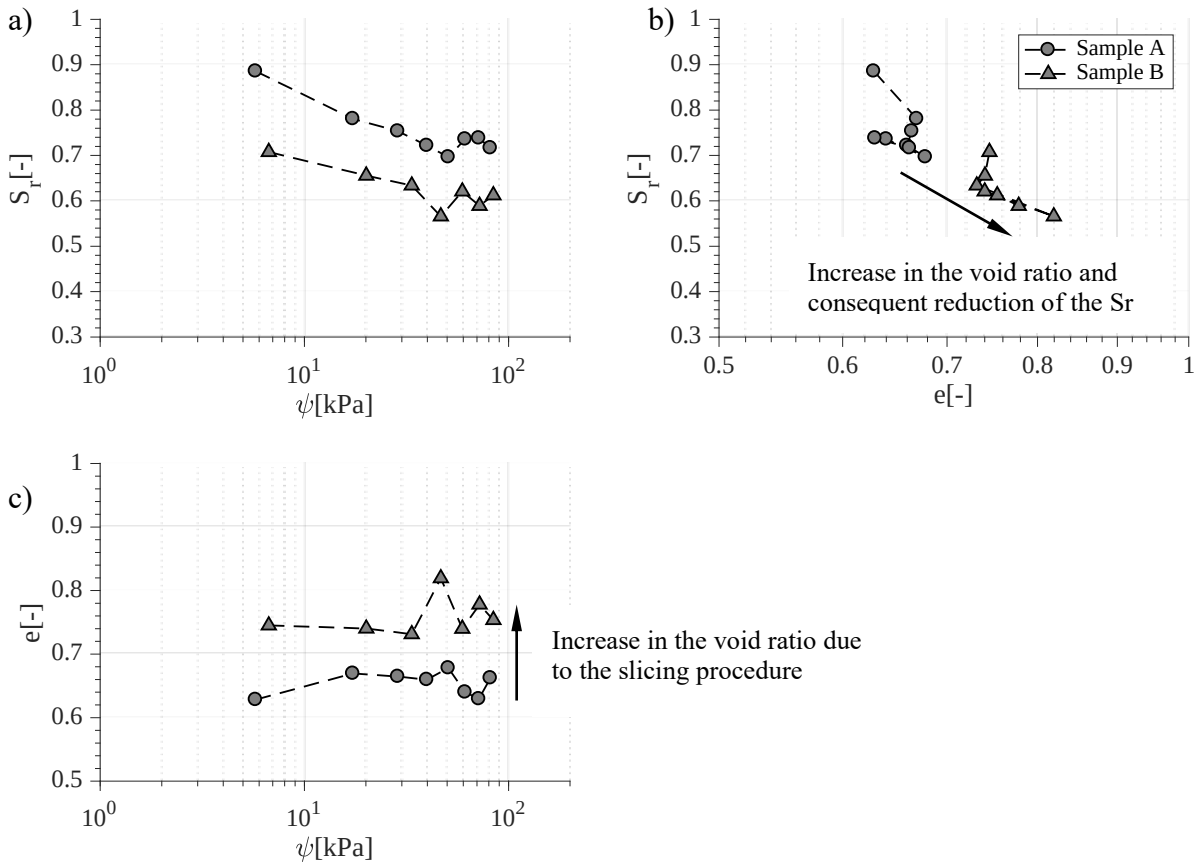

Figure 68. Plane views of the SWRS from Test# 1: a) Representation of SWRC in the Sr-ψ plane, and complementary views, b) lateral view Sr-e, and c) top view e-ψ.

8.4.2 Hydrostatic test: Results using Non-destructive (ND) measurement technique

In typically infiltration columns set-up, the information needed to define the soil SWRC can be obtained by monitoring the volumetric water content and suction with sensors at the same location. The changes in density are typically ignored and the soil is assumed to remain rigid.

In this research component, the determination of SWRS data points includes measuring both the density and the water content in-flight without disturbing the soil sample. This procedure is referred to as Non-Destructive (ND) measurement technique.

Several benefits can be recognized from the implementation of this technique. Measurements are performed in-flight at the corresponding state of stresses. Also, both measurement systems are non-intrusive and in consequence they do not interfere with the soil deformation. In addition, the transient response of the soil can be monitored upon wetting and drying; there are no limitations in the range of values being measured. Finally, in comparison to the previously presented SD and D measurement techniques, several drying stages can be performed over the same sample if desired.

8.4.2.1 Non-intrusive sensor set-up

Figure 69(a) illustrates the discretization of the soil layers used to calculate the unit weight, and the void ratio profile along the soil sample. The change in height of each soil layer is calculated as the difference between the displacement of the top and bottom marker using the protocols described in Chapter 6. This information can be used to estimate the volume changes along the soil sample during the test. Figure 69(b) shows the sections where the volumetric water content is measured using the non-intrusive sensors GTDR described in Chapter 5. While the density is discretized in eight layers, only three nodes are available to determine the moisture content profile.

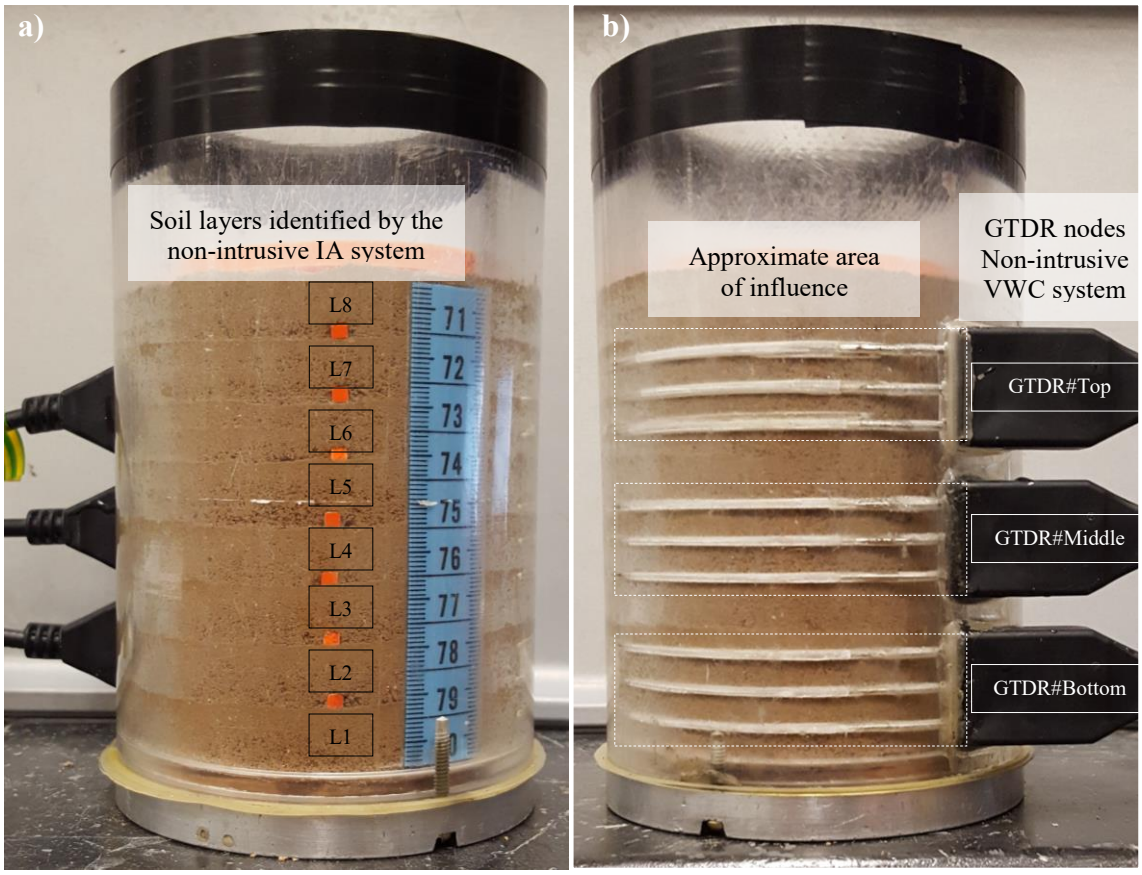

Figure 69. Scheme for Non-Destructive measurement technique indicating: a) soil layering to calculate deformation and density profiles, and b) GTDR nodes to measure the volumetric water content.

8.4.2.2 Deformation measurements time response

The results obtained from Sample A of Test #1 are presented in order to demonstrate the capabilities of the ND measurement technique. In this particular test, the RMA soil compacted at 90% RC and tested at 90 g's, showed small displacements for all the layers. Figure 70 illustrates the change in height of each layer during the test. The dry unit weight of each layer can be calculated based on the updated height of the layer at any time during the test. The dry unit weight profile at the end of the test for Sample A was presented in Figure 63(a).

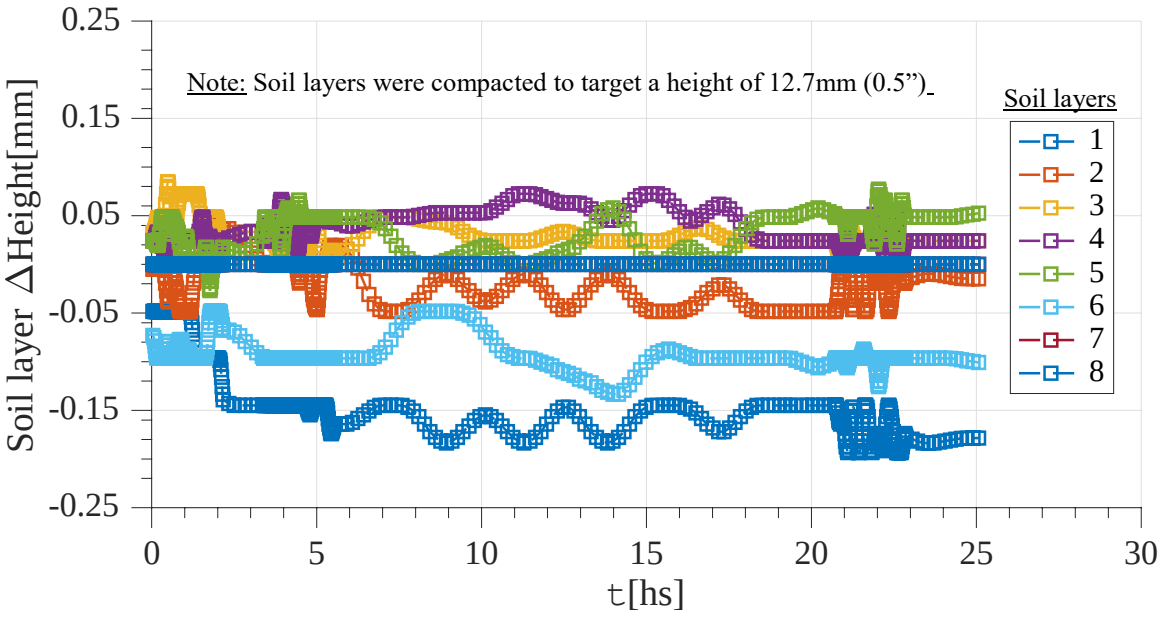

Figure 70. Change in height of each soil layer for Sample A during Test #1.

8.4.2.3 Volumetric water content time response

The time response of the three GTDR for Sample A of Test #1 is presented in terms of the apparent dielectric conductivity in Figure 71(a). These values are obtained after filtering the raw results provided by CSI software. In this case, the average response of the top and middle GTDRs is clearly defined. On the other hand, the apparent dielectric conductivity values obtained for the bottom GTDR have a considerable scatter. However, the scatter in these measurements is created as result of a wrong interpretation of the waveforms and not due to a malfunction of the sensor itself.

A calibration curve is used to obtain the volumetric water content presented in Figure 71(b). Since the calibration curve is an increasing function (third degree polynomial) the transient response in both Figure 71(a) and Figure 71(b) is very similar, and the analysis of the time response of the sensors could be done using any of these figures.

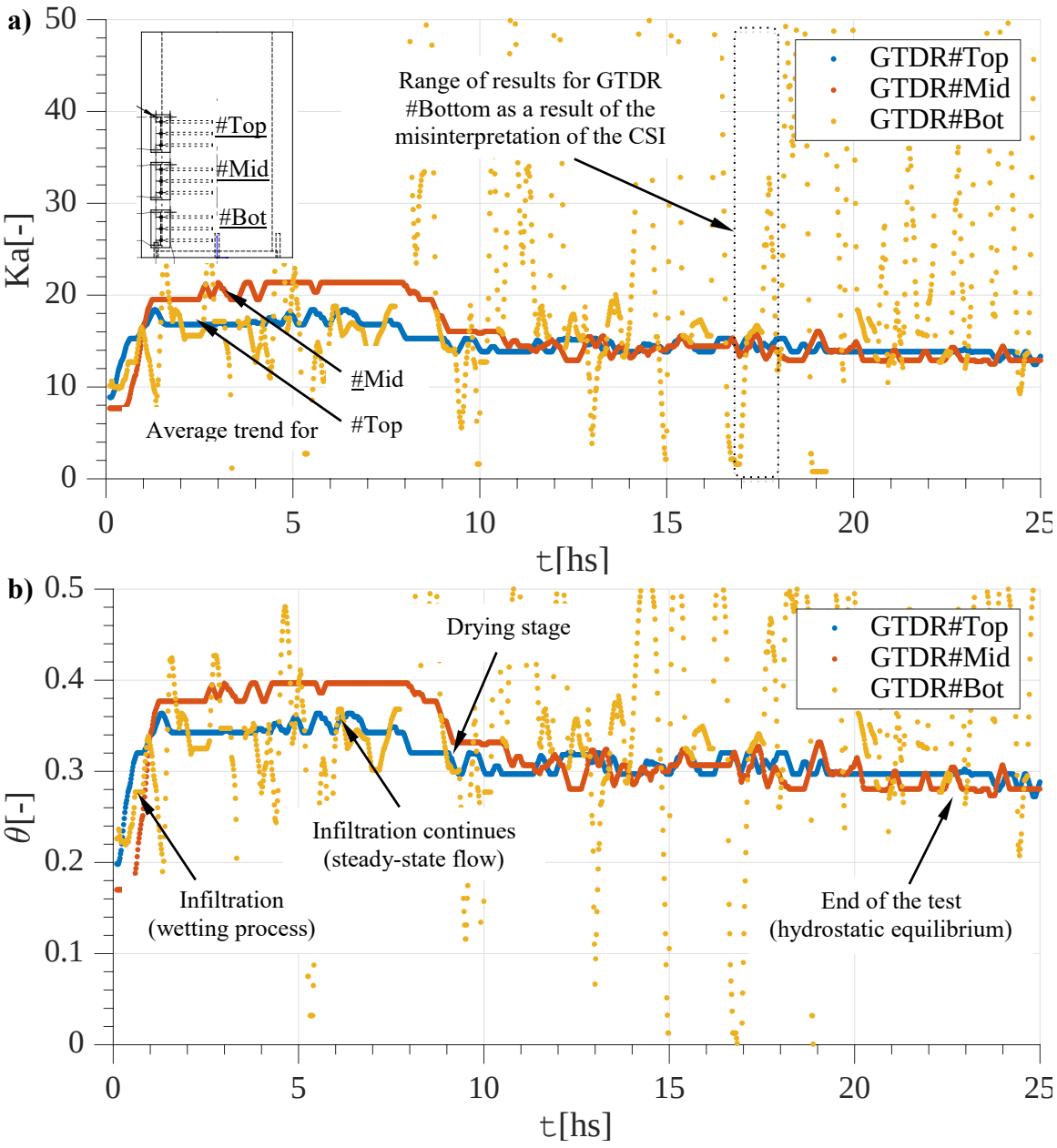

Figure 71. GTDRs time response represented by: a) apparent dielectric conductivity, and b) volumetric water content.

The infiltration process presented in Figure 71(b) is characterized by a gradual increase of the water content during the first two hours until a constant value is observed for each sensor. A delay between the top and middle sensor is observed as result of the

water advance. The inflow rate was maintained constant to confirm the steady state condition (constant inflow and outflow, and constant water content in the soil column). After 7 hours, the inflow pumps were shut down and the drying process began. The test was continued until no outflow was observed and the water content at hydrostatic equilibrium remained constant at the location of the three sensors.

The results provided by the CSI software for the bottom GTDR in Test #1 showed a significant scatter in the measurements. This outcome was repeated in other tests and sensors. In order to address this problem, the AWIGF algorithm (Scwartz et al. 2013) was used to re-analyze the recorded waveforms, and to obtain an additional set of apparent dielectric conductivity values. A calibration curve specifically obtained for this procedure was also used to obtain the corresponding volumetric content values.

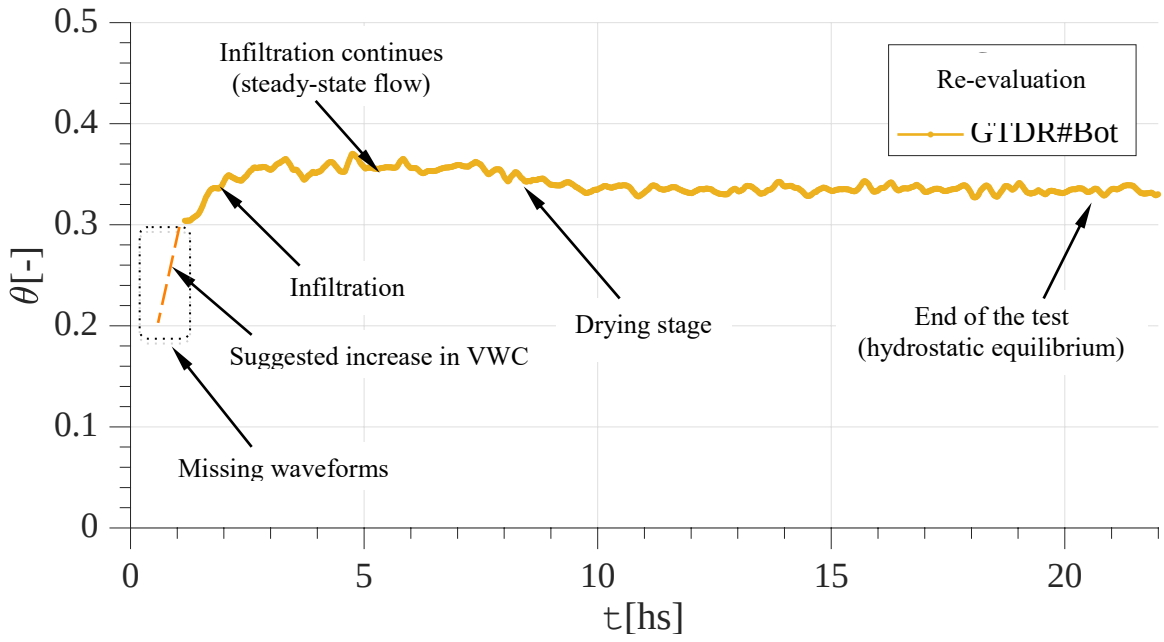

Figure 72. Reinterpretation of GTDR #Bottom waveforms using AWIGF algorithm to determine the volumetric water content.

Figure 72 provides the volumetric water content measurement for the bottom GTDR in Test #1 using AWIGF. Since the waveforms were only recorded between 1.5 and 25 hours of testing, the initial gradual increase in the water content is not observed during the infiltration. However, the water content reaches a steady value after two hours. A reduction of the water content is observed between the 7 and 10 hours of testing during the drying stage. These times match the dynamics of the top and middle sensors described in Figure 71(b). The results presented in Figure 72 confirm that for the same sensor and waveforms using the AWIGF algorithm provides a much more stable result.

8.4.2.4 Comparison of results for hydrostatic test between Non-Destructive, Semi-Destructive and Destructive measurement techniques

After hydrostatic equilibrium has been achieved an average water content value is obtained for each GTDR sensor. This value is associated with a suction value at estimated at the center location of the GTDR.

Figure 73 provides a direct comparison between the results from the GTDR (ND), and the SD and D measurement for Test #1. The results show a good agreement between the different techniques for the top and mid sensor based on the CSI results. The bottom sensor matches the SD results after reinterpreting the waveforms using AWIGF.

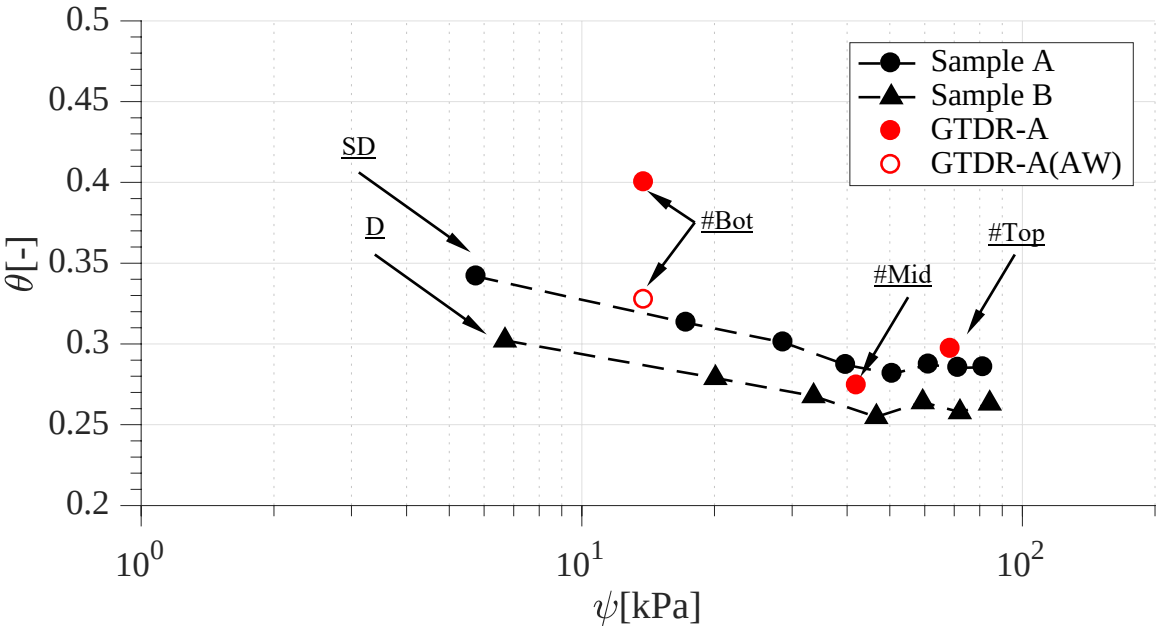

Figure 73. SWRC information based on ND measurements (GTDR).

In order to calculate the degree of saturation at the location of each sensor it is necessary to estimate a representative void ratio for each GTDR node. The void ratio values associated to each GTDR are calculated as an average void ratio from the soil layers in the area of influence of each sensor (Figure 69). Figure 74 provides a comparison of the ND, SD, and D measurement techniques results in the SWRS space.

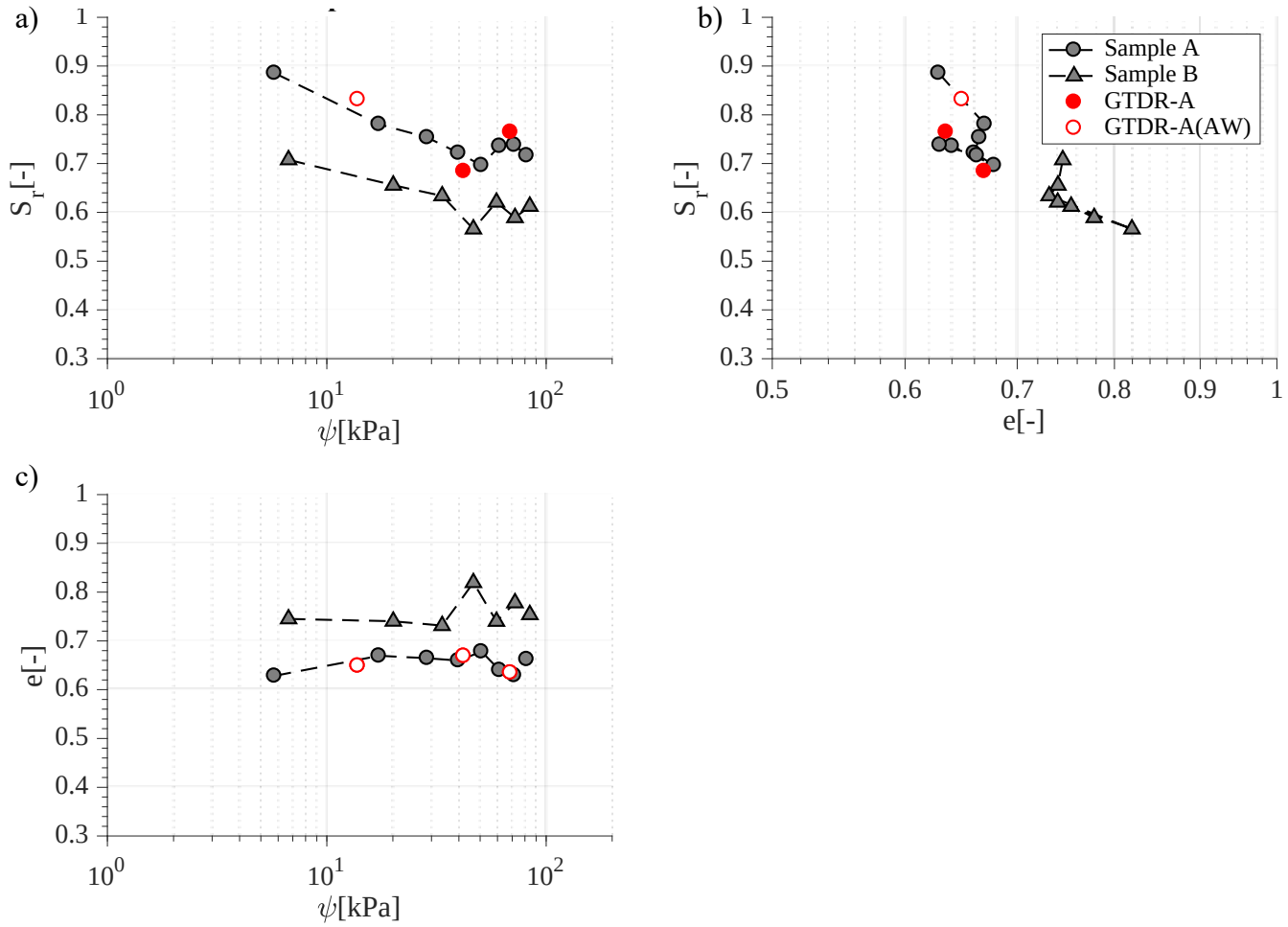

Figure 74. Comparison of SWRS results for Sample A of Test #1 using. ND, SD and D measurement techniques: a) Representation of SWRC in the Sr-ψ plane, and complementary views b) Sr-e, and c) e-ψ views.

8.4.3 Transient analysis based on ND measurements from a hydrostatic test

The ND measurement technique can provide additional insight about the transient flow process. The sample is divided in soil layers delimited between markers and this information is used to determine the dry unit weight and void ratio of each layer. However, there are only three GTDR sensors to estimate the distribution of the volumetric water content along the soil column. In order to produce a more detailed profile a volumetric water content value is assigned to each layer according to their relative position with the GTDRs (Figure 75a). This is a simplified interpretation, but useful particularly to describe a transient flow process.

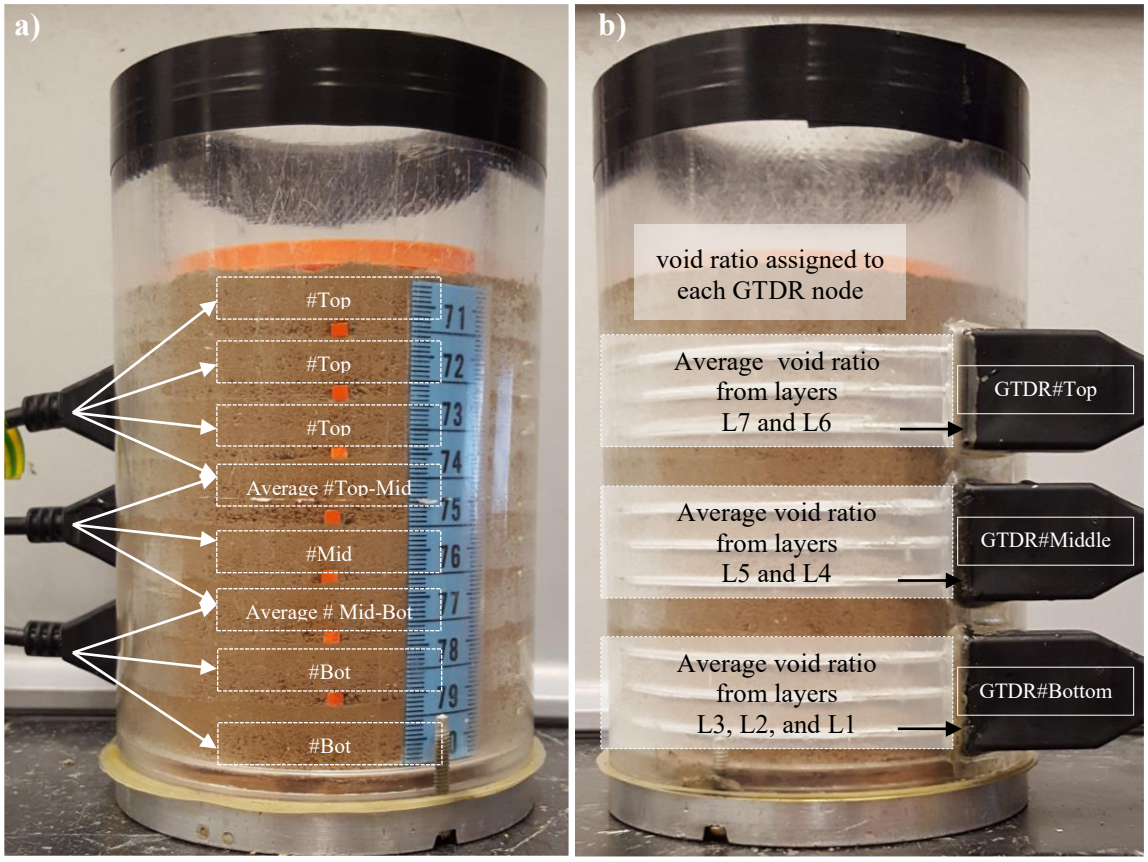

Figure 75. Combination of ND measurements: a) water content assigned to each soil layer, and b) void ratio for each GTDR node.

Figure 76 summarizes the values obtained for Sample A during the infiltration process of Test #1. Figure 76(a) shows the unit weight profile obtained using the image analysis tool, Figure 76(b) presents the volumetric water content profile estimated using the three GTDR sensors, and Figure 76(c) illustrates the degree of saturation (Sr) profiles that combines both previous measurements. These profiles were defined at different intervals to show the advance of the water through the soil sample.

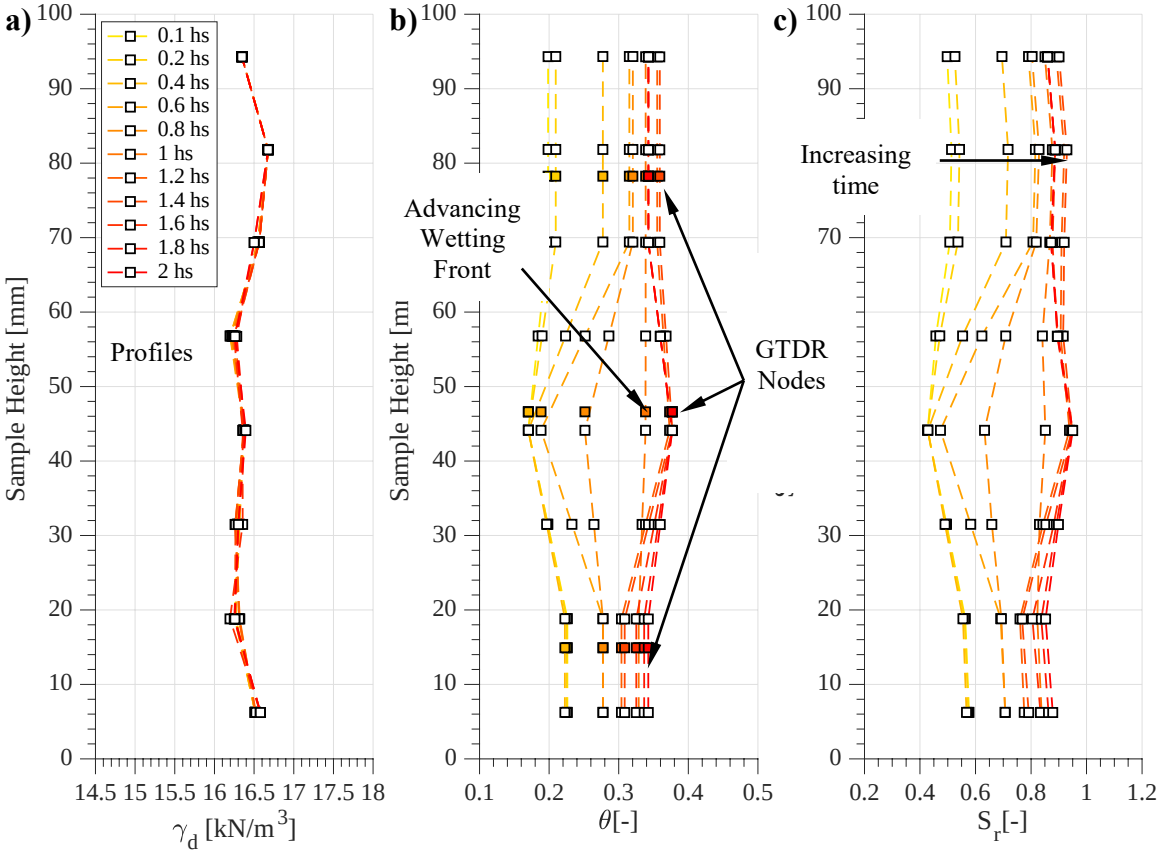

Figure 76. Infiltration stage profiles for Sample A of Test #1 including: a) dry unit weight calculated using image analysis, b) volumetric water content estimated using GTDRs, and c) degree of saturation.

After 2 hours of testing the degree of saturation, the profile reaches its maximum value at the bottom of the sample and it remains constant. In Test #1 the beginning of constant outflow was measured approximately after two hours of testing as well.

The drying stage started after 7 hours of testing. The transient profiles during this stage are presented in Figure 77. The drying stage is completed when hydrostatic equilibrium is achieved. This condition matches the end of outflow and a steady saturation profile. In Test #1 hydrostatic equilibrium was achieved after 17 hours of drying (24 hours of testing).

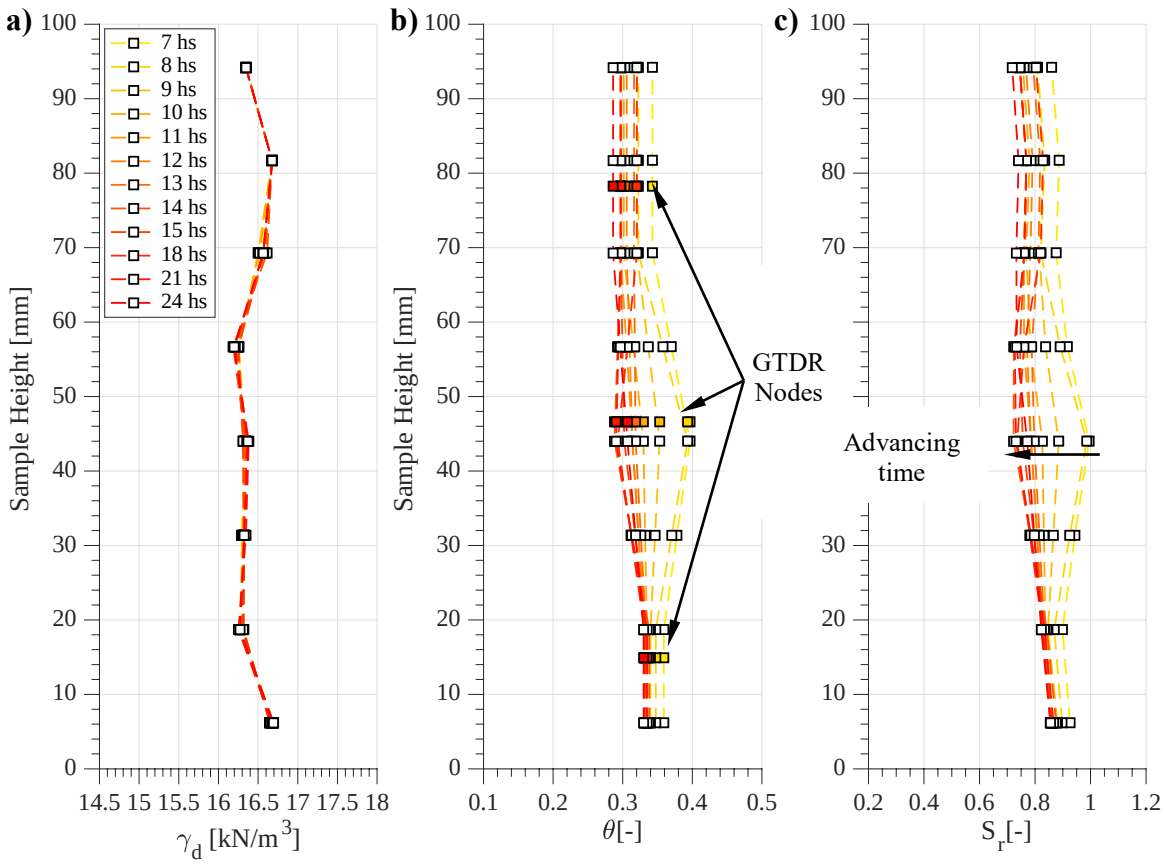

Figure 77. Drying stage profiles for Sample A of Test #1 including: a) dry unit weight calculated using image analysis, b) volumetric water content estimated using GTDRs, and c) degree of saturation.

8.4.4 Multistage hydrostatic test using ND measurements

In Test #3 multiple drying stages were carried out in order to obtain multiple data sets from the same soil sample using the ND measurement technique. Each drying stage is initiated when the rotational speed is increased, consequently increasing the gravitational forces and the "suction" imposed to reach hydrostatic equilibrium. As a result the water content on each layer is reduced progressively on each stage. The response of the GTDR sensors and the outflow recorded for Sample A are presented in Figure 78 (a) and (b) respectively, including the infiltration and the four drying stages.

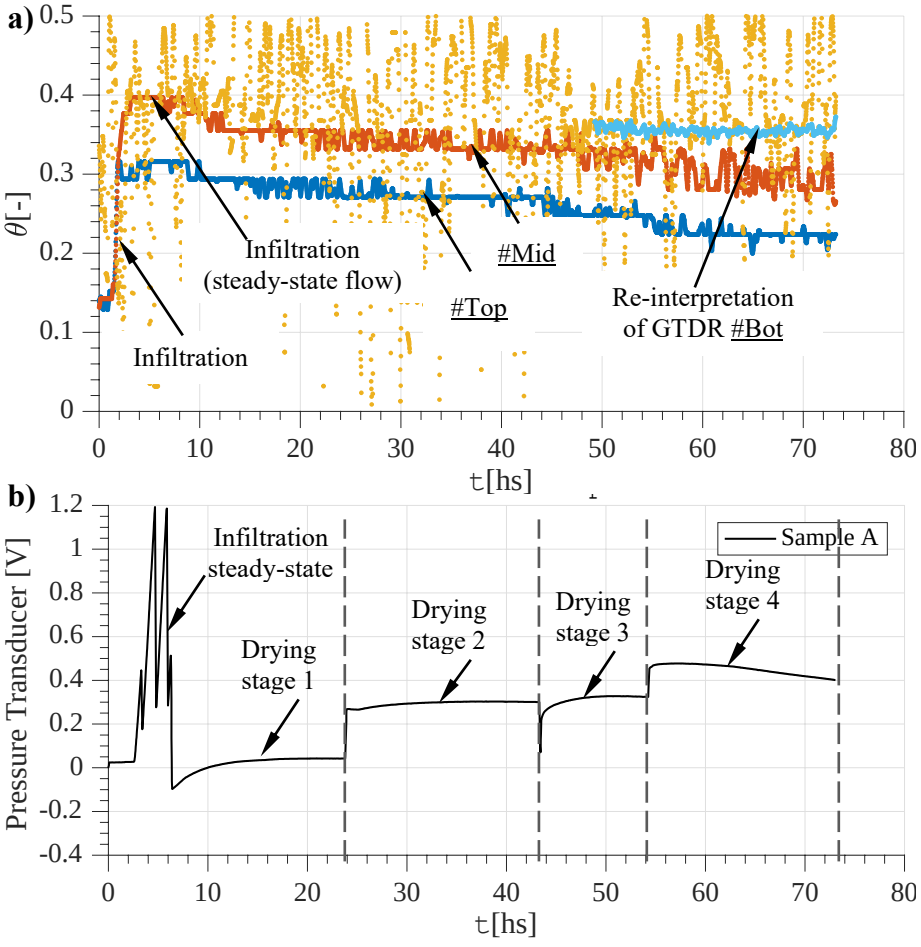

Figure 78. Transient response in a multistage test: a) water content, and b) outflow.

Figure 78(a) shows a gradual increase of the water content during the infiltration stage until a maximum value is reached in all sensors. At this point in time water reached the far end and the outflow sensor reports a change in voltage. The constant slope of the change in voltage with time also indicates that a steady state outflow has been reached.

A similar transient behavior is observed after each drying stage is initiated. The GTDR sensors show a reduction in their values and the outflow voltage readings increase following a parabolic curve with an outflow rate that decreases with time. Hydrostatic equilibrium is achieved after all the sensors reach a steady value.

A few singularities can be indicated in Figure 78(b). During the infiltration process several steps down in the voltage readings of the outflow sensor were observed as result of flushing of the reservoir. Every time a new drying stage was initiated, a step up in the voltage readings were observed as consequence of the increase in stresses applied to the pressure sensor. In the last stage, a reduction in the voltage readings was reported, this could indicate the presence of leakage in the outflow system at high speeds.

Figure 78(a) illustrates the readings from the GTDR sensors in Test #4, the sensor located at the bottom of the soil column presented considerable scatter in the results obtained using the CSI software. In this test the waveforms were saved only for the last stage and therefore, the re-interpretation using AWIGF was limited to the last hours of testing. The results are superimposed in Figure 78(a), where it can be observed that the scatter in the readings was considerably reduced indicating a good performance of the sensor..

Figure 79 show the dry unit weight, water content and degree of saturation profiles at the end of each drying stage. The suction profile at hydrostatic equilibrium estimated for each stage is also included.

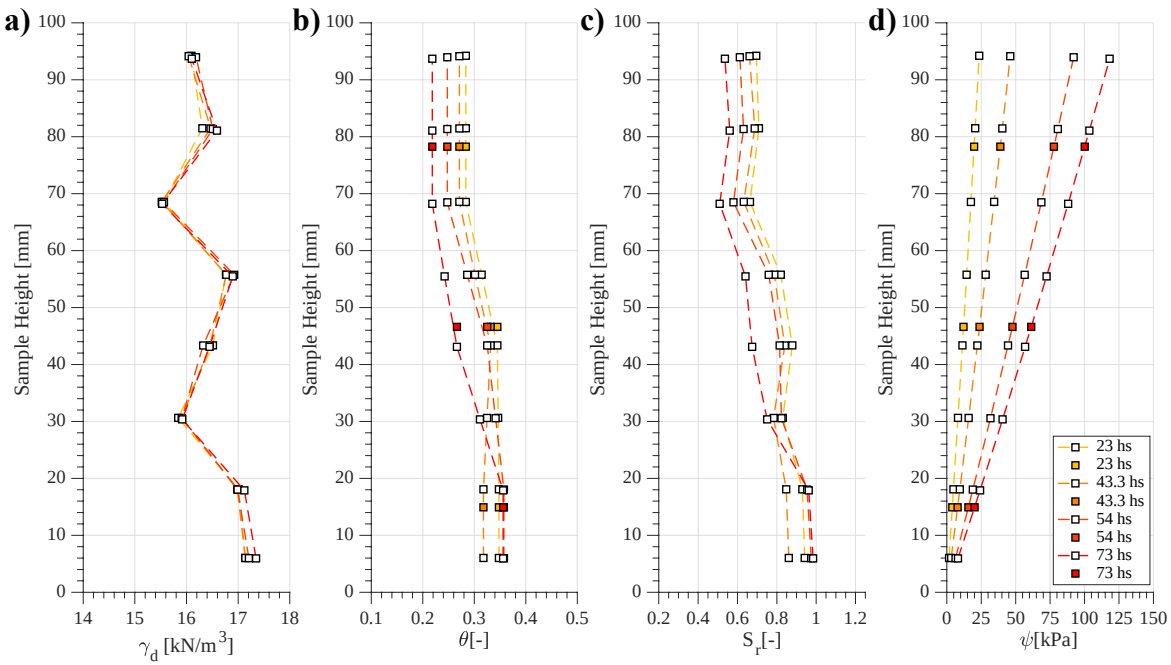

Figure 79. Profiles at hydrostatic equilibrium for 25,50,100 and 125g's of Test #3: a) dry unit weight, b) volumetric water content, c) degree of saturation, and d) suction.(imposed) at equilibrium.

After the multi-stage test was finished at 125g's, additional measurements were obtained using the SD measurement technique. All These results are used to define the SWRS and are compared together in Figure 80.

Figure 80(a) illustrates the correlation between the degree of saturation and the suction at each equilibrium stage. It can be observed that for all GTDR nodes (top, mid, bottom) every time the rotational speed increases, the suction increases and this creates an offset of the data points along the suction axis. Also, for each GTDR node the degree of saturation is reduced with each stage. While the bottom GTDR remains almost constant for imposed suction between 4 to 20 kPa, the soil around the top GTDR undergoes a substantial change in water content when changing from 20 to 100 kPa. Although the results show a certain scatter in the degree of saturation measured at the same suction, all the measurements lie within a narrow range.

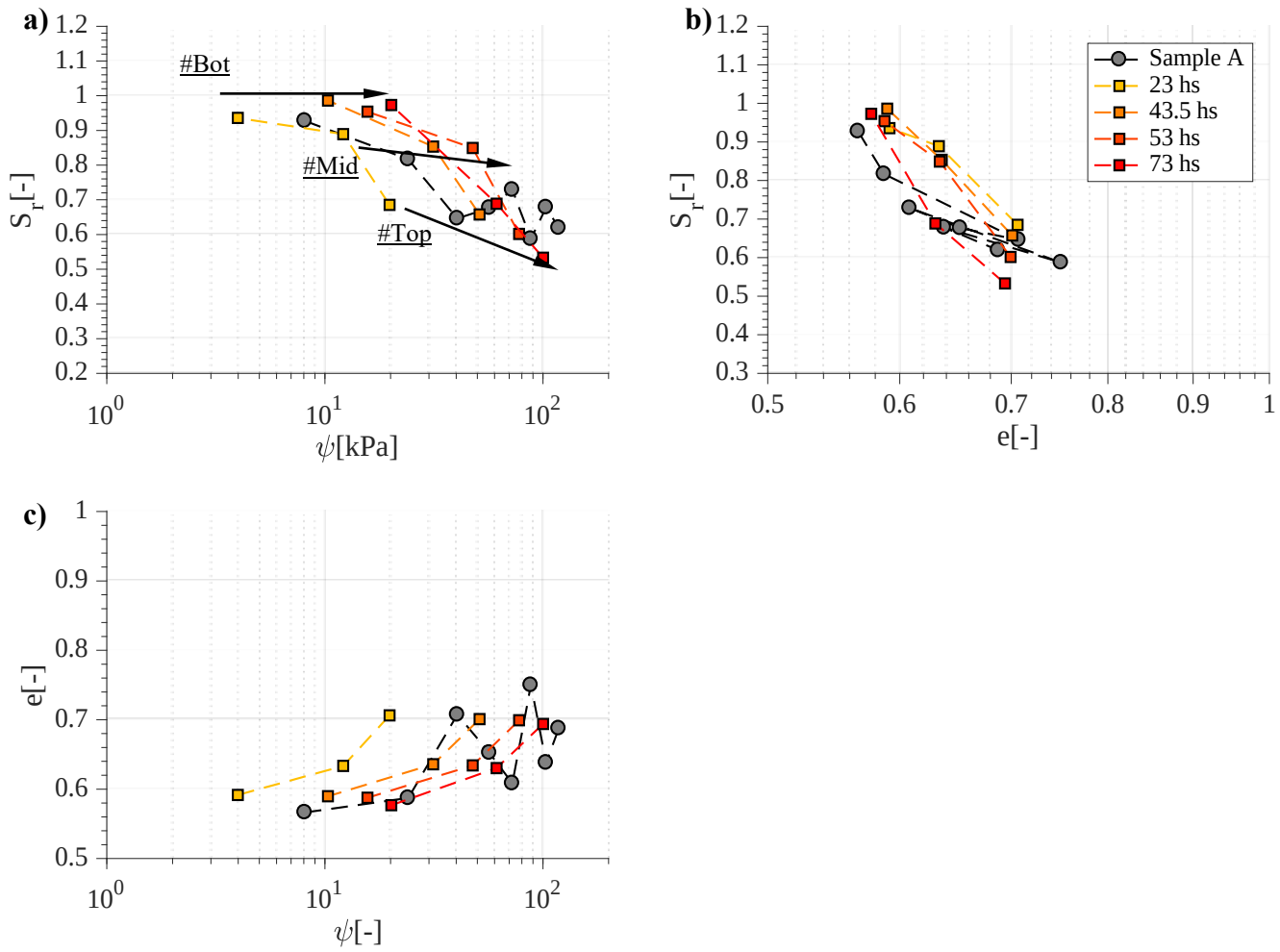

Figure 80. SWRS plane views for multistage test: a) SWRC in Sr-ψ, b) lateral view Sr-e, and c) top view e-ψ.

8.4.5 Hydrostatic test: effect of the initial conditions in the mechanical response during centrifuge testing

In order to fully define the SWRS it is necessary to prepare and test soil samples over a broad range of void ratio and suction values. However, the different initial conditions of the soil sample have an impact not only in the hydraulic properties but also in the mechanical properties. As a result, the changes in unit weight during centrifuge testing will depend upon the level of stresses imposed by the centrifuge, and the initial condition of the soil samples, particularly the dry unit weight and water content. Figure 81 illustrates the unit weight profiles at the beginning and end of Test #2.

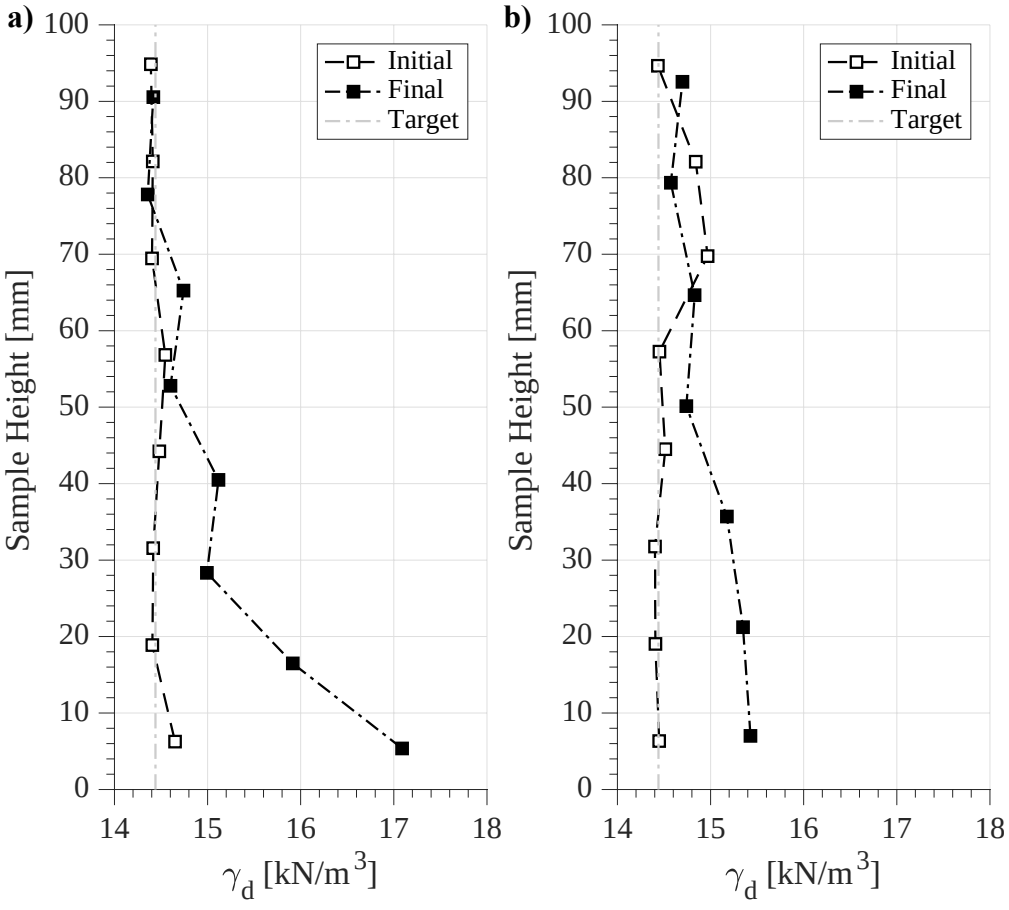

Figure 81. Dry unit weight profiles for Test #2: a) Sample A (SD) and b) Sample B (D).

While in test #1 the dry unit weight profile of Sample A remains almost constant during testing (Figure 63a), in test #2 the unit weight of Sample A changes after testing. Both tests were carried out at the same rotational speed and in consequence the stresses imposed are relatively similar. However, in test #2 the samples were compacted at a lower relative compaction. This comparison shows that volume changes can be relatively significant even for low plasticity clays.

The results presented in Figure 81(a) for Sample A were obtained using a SD measurement technique. In consequence, the volume changes measured in-flight were only caused by the imposed stresses. However, in Figure 81(b) the results for Sample B were obtained using a D measurement technique. In this case, the changes in dry unit weight are coupled with those created by the measurement technique during slicing.

Figure 63(b), shows that for Sample B in test #1, the final dry unit weight is lower than the initial one, however in test #2 the final dry unit weight is higher than the initial despite of the decompression created by the slicing. This decompression is partially masked by the initial compression caused by the increased stresses in the centrifuge

The decompression created by the slicing procedure could be estimated as the difference in dry unit weight between the Sample A profile (assuming it to be the "expected" final result) and the Sample B profile at the end of the test.

Figure 82 shows a representation of the SWRC for both samples of test #2. Different from Test #1 where an offset between the results of both samples was observed, in test #2 the overall volume change (due to stresses and to the slicing) has mainly an impact on the lower end of the soil sample.

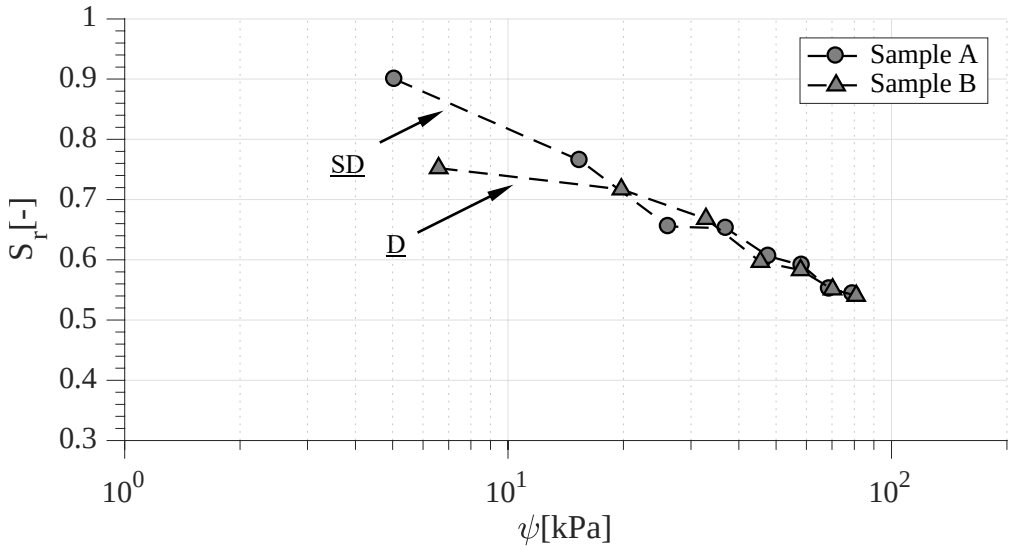

Figure 82. Representation of the SWRC results from Test #2.

As a conclusion of this analysis, it can be state that instead of assuming a soil matrix rigid or deformable, volume changes should always be considered and measured inflight with non-intrusive systems to avoid creating additional deformations.

The initial compaction (unit weight and moisture content) conditions create a preconsolidation. If the imposed stresses are relatively lower than the preconsolidation, a "quasi-elastic" behavior could be expected and the deformations are negligible (Test #1). However, if the imposed stresses surpass the preconsolidation state the soil sample could undergo considerable volume changes that must be taken into account to define the SWRS (Test #2).

8.4.5.1 Limitations to the definition of the SWRS based on the mechanical response of the soil

A consequence associated to the mechanical behavior of the soil during centrifuge testing is the limitation of the testing methodology to target results at low dry unit weights (high void ratio values) and low suction (lower layers), especially when testing at

high g-levels (high stresses) to obtain a broad range of suction values, or to reduce the testing time.

8.4.6 Summary of results for hydrostatic tests to define the SWRS

The results from all the hydrostatic tests listed in Table 7 performed to define the RMA soil SWRS using centrifuge technology are compiled in Figure 83. Through this experimental program it has been possible to cover a reasonable range of void ratio, water content, and suction values.

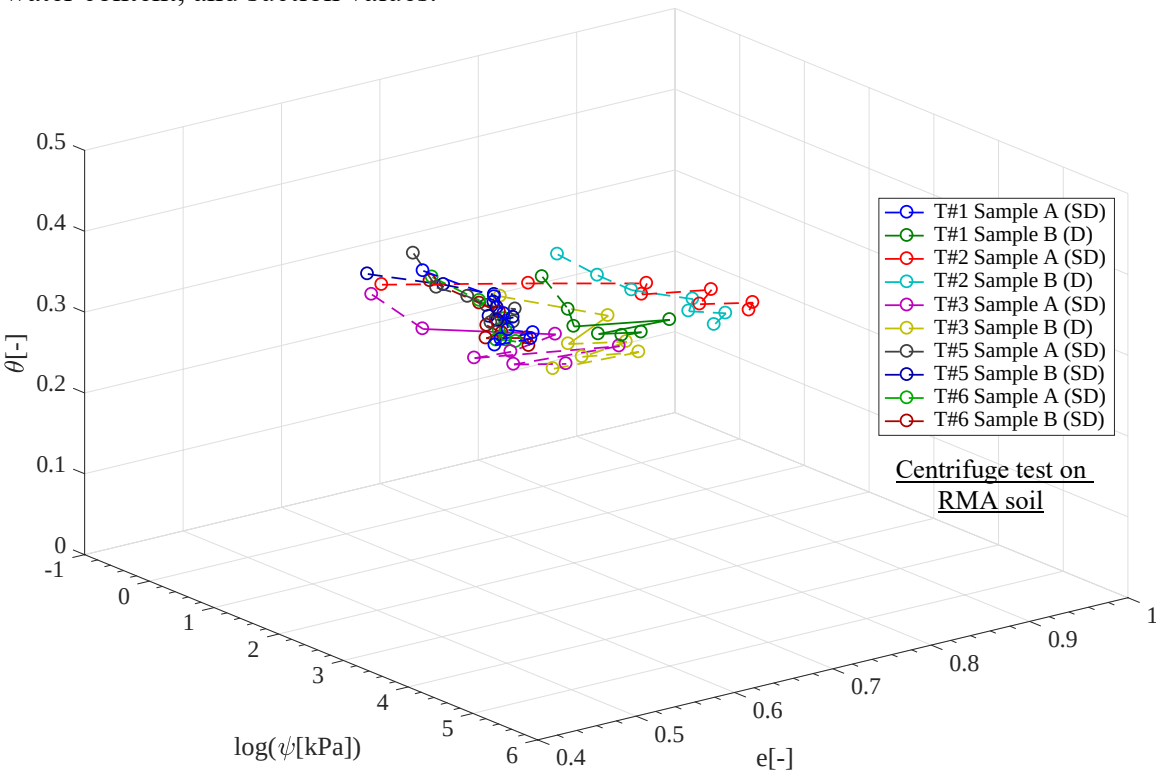

Figure 83. SWRS results from centrifuge testing for RMA soil.

A more detailed view is presented in Figure 84 to facilitate the comparison of the results on each two-dimensional plane. Figure 84(a) show that most tests overleap in a narrow range in the SWRC plane, but some tests are far from this range. The inclusion of the void ratio allows observing the influence of the soil unit weight in the retention

capabilities. As previously indicated the initial unit weight impacts the mechanical response of the soil sample. In consequence, in Figure 84(c) it can be observed that due to the stresses imposed by the centrifuge it was not possible to obtain results at high void ratio and low suction values.

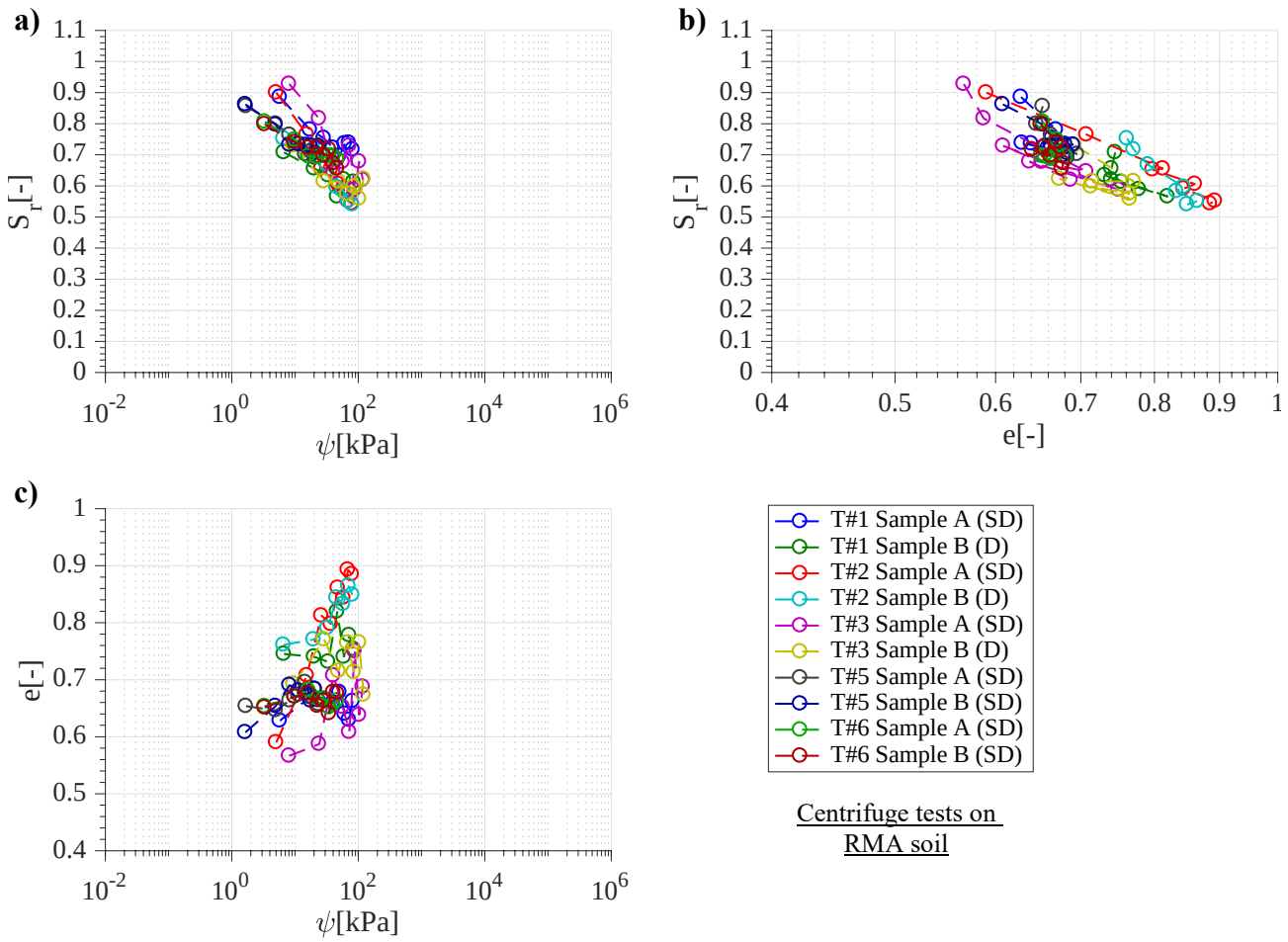

Figure 84. Plane views of the data points used to define the SWRS for RMA soil using centrifuge testing: a) SWRC in Sr-ψ, b) lateral view Sr-e, and c) top view e-ψ.

8.4.7 Imposed flow test: determination of the unsaturated hydraulic conductivity

The unsaturated hydraulic conductivity for RMA soil was measured in the centrifuge through imposed flow test (IF). In Test #4, semi-destructive and non-destructive measurements were obtained from Sample A, and Destructive from sample B. Alike the SWRS, the measurement technique has an impact on the soil dry unit weight density (Figure 85) and consequently in the volumetric water content profile (Figure 86a).

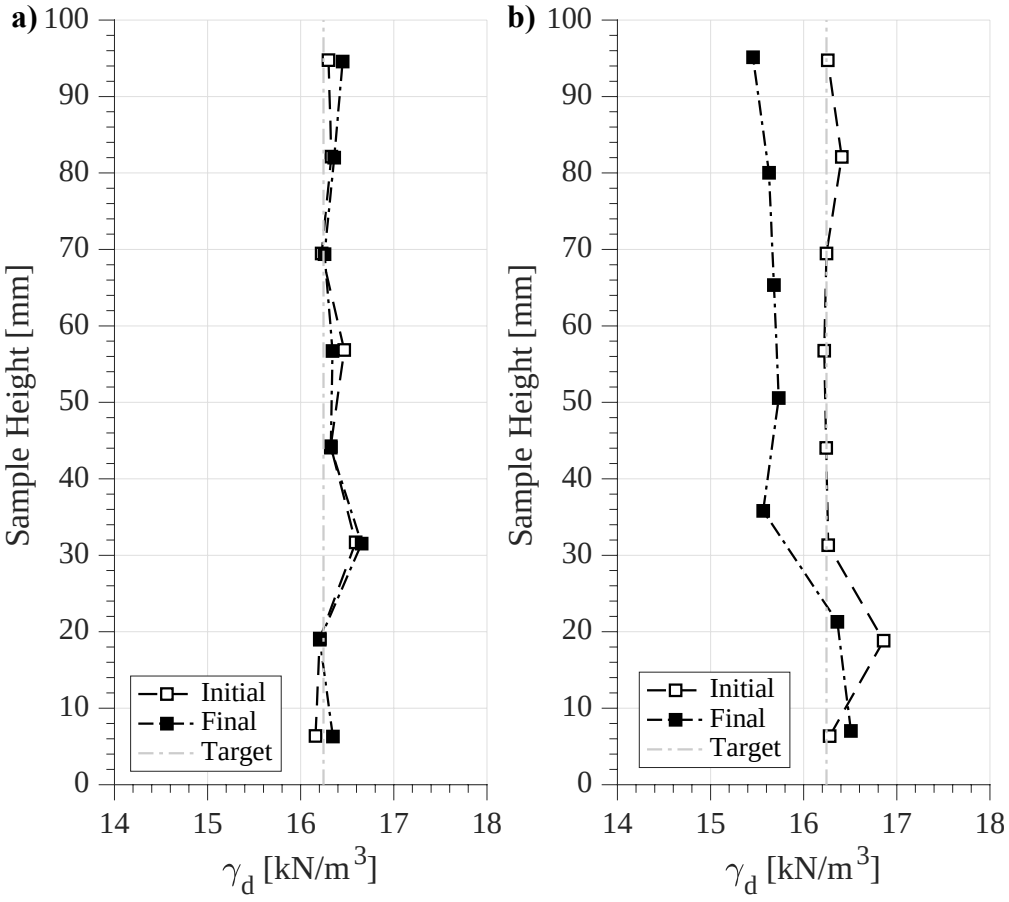

Figure 85. Dry unit weight profile for: a) sample A (SD), and b) sample B (D) of Test #4.

The suction profile was obtained implementing the SWRS for the RMA soil (Figure 86b). The details about the construction of the SWRS are described later in Chapter 9.

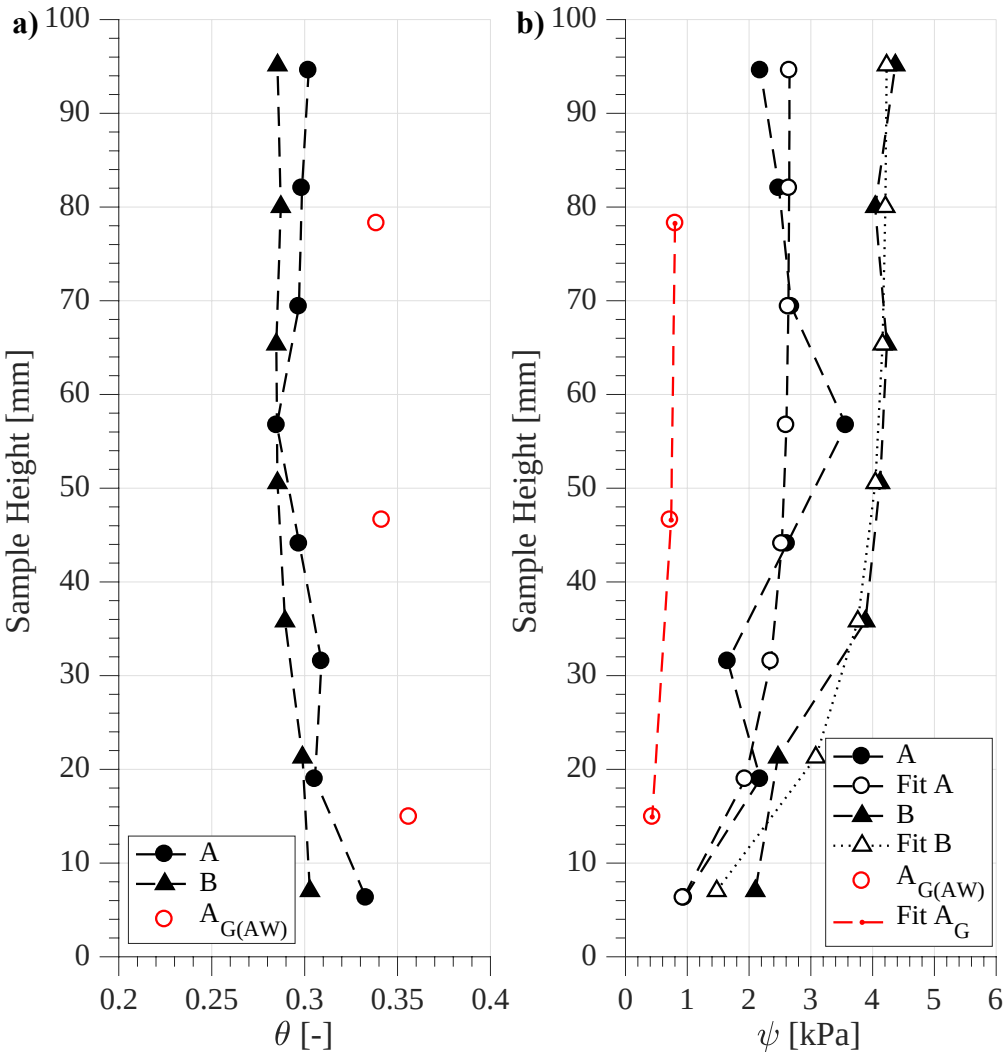

Figure 86. a) Measured water content, and b) derived suction profiles and fits for Test #4.

For this particular case, the SWRS used to estimate the suction at each soil layer corresponds to Set 2. The following fitting function presented by Plaisted (2014) was used to define a smooth suction profile.

$$\psi(z) = a\left(1 - e^{-bz}\right) \quad (24)$$

where a and b are two fitting parameters, ψ is the matric suction expressed in [kPa], z is the position in the sample starting from the base [cm], and r_o is the radius at the base of the sample (60 cm). The correlation between the radius and the position in the sample is given by the next equation:

$$r = r_o - z \quad (25)$$

This functional form simplifies the calculation of the suction gradient necessary to be incorporated in equation (23) in order to determine the hydraulic conductivity. Consequently, the gradient due to the suction can be calculated along the sample using the following function:

$$-\frac{dh_p}{dr}(z) = -\frac{dh_p}{dr}\frac{dr}{dz} = 10.197(b.a)e^{-bz} \quad (26)$$

where 10.197 is a correction factor to express suction as water head [cm]. Because the suction was treated as a positive pressure for the fitting, an inversion in the sign of the gradient was included.

The volumetric water content measured with the SD and D techniques and by the GTDR on "Sample A" are included in Figure 86(a). Figure 86(b) shows the estimated suction values. It can be observed that a slight difference in the volumetric water content between the samples almost duplicates the suction values. However, this difference in suction values does not correspond to a difference in the suction gradient, and therefore, in the hydraulic conductivity.

Figure 87(a) shows the suction gradient (i_S) for each layer, with values from 0 to 20. Figure 87(b) shows the total gradient (i_T) values, and a line describing the theoretical gravitational gradient along the soil sample. Due to the water content distribution, the suction gradient has an opposite direction with respect to the gravitational gradient.

Also, it can be observed that the influence of the suction gradient is negligible in the upper half of the sample. Figure 87(c) illustrates the estimated hydraulic conductivities values for each layer of the soil sample. In test #4 the imposed inflow was 10 mlh. All the figures include the results for Sample A (SD and ND) and Sample B (D). The hydraulic conductivity measured on sample B is higher because the area of the slip ring tube was smaller and the same total inflow rate (10mlh) was used for both.

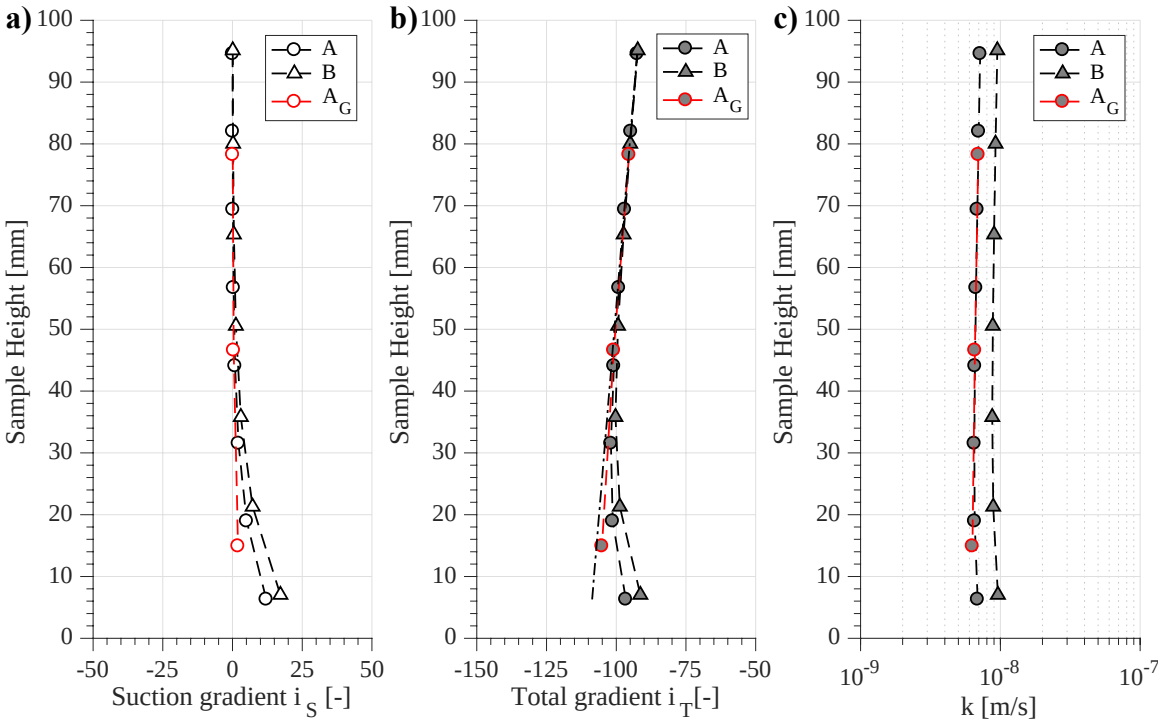

Figure 87. Test #4: a) suction gradient, b) gravitational and total gradients, and (c) derived unsaturated hydraulic conductivity for sample A, sample B and sample A with ND measurements (A_{GTDR}).

Although the GTDR predicted higher water contents than the SD and D measurements, and consequently lower suctions values, the predicted hydraulic conductivity based on fully non-intrusive sensors (ND measurement technique) is in good agreement with the results obtained using SD and D measurement techniques.

8.5 SUMMARY AND CONCLUSIONS

The objectives of this research component included: proposing modifications and incorporating the non-intrusive sensors detailed in Section 1 (Chapter 5 and Chapter 6); evaluating the response of the non-intrusive sensors and comparing them with other measurement techniques. An additional objective was to gain insight into the hydro-mechanical characterization of RMA soil using centrifuge testing. These goals were accomplished performing a series of tests in the centrifuge permeameter, the analysis of the results showed that:

- The inclusion of non-intrusive sensors (GTDRs and image analysis) was found to be successful. Specifically, deformation and water content profiles could be obtained using Non-destructive (ND) and Semi-Destructive (SD) measurements in addition to the Destructive (D) measurements.
- In addition to determining the retention capabilities and the hydraulic conductivity, the sensors were found to provide information about transient response of unsaturated soils during centrifuge testing.
- The mechanical response of the soil sample was found to depend on the initial conditions (unit weight and water content).
- The level of deformation was found to depend on the combination of both the initial conditions and the stress imposed during centrifuge testing.

- Using destructive measurements (slicing) generated an increase in the volume of the soil layers reducing the volumetric water content and the degree of saturation at hydrostatic equilibrium. Incorporating non-intrusive volumetric measurements solved this problematic allowing a better definition of the SWRS.
- The three-dimensional space used to define the soil SWRS allowed representing the water-retention capabilities of the soil measured in the centrifuge environment incorporating the volume changes occurred during testing.
- The ND measurement technique allowed carrying out multistage hydrostatic test. The results showed a good level of agreement with the results obtained using SD measurements.
- Although it was not found to be a significant factor, the suction gradient should be incorporated into the derivation of the unsaturated hydraulic conductivity, as it was previously shown by Plaisted (2014).
- The ND measurement technique can provide volumetric water content and void ratio profile useful to determine the corresponding suction profile during steady state conditions.
- The hydraulic conductivity values obtained with the ND measurement agree with those obtained using SD measurement. In addition, using ND measurement could be possible to target different hydraulic conductivity values using the same sample.
- The CSI software was found to occasionally create a significant scatter in the GTDR readings. Interpreting the GTDR waveforms using AWIGF algorithm provided a clearer trend.

Chapter 9: Analysis of the Hydro-Mechanical Characterization of Unsaturated Low Plasticity Clays

9.1 INTRODUCTION

Several methods are available to obtain the hydraulic characterization of unsaturated low plasticity clays. Typically, the determination of the soil-water retention characteristics (SWRC) of the soil requires the combination of low and high suction standard procedures as it was shown in Chapter 3. Direct measurement of the unsaturated hydraulic conductivity (k-function) is rarely conducted and more often these values are derived from the retention properties.

The development of a centrifuge permeameter (CPUS) has helped to reduce the time required for this labor and provides a useful tool to evaluate both the SWRC and k-function. In Chapter 8, different measurement approaches implemented in the CPUS were described (fully instrumented, destructive, etcetera) and proved to be successful.

This research component focuses, first, on the construction of the SWRS for RMA soil based on the results obtained in Chapters 7 and Chapter 8. The analytical model and the numerical optimization procedure are described, and a series of results obtained for different data sets is presented. This analysis also includes a comparison between the fitted functions in order to understand how well the functions fit the data, and to evaluate the extrapolation capabilities.

Secondly, a series of unsaturated hydraulic conductivity results were obtained from the transient response of standard (1.g) and centrifuge (N.g) tests previously employed to define the SWRS A simple analytical solution proposed by Gardner (1956) was used to analyze the transient flow response of the ATX Cell Test. The transient response of the centrifuge was evaluated using the commercial code Hydrus (Simmunek et al. 1998) modified for centrifuge testing (Simmunek and Nimmo, 2005).

9.2 DETERMINATION OF THE SWRS

The approach selected to define a function to describe the SWRS was to use Van Genuchten (1968) SWRC equation, including a linear relationship of its parameters (α, n, θ_s, and θ_r) as function of the void ratio.

This hypothesis was previously tested analyzing a series of parameters obtained after using a curve fitting procedure with Van Genuchten (1968) SWRC model. This fitting procedure was carried out using results from the ATX Cell. In these tests the soil samples did not show substantial volume changes and, consequently, each set of fitting parameters could be associated to the initial void ratio. Additional details about this analysis are incorporated in Appendix 3. This model was previously used by Plaisted (2014) but only including centrifuge test results.

9.2.1 Analytical formulation of the SWRS model

The analytical formulation of the SWRS is presented in terms of the volumetric water content as function of suction and void ratio according to the following equations:

$$\theta\left(\psi,e\right)=\theta_r(e)+\left(\theta_s(e)-\theta_r(e)\right)\left[1+\left(\alpha_{VG}(e).\psi\right)^{n_{VG}(e)}\right]^{-m_{VG}(e)} \quad (27)$$

In this formulation, the residual and saturated moisture content (θ_r and θ_s) and the parameters α_{VG}, n_{VG}, and m_{VG} are change into linear functions. In this case the set of parameters to be optimized are a_i and b_i for each of the following linear equations.

$$\theta_s(e)=a_1+b_1.e \quad (28)$$

$$\theta_r(e)=a_2+b_2.e \quad (29)$$

$$\alpha_{VG}(e)=a_3+b_3.e \quad (30)$$

$$n_{VG}(e) = a_4 + b_4.e \quad (31)$$

$$m_{VG} = \left(1 - 1/n_{VG}\right) \quad (32)$$

9.2.2 Numerical optimization

The numerical optimization of this customized non-linear model was performed using Matlab's Optimization Toolbox™, with an equation solver based on trust-regions (Moré and Sorensen, 1983). This algorithm allows performing non-linear optimizations and handle at the same time a set of constrains in each variable.

The initial values and constrains for each variable were obtained from the curve fitting procedure included in Appendix 2A. Additional constrains were taken into account for the variables to remain physically meaningful (e.g. residual volumetric water content higher than zero for all the void ratio values). Table 8 presents the upper and lower constrains as well as the initial searching values for each parameter. Initial values were further modified in order to evaluate the robustness of the solution obtained through numerical optimization.

Table 8. Constrains applied during non-linear optimization

Parameter	a_1	a_2	a_3	a_4	b_1	b_2	b_3	b_4
	[-]	[-]	[kPa^{-1}]	[-]	[-]	[-]	[kPa^{-1}]	[-]
Initial	0.167	0.10	0.25	0.50	0.33	-0.10	2.0	0.50
Upper B	1	0.15	-	-	-	0	-	-
Lower B.	0	0	0.01	0	0	-	0	0

9.2.3 Data sets for SWRS calibration

It is expected that the final shape of the SWRS described by the analytical model proposed depend significantly on the experimental. Moreover, the ability to extrapolate and values out of the testing range is also affected by the data set selected. Four data sets

were created incorporating different combinations of experimental data in order to evaluate the impact of the data in the shapes of the SWRS, and the prediction capabilities of this tool. Table 9 shows the experimental data incorporated on each set, including results from standard testing (1.g) presented in Chapter 7, and centrifuge testing (N.g) from Chapter 8.

Table 9. Data sets created for SWRS optimization

Testing			Experimental data			
Methodology	Path	Suction range	Set 1	Set 2	Set 3	Set 4
ATX Cell (1.g)	Wetting	0 - 100 kPa	X	X	-	-
WP4C (1.g)	-	0.3 - 100 MPa	-	X	-	X
Centrifuge (N.g)	Drying	0 - 100 kPa	-	-	X	X

These data sets were specifically selected to evaluate specific conditions. For example, Sets 1 and 3 contain experimental data at low suctions (less than 100 kPa), but set 1 uses results from standard tests and set 3 from centrifuge testing. Also, the samples in set 1 correspond only to results from wetting path tests, however in centrifuge testing the experimental data is obtained drying the soil. These data sets will allow evaluating the impact of the experimental technique selected in the SWRS predicted when using experimental data within the same suction range.

Data sets 2 and 4 combine experimental data obtained using different testing techniques at low and high suction values. While Set 2 includes only data from standard characterization tests, Set 4 combines results from standard and centrifuge testing. It is expected that these sets provide a better definition of the SWRS along a wide range of suction and void ratio values. In both sets, the experimental data at high suction values was obtained using the WP4C test, where samples are compacted at target water content and tested and wetting or drying paths.

9.2.4 SWRS model calibration

In this section the results for each optimization are presented together with the corresponding residuals values. Table 10 includes the best set of parameters obtained for each data set.

Table 10. Fitting parameters for SWRS

	Set 1	Set 2	Set 3	Set 4
Parameter	[-]	[-]	[-]	[-]
a_1	0.1746	0.1722	0.3482	0.3482
a_2	0.0037	0.0230	0.1500	0.1500
a_3	0.0126	0.0100	0.0100	0.0100
a_4	1.0634	1.0537	1.0912	1.0912
b_1	0.3131	0.3214	0.0020	0.0020
b_2	-0.0234	-0.0447	-0.0001	-0.0001
b_3	2.7535	3.5727	0.9375	0.9375
b_4	0.1204	0.1224	0.0605	0.0605

The fitting procedure using the analytical formulation proposed for the SWRS was proven successful. In general for all the data sets evaluated, the fitted functions approximate the experimental data with an error below 6% for all the range of suction and void ratio values evaluated.

The following figures illustrate the SWRS fitted functions together with the experimental data included in each set. Figure 88 and Figure 89 show the SWRS and the residuals for set 1. Residuals represent the difference in the volumetric water content between the data and the surface. Since experimental data is available for suction values under 1 kPa the SWRS in Figure 88 shows the volumetric water content parameter (θs) is almost equal to the porosity for every void ratio value.

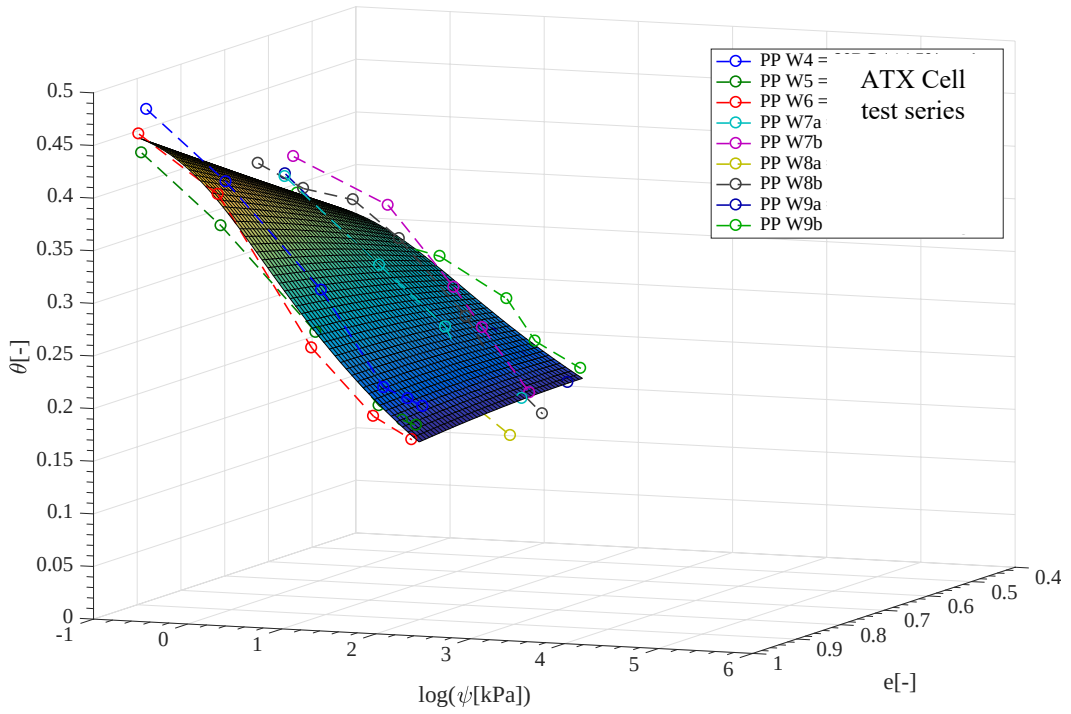

Figure 88. SWRS for Set 1.

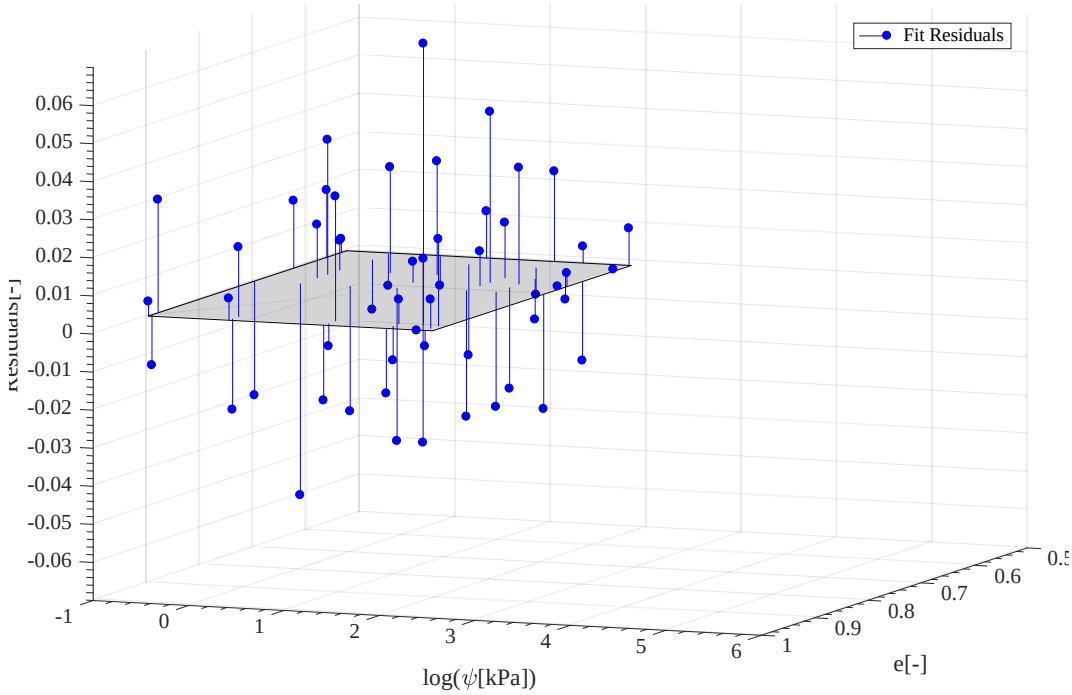

Figure 89. Residuals from SWRS fitting for set 1.

Figure 90 and Figure 91 show the SWRS and residuals for set 2. This set includes the experimental data through the largest range of suction values 0.1 kPa to 1000 MPa. In consequence it is possible to observe in Figure 90 that the SWRS has a double curvature along the void ratio axis.

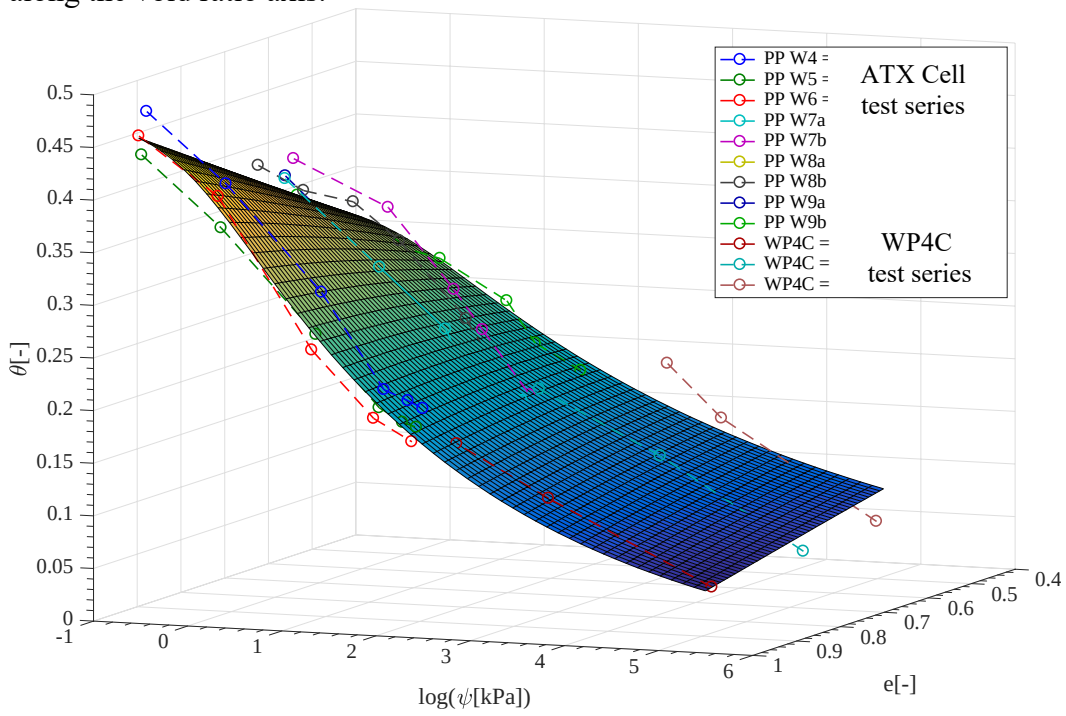

Figure 90. SWRS for Set 2.

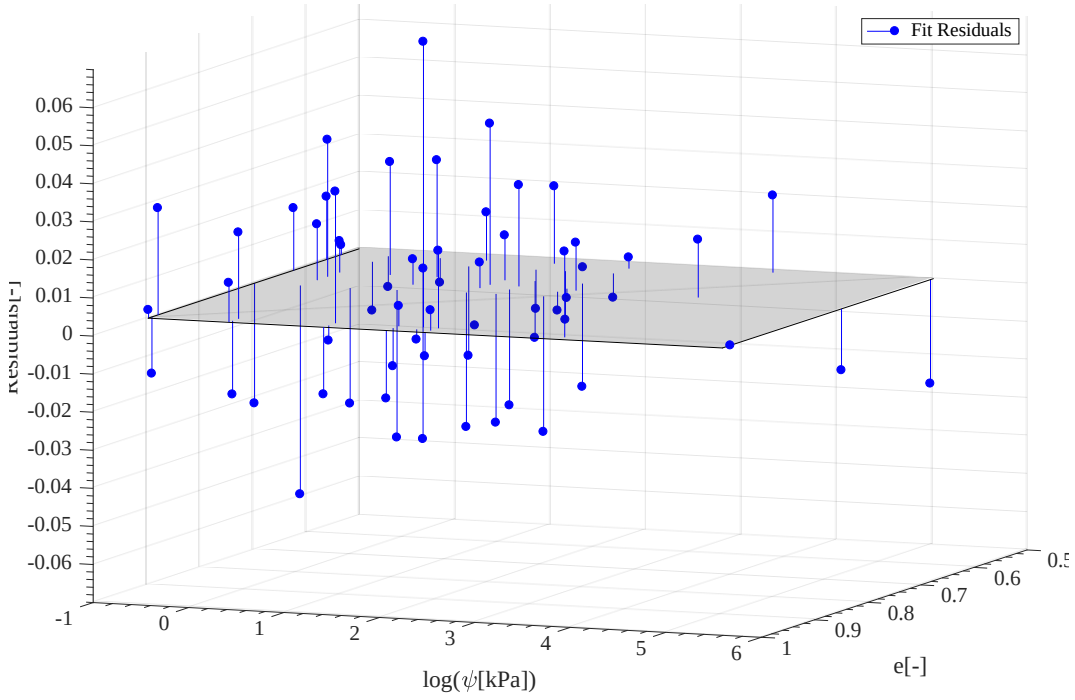

Figure 91. Residuals from SWRS fitting for set 2.

Figure 92 shows the results for Set 3. In this case, only the results obtained with the semi-destructive (SD) measurement technique were included, since the results obtained with the destructive (D) technique have a reduced water content product of the measurement procedure. This experimental data also represents the narrowest suction range and, therefore, a higher consistency in the actual data was expected. Figure 93 illustrates that in this set all the residuals are lower than a 3%.

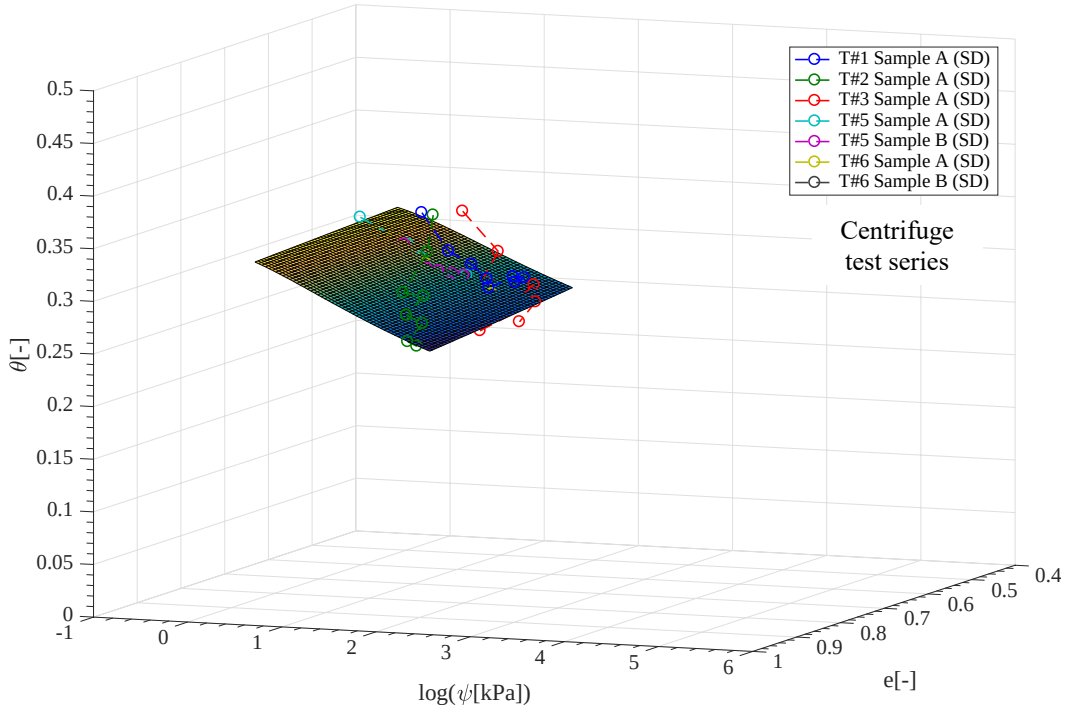

Figure 92. SWRS for Set 3.

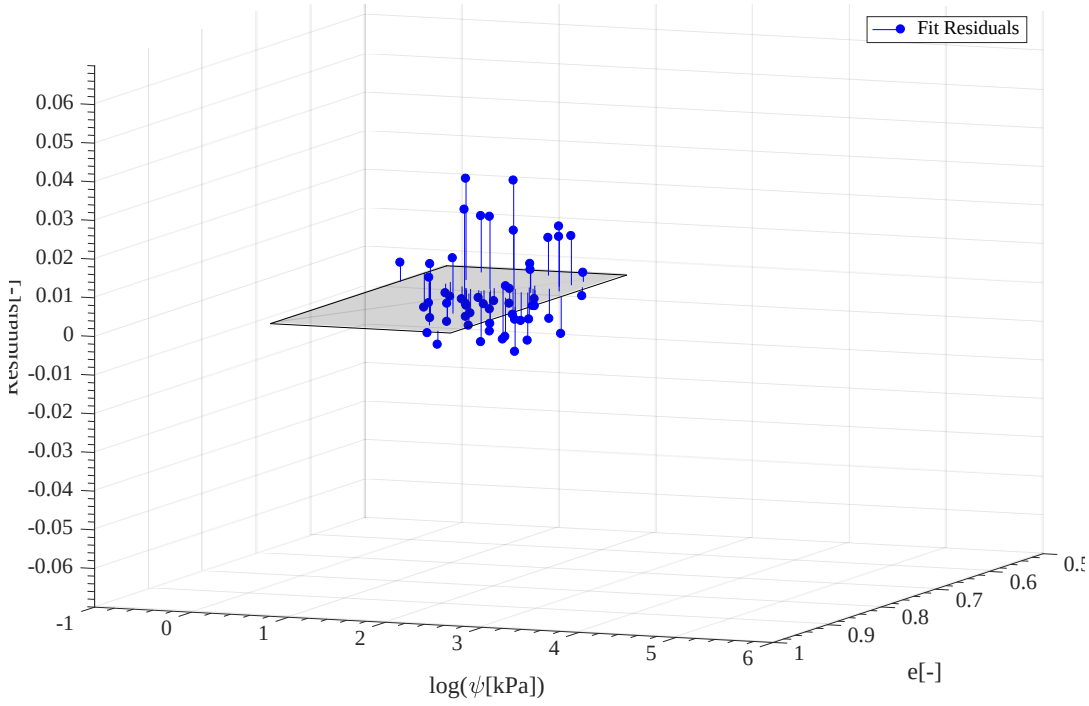

Figure 93. Residuals from SWRS fitting for set 3.

Similar to set 2, the inclusion of experimental data at high suction values in sets 4 allows a better definition of the SWRS. The SWRS in Figure 94 has a less marked double curvature along the void ratio axis in comparison to the SWRS in Figure 90. Figure 95 presents the residual values for set 4, and similar to set 3, values lie within a 3% to 4%.

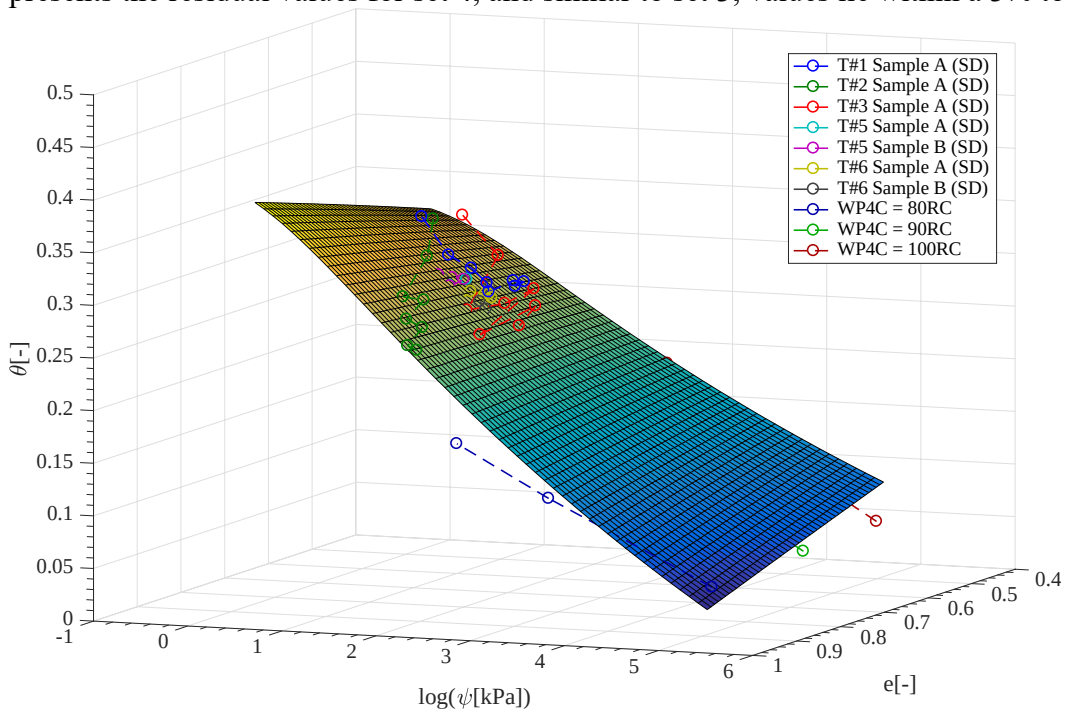

Figure 94. SWRS for Set 4.

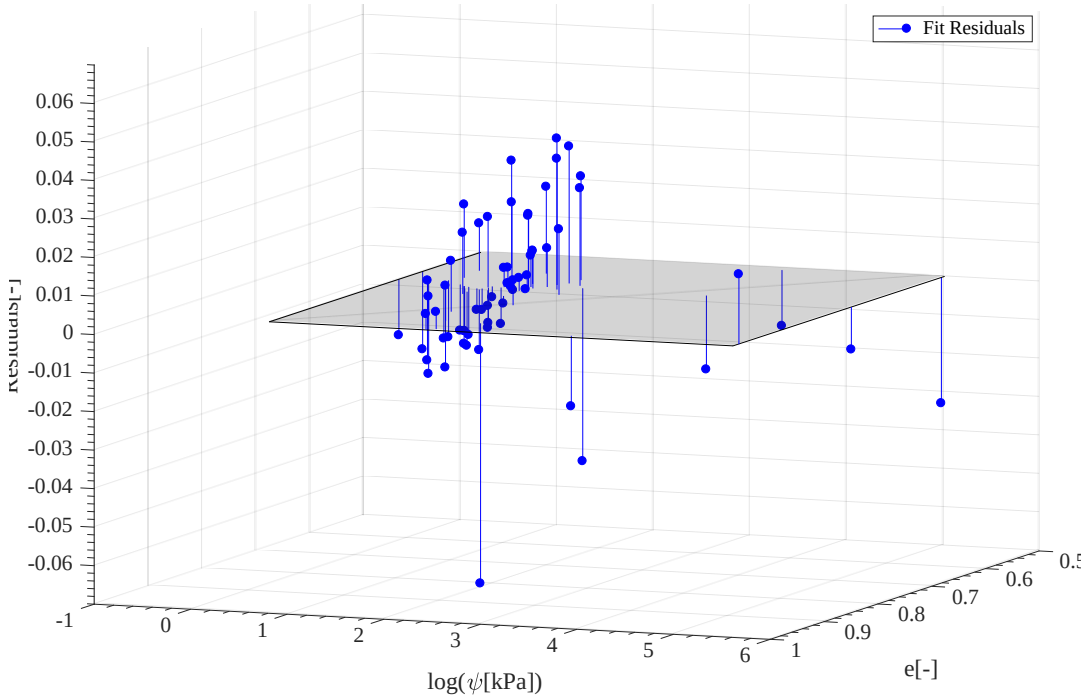

Figure 95. Residuals from SWRS fitting for set 4.

9.2.5 Performance of the predicted SWRS

The performance of the surfaces obtained in section 9.2.4 can be evaluated visually using the residuals plot in order to understand how well the SWRS approximate the experimental data. In addition, a series of statistical metrics are used to quantify the SWRS performance. Table 11 summarizes the results obtained for each data set including the following metrics: SSE, R-square, Adjusted R-square, and RMSE from the Matlab's Optimization Tool Box™.

Table 11. Goodness of fit metrics for SWRS optimization

Metric	Set 1	Set 2	Set 3	Set 4
SSE	0.0307	0.0351	0.0058	0.0231
R-square.	0.9193	0.9402	0.7686	0.9158
Adj. R-square.	0.9073	0.9328	0.7349	0.9055
R.M.S.E.	0.0256	0.0250	0.0110	0.0201

In general, the first evaluation performed observing the residuals showed errors that were lower than a 6%. The metrics show a good performance of the SWRS model for all the data sets, with R-square values acceptable for all the surfaces.

Set 3 shows a comparatively lower value than the other sets since a group of experimental data points are distant from the SWRS. However, at the same time this set has the residuals with lower values, and this distribution of the data is represented by a low SSE (sum of square residuals) value.

Yet, these metrics compares only the experimental data used in each set with the fitted surface. In order to provide an additional evaluation a series of figures were prepared to show a direct comparison between the surfaces fitted.

Figure 96 and Figure 97 illustrates the comparison between the SWRS for Sets 1 and 3. The most significant discrepancy is observed between the predicted water content values for suctions below 1.0 kPa. This range is not well defined by the centrifuge data (Set 3) and consequently an almost constant water content value is predicted. Depending on the void ratio, the SWRS fitted for Set 3 could be over or under predicting the water content at low suctions.

The inclusion of tests at high suctions does not modify considerably the predicted SWRS for Set 2 (in comparison for set 1). However, the prediction for Set 3 changes considerably when adding data at high suction values in Set 4. A comparison between the SWRS for Sets 2 and 4 is presented in Figure 98 and Figure 99.

Although no experimental data was incorporated at suctions values below 1 kPa in Set 4, it can be observed that the shapes of Set 2 and Set 4 are similar. The plateau of the SWRS for Set 3 was modified forced by curvature induced by the inclusion of data at high suction values. The difference in water content predictions between these surfaces based on wetting or drying tests remains under 0.07.

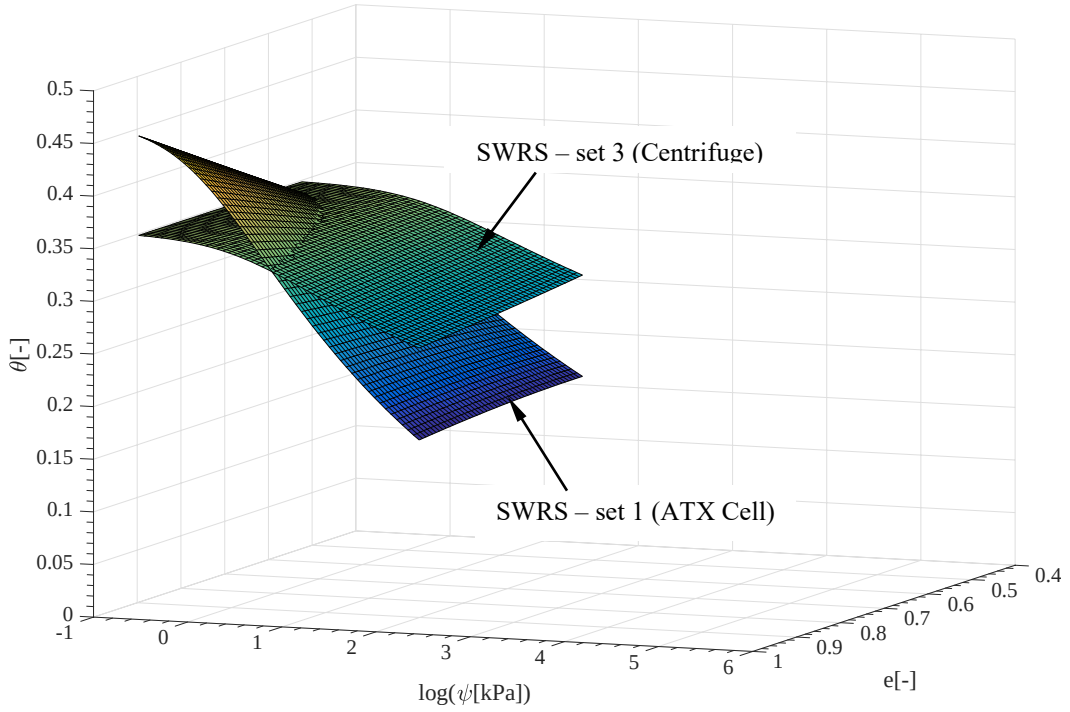

Figure 96. Comparison between surfaces for Set 1 and Set 3.

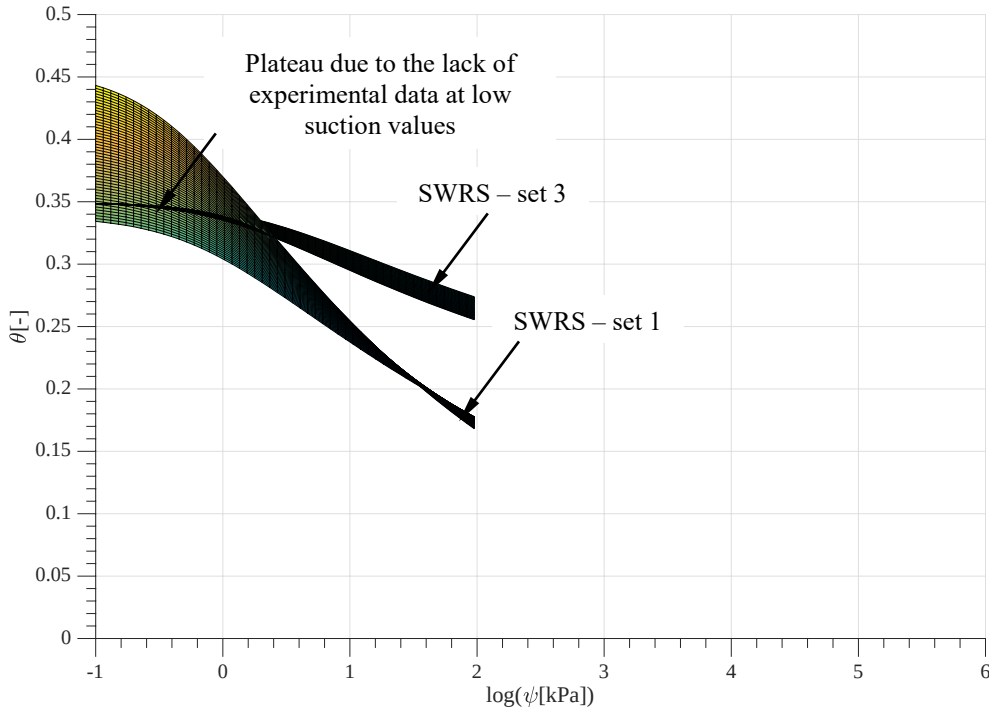

Figure 97. Comparison between surfaces for Set 1 and Set 3.

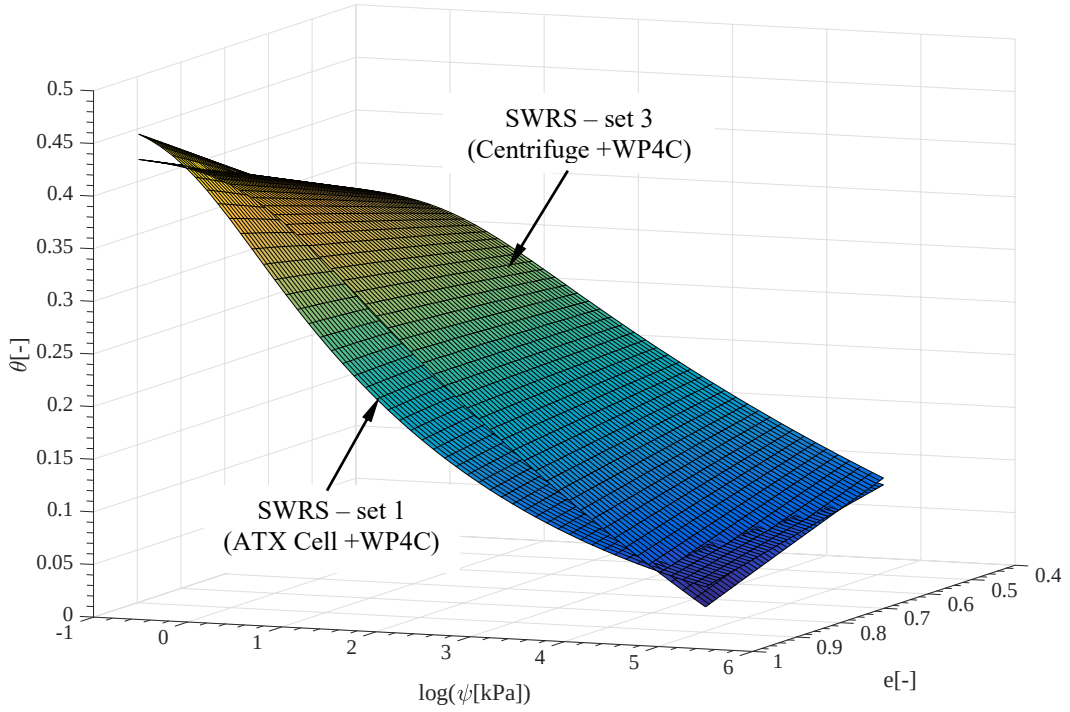

Figure 98. Comparison between surfaces for Set 2 and Set 4.

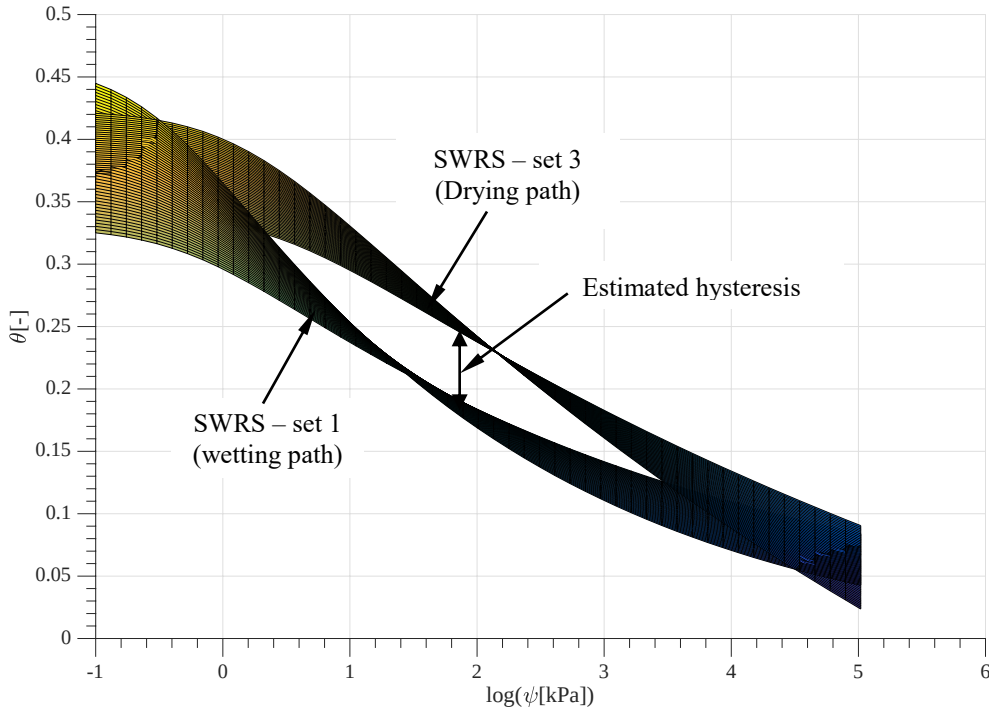

Figure 99. Comparison between surfaces for Set 2 and Set 4.

9.3 DETERMINATION OF HYDRAULIC CONDUCTIVITY FROM TRANSIENT ANALYSIS

The determination of the unsaturated hydraulic conductivity can be a time-consuming task. Even with the implementation of centrifuge testing, the time required to establish steady-state flow under very low flow rates may become unpractical.

The analysis of transient flow processes can provide useful information to determine the unsaturated hydraulic conductivity of the soil. The objective of this section is to evaluate available methodologies to analyze the transient process of tests performed to characterize the SWRS.

The transient wetting stages from the ATX Cell tests were analyzed using Gardner's (1956) multi-step outflow method. The transient inflow process in the centrifuge was back analyzed using the commercial code HYDRUS with a modification to account for the increased gravitational field (Simmunek and Nimmo 2005).

9.3.1 Analytical solution for ATX Cell transient response (1.g)

Gardner's (1956) multi-step approach was applied to the transient response of the samples tested with the ATX Cell (Figure 52) to estimate the unsaturated hydraulic conductivity of the RMA soil. This method was selected from all the analyses available described in Appendix 1.

Garder's method provides a simple solution to Fick's second law that can be applied to the inflow time series recorded during each testing stage. Every time a new testing stage begins, the applied suction in the ATX cell is reduced (or increased) and the inflow (or outflow) is monitored to determine the change in volumetric water content.

9.3.1.1 Analysis of transient response

All stages from test W9 performed on RMA soil compacted at 100% proctor standard dry density and optimum water content were analyzed using Gardner's solution.

Figure 100 shows the water inflow recorded by the scale corresponding to the reduction in suction from 95 to 30 kPa of test W9. The secondary vertical axis shows the values of the same inflow data after applying a logarithmic linearization with the following equation

$$\ln\left(V\right) = \ln\left(\frac{V_f - V_t}{V_f}\right) \quad (33)$$

The procedure is completed searching for the soil diffusivity constant (slope of the linear trend) that provides the best fit between the linearized data and the results provided by the following equation:

$$\ln\left(\frac{8}{\pi^2}\right) - D \cdot t \frac{\pi^2}{4L^2} \quad (34)$$

where V_t is the outflow at a given time, V_f, is the final outflow (for that stage), D is the diffusivity and L is the length of the specimen.

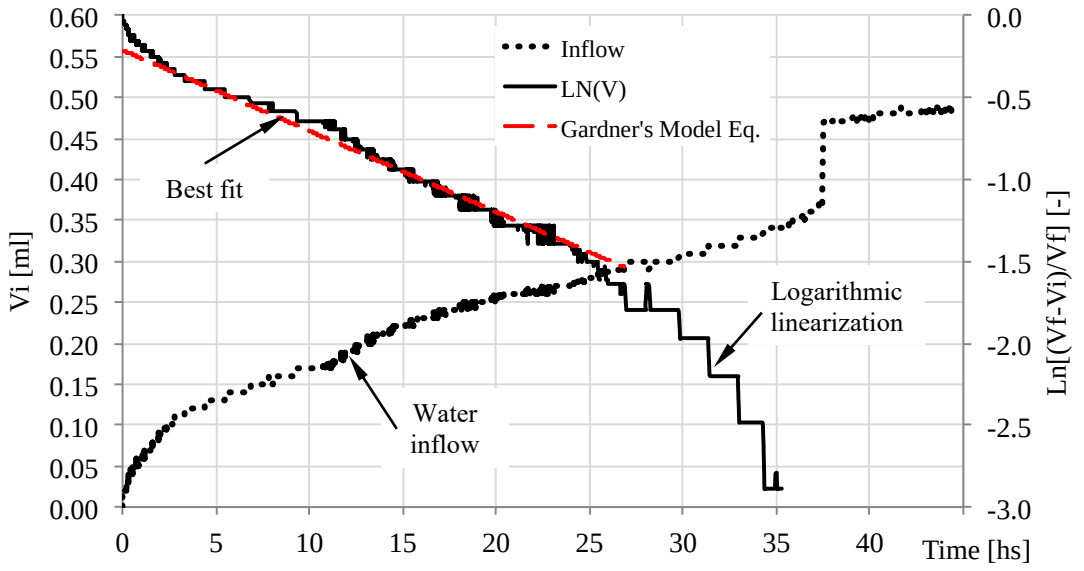

Figure 100. Analysis of inflow time response for suction reduction from 95 to 30 kPa.

The fitting procedure was repeated for all the stages of the W9 test, and the unsaturated hydraulic conductivity can be derived for each step using this definition, the results are summarized in Table 12.

$$k(\theta) = D\frac{\Delta\theta}{\Delta\psi} \qquad (35)$$

where k(q) is the unsaturated hydraulic conductivity associated to a given water content, $\Delta\theta$ and $\Delta\psi$ are the finite steps in water content and suction for the same testing stage.

In general, the results showed that: a) the linear relationship proposed is not accurate at describing all the water inflow process, however it can fit a broad range of data, b) the discontinuity in the inflow data is due to the presence of bubbles creates, this is an error in the measurement technology and it is not related to the flow process, if possible, the time window including this discontinuity should be avoided in the fitting procedure (Figure 100), c) the lower the suction range evaluated (higher water contents),

the smallest the ordinates values for the linear fitting, this indicates that for high water contents the base plate has more influence in the flow process since the ceramic disc saturated hydraulic conductivity is more comparable the hydraulic conductivity of the soil.

Table 12. Derived unsaturated hydraulic conductivity

Testing stage	ψ_{avg}	θ_{avg}	$\square_{avg}$	k
[kPa]	[kPa]	[-]	[-]	[m/s]
0.3 to 0.1	0.2	0.335	0.561	2.01E-10
1.0 to 0.3	0.5	0.302	0.560	6.26E-11
3 to 1	1.7	0.264	0.559	7.31E-11
15 to 3	6.7	0.229	0.558	1.30E-11
30 to 15	21.2	0.205	0.558	9.97E-12
95 to 30	53.4	0.192	0.557	1.29E-12

9.3.1.2 Estimated hydraulic conductivity vs. indirect k-function

Each hydraulic conductivity value listed in Table 12 was matched with the average water content, void ratio, and a log linear average suction testing stage. Figure 101 illustrates the relationship between and suction.

In addition, a comparison is presented with the values obtained using the Van Genuchten-Mualem (VGM) model prediction. These hydraulic conductivity values were generated using the set of fitting parameters obtained for test W9 using van Genutchen a SWRC model.

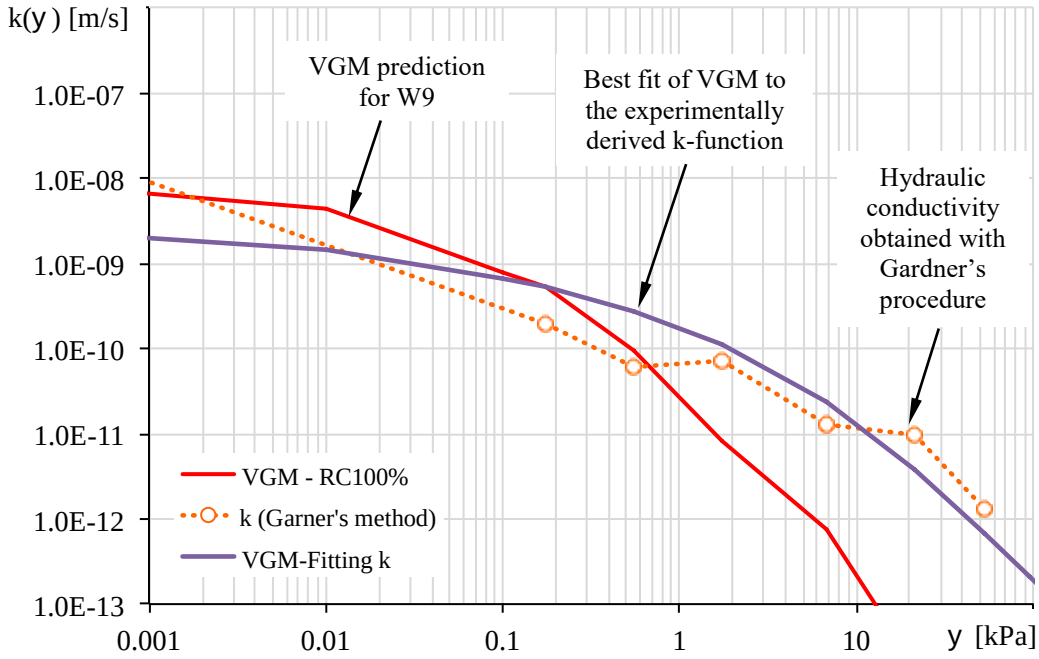

Figure 101. Hydraulic conductivity as function of suction for RMA soil.

Despite of the limitations in Gardner's (1956) method a reasonable trend in the derived results can be observed. When compared to VGM model at high suction values the laboratory results are one or more orders of magnitude higher. Also, the decrease rate in the k-function with increase in suction is lower than the decrease rate obtained through the VGM prediction. In addition, VGM prediction is highly influenced, by the saturated hydraulic conductivity and the parameters derived from the SWRC. The saturated hydraulic conductivity was extrapolated for test W9 from previous research on RMA soil (McCartney, 2007 and Plaisted, 2014). Although this indirect method is simple, the best set of fitting parameters for the SWRC do not represent always the best set of parameters for the k-function.

9.3.2 Hydraulic conductivity based on Centrifuge

The commercial code Hydrus (Simunek et al., 1998) was selected to analyze the transient flow process in the centrifuge in order to derive the RMA soil k-function. Particularly, a modified version of Hydrus 1-D (Simmunek and Nimmo, 2005) that accounts for the increased gravitational field was implemented to reproduce the infiltration stage of the hydrostatic characterization tests. The results obtained include a set of parameters for the van Genutchen-Mualem model (Mualem, 1976) that allows describing the relationship between the hydraulic conductivity and the soil water content (or matric suction).

9.3.2.1 Transient analysis model with Hydrus

The model was created to reproduce the infiltration stage in the hydrostatic test performed in the CPUS. Test #1 was selected as a representative case in order to evaluate Hydrus as a tool to derive the soil unsaturated hydraulic conductivity.

The geometry of the model includes only one material (soil sample) of 100 mm height, spinning at a rotational speed of 378 r.p.m. (6.30 1/s). The radius indicated in the model was 0.50 m corresponding to the top of the sample. The base of the bucket that holds the sample is located at 0.60 m.

The boundary conditions were selected as: inflow at the top and free drainage at the bottom. The imposed inflow in this stage was 40 mlh ($2.653.10^{-4}$ cm/s). During the first two hours of the infiltration process no outflow was observed. This is the time that was necessary for the water to reach the far end and establish a steady flow condition.

Test #1 was compacted to target 90% relative compaction, which corresponds to an average dry unit weight of 16.3 kN/m^3 (void ratio of 0.671). The initial condition of the soil sample in the model was indicated in terms of the volumetric water content at compaction (0.20 to 0.24).

9.3.2.2 Hydrus model optimization

Hydrus package modified by Simmunek and Nimmo (2005) counts with direct and inverse solvers of the Richards equation to predict water flow in unsaturated soils in the centrifugal field. The parameter optimization in this software is obtained following the Levenberg-Marquardt non-linear optimization method (Marquardt, 1963).

The time variable information used to calibrate the model corresponds to the readings obtained from the three GTDR nodes (top, bottom and middle) during the first two hours of the infiltration stage. Since the bottom GTDR presented a large scatter, a synthetic time history was created using the available values, at the beginning and at steady state, and using a transition similar to the top and middle sensors.

A set of initial parameters used for the inverse solution is listed in Table 8. These values were obtained from the SWRC fit for test W8b (ATX Cell, Appendix 3), that corresponds to a soil sample compacted at the same void ratio that Test #1. Although, α has units of [kPa^{-1}] in the SWRC fitting and k_{sat} [m/s], the values and units for this model are indicated for a direct input on Hydrus.

All the parameters were included in the optimization except the parameter "l" incorporated by Mualem (1976), which was found to have almost to no impact in the fitting procedure, and therefore a fix value was assigned to it.

Table 13. Initial values for Hydrus model optimization

Parameter	θ_r	θ_s	α^*	n	k_{sat}	l
	[-]	[-]	[cm^{-1}]	[-]	[cm/s]	[-]
Initial estimate	0.02	0.3815	0.0557	2.0	0.00015	0.50
Fitted	yes	yes	yes	yes	yes	no

9.3.2.3 Model Results

The results obtained through the inversion process with the Hydrus 1-D model are summarized in Table 14. The best fit was obtained following a non-linear least-squares analysis, and the regression coefficient was 0.917.

Table 14. Best set of parameters and 95% confidence limits

Parameter	θ_r	θ_s	α^*	n	k_{sat}	l
	[-]	[-]	[cm^{-1}]	[-]	[cm/s]	[-]
Best fit	0.096	0.354	0.0423	1.724	$1.74\ 10^{-4}$	0.50
S.E Coeff.	0.0205	0.0074	0.0103	0.3383	$1.41\ 10^{-4}$	-
Lower value	0.055	0.339	0.0219	1.059	$-1.05\ 10^{-4}$	-
Upper value	0.136	0.368	0.0626	2.389	$4.52\ 10^{-4}$	-

The results presented in Table 14 show that the residual and saturated water content parameters lay within a small range forced by the experimental data, but the saturated hydraulic conductivity shows a higher variability. The hydraulic conductivity obtained with the model is in the higher end from all the measurements previously done for RMA soil. However, the model would not converge if the initial values were lower than $1.0\ 10^{-4}$ cm/s.

Figure 102 shows a comparison between the model response and the readings at the observation points. In general, the results for the three sensors show a good agreement between the model and the measurements. While the transient response is represented correctly for the three sensors, the initial and final water content values are matched only for the top and bottom sensor. However, the values obtained at the beginning and end of the test are within a 3% error in the volumetric water content.

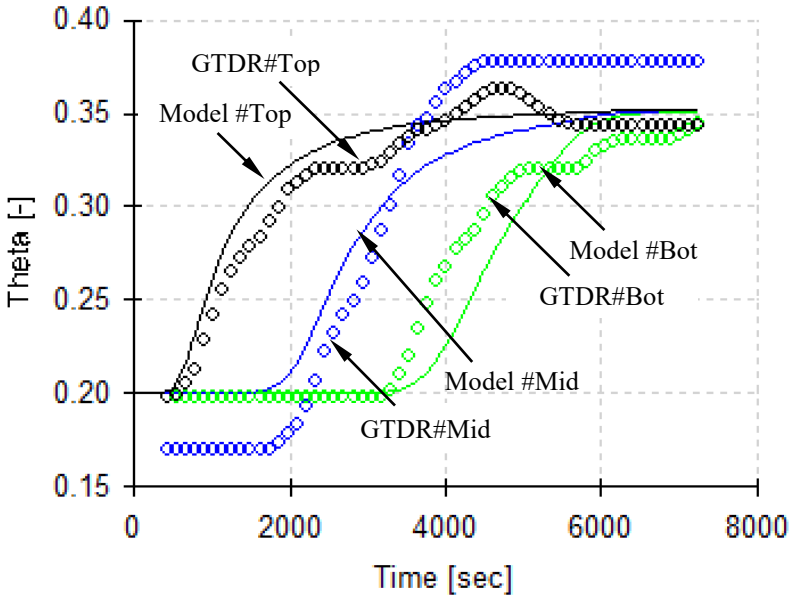

Figure 102. Comparison between the predicted behavior in Hydrus model and the measured water contents at the three GTDR nodes during the infiltration stage of Test #1.

Figure 103 illustrates de advance of the water content in the soil sample. The profiles were selected at the same times than the ones used in section 8.4.3 for the transient analysis. However, in this case the flow response presents a more defined plug-flow, while the results presented in Figure 76 using the same experimental data set indicates a transition where the water content increases more evenly along the sample.

This difference could be attributed to the presence of the ceramic disc at the base of the soil sample, and the availability of water on it. In such case, water could be migrating upwards from the base towards the soil, and this is a feature that the model cannot represent as it is. However, not taking it into account or accommodating the readings of the bottom GTDR based on the top and middle readings, allows reproducing the flow in the centrifuge environment at the selected speed and related only to the

imposed inflow at the top of the sample. In consequence, this difference in the profiles does not have a negative effect in the parameters predicted.

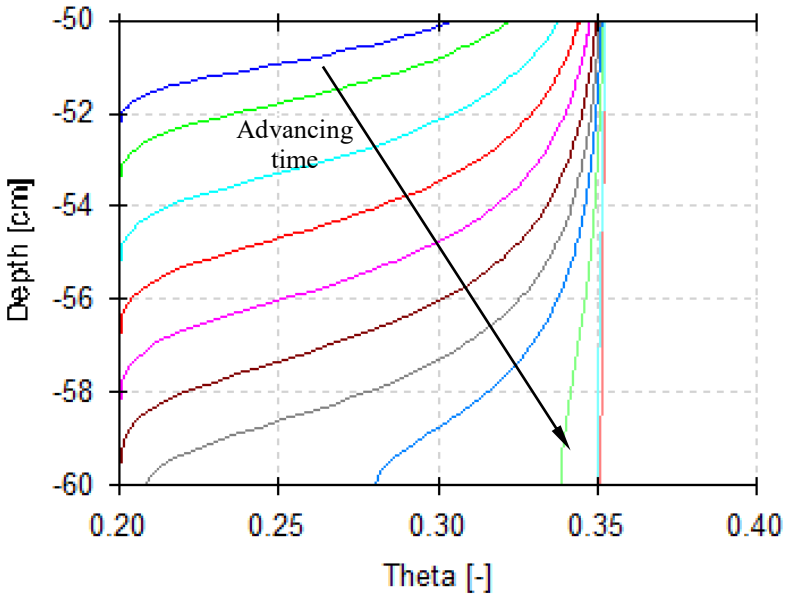

Figure 103. Water content profiles during the infiltration stage predicted in Hydrus model for Test #1.

Figure 104 shows a comparison between the derived k-function from Test #1 using Hydrus and the result obtained in one stage of an imposed flow test (Test #4). In this second case only one value of the unsaturated hydraulic conductivity function was obtained when reaching steady state flow under unsaturated conditions. Also, these results are comparable because both soil samples were prepared at the same void ratio (or relative compaction).

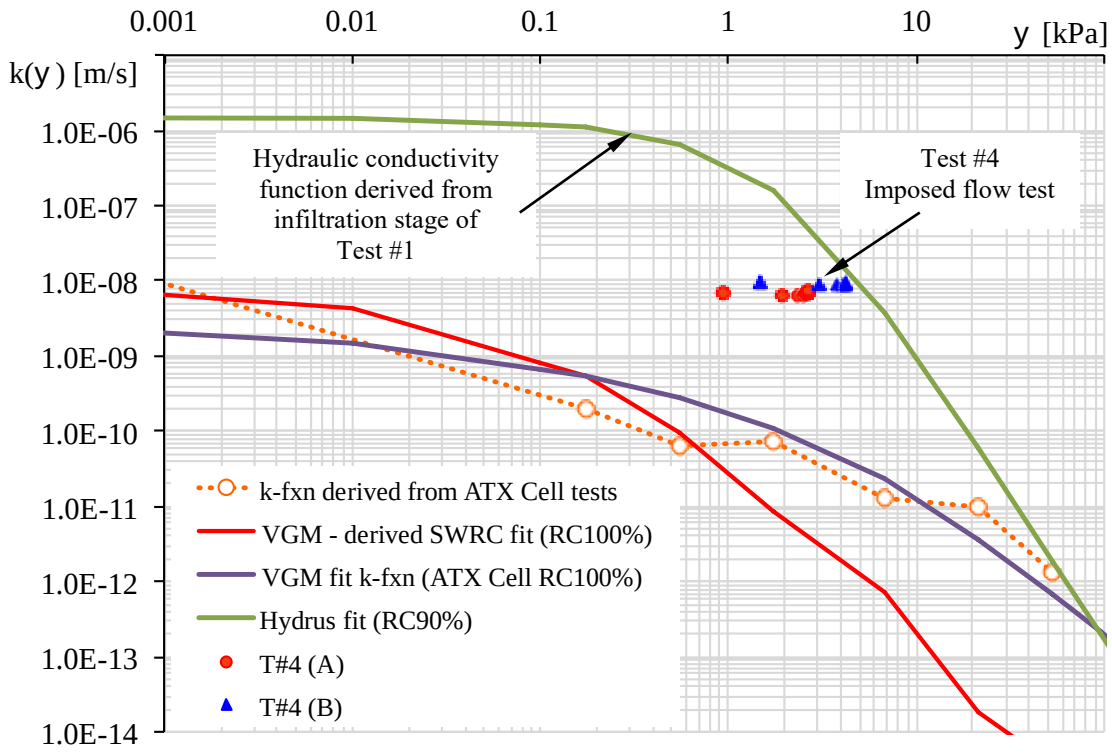

Figure 104. Comparison between the derived k-function from Test #1 using Hydrus transient analysis and measurement performed in Test #4 under unsaturated steady state flow conditions, hydraulic conductivity derived from ATX cell test and VGM model k-function prediction.

9.4 Summary and Conclusions

The summary and conclusions of this research component are presented in two sections: the definition of the SWRS based on the results obtained in Chapters 7 and 8, and the derivation of the unsaturated hydraulic conductivity based on transient analyses.

9.4.1 Development of SWRS

The implementation of an analytical SWRS approach based on the van-Genuchten SWRC model was proven to be successful. The fitting procedure and the results showed that:

- The SWRS model allowed fitting experimental data generated with different experimental techniques (standard -1.g- or centrifuge -N.g-) and it is independent of the hydro-mechanical behavior of the soil (volume changes during wetting or drying) in response to the testing technique selected.
- The linearization of the fitting parameters with respect to the void ratio was deemed an acceptable hypothesis, and transformed the problem into a numerical optimization of eight constants for each surface.
- Trust-Region methods implemented through Matlab's Optimization Tool Box required a reasonable estimate of the initial values of each constant, however the boundary constrains did not have a significant effect in the optimization.
- Four different data sets were used to evaluate the response of the SWRS model. In all cases (independently of the testing technique or the testing path) the error between the measured and predicted volumetric water content was lower than 0.06. The closest fitting obtained (set 2, centrifuge data only) had an error lower than 0.03.
- The range of suction values in the experimental data was found to highly influence the shape of the SWRS. This is particularly important if extrapolations are going to be considered using this tool.
- In particular, for RMA soil important differences were observed in the shape of the SWRS when data below 1 kPa was incorporated to the experimental data (e.g set 1 vs. set 3), allowing a better definition in the relationship between the saturated volumetric water content and the void ratio.
- The inclusion of experimental data at high suction values (set 2 and set 4) showed that in addition to the curvature along the suction axis (alike the SWRC), there is a double curvature in the SWRS along the void ratio axis.

- The comparison of SWRS based on experimental obtained with wetting and drying path test methodologies showed that hysteresis varies with suction and the void ratio, and for RMA soil was estimated than 0.07.
- In addition to the inspection of the errors (residuals) in the fitting procedure, it was found convenient to evaluate the performance of the SWRS using additional metrics. In this case best R-square values were around 0.91 to 0.94 and SSE lower than 0.035.

9.4.2 Transient analysis

The analysis of transient flow processes provides an indirect method to estimate the unsaturated hydraulic conductivity of the soil. In this research component two methodologies available were applied: Gardner's (1956) multi-step outflow method, to analyze the transient response from the ATX Cell test, and the software Hydrus (Simmunek and Nimmo, 2005) to back-analyze the readings from the infiltration stage in the centrifuge environment. These analyses showed that:

- Gardner's method was applied to the inflow readings obtained with the ATX Cell, and an average value of the hydraulic conductivity can be obtained for each stage.
- For RMA soil the unsaturated hydraulic conductivity measured in the range from 0.1 kPa to 100 kPa ranges between 2.0 10^{-10} m/s to 1.3 10^{-12} m/s, for a sample compacted at 100% relative compaction (void ratio of 0.504).
- It could be expected that Gardner's method underestimates the soil hydraulic conductivity at high water contents where it becomes similar to the conductivity of the base porous plate.
- The comparison of the estimated values with Gardner's method against the prediction created with the van-Genuchten-Mualem (1976) model showed that the hydraulic conductivity values derived from transient measurements could be orders of

magnitude higher, particularly at high suctions. This occurs as consequence of a higher decrease rate in the VGM model.

- The commercial code Hydrus 1-D (Simunek et al., 1998b) provided a robust tool to back-analyze transient data obtained from centrifuge testing.
- The model predictions showed good agreement with the observations at the three GTDR nodes, during the transition and estimating the initial and final water contents. The regression coefficient obtained was higher than 0.91.
- The k-function derived for RMA soil showed that in the range from 0.01 kPa to 100 kPa the hydraulic conductivity ranges between 1.0 10^{-6} m/s to 1.0 10^{-12} m/s, for a sample compacted at 90% relative compaction (void ratio of 0.607).
- The k-function derived with Hydrus from transient analysis showed good agreement with the values obtained in the centrifuge using steady-state (imposed inflow) tests.

SECTION 3: HYDRO-MECHANICAL CHARACTERIZATION OF UNSATURATED EXPANSIVE CLAYS

Section 3 of this dissertation build upon the outcomes of Sections 1 and 2 to investigate the hydro-mechanical characterization of unsaturated expansive soils. The incorporation of the void ratio (e) as an additional variable is central to describe the hydraulic properties of unsaturated expansive clays and their mechanical response during wetting or drying processes. Eagle Ford ford clay was selected as the soil to investigate in order to reach the main goal of this section.

Chapter 10 includes the results from a series of standard (1.g) laboratory tests in order to provide the characterization of the unsaturated hydraulic properties of the Eagle Ford clay (EF). Specifically, a series of tests were conducted using the ATX Cell, filter paper method and chilled mirror hygrometer (WP4C) tests. The experimental data generated provides a base line for the determination of Eagle Ford's Soil-Water Retention Surface (SWRS).

The results from a centrifuge testing program is presented in Chapter 11. The tests incorporated the non-intrusive techniques developed in this research. Centrifuge tests were carried out, according to the procedures described in Chapter 8, in the centrifuge in order to generate experimental data for the SWRS. The objective was to evaluate the unsaturated hydraulic conductivity of Eagle Ford clay using steady-state procedures, and ultimately to evaluate the hydro-mechanical response of the expansive clays (moisture and volume changes) during centrifugation.

Chapter 12 presents the determination of Eagle Ford clay SWRS using the experimental data obtained in previous chapters. The numerical procedure, initial values, constrains and the performance of the model are discussed. A validation of the model is

presented in order to evaluate the impact of the imposed loads and a comparison between the different testing techniques. A series of transient analysis were performed in order to derive the unsaturated hydraulic conductivity function from standard (1.g) and centrifuge (N.g) characterization tests.

Chapter 13 presents the analysis of swelling tests on Eagle Ford clay incorporating the non-intrusive sensors (GTDR and image analysis) in order to illustrate the evolution of the global testing variables: soil volume, water content, degree of saturation and outflow during the wetting process. The correlation between the swelling rate and the rate in the moisture changes is evaluated for a typical test, as well the expansion along the column in comparison to expansion obtained measuring the overall deformation of the soil sample. Finally, the results of the swelling tests are represented in the [θ, e] plane to provide a different analysis of the swelling test data, and to compare the evolution of the main variables when testing soil samples at different water contents. Also, the measurements performed with the ATX Cell (at 1.g) are compared with those from the swelling test to show the evolution of the water content and void ratios using two different testing perspectives.

Chapter 10: Hydraulic Characterization of Unsaturated Expansive Clays Using Standard (1.g) Testing

10.1 INTRODUCTION

The objective of the research component presented in Chapter 10 is to provide the characterize the unsaturated hydraulic properties of the Eagle Ford clay (EF) using standard (1.g) laboratory tests.

Tests were conducted to cover a broad range of suction and void ratio values by combining the results from ATX Cell, filter paper method, and chilled mirror hygrometer (WP4C) tests. The experimental data generated in this Chapter allows determination of the Soil-Water Retention Surface (SWRS) for EF clay.

These tests allow evaluating additional aspects of Eagle Ford clay, including: changes in the void ratio when the soil samples are subjected to progressive wetting in the ATX Cell under different loading conditions; osmotic suction values (filter paper results), and a methodology to obtain matric suction values from the WP4C tests (total suction) in order to combine all the results in one SWRS appropriately.

10.2 MEASUREMENT OF THE RETENTION CAPABILITIES OF HIGH PLASTICITY CLAYS AT LOW SUCTION VALUES

10.2.1 ATX Cell

The ATX Cell was used to evaluate the hydro-mechanical behavior of the Eagle Ford Clay soil over a broad range of suction and void ratio values and different loading conditions. The final goal of this testing program is to obtain discrete data points to define the continuous representation of the Soil-Water Retention Surface (SWRS).

In addition, these tests allow evaluating the volumetric changes in response to progressive wetting under different initial conditions. The ATX cell allows imposing an overburden independently of the imposed suction stage.

10.2.1.1 Testing program

A testing program conducted as part of this research used soil from a batch obtained from Eagle Ford shale formation (EF) near Austin, Texas (Kuhn, 2010). This soil was processed and sieved through a #10 sieve. Grain size distribution shows that its fine-grained fraction (passing #200 sieve) is nearly 89.5%, and clay fraction is 64%. The Atterberg's limits measured for the soil batch tested in this research are LL=88 and PL=39, and specific gravity is Gs=2.74. Eagle Ford clay is typically indicated as a expansive clay, but it should be observed the for Eagle Ford formation plasticity index ranging between 16 and 113 have been reported (Hsu and Nelson, 2002, Kuhn, 2010).

The maximum dry unit weight ($\gamma_{d.max}$) is 15.2 kN/m^3 using the standard proctor compaction effort, and its optimum water content is w_{opt}=24%. Saturated hydraulic conductivity values measured in flexible wall permeameter tests for saturated soil samples compacted at the optimum water content and maximum dry unit weight (Figure 105) have been reported in the range of 5.0 10^{-10} m/s to 5.0 10^{-11} m/s (Khun, 2010).

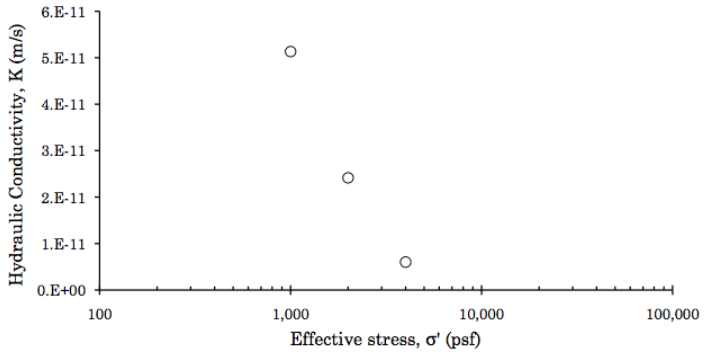

Figure 105. Hydraulic conductivity values for Eagle Ford clay samples (Khun, 2010).

Soil samples were prepared using a target moisture equal to the optimum water content and to several unit weights to cover a wide range of void ratio values. The ATX cell allows imposing an independent vertical load through the air piston. This system was used to test three different loading conditions: a) 20 kPa net stress, which is calculated at each stage as the difference between vertical stress and suction ($\sigma_{vne} = \sigma_v - \psi$), b) 25 kPa total vertical stress, and c) 1 kPa total vertical stress. A summary of the characteristics for the initial conditions of the soil samples is presented in Table 15.

Table 15. Testing scope for Eagle Ford clay

Test	RC_t	w_c	γ_d	e	σ_v
[#]	[%]	[%]	[kN/m^3]	[-]	[kPa]
EFW1a	100	24.0	15.2	0.768	20.0*
EFW1b	100	24.0	15.2	0.768	20.0*
EFW2a	100	24.0	15.2	0.768	25.0
EFW2b	100	24.0	15.2	0.768	25.0
EFW3a	100	24.0	15.2	0.768	1.0
EFW4a	90	24.0	13.7	0.964	1.0
EFW5b	80	24.0	12.2	1.210	1.0

* values corresponding to net stress, not total stress.

10.2.1.2 Experimental Results

Experimental results were obtained from multistage ATX Cell tests applying the testing procedure described in Chapter 4 and applied in Chapter 7 for a low PI clay. Each testing stage involved imposing a target matric suction (ψ) value and a vertical stress (σ). The data obtained in each test includes the volumetric water content (θ) and void ratio (e). The equilibrium points at the end of each testing stage were used to define a three-dimensional representation of the hydro-mechanical path of each test in the (ψ, θ, e) space.

Figure 106 shows the results of the tests listed in Table 15. This representation provides insight on the impact of the void ratio over the retention capabilities, as well as on the impact of the imposed stress in the volume changes measured during the test.

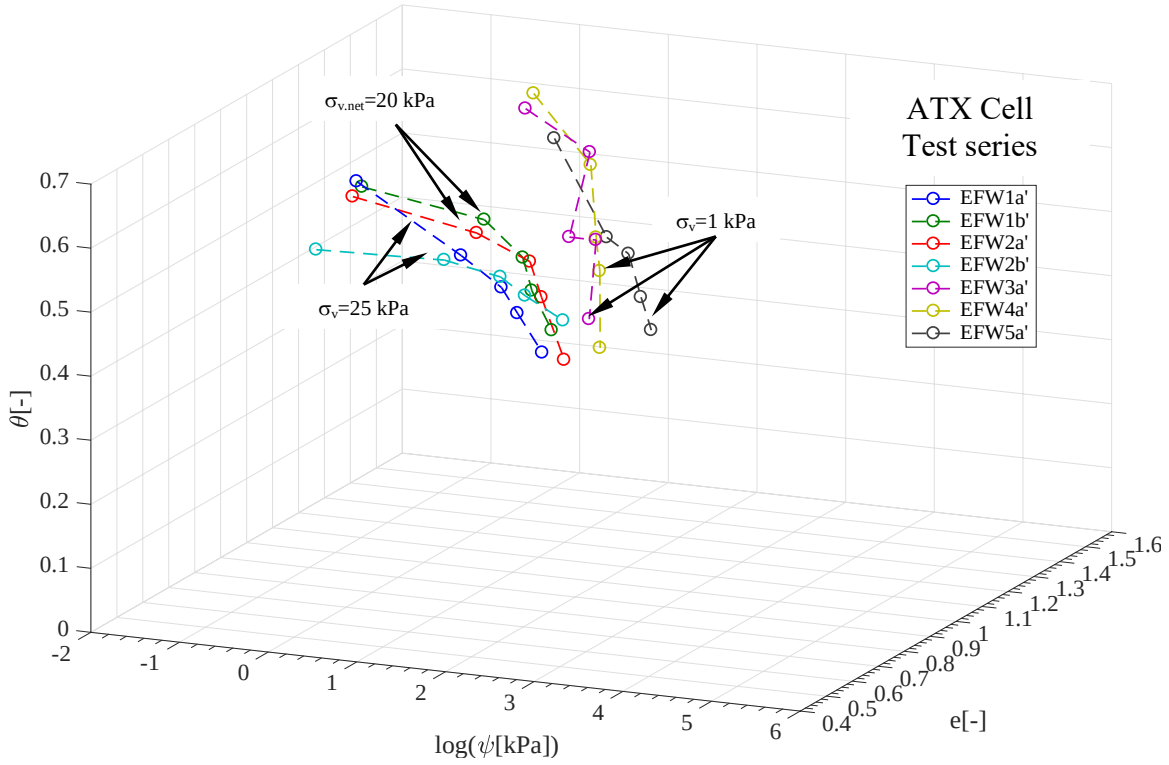

Figure 106. ATX Cell test results for Eagle for clay in three-dimensional (θ, ψ, e) space.

Three two-dimensional views of the same experimental data are shown in Figure 107 to illustrate the relationship among the three variables. Figure 107(a) illustrates the data in the θ-ψ plane together with three SWRC (defined at relative compactions of 80%, 90% and 100%) included as a reference. It can be observed that the experimental data in this plane does not follow any of the reference curves except at very specific points where the tests have the same void ratio than the SWRC.

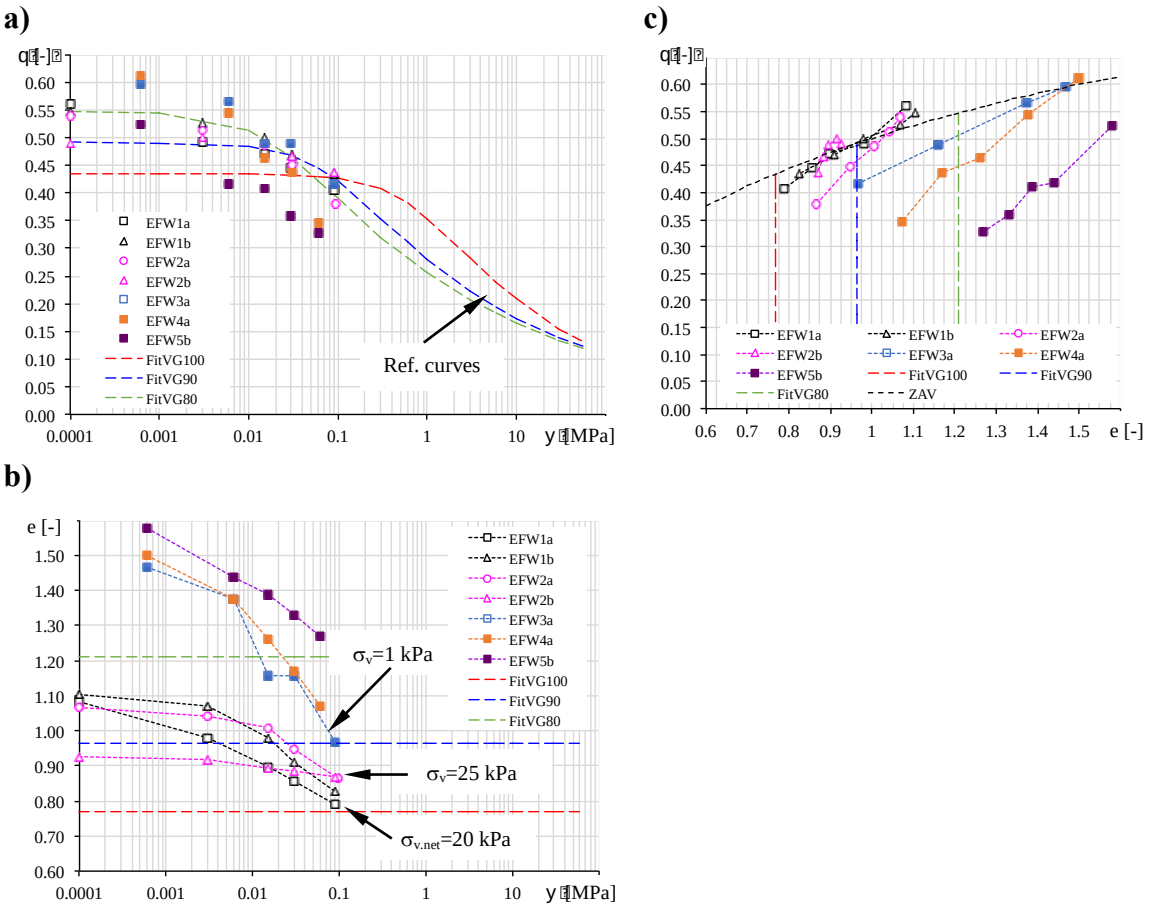

Figure 107. Two-dimensional views of the SWRS for Eagle Ford clay: a) θ vs ψ plane, b) θ vs e plane and c) e vs ψ plane.

Figure 107(b) illustrates the changes in void ratio through the successive testing stages for all ATX cell tests. A comparison between tests EFW2a and EFW3a, where both samples were compacted at the same initial conditions, but different vertical stresses were applied (25 kPa and 1 kPa respectively) shows that the higher the vertical stress the lower the associated volume changes.

Figure 107(c) shows that the increment of the volumetric water content not only depends on the suction stage applied, but also on the void ratio achieved. In previous examples (EFW2a vs. EFW3a), the amount of water incorporated was found to be proportional to the void ratio, and in both cases the soil sample becomes saturated.

In general, for the range of suction tested (100 kPa to 0.1 kPa) and the targeted water content and void ratio, the degree of saturation measured is higher than 80%, with the exception of test EFW5b (the highest void ratio) where the sample starts at 60% and only achieves an 85% saturation.

10.2.2 Transient response

As explained in Chapter 4, every testing stage in the ATX cell involved changing the air pressure to impose a new equilibrium condition results in changes in water content and volume. Figure 108 illustrates the successive time responses for test EFW3a.

The ATX Cell allows measuring the changes in total weight and in height of the soil sample to calculate the relevant variables (e.g. volumetric water content or the void ratio).

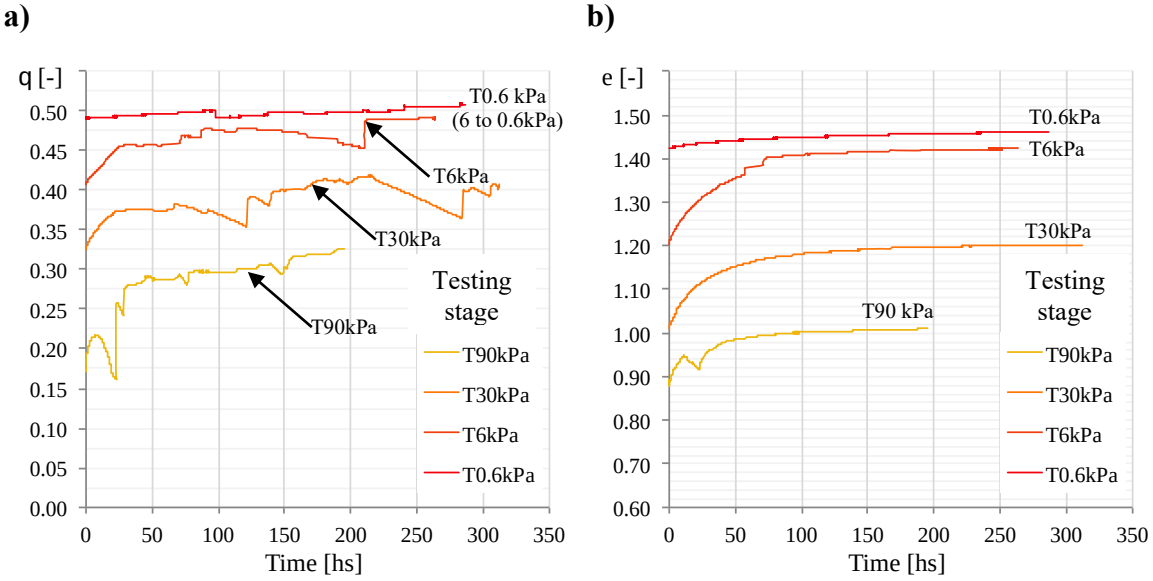

Figure 108. Transient response in ATX Cell test EFW3a for each testing stage described by: a) water content, and b) void ratio time histories.

In this case, it can be observed in Figure 108(a) the presence of discrete changes in the volumetric water content due to the presence of bubbles in the system. However,

volume changes are not affected by these bubbles and smooth transitions could be achieved, as shown in Figure 108(b).

For every stage, independently of the suction applied, most of the changes in both the water content and void ratio occur during the first 50 hs of testing. Also, with this information a coupled behavior could be identified between both variables. When the swelling rate decreases (lower changes in void ratio with time), the inflow rate decreases as well (lower changes in volumetric water content with time).

The main differences of this test in comparison with the results presented in Figure 55 for RMA soil are: a) the duration of each stage was approximately 300 hs for Eagle Ford clay vs. 100 hs for RMA soil; and b) the amount of deformation as a result of the expansive behavior of the Eagle Ford clay against an almost rigid behavior of RMA soil. In both tests the total vertical pressure imposed was 1 kPa.

10.3 MEASUREMENT OF THE RETENTION CAPABILITIES OF HIGH PLASTICITY CLAYS AT HIGH SUCTION VALUES

Two testing techniques were selected to characterize Eagle Ford clay's SWRS at comparatively high suctions values: the filter paper test (ASTM D5298-94), and the chilled mirror hygrometer (ASTM D6836 - 02(2008)). While the filter paper test provides results for the matric and total suction, the WP4C only allows determining the total suction of soil samples.

In order to include this experimental data in Eagle Ford clay SWRS, all values must be matric suction measurements. The WP4C provides a much faster testing than the filter paper, but it is necessary to subtract the osmotic suction component before using it to define the SWRS.

10.3.1 Testing program

Three sets of soil samples, prepared at different relative compactions (80%, 90% and 100% maximum proctor standard dry unit weight), were compacted using a broad range of water contents for the filter paper test. Each soil sample contains two filter papers that allow measuring the total and matric suction of each sample.

After equilibrium was reached and the soil samples were removed from the containers, a piece of each sample was tested to measure the total suction using the WP4C device. This provides a comparison of the total suction measurements for the exact same samples using two testing techniques. Also, using this information it became possible to determine the osmotic suction values.

In addition, a series of tests were carried out using the chilled mirror hygrometer to determine the total suction over a broad range of unit weights and water contents. The total suction values were compared to determine the matric suction.

10.3.2 Experimental results

Filter paper test samples were stored for 14 days and tested according to the procedures described in Appendix 1 (Section 1.4). Figure 109 illustrates the results obtained from the filter paper test (total suction and matric suction), and from the WP4C test (total suction) for a series of samples compacted at a constant void ratio (equivalent to 90% of relative compaction). A clear trend can be observed in the matric suction values from filter paper; however, the experimental data for total suction shows a comparatively high scatter. The inclusion of the WP4C test provides a consistent definition of the total suction, and allowed measuring the difference between total and matric suction at different water contents.

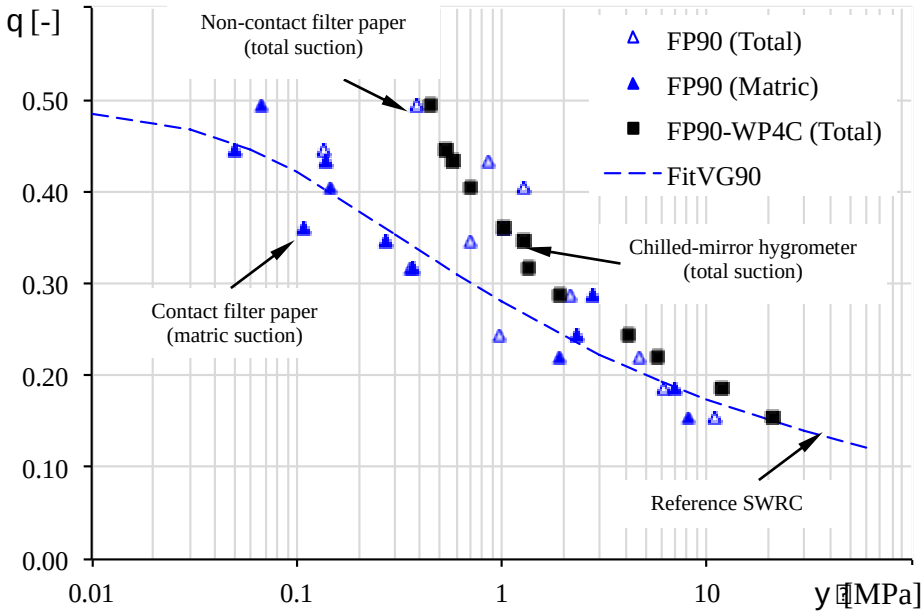

Figure 109. Experimental data from Filter Paper (total and matric suction), and WP4C test (total suction) for Eagle Ford clay samples compacted at 90% relative compaction proctor standard.

Figure 110 shows the matric suction measurements on Eagle Ford clay for a series of samples compacted at three different unit weights and a wide range of gravimetric water content values (6% to 30%). Since the samples have not been subjected to a wetting or drying process (considering negligible the amount of moisture interchanged with the filter papers) it may be assumed that they have remained at a constant volume.

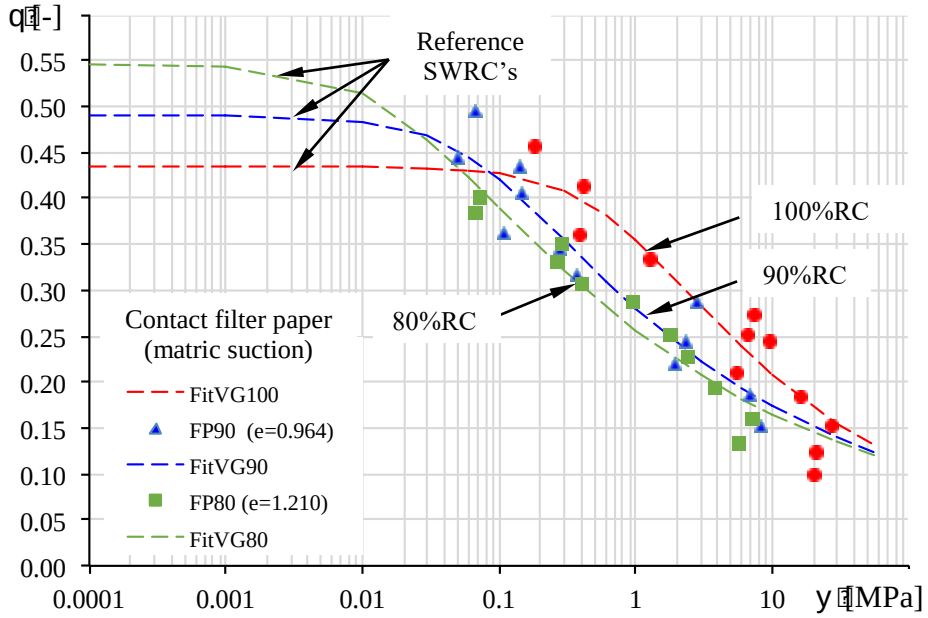

Figure 110. Experimental data from Filter Paper (matric suction) for Eagle Ford clay samples compacted at three different relative compactions.

The results show values as low as 50 kPa and as high as 30 MPa. The impact of the void ratio can be observed in the slope of each series of tests. Three SWRC (van-Genuchten model) were included as reference for each constant void ratio. This comparison indicates that all the measurements correspond to suction values that are higher than the air entry pressure (for each void ratio), although this should be confirmed with the inclusion of measurements at lower suction values (e.g. using the ATX cell).

In order to use the filter paper and WP4C measurements to define a SWRS defined using matric suction values (ATX Cell, and contact filter paper) it is necessary to subtract the osmotic component from the total suction value.

In unsaturated flow problems in soils, the osmotic potential has often been typically considered uniform in space, therefore the gradient is deemed negligible and it does not induce flow. Then, suction values are represented in the SWRC in terms of the matric suction, which is responsible for flow along with the gravitational gradient.

Figure 111 shows the results previously presented in Figure 109 and a matric suction data set derived using WP4C results subtracting a constant suction value. Using this procedure the derived values lay near the fit proposed for the matric suction values. The subtracted suction value (difference between total suction and derived matric suction) may be assumed to correspond to the osmotic suction. In this case, the constant value assumed as osmatic suction was found to be 630 kPa.

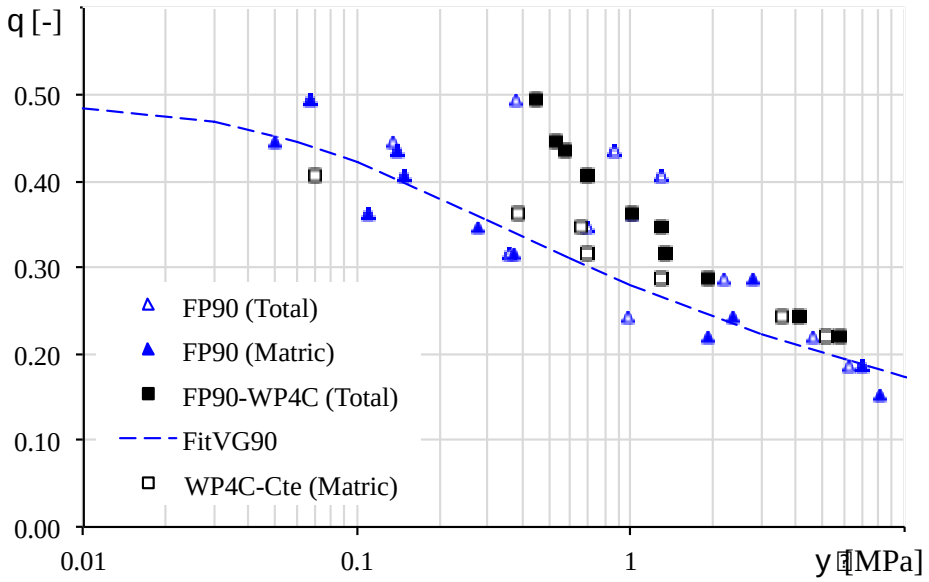

Figure 111. Derivation of matric suction values using WP4C test results (total suction) for Eagle Ford clay samples compacted at 90% relative compaction.

The same procedure was performed to define the total suction values obtained using the WP4C device with all the samples of the three data sets in Figure 110 in order to derivate the matric suction values at different void ratio values. Figure 112 shows the correlation established between the volumetric water content and the matric suction for three different void ratio values.

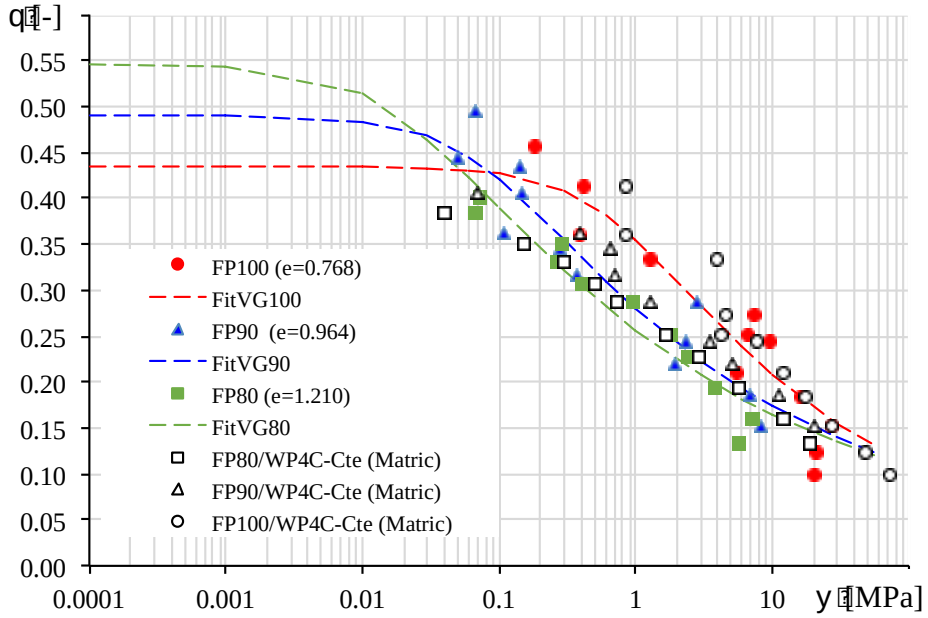

Figure 112. Derivation of the correlation between volumetric water content and matric suction values using WP4C test results and a correction factor for Eagle Ford clay samples compacted at three relative compactions.

The chilled mirror hygrometer test has the advantage of considerably reducing the testing time required to produce results (5 to 15 minutes per sample) while a filter paper test that requires 7 to 14 days.

A series of tests were carried out using only the Chilled Mirror Hygrometer (WP4C) device. Figure 113 illustrates the correlation between the volumetric water content and total suction for Eagle Ford clay, covering a broad range of water contents, from saturation to air dry condition, and dry unit weights, from a very loose condition (65% RC), passing for a barely compacted soil sample (75% - 80% RC), to a heavily compacted soil sample (95% RC). The total suction values range between 0.3 to 80 MPa for water content ranging between 0.45 to 0.05. In addition, this experimental data was produced in a fraction of the time required for the filter paper tests.

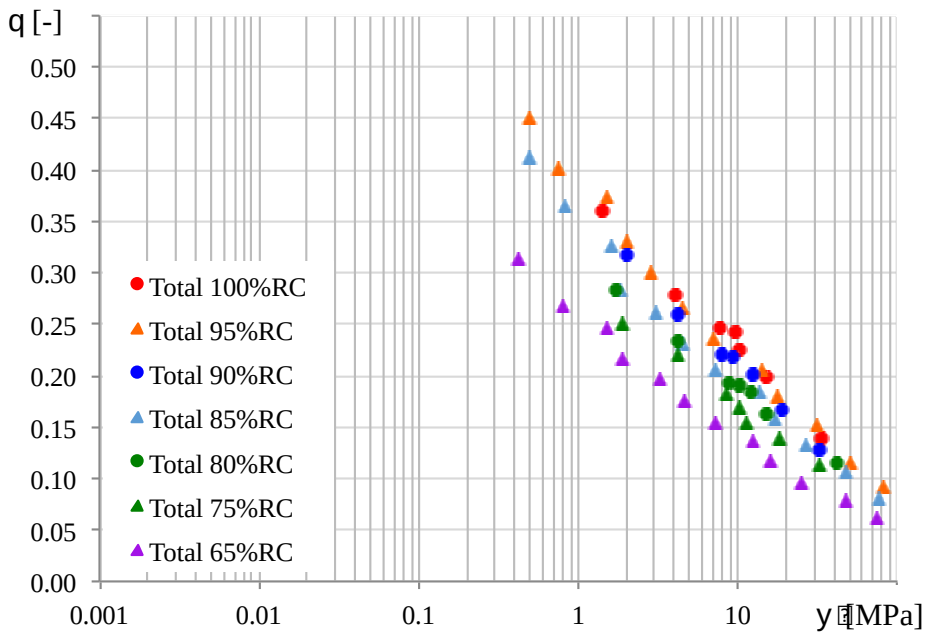

Figure 113. Correlation between total suction and volumetric water content factor for Eagle Ford clay samples compacted at three relative compactions.

The correction procedure was also applied to the WPC4-generated total suction values to define the correlation between volumetric water content and matric suction for all these samples and dry unit weights (Figure 114). The three SWRCs defined using filter paper test results (matric suction) at constant void ratio are included in Figure 114 to evaluate the accuracy of the correction procedure.

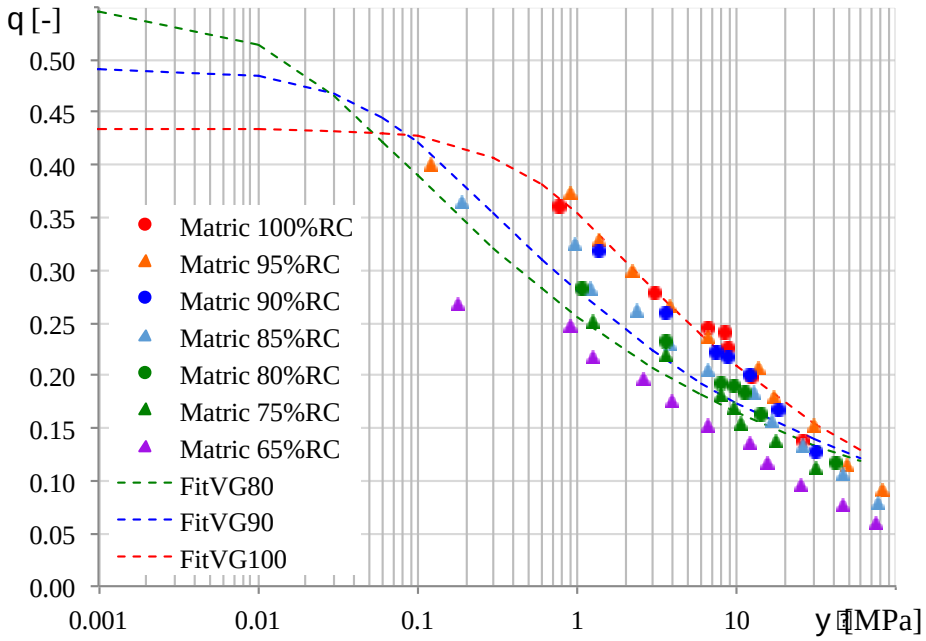

Figure 114. Derivation of matric suction values using WP4C test results (total suction) for Eagle Ford clay samples compacted at dry unit weights ranging from 65% to 95% relative compaction.

10.4 SUMMARY AND CONCLUSIONS

Characterization of the unsaturated hydraulic properties of an expansive soil, Eagle Ford clay (EF) was successfully achieved by implementing standard (1.g) laboratory tests. The information compiled to define the SWRS includes a comparatively wide range of dry unit weight and suction values, ranging from 0.1 kPa to 100 MPa.

In order to combine hydraulic test results from multiple sources, all of them were expressed in terms of the same suction component (matric suction). Based on the results obtained in the research component presented in this chapter, the following conclusions can be drawn:

- The ATX Cell was found to facilitate the hydro-mechanical characterization of a high plasticity clay, Eagle Ford, providing continuous measurement of void ratio, matric suction, and water content.

- The experimental data obtained using the ATX cell (pressure extractor test) cannot be displayed as a SWRC. The void ratio changes throughout the path.
- Measured volume change depends on the initial void ratio and the stresses imposed. For example, Samples EFW2a and EFW3a were compacted at the same initial conditions, but the imposed vertical stresses were 25 kPa and 1 kPa, respectively. Volume change for EFW2a was found to be less than half of that for EFW3a.
- Water content was found to be proportional to the volume changes. In both cases (EFW2a and EFW3a) the water content values were high enough to achieve full saturation.
- In general, for the range of suction values tested in this study (100 kPa to 0.1 kPa), as well as for the targeted water content and void ratio, the measured degree of saturation was higher than 80%
- During each testing stage, a coupled behavior could be identified between volume changes and water content. The swelling rate and the inflow rate were found to follow the same pattern with time for all suction values.
- The total duration of each testing stage for Eagle Ford clay was 300 hs, in comparison to the 100 hs necessary for RMA soil. For every stage, independently of the suction applied, most of the changes in both the water content and void ratio were found to occur within the first 50 hs of testing.
- While the volumetric water content defined using direct measurements of weight is affected by the entrapped air in the system, the void ratio defined using direct measurements of the sample height was found to show a smooth relationship.
- Both, filter paper and WP4C techniques provided useful experimental data to define the retention characteristics of Eagle Ford clay in a wide range of suction values, ranging 300 kPa to 100 MPa.

- While the filter paper test provided a clear trend for the matric suction values, the total suction measurements (non-contact filter paper) showed considerable scatter. Yet, the WP4C tests carried out in the same soil samples provided a more consistent trend of the total suction for the void ratio values tested in this study.
- Comparison of the filter paper results with analytical curves indicates that the matric suction measurements obtained with filter paper are higher than the estimated air entry pressure, for the range of void ratio values tested with this technique.
- Subtracting a constant value of 630 kPa from the total suction measurements (WP4C) allowed representing these measurements as matric suction values. This value may be considered as the osmotic suction for the Eagle Ford clay Samples. This procedure assumes a uniform osmotic value in space that is independent of the water contents.

Chapter 11: Hydro-Mechanical Characterization of Unsaturated Expansive Clays Using Centrifuge (N.g) Tests

11.1 INTRODUCTION

An important goal of this research is to develop a technique to characterize the hydraulic properties of unsaturated high plasticity clays in an expeditious way using centrifuge technology. The research component presented in this Chapter benefits from the sensors, testing techniques, and results previously reported in the previous components of the research.

In this research component, a series of tests was carried out in the centrifuge in order to evaluate the hydro-mechanical response of the expansive clays and, ultimately, measure the unsaturated hydraulic properties of Eagle Ford clay. In particular, the goals of the research presented in this chapter are:

- Assess the infiltration results from standard (1.g) column tests in high plasticity clays.
- Evaluate the in-flight time response of the expansive clay due to wetting using a setup that implements the previously developed non-intrusive sensors.
- Gain insight into the characterization of the unsaturated hydraulic properties of Eagle Ford clay using centrifuge technology.
- Identify the advantages and disadvantages of centrifuge testing for the case of expansive clays, both for steady-state and for transient conditions.

11.2 BACKGROUND

Infiltration column tests in unsaturated soils have been conducted using suction and the volumetric water content sensors placed at different levels. The information

collected during the wetting phase can be used to determine the SWRC of the soil and the transient response analyzed to determine the hydraulic conductivity (Cui et al. 2010).

Although this has been shown to be a useful approach, there are several limitations that need to be addressed when testing on high plasticity clays:

- The soil column needs to be high enough to accommodate the suction and water content sensors, and they should not interfere with the soil swelling or induce a preferential flow path.
- While water content sensors can be used for a broad range of values, it may not be possible to measure a wide range of the suction values with only one type of sensor.
- Sensors time response must be compatible with the velocity of moisture changes. While water content sensors based on electric properties (TDR, surface resistivity, or capacitance) provide a comparatively fast response, suction sensors using a surrogate medium (e.g. tensiometer ceramic cup, or HDU porous block) may require longer equilibrium times (specially at high suction values).
- Volume changes must be taken into account in order to incorporate void ratio as an additional variable to characterize correctly the SWRS and K-function.

Above all, unsaturated soil column tests may be extremely time consuming. They should be built on a full-scale to accommodate all the sensors, and to evaluate a broad range of stresses. Also, flow is driven only by the gravitational and suction potentials, and the infiltration process may be particularly slow. For this reason, infiltration column tests in expansive clays have been rarely reported. For example, Cui et al. (2010) evaluated the hydro-mechanical behavior of compacted Romainville clay using a 1.0-meter height infiltration column that was monitored for 338 days.

An alternative to infiltration column models is to use adapted devices that allow imposing elevated hydraulic gradients. These methods can be at constant volume (rigid cells), controlled or free swelling cells (e.g. double flexible wall permeameter cell, Masrouri et al. 2008), or as proposed in this research, using centrifuge testing (in rigid free swelling columns) taking into account all the aforementioned difficulties and limitations.

11.3 TESTING PROGRAM

11.3.1 Procedures and measurement techniques

In this research component the CPUS was used to assess the unsaturated hydraulic properties of high plasticity (expansive) clays. Non-intrusive sensors were implemented in to the tests to determine: the water content profile (using GTDRs as described in Chapter 5), and the deformation and consequent void ratio profile (using image analysis techniques as described in Chapter 6). Due to space limitations, time response, and sensing range suction probes were not included in the acrylic permeameter cups. As in Chapter 8, the suction profile is either imposed in "hydrostatic tests" or derived (from water content and void ratio measurements) using a previously defined SWRS for "Imposed flow tests".

In the tests presented in this Chapter, the measurement techniques described in Section 8.3.2 were implemented. This includes Non-Destructive (ND), Semi-Destructive (SD) and Destructive (D) measurements.

11.3.2 Scope of the testing program

A summary of the test series conducted in this research component, including the initial soil conditions, drying stages, and measurement techniques is provided in Table 16.

Based on the results presented in Chapter 10 and the range of imposed suction expected in the centrifuge during hydrostatic tests (< 300 kPa), a low relative compaction (80% in relation to standard proctor) was selected in order to generate useful (unsaturated) experimental data on from each soil sample.

In addition, several centrifuge speeds were adopted in order to evaluate the advantages of speeding up the flow process and increasing the imposed suction, versus the disadvantage of increasing the imposed stresses.

Table 16. Scope of centrifuge tests performed using Eagle Ford Clay

Test	Date	Initial RC	Initial w_c	Test Type	Testing Stages	Equivalent g-level	Measurement technique	
[#]	[-]	[%]	[%]	[-]	[#]	[N]	A	B
EF1	2/15/17	80	24.0	H	1	125	ND/SD	D
EF2	3/04/17	80	24.0	H	1	200	ND/SD	ND/SD
EF3	3/11/17	80	24.0	IF	1	100	ND/SD	ND/SD

11.4 EXPERIMENTAL RESULTS

The results from the Hydrostatic and Imposed Flow tests are presented in this Section. As indicated in Chapters 8 and 10, the initial soil density and water content (as compacted) impact the coupled hydro-mechanical response of the soil structure during testing, as well as the imposed stresses.

The Hydrostatic and imposed flow tests conducted to define the SWRS and the unsaturated hydraulic conductivity of Eagle Ford Clay were carried out according to the testing procedures described in Section 8.3.1.

11.4.1 Hydrostatic test on expansive clays

11.4.1.1 Comparison of measurement techniques

A comparison of the results using SD, D, and ND measurement techniques is provided for test #EF1. Figure 115 illustrates the dry unit weight and Figure 117 the gravimetric water content profiles obtained using Semi-Destructive (Sample A) and Destructive (Sample B) measurements techniques.

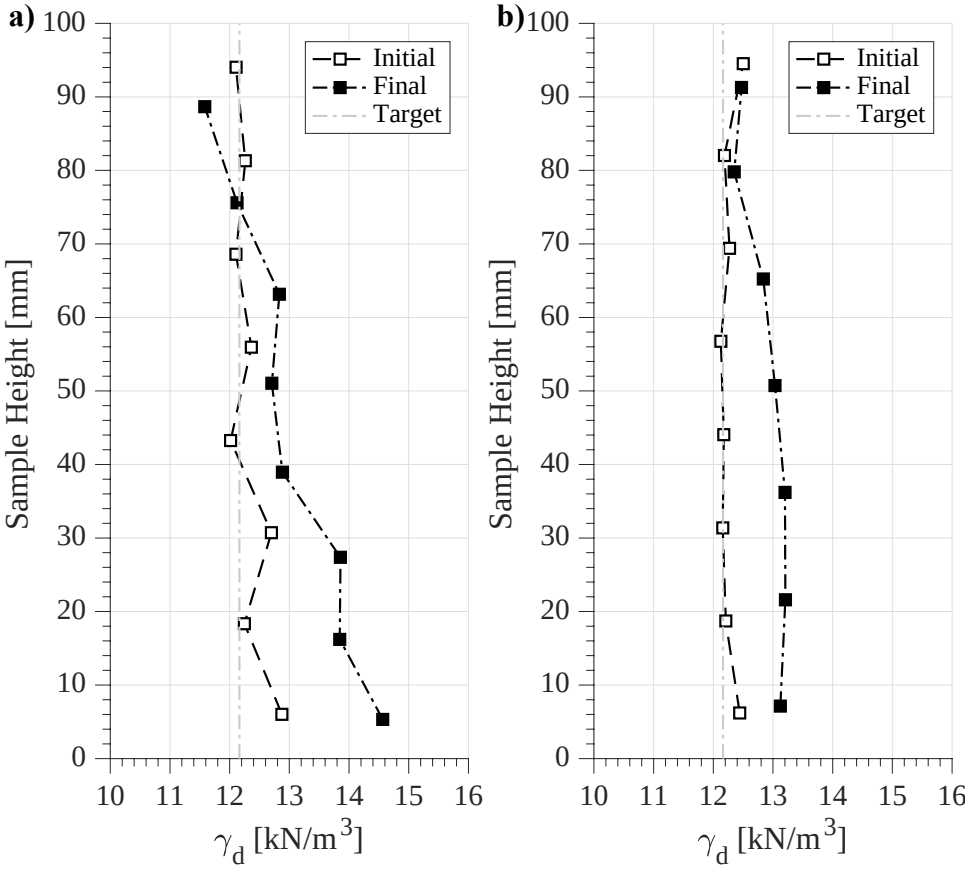

Figure 115. Dry unit weight profiles of Test #EF1 for: a) Sample A (SD) in-flight and b) Sample B (D) after slicing.

The dry unit weight measurements (conducted using image analysis for sample A and slicing for sample B) follow the same trend as the results presented for low plasticity

clays (see Test #2 in Figure 81), increasing towards the base (higher stresses) and showing the effect of slicing the sample (generally reducing the unit weight).

At the top of the sample A, a reduction in the unit weight can be observed as a consequence of the expansion due to wetting. Although all the layers are subjected to wetting, the combined effect of expansion and imposed additional stresses led to swelling only on the top part of the sample. These results can be explained observing the change in height of each soil layer in Figure 116.

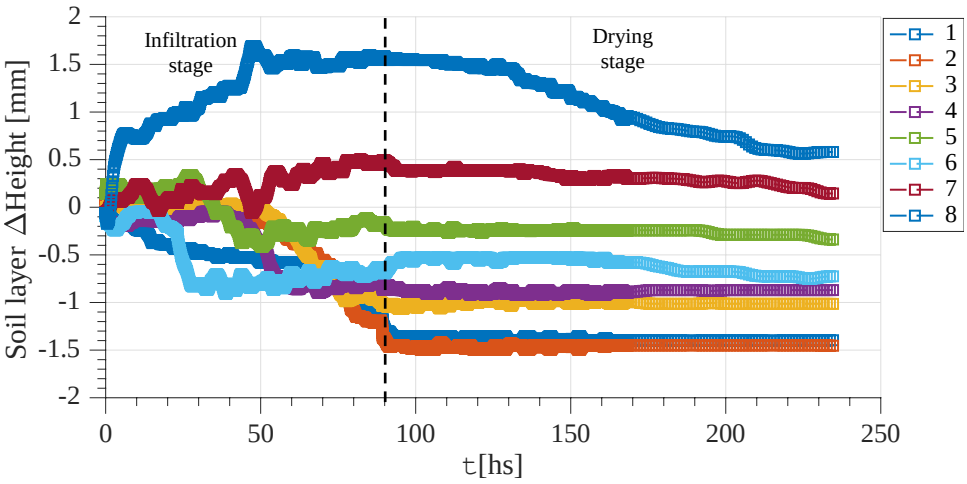

Figure 116. Change in height of each soil layer for Sample A during Test #EF1.

Figure 116 shows the expansion during the infiltration stage, which corresponds to the initial 89 hs of the test and a reduction in the sample volume during the drying stage, which corresponds to the final 146 hs of the test between 89 hs and 235 hs.

On the other hand, the gravimetric water content profile presented in Figure 117 contradicts the expected trend in these tests. The upper section (at higher suction) shows higher gravimetric water content than the lower section. This illustrates that not

incorporating the void ratio measurements as an additional variable during testing can lead to incorrect interpretation.

Figure 118 illustrates the volumetric water content (θ) and the degree of saturation (Sr) profiles at equilibrium. The inclusion of the variable void ratio along the sample provides a more intuitive profile with the low water content and degree of saturation values observed in the sections with high imposed suction values (at the top of the sample) and high water content values at the bottom of the sample (at low suction values).

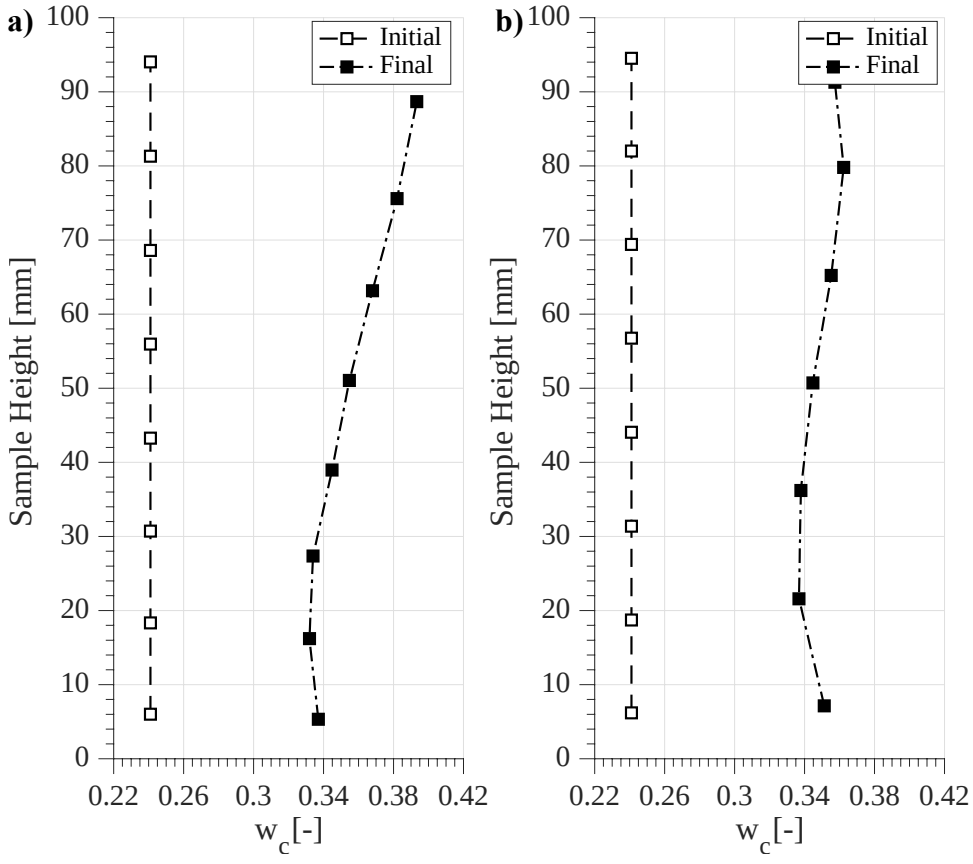

Figure 117. Water content distribution of Test #EF1 after slicing: a) Sample A (SD) and b) Sample B (D).

Although the gravimetric water content profiles are very similar (both were obtained through slicing and oven drying) the volumetric water content and saturation profiles in Sample B are lower than in Sample A as a result of the lower unit weight created by the slicing process.

The experimental data from test #EF1 is represented in the [Sr, e, ψ] space to define the SWRS (Figure 119). This figure now presents all the available information, the impact in the degree of saturation as a result of the changes in the sample density during centrifuge testing can be directly observed.

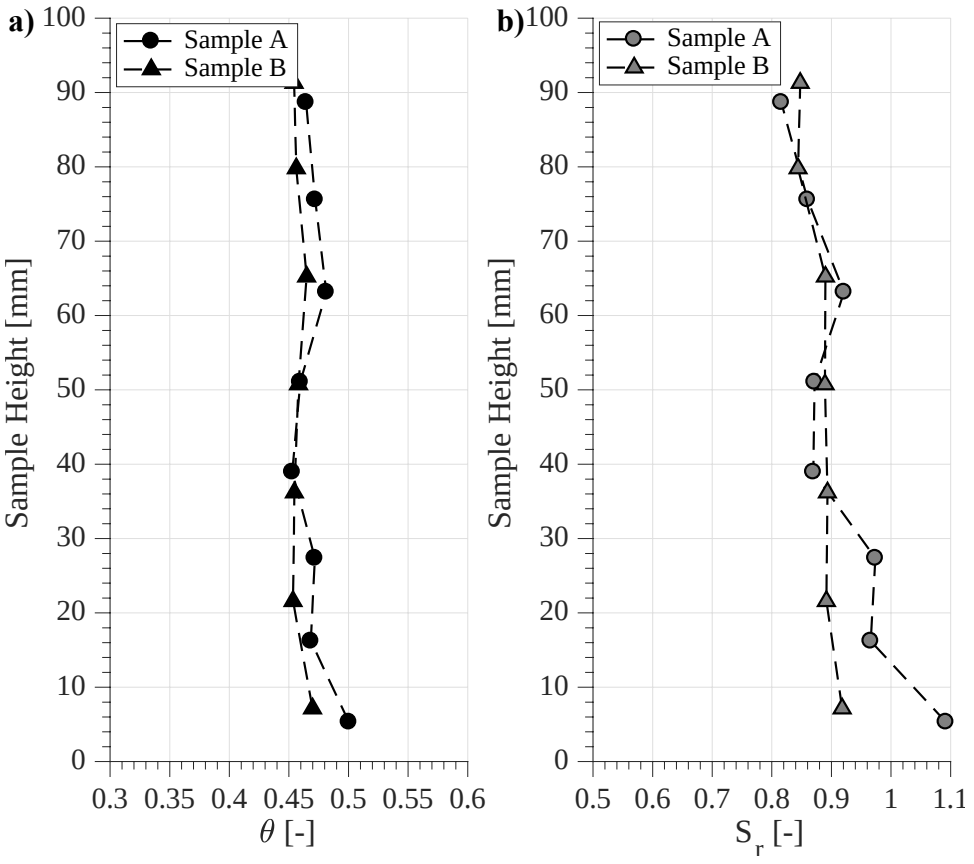

Figure 118. Comparison of samples A and B of Test #EF1 using: a) volumetric water content (θ), and b) the degree of saturation (Sr) profiles.

Figure 119(a) shows the correlation between the degree of saturation and the imposed (hydrostatic) suction. In general, for all suction values imposed below 112 kPa (top of the sample at 125g's), the degree of saturation is higher than 80%. Figure 119(b) shows how the void ratio changes across the sample, with a reduction at the base (at low suction values) and increment at the top (for high suction values). The impact in the degree of saturation of these volume changes can be observed in Figure 119(c) and as well as in Figure 119(a).

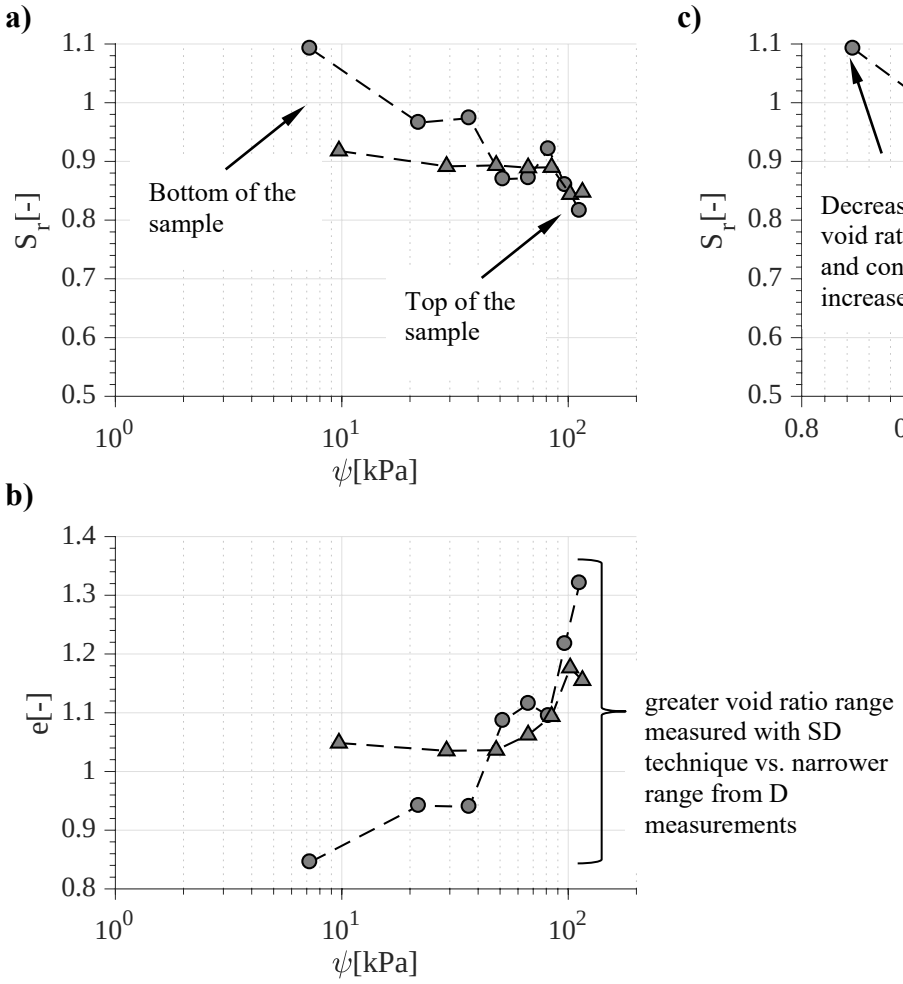

Figure 119. Plane views of the SWRS from Test #EF1: a) Representation of SWRC in the Sr-ψ plane, and complementary views b) lateral view Sr-e, and c) top view e-ψ.

In addition, ND measurements were also obtained from Sample A. Figure 120(a) shows the values reported for each GTDR. In this test, the CSI software did not produce results for the GTDR at the bottom of the sample. However, the AWIGF algorithm was used instead for the recorded waveforms of each GTDR, Figure 120(b) shows the results obtained following this procedure.

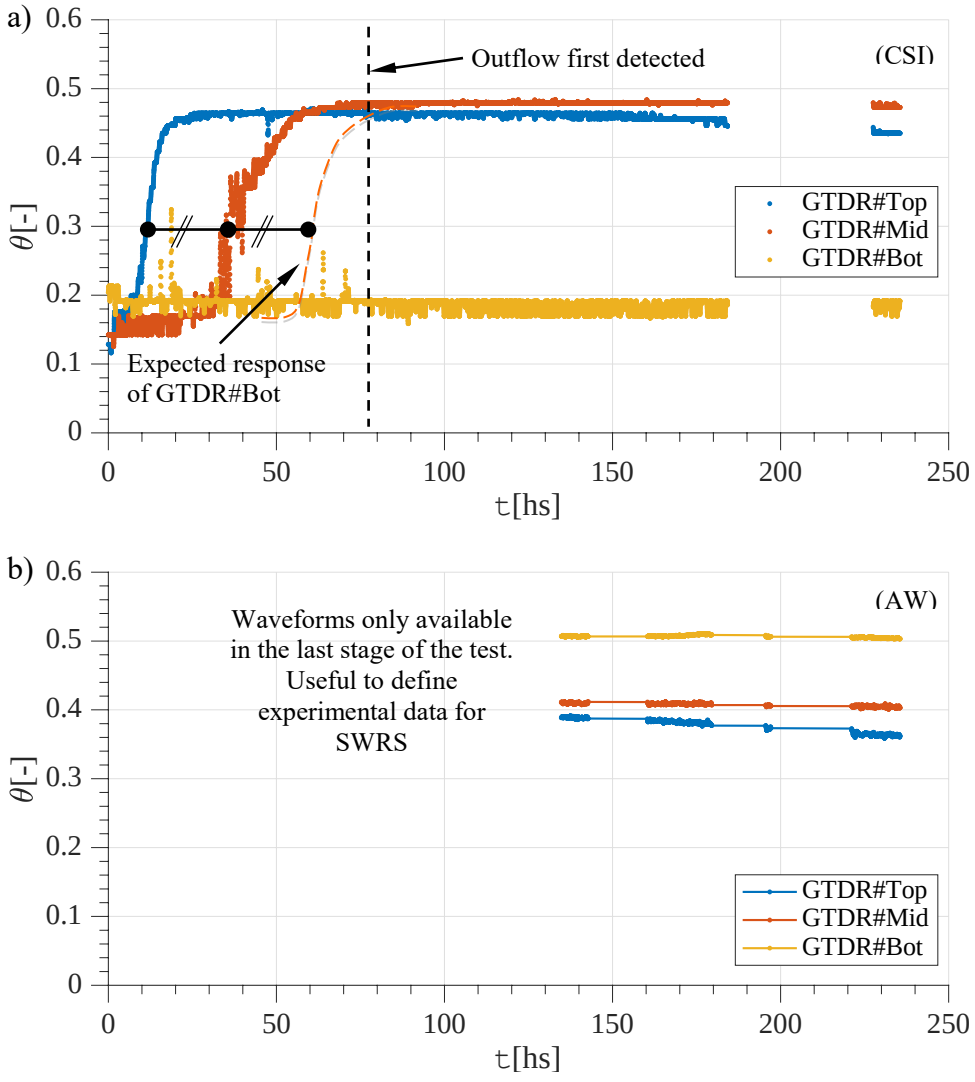

Figure 120. GTDRs time response results represented by volumetric water content using: a) CSI, and b) AWIGF algorithms.

Since the waveforms were recorded only during the drying stage, it was not possible to observe the transient behavior of the sensors during the infiltration process. However, if a similar transient behavior (increment of the water content in time) were adopted for this sensor, it would be expected to reach the maximum water content at a similar time that the outflow was first detected at below the infiltration column (78 hs).

Figure 121 shows the volumetric water content values registered at the end of the test (hydrostatic equilibrium) at the corresponding suction values (at each sensor elevation). While the results obtained with the CSI algorithm show good agreement with the SD measurements, the values reported with AWIGF match for the GTDR #Bot but are lower than the SD results for the upper sensors.

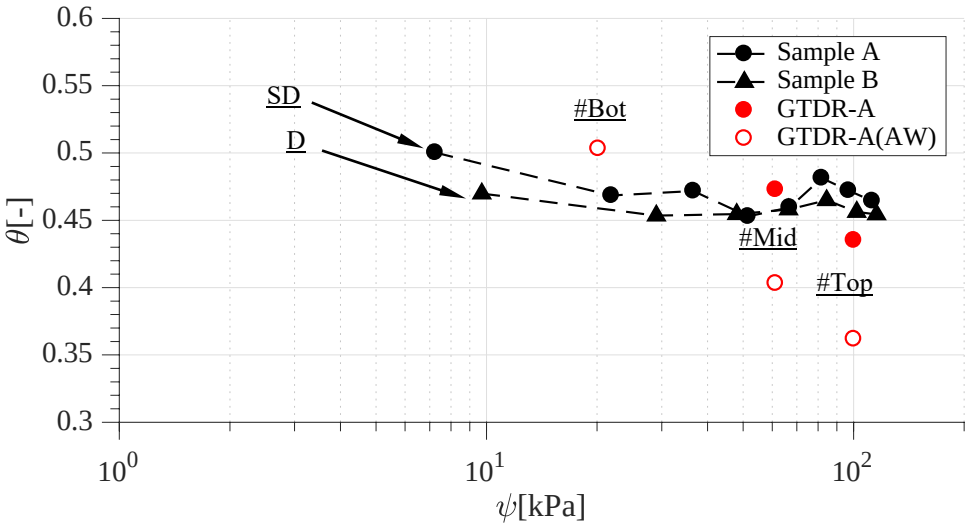

Figure 121. SWRC information of Test #EF1 including ND, SD (Sample A), and D (Sample B) measurements.

The results of the GTDRs were combined with those from the image analysis in order to represent the experimental data in the [Sr, ψ, e] space, and to provide a comparison of the ND, SD, and D measurement techniques (Figure 122).

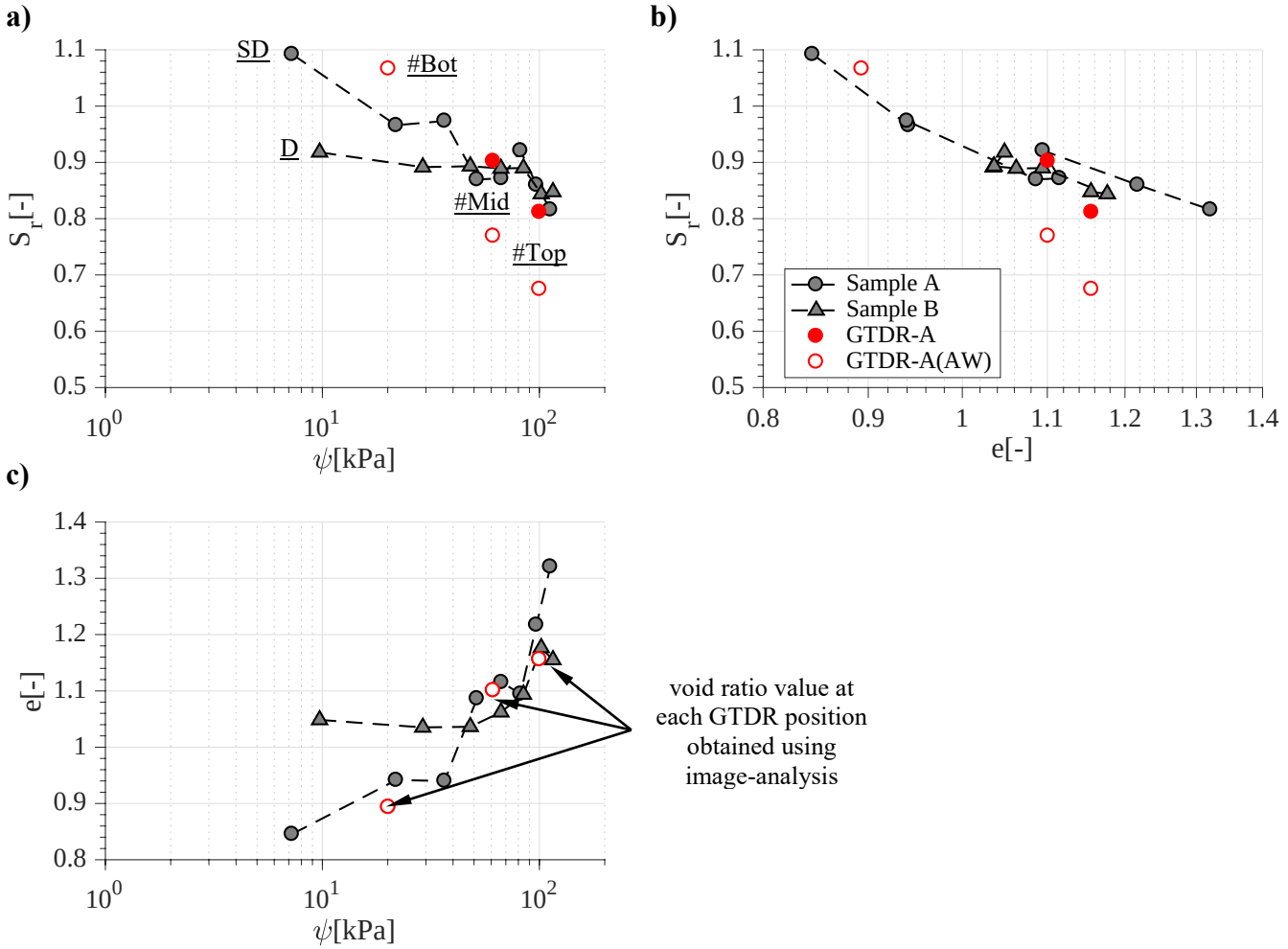

Figure 122. Plane views of the SWRS from Test #EF1: a) Representation of SWRC in the Sr-ψ plane, and complementary views b) lateral view Sr-e, and c) top view e-ψ.

11.4.1.2 Impact of increasing centrifuge speed

Centrifuge testing results in an increasing "gravitational" field along the infiltration column by increasing the centrifuge speed. The CPUS can reach 875rpm (or 600 g's at 0.70 m radius). As a result, the gravitational potential increases, speeding up the infiltration process, as well as the imposed suction at hydrostatic equilibrium. The shortcoming of this technique is that as the imposed gravitational field also increases the mass forces, increasing the stresses in soil particles, resulting in load-induced deformations.

In test #EF2, the gravitational field was increased up to 200g's in order to generate experimental data at comparatively high suction values (and expected low degree of saturation) to define the SWRS, and to assess the advantages and disadvantages of increasing the gravitational field in the centrifuge environment.

Figure 123 illustrates the time response of the GTDRs sensors from both samples of test #EF2. In this test, the waveforms of all the GTDRs were recorded, and the results correspond to the readings obtained using AWIGF algorithm.

In both samples it can be observed the GTDR at the bottom of the sample does not follow the expected trend in response to the advancing wetting front. It shows increasing values since the beginning of the test. This could be related to the presence of water in the base being soaked by the clay.

Outflow was detected around the same time that the GTDR at the bottom of the sample leveled up, indicating that the sample reached a steady state condition. The times registered were approximately 65 hs for Sample A, and 55 hs for Sample B. This can be considered a reduction in the infiltration time when compared with the 78 hs required for test #EF1, although the improvement was not significant.

Figure 123(a) and Figure 123(b) show similar transient sensors responses, with a travel time from the top water content sensor the middle water content sensor of approximately 32 to 40 hs for Sample A and 35 hs for Sample B. However, these times were higher than the 25 hs registered in test #EF1.

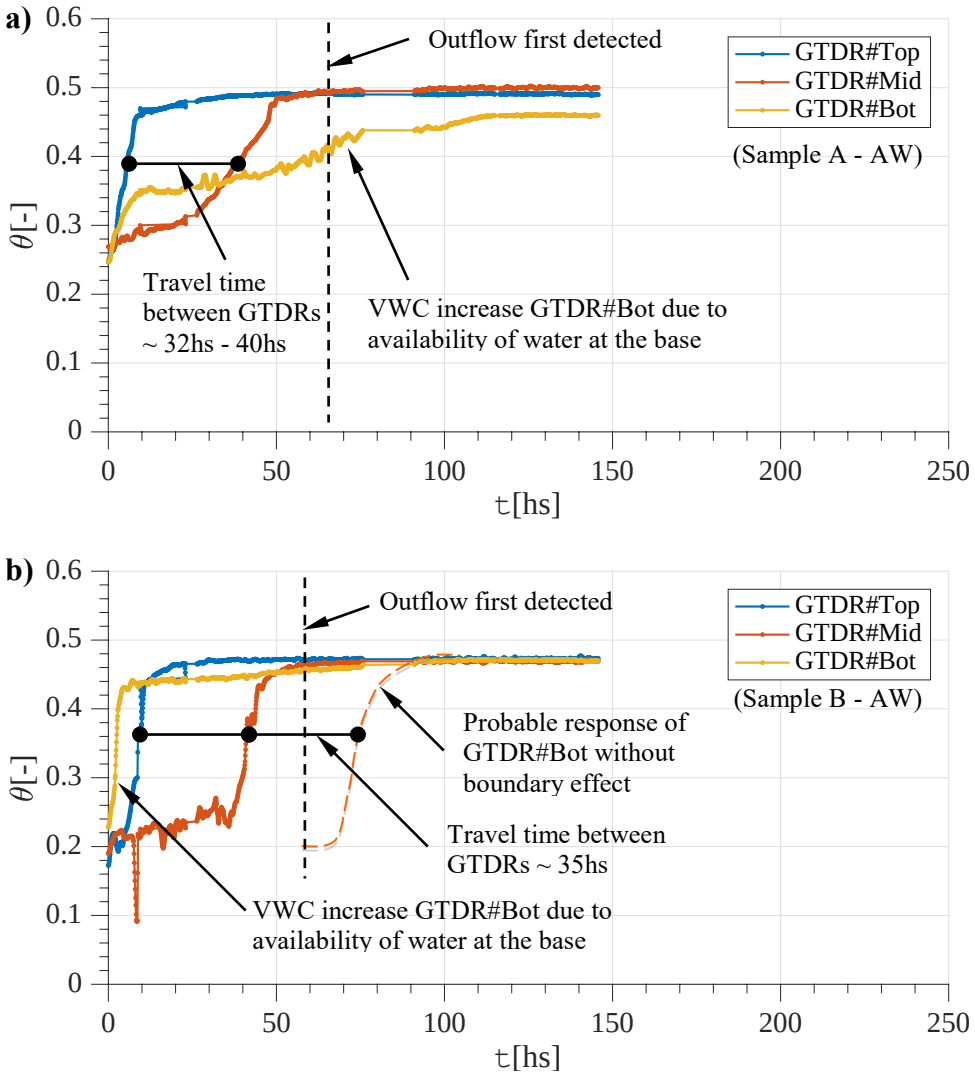

Figure 123. Volumetric water content readings from GTDR's using AWIGF algorithm on test #EF2 for: a) Sample A, and b) Sample B.

The transient response presented in Figure 123 indicates that it should have taken longer for the water to advance through the column and report outflow when compared with test #EF1 (Figure 120(a)). Since the gravitational gradient was increased as a result of the higher centrifuge speed, it could be possible that due to the higher stresses in test #EF2 the hydraulic conductivity was reduced due to a reduction in the void ratio, and this counterbalanced the increased potential. However, the presence of water at the based helped to reach steady state in advance, reducing in the time required to detect outflow.

Figure 124 shows the dry unit weight profiles for both samples of test #EF2, including a comparison with the average dry unit weight obtained for Sample A #EF1.

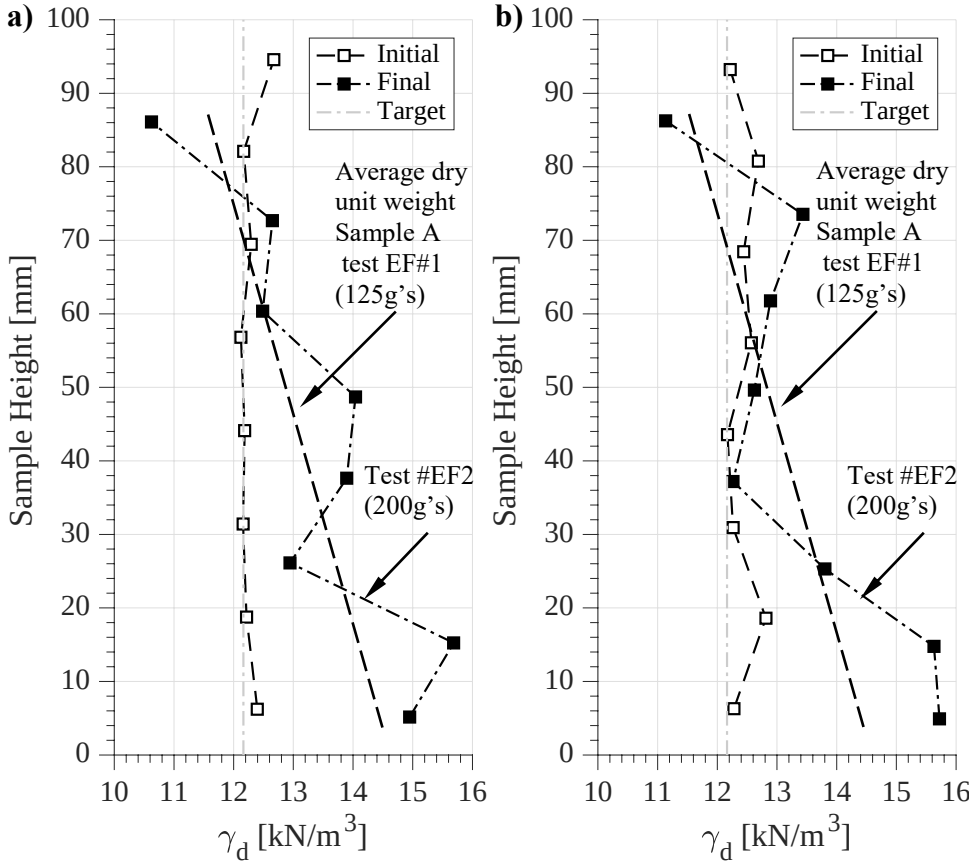

Figure 124. Dry unit weight profiles of Test #EF2 for: a) Sample A and b) Sample B using SD measurements and comparison against average trend from #EF1.

Although the unit weight profile presented in Figure 124 (#EF2) is not comparatively higher than that obtained from the test #EF1 results, the changes in void ratio may be enough to reduce the hydraulic conductivity.

A second objective to increase the centrifuge speed was to reach comparatively higher suction values to characterize the SWRS. Figure 125(a) and (b) shows two planes of the SWRS from test #EF1, and Figure 125(c) and (d) the same information corresponding to #EF2. It can be observed that the suction range increased from 112 kPa (Figure 125a) to 189 kPa (Figure 125b).

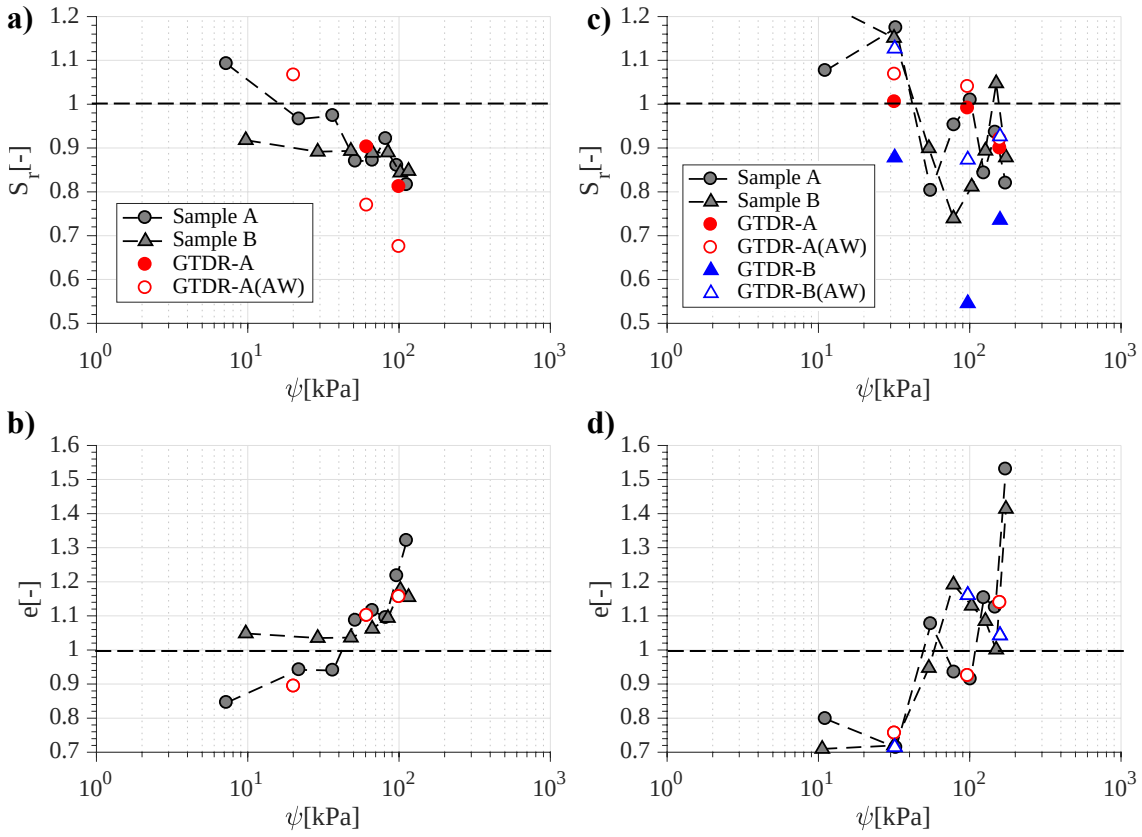

Figure 125. Plane views of the SWRS including a representation in the Sr-ψ plane, and complementary top view e-ψ plane for tests: a) #EF1 and b) #EF2.

However, this increment also created a reduction in the void ratio. While in Figure 125(a) only one-third of the sample remains saturated (as consequence of the low suction and void ratio below 1.0), in Figure 125(b) almost half of the sample has a void ratio below 1.0 and remains saturated despite having a higher imposed suction.

In conclusion, results from test EF#2 showed that increasing the centrifuge speed might lead to reduced testing time if the hydraulic potential increases is counterbalanced by a reduction in the void ratio (and consequently in the hydraulic conductivity). Similar results could be observed in the hydrostatic tests. That is, increasing the suction range leaded to a reduction in the void ratio such as a considerable portion of soil sample remain saturated, even for higher suction values.

11.4.2 Imposed Flow test on expansive clays

The unsaturated hydraulic conductivity for EF clay was measured in the centrifuge by conducting Imposed Flow (IF) tests. Steady state was reached after 350 hours (more than 14 days) with an imposed flow of 0.1 mlh (the lowest inflow rate available in the current configuration) and a centrifuge speed of 405 rpm (equivalent to 100 g's).

In Test EF#3, semi-destructive (SD) and non-destructive (ND) measurements were conducted using Samples A and B. Figure 126(a) illustrates the volumetric water content profile and Figure 126(b) the degree of saturation profile for both samples. Although both profiles are relatively constant along the soil sample height, the water content and degree of saturation are higher at the top, which indicates a suction gradient that could force downwards flow.

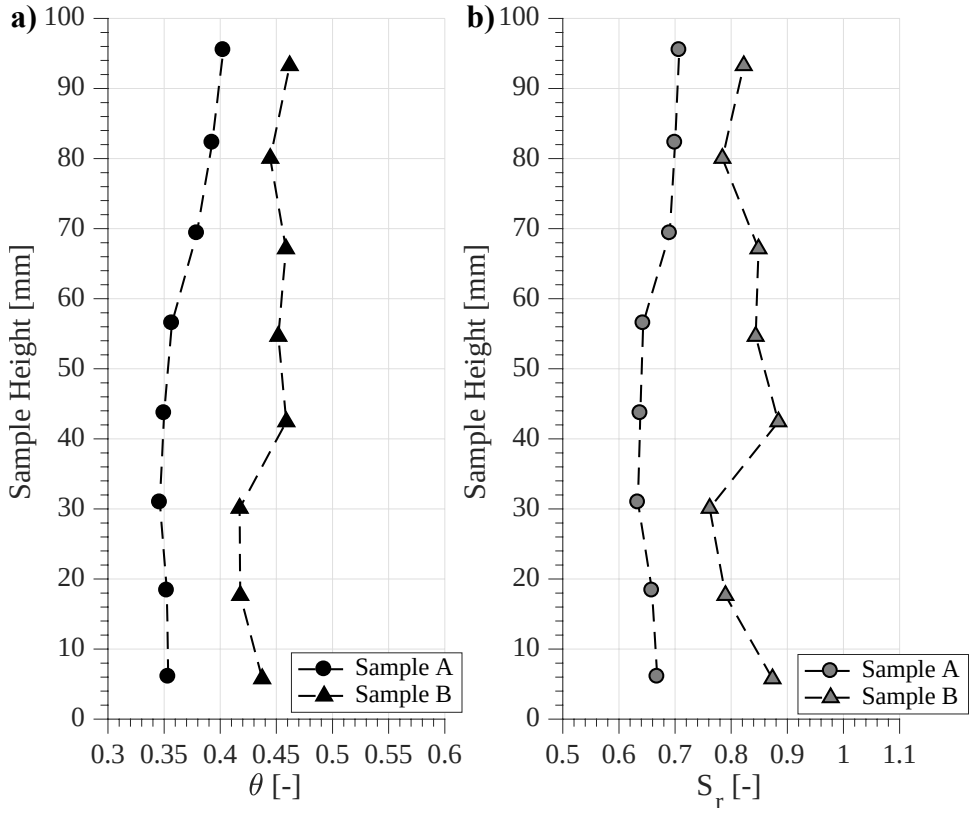

Figure 126. Comparison of samples A and B of imposed flow test #EF3 using: a) volumetric water content (θ), and b) the degree of saturation (Sr) profiles.

Figure 127(a) illustrates the water content profiles (obtained with SD measurements) and the GTDR readings at steady state on each soil sample. Figure 127(b) shows the suction profiles obtained implementing the SWRS for the Eagle Ford Clay.

The water content profiles did not follow the distribution previously observed in Chapter 8 for low plasticity clays. A third-degree polynomial function was selected to define a smooth suction trend (along the samples) and a second-degree polynomial function was used to fit the GTDR data points (Figure 127b).

In general, these polynomial fitting equations allowed accommodating the less uniform profiles, and simplified the derivation of the suction gradient included in the total hydraulic gradient in order to back calculate the hydraulic conductivity.

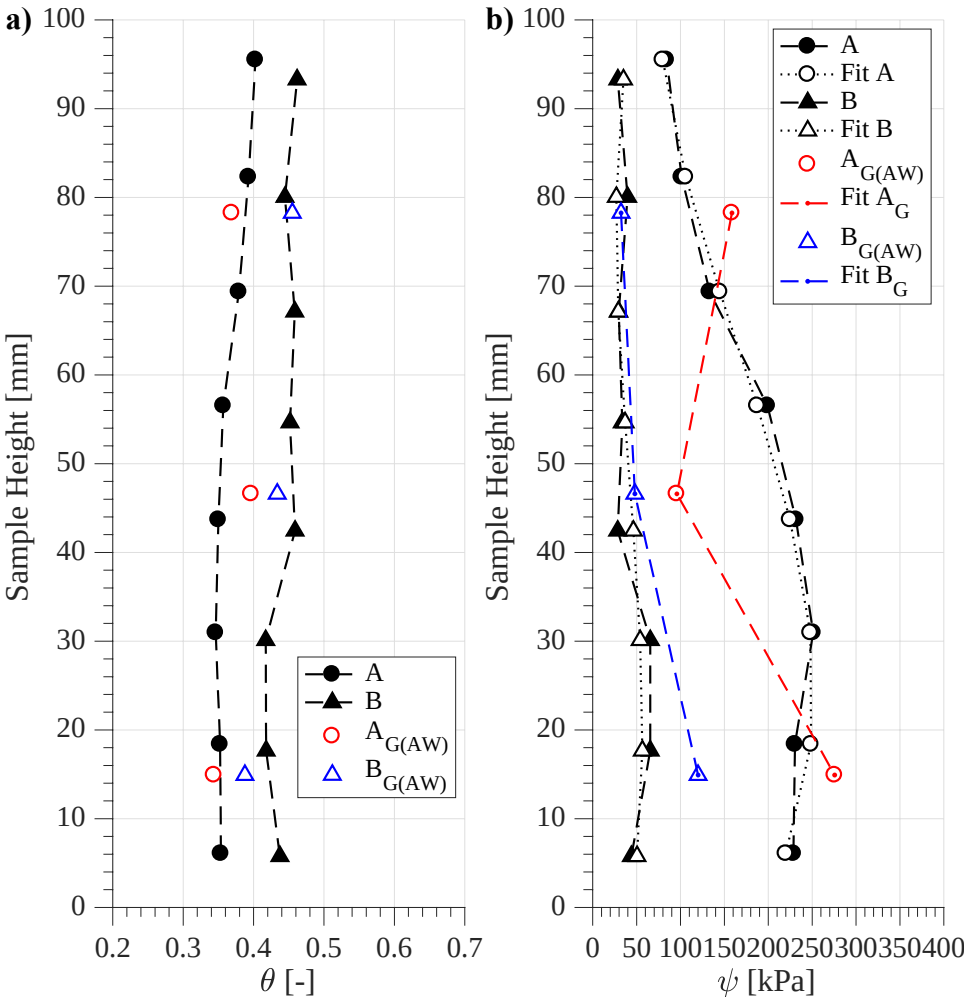

Figure 127. Comparison of sample profiles for test #EF3 including: a) SD and ND measurements of measured water content, and b) derived suction profiles.

It can be observed that the difference in the volumetric water content (based on the SD measurements) between the samples can lead to relatively big differences in the suction profiles. However, this difference in suction values does not necessary result in significant differences in suction gradients (Figure 128a).

Figure 128(b) shows that, for Sample A, the inclusion of the suction gradient in the total gradient creates a deviation of +/-30% from the gravitational gradient.

Consequently, the derived unsaturated hydraulic conductivity ranges between 5.10^{-11} m/s to 1.10^{-10} m/s (Figure 128c).

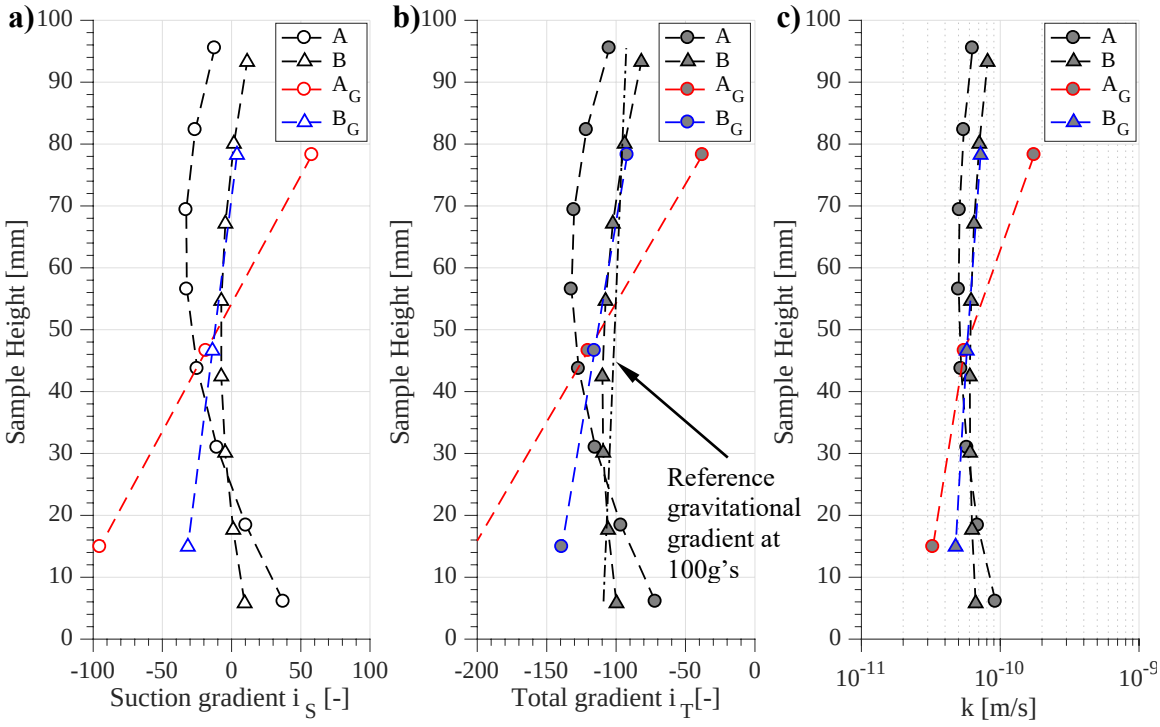

Figure 128. Profiles derived for test #EF3: a) suction gradient, b) total gradients, and (c) derived unsaturated hydraulic conductivity for Sample A, Sample B, and ND measurements on both samples (A_G and B_G) respectively.

When using only ND measurements (GTDR's) the scatter in the readings a significantly affect the suction gradients (e.g. Sample A, Figure 128a). However, the unsaturated hydraulic conductivity values derived using only ND show good agreement with those from SD techniques. Special attention must be placed in this case to the filtering of the sensors readings in order to determine the volumetric water content values at steady state conditions.

11.4.2.1 Comparison with low plasticity clay experimental results

Although it was possible to determine the unsaturated hydraulic conductivity of an expansive clay using a steady-state methodology in the centrifuge environment, it was found to require a considerable amount of time. In comparison with the results presented in Section 8.4.7, the imposed flow test (IF) carried out using Eagle Ford clay Samples required 350 hs (more than 2 weeks) instead of the 5 hs required to achieve steady state flow in RMA soil.

In test EF#3 the imposed inflow rate was 0.1 mlh, which is the lowest constant inflow rate that can be imposed currently in the CPUS. This value represented a tenth of the inflow rate used to fully saturate the sample (1 mlh) at a centrifuge speed of 100g's. With this set up, the degree of saturation achieved for this expansive clay ranged from 0.65 to 0.8, these values could represent a lower bound in the degree of saturation that can be achieve for this expansive clay, which corresponds the unsaturated hydraulic conductivity values between 5.10^{-11} m/s to 1.10^{-10} m/s. These hydraulic conductivity values are in the lower end of the results reported by McCartney (2007) for centrifuge testing when describing the capabilities of the CPUS.

The inflow rate used to saturate the RMA soil sample was at 100 g's was 40 mlh. In Test #4, where an imposed inflow rate of 10 mlh was used, the degree of saturation achieved also ranged from 0.65 to 0.8, and the corresponding unsaturated hydraulic conductivity values ranged from 7.10^{-9} m/s to 1.10^{-8} m/s.

11.5 SUMMARY AND CONCLUSIONS

This research component focuses in the development of a testing technique to characterize the hydraulic properties of unsaturated, high plasticity clays using centrifuge technology. In particular, the goals were: evaluating the in-flight response of the non-intrusive sensors; provide insight on the characterization of the unsaturated hydraulic

properties of Eagle Ford clay; and identifying the advantages and disadvantages of centrifuge testing of expansive clays. The analysis of tests and results showed that:

- It was observed that the coupling between the induced stresses and the expansion/contraction in response to changes in water content, modifies the void ratio along the sample depending on the initial test conditions (i.e. water content, relative compaction) and the imposed centrifuge speed.
- The gravimetric water content distribution in hydrostatic tests was found to contradict the typical distribution observed in centrifuge testing, with higher values at higher suction values.
- The hydro-mechanical characterization of unsaturated expansive clays required measuring the void ratio during testing to define the volumetric water content (or the degree of saturation) to avoid counterintuitive interpretations.
- Despite of the expansive nature of the clay, image analysis was found to successfully detect swelling and contraction during hydrostatic tests.
- The dry unit weight measurements followed a similar trend as that for low plasticity clays: increased unit weight at the base (higher stresses) and swelling near the top.
- It was observed using the image analysis system that during the wetting process only the top layers of the centrifuge samples expanded, while the rest of the layers compressed due to the imposed stress.
- It was found that the implementation of destructive measurement techniques also has an impact in the determination of the void ratio, and consequently in the definition of the volumetric water content, and degree of saturation of high plasticity clays,

- The volumetric water content data gathered using the GTDR's were in good agreement with the SD results obtained in hydrostatic tests.
- In hydrostatic tests, and for all suction values imposed in Test #EF1 at 125 g's (max. 112 kPa), the degree of saturation values measured were higher than 80%.
- Increasing the centrifuge speed up to 200 g's resulted in an increased imposed suction (max. 189 kPa), but the degree of saturation was not necessarily reduced. Indeed, a comparatively larger portion of the specimen remained saturated as a consequence of the reduction in the void ratio along the sample.
- Transient analysis showed that reaching steady state water content values along the column matched with the first detection of outflow below the infiltration column.
- For Eagle Ford clay samples compacted at optimum water content and 80% relative compaction about, 78 hs of were required to reach saturation at 100 g's.
- Comparatively high testing times were observed with the GTDR for the water to advance through the sample when using higher centrifuge speeds (200 g's). This was found contrary to the results expected for a comparatively higher hydraulic gradient imposed.
- The presence of water in the base of the permeameter cup allowed the lower section of the sample to saturate before the wetting front reached this portion of the soil specimen, and to trigger outflow earlier.
- The inflow rate (0.1 mlh) used to measure the unsaturated hydraulic conductivity was the lowest available in the CPUS, with which 350 hours (more than 14 days) were necessary to reach steady state.
- The unsaturated hydraulic conductivity measured under steady state condition ranged from 5.10^{-11}m/s to 1.10^{-10} m/s for the corresponding suction values ranging

from 50 kPa to 250 kPa, and degree of saturation values ranging from 0.65 to 0.85.

- It was observed that the scatter in the water content measurements obtained with the GTDR had a significant impact in the determination of the suction gradient and consequently in the hydraulic conductivity.
- The inclusion of the suction gradient in steady state conditions may account for roughly a difference of +/-30% in the total gradient. Higher differences were found when using data from non-destructive measurements.

Advantages and Disadvantages

- In general, increasing the centrifuge speed might not result in a testing time reduction or lower water contents since the increased gravitational gradients may be counterbalanced by reduced void ratios and a consequently higher air entry pressure and lower hydraulic conductivity.
- The suction range useful to describe unsaturated properties in hydrostatic tests depends on the clay hydraulic properties, but also on the mechanical response of the sample.
- Although it was possible to determine the unsaturated hydraulic conductivity of expansive clays using steady-state tests, a considerable amount of time was required.
- The transient information provided by the non-intrusive sensors was found to be clearly determined and provides useful information to determine the unsaturated hydraulic conductivity.

- Running centrifuge testing in expansive clays may provide a useful tool to evaluate the transient behavior of the clay throughout a wide range of stresses in a reduced amount of time, in comparison to real scale infiltration column models.

Chapter 12: Analysis of the Hydro-Mechanical Characterization of Unsaturated High Plasticity Clays

12.1 INTRODUCTION

Determination of the unsaturated hydraulic properties of clays requires the combination of several measurement techniques. Also, assessment of the hydro-mechanical behavior of expansive clays is time consuming and it involves quantifying all the relevant variables (volumetric water content, suction and void ratio) during testing. The objective of this research component is to define the SWRS and the unsaturated hydraulic conductivity for Eagle Ford clay.

Determination of the SWRS involves incorporating the experimental data obtained in Chapters 10 and 11 using different testing techniques. Numerical optimization of the SWRS model was performed using two different data sets in order to evaluate the ability of the analytical model to incorporate data from different tests, at different suction and void ratio values.

A validation of the SWRS was performed to evaluate the hypothesis that although imposed stresses affect the mechanical response of unsaturated soils, all the measured equilibrium points belong to a unique SWRS.

While centrifuge testing provides a methodology to expedite the flow process in unsaturated clays, a series of advantages and disadvantages of this testing technique were evaluated when measuring the SWRS and the unsaturated hydraulic conductivity of expansive clays using steady-state approaches.

In addition to steady-state approaches, the transient information from standard (1.g) and centrifuge (N.g) characterization tests was analyzed to derive the unsaturated hydraulic conductivity of Eagle Ford clay.

12.2 DETERMINATION OF THE SWRS

The SWRS for Eagle Ford clay was determined using the experimental results obtained in Chapters 10 and 11, and the same models and procedures presented in section 9.2. Although in some tests suction measurements were performed at a given water content and void ratio, in all those cases where the samples were subjected to wetting or drying, due to changes in the imposed suction values, volume changes were measured.

This experimental data cannot be fitted by a single, two-dimensional SWRC (at a fix void ratio), however a single, three-dimensional SWRS can incorporate data from different tests independent of the void ratio measured at equilibrium.

12.2.1 Numerical optimization

The SWRS model is an extension of Van Genuchten (1968) SWRC equation, which includes a linear relationship of its parameters (α, n, θ_s, and θ_r) as function of the void ratio. The numerical optimization of this customized non-linear model was performed using Matlab's Optimization Toolbox™.

The initial values and constrains for each variable were obtained taking into account the values presented in Table 8 for RMA soil SWRS, and after performing several iterations with the curve fitting procedure to observe the influence of the different parameters. Initial values were iteratively updated in order to evaluate the robustness of the solution obtained through numerical optimization. The initial values and constrains (lower and upper bound constrains) presented in Table 17 provided the best optimization for both sets, while minimizing the influence of the constrains imposed to each variable.

Table 17. Constrains applied during non-linear optimization

Parameter	a_1	a_2	a_3	a_4	b_1	b_2	b_3	b_4
	[-]	[-]	[kPa^{-1}]	[-]	[-]	[-]	[kPa^{-1}]	[-]
Initial	0.2	0.10	0.25	0.50	0.50	-0.01	2.0	0.50
Upper B	1	0.15	-	-	-	0	-	-
Lower B.	0	0	0.01	0	0.1	-	0	0

12.2.2 Experimental data sets

In order to define Eagle Ford's SWRS and provide comparison between experimental results two data sets were identified (Table 18) combining the experimental obtained from standard testing (1.g) presented in Chapter 10, and centrifuge testing (N.g) presented in Chapter 11. All experimental data points correspond to matric suction values measured or derived from other measurements.

Table 18. Data sets created for SWRS optimization on Eagle Ford Clay

Testing		Experimental data		
Methodology	Path	Suction range	Set 1	Set 2
ATX Cell (1.g)	Wetting	0 - 100 kPa	X	-
WP4C (1.g)	-	0.3 - 100 MPa	X	X
Filter Paper (1.g)	-	0.05 - 30 MPa	X	X
Centrifuge (N.g)	Drying	0 - 200 kPa	-	X

Data Sets 1 and 2 combine experimental data obtained using different testing techniques at low and high suction values. Set 1 incorporates only results from standard (1.g) characterization tests, and Set 2 combines centrifuge testing (N.g) results at low suction values and standard test results at suctions above 50 kPa.

In order to validate the SWRS model, and to evaluate the impact of the imposed stresses in the hydro-mechanical response of the expansive clays, the tests EFW2a and EFW2b performed in the ATX Cell were excluded from Set 1.

12.2.3 SWRS model calibration

Table 19 shows the best set of parameters obtained to define the SWRS for each data set. The subsequent figures illustrate the SWRS fitted functions together with the experimental data included in each set.

Table 19. Fitting parameters for Eagle Ford SWRS

	Set 1	Set 2
Parameter	[-]	[-]
a_1	0.444	0.428
a_2	0.00	0.00
a_3	0.01	0.00
a_4	1.074	1.11
b_1	0.10	0.10
b_2	-0.328	-0.205
b_3	0.110	0.028
b_4	0.00	0.00

Figure 129 and Figure 130 show the SWRS and the residuals for Set 1. Residuals provide a measurement of the difference between the volumetric water content in the experimental data and the value predicted in the surface.

The results shown in Figure 129 indicate that the data from filter paper and WP4C tests at relatively constant void ratio define a change in the slope of the SWRS along the suction axis. On the other hand, the experimental data incorporated with the ATX cell, allows defining the SWRS at low suction values, including a reasonable correlation between the saturated volumetric water content (θs) and the void ratio.

Residuals in Figure 130 show that the errors are generally below 8%. The experimental data obtained from test #EFW5a (80% relative compaction) shows comparatively larger errors (up to 12%) due to low water contents in a section of high void ratio where few experimental data is available.

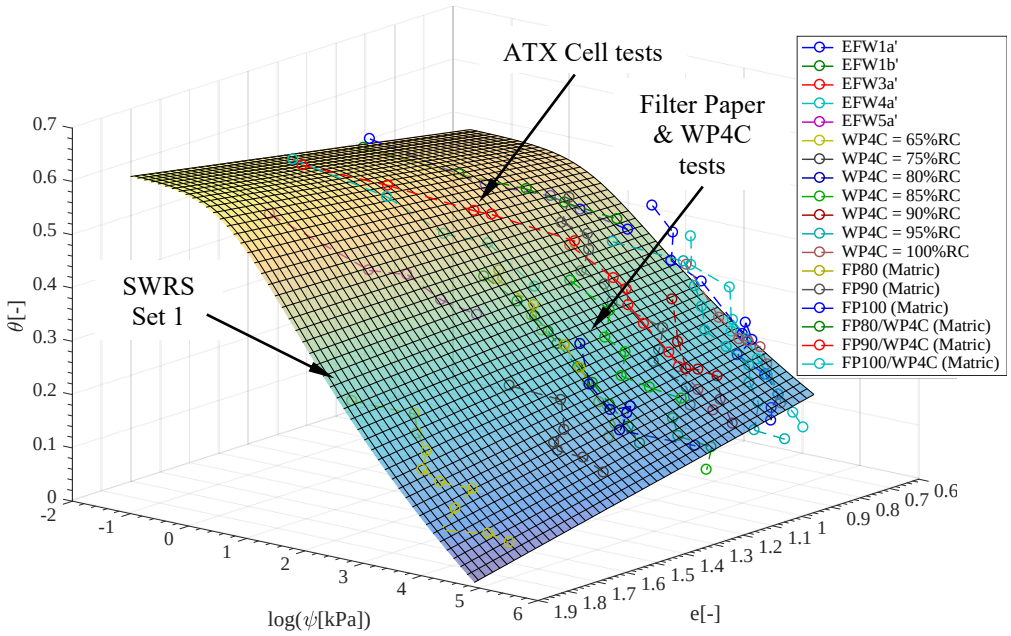

Figure 129. Definition of Eagle Ford clay SWRS for data set 1.

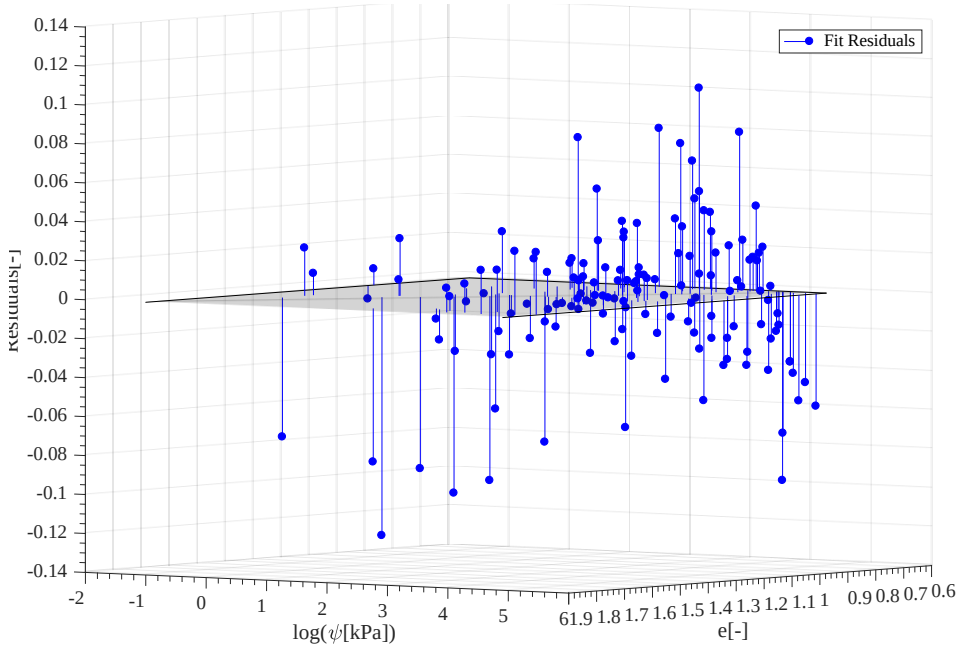

Figure 130. Residuals measured between experimental data and SWRS model for set 1.

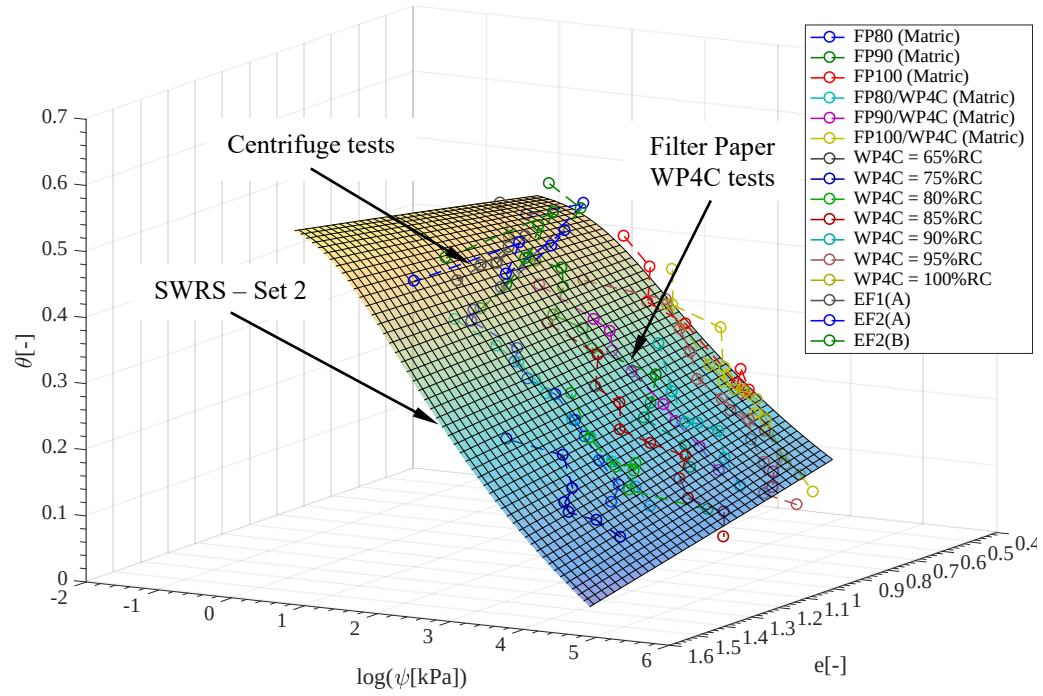

Figure 131. Definition of Eagle Ford clay SWRS for data set 2.

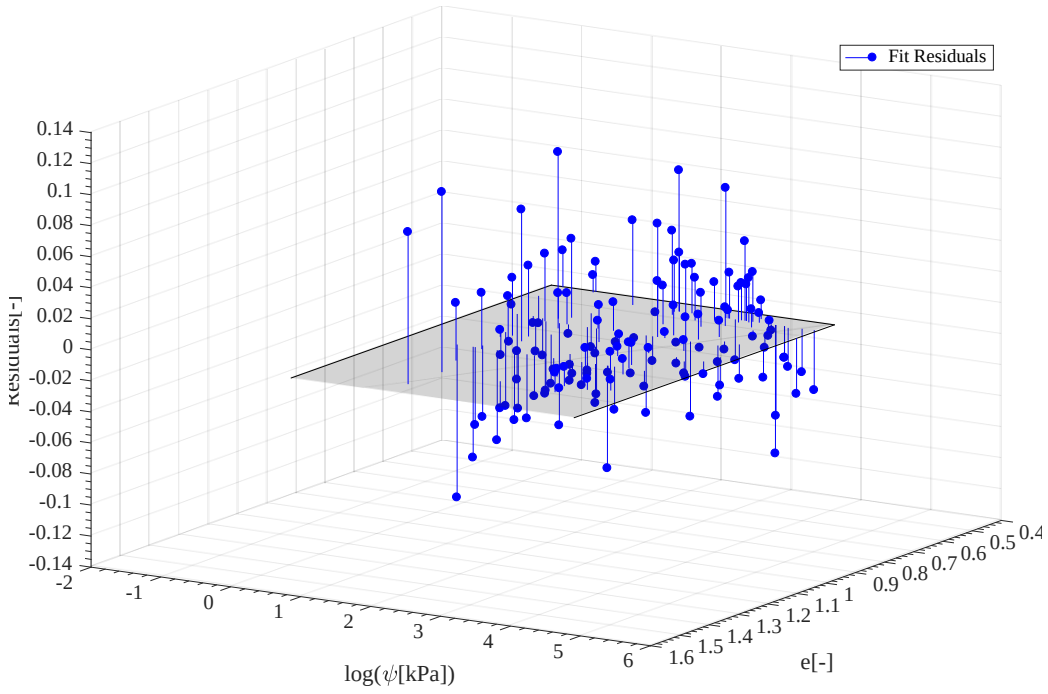

Figure 132. Residuals measured between experimental data and SWRS model for set 1.

Figure 131 shows the SWRS defined for Set 2 including the centrifuge testing (N.g) results in low suction values, and Filter paper and WP4C testing result in high suction values. The SWRS from Set 2 is similar to the one presented in Figure 129 since a considerable amount of data is shared between the two sets. However, the limitation of the centrifuge results at describing low suction values may have an impact in the shape of the SWRS at low suctions.

Figure 132 illustrates the residual distribution of Set 2. In this case smaller errors were observed in comparison to Set 1 (Figure 130). In general the errors were measured within a 6% difference between the experimental data and the surface values.

In both sets, the availability of a significant source of experimental data at high suction values allowed a clear definition of the SWRS slope. On the other hand, the limited availability of experimental data at low suction values did influence the shape of the surface. A sensitivity analysis showed that, due to the scarcity of data in this region, the values obtained for the parameter b_1 (used to define θs) were the ones most impacted by the lower limit constrains defined for this parameter.

In order to improve the definition of the SWRS, data at low suction and low void ratio values may be necessary. This data could be generated using the ATX Cell under a high vertical pressure in order to limit the expansion of the sample. In Set 2 it would be required to run centrifuge tests at comparatively low centrifuge speeds (lower suction values), but this could limits the real benefit of the technique, which is to reduce the testing time.

12.2.4 Performance of the predicted SWRS

The performance of the SWRS was evaluated using the residuals plots and a series of statistical metrics including: SSE, R-square, Adjusted R-square, and RMSE

from the Matlab's Optimization Tool Box™. Table 20 summarizes the results obtained for each data set.

Table 20. Goodness of fit metrics for Eagle Ford clay SWRS optimization

Metric	Set 3	Set 4
S.S.E.	0.1623	0.1709
R-square.	0.9327	0.9235
Adj. R-square.	0.9309	0.9219
R.M.S.E.	0.0334	0.0342

The SWRS model showed a good performance when evaluating the residual plots, this was confirmed with R-square values above 90% for both data sets. The metrics between both sets are similar and this principally influence by the amount of experimental data shared.

In comparison to the metrics values obtained when fitting SWRS models for RMA soil the S.S.E. values are higher for Eagle Ford SWRS models. It could be presumed that the measurement of the volume changes are more difficult in expansive clays and the impact in the scatter of the experimental data is higher when defining the volumetric water content at each equilibrium point.

Figure 133 illustrates Eagle Ford SWRS obtained for the experimental data sets Set 1 and Set 3. As it was previously observed from the definition of the coefficients, both surfaces are very similar and a maximum hysteresis value could be indicted as 0.05.

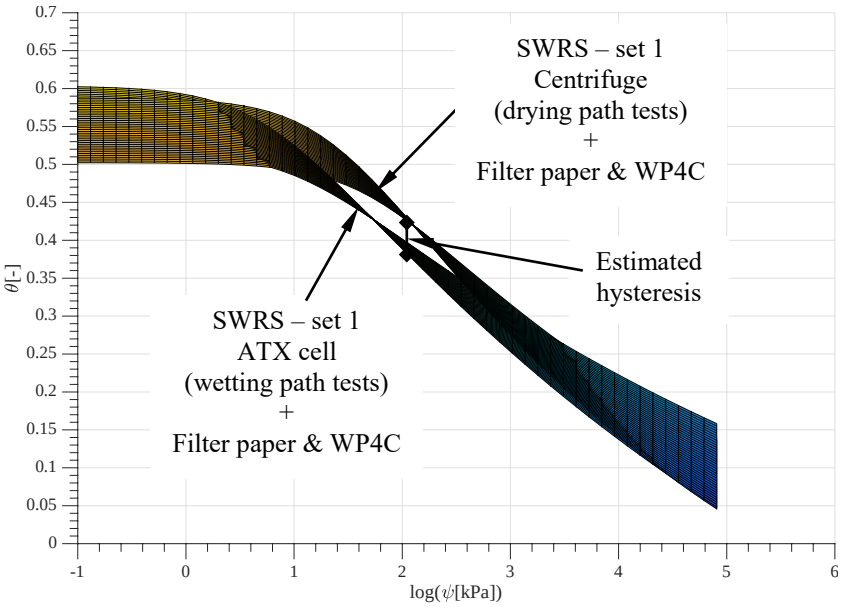

Figure 133. Comparison of Eagle Ford SWRS obtained for Set 1 and Set 2.

12.2.5 Validation of SWRS

Tests EFW2a and EFW2b were not included in the experimental data Set 1 in order to perform a validation of the best fit for the SWRS model obtained for ATX Cell results (Set 1). These tests were carried out in the ATX Cell under 20 kPa of vertical pressure. Since no other test was performed under this condition, a priori no experimental data could bias the model to fit correctly the data from the two tests selected.

Figure 134 shows the three-dimensional view of the SWRS (Set 1), the results from tests EFW2a and EFW2b, and the distribution of the experimental data used to define the SWRS. Although the volumetric changes depend on the imposed overburden it can be observed that the equilibrium point follow the SWRS proposed. The comparison between these observations and the model have an error lower than a 4% (Figure 135).

It could be conclude that this model can represent the changes in volumetric water content and void ratio for the successive suction stages imposed independently of the imposed loads.

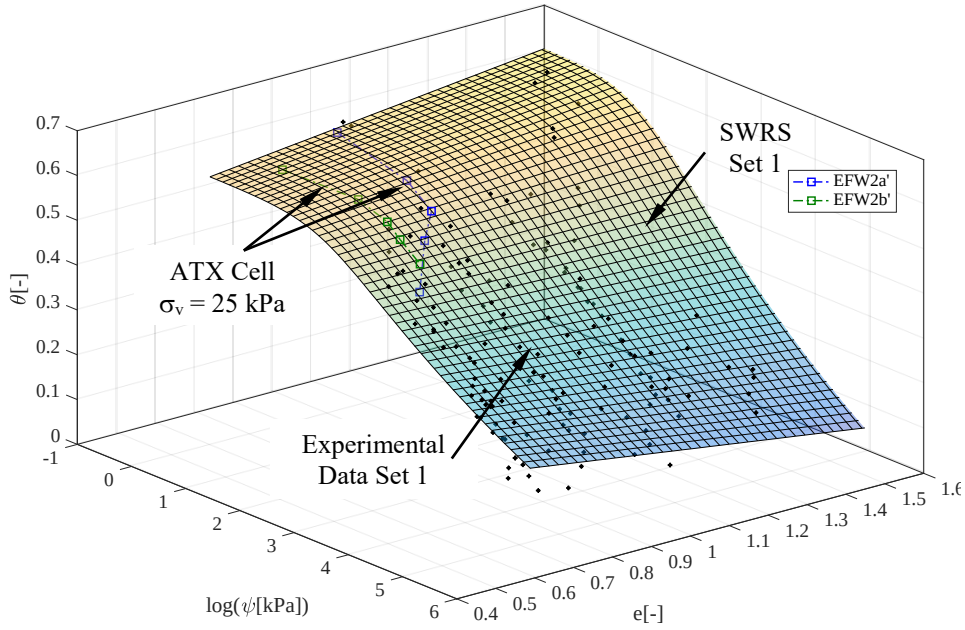

Figure 134. Validation of SWRS model for Eagle Ford clay by comparing the equilibrium stages of test EFW2

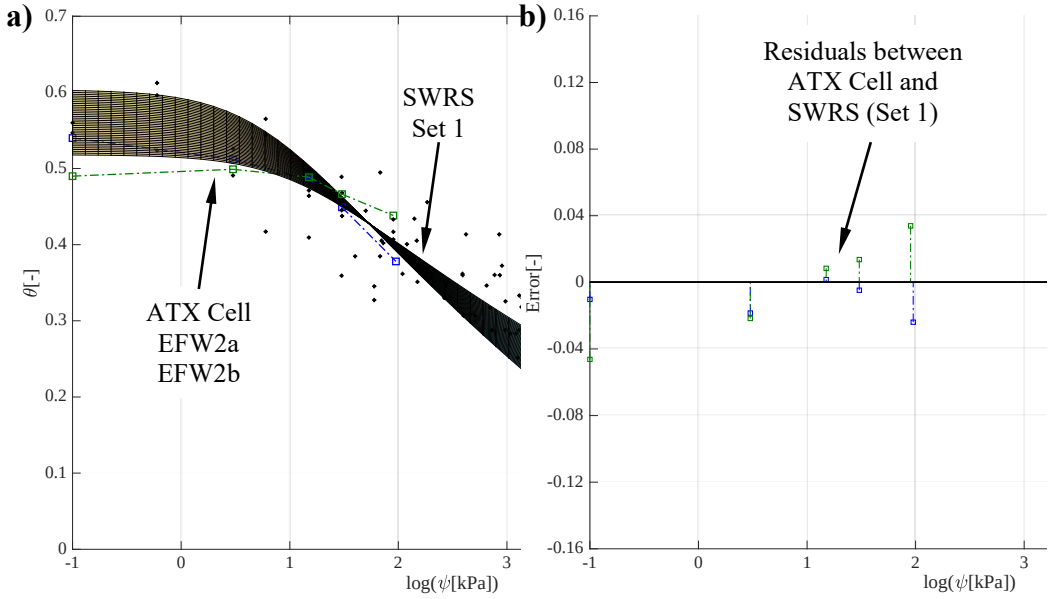

Figure 135. Validation of SWRS model for Eagle Ford clay including: a) side-view of the comparison between SWRS model and EFW2 testing stages, and b) residuals measured between tests EFW2 and model prediction.

The second analysis presented in this section involves comparing the SWRS from Set 1 with the results from centrifuge test. Figure 136 shows that although the centrifuge data is contained within a small range of suction values (8 kPa to 200 kPa) the void ratio values in these tests (0.6 to 1.6) cover the entire range of the SWRS.

Figure 136 illustrates that for suction values above 100 kPa the volumetric water content measured are larger than the ones predicted by the SWRS, with errors up to 16% (Figure 137). In this case the comparison is not strictly correct since the SWRS was developed using Set 1, which included experimental data from wetting path tests, and centrifuge results correspond to drying path tests. It can be observed in Figure 137(b) that the errors measured between the surface and the experimental data at high suction values were higher (0.14) that the estimated hysteresis (0.05). However, these errors were also measured for those specific four data points when defining the SWRS of Set 2.

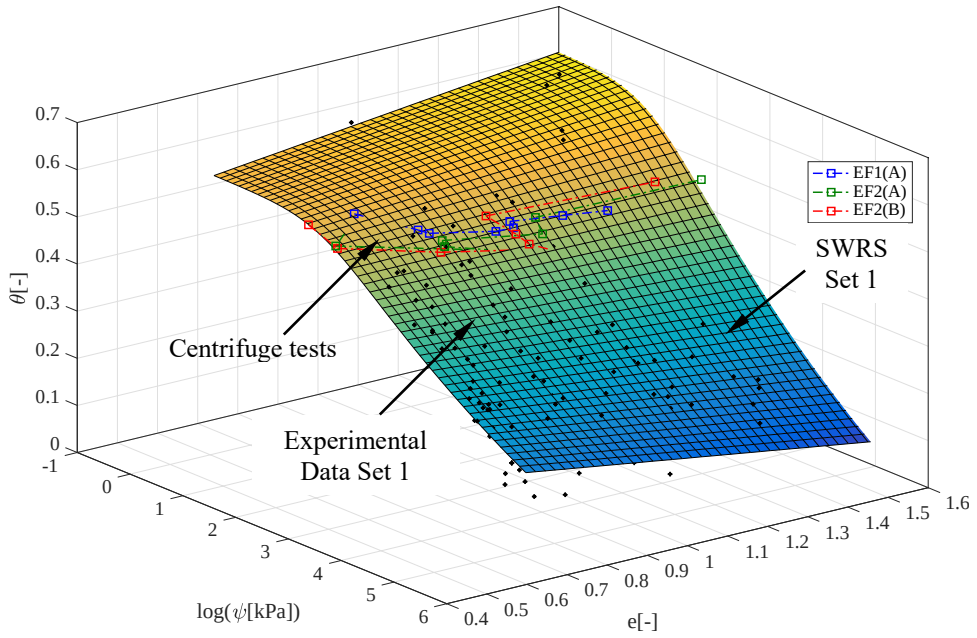

Figure 136. Comparison of SWRS model for Eagle Ford clay (Set 1) vs. results from centrifuge testing.

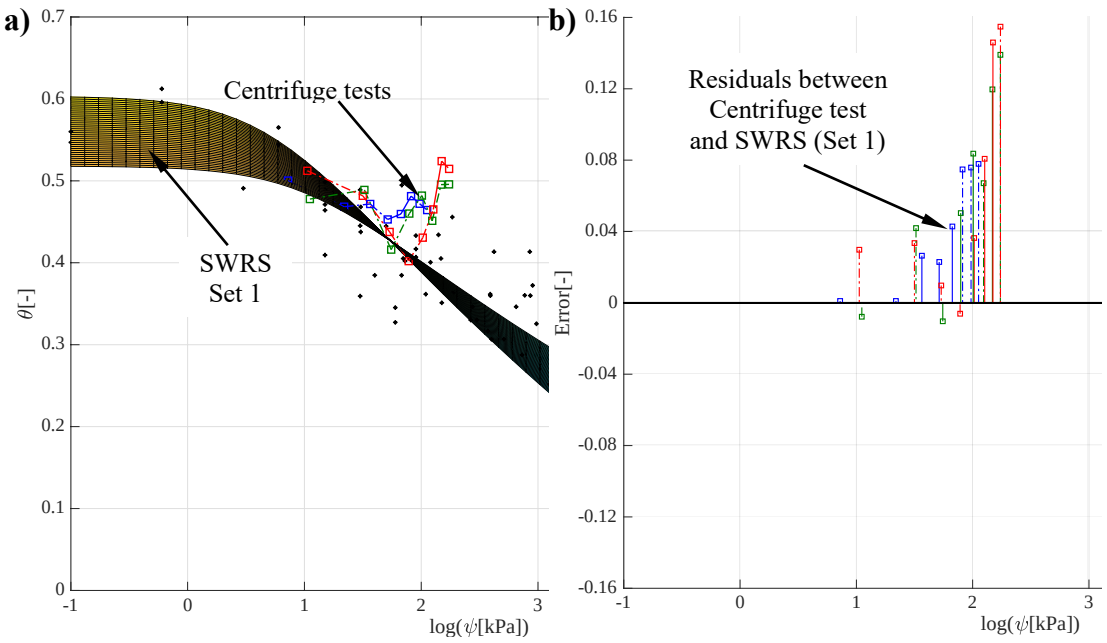

Figure 137. Evaluation of SWRS model for Eagle Ford clay (Set 1) including: a) side-view of the comparison between SWRS model and centrifuge testing, and b) residuals measured between centrifuge results and model prediction.

12.3 DETERMINATION OF HYDRAULIC CONDUCTIVITY FROM TRANSIENT ANALYSIS

The analysis of the transient flow processes presented in section 9.3 was applied to the data obtained from tests performed on Eagle Ford clay. Although this methodology does not account explicitly for volume changes during the tests, the advantages and limitations of applying these procedures are discussed.

12.3.1 Analytical solution for ATX Cell transient response (1.g)

ATX Cell tests (Figure 106) were analyzed using Gardner's (1956) multi-step outflow method. Although one of the hypothesis in Gardner's method is to consider the soil as a rigid body, the analysis procedure can be applied to the inflow/outflow readings independently of the volume changes.

12.3.1.1 Analysis of transient response

All stages from test EFW3a were analyzed using Gardner's solution. The soil sample in EFW3a was compacted at the optimum water content and 100% relative compaction (proctor standard dry unit weight). The unsaturated hydraulic conductivity values derived from tests are summarized in Table 21.

Table 21. Derived unsaturated hydraulic conductivity

Testing stage	ψ_{avg}	θ_{avg}	e_{avg}	k
[kPa]	[kPa]	[-]	[-]	[m/s]
6 to 0.6	1.9	0.507	1.471	5.64E-12
6 to 15	9.5	0.449	1.313	1.86E-11
90 to 30	52.0	0.367	1.106	1.85E-12
Comp. to 90	210	0.250	0.944	7.08E-13

Each hydraulic conductivity value listed in Table 21 was associated with an average water content, average void ratio, and a log linear average at each suction testing stage.

12.3.1.2 Estimated hydraulic conductivity vs. indirect k-function

Figure 138 illustrates the unsaturated hydraulic conductivity values derived from the transient stages of test EFW3a. Also, two sets of reference curves were incorporated. Each set consists of three curves depicting the predicted hydraulic conductivity values using the van Genuchten-Mualem (VGM) model.

The parameters used to calculate the values with the VGM model were obtained from the equations implemented to describe the SWRS indicating a fix void ratio. The difference between the two set of curves is the saturated hydraulic conductivity value incorporated in the model.

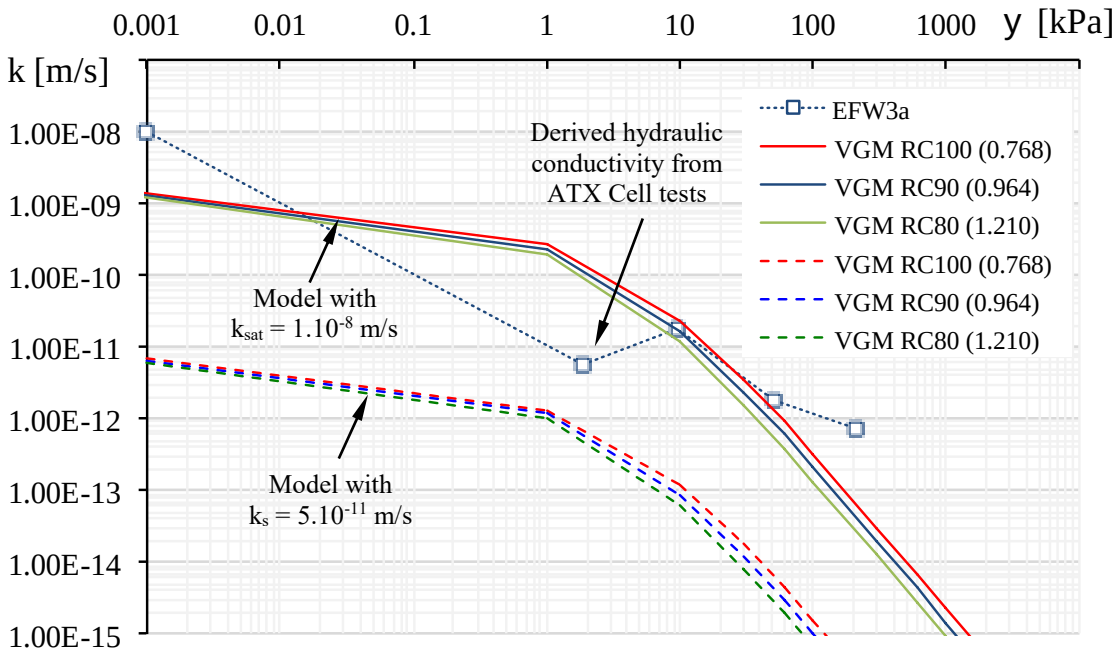

Figure 138. Hydraulic conductivity as function of suction for Eagle Ford clay including: values derived from ATX Cell tests soil, and indirect values obtained with van Genuchten-Mualem model.

Despite of the limitations in Gardner's (1956) model, the measurements from the transient flow process can be analyzed to estimate the unsaturated hydraulic conductivity. If the changes in suction are small enough an average void ratio could be indicated to represent each testing stage, and the testing conditions would closer to the hypothesis indicated in the analysis method

The comparison with the VGM model shows that a higher saturated hydraulic conductivity should be necessary in order to approximate the results derived from the ATX Cell. The lower saturated hydraulic conductivity was obtained from the flexible wall permeameter test presented by Kuhn (2010) at approximately 48 kPa (1000 psf).

12.3.2 Hydraulic conductivity based on Centrifuge

The transient inflow process during the characterization tests carried out in the centrifuge was back-analyzed using the commercial code HYDRUS with a modification to account for the increased gravitational field (Simmunek and Nimmo 2005).

The outcome of this analysis is a set of parameters for the van Genuchten-Mualem model (Mualem, 1976) that allows describing the relationship between the hydraulic conductivity and the soil water content (or matric suction).

12.3.2.1 Transient analysis model

The Hydrus simulations reproduce the infiltration stage in the hydrostatic test performed in the CPUS in test #EF1, following the approach indicated in Section 9.3.2. The experimental data corresponding to each test is indicated in Table 22.

This numerical code does not account for the volume changes along the soil as a result of the deformation created by the imposed stresses in the centrifuge or the expansion in response to wetting.

In order to incorporate evaluate the impact of the different properties along the soil column two models were evaluated: a) using a single material that could represent the average hydraulic properties of the soil sample, and b) using three different materials along the column. In this second geometry it is expected to capture indirectly the impact in of the different void ratio in the hydraulic properties of the clay. Figure 139 illustrates the position of the observation nodes and the discretization of the different materials along the column for the second geometry.

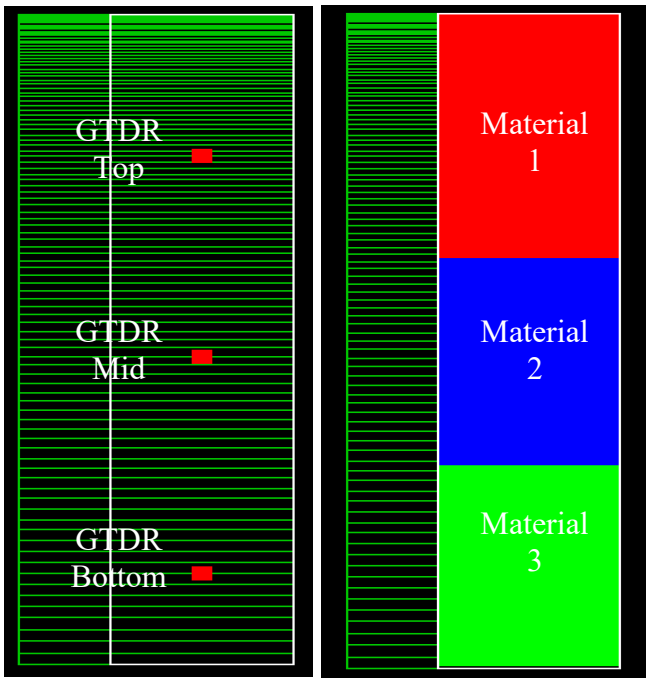

Figure 139. Hydrus model geometry including: a) the node discretization and the location of the observation points (GTDR), and b) the geometry of the three materials.

Table 22. Hydrus model parameters for centrifuge testing on Eagle Ford clay

Model	Unit	Test
	[-]	#EF1a
Speed	[rpm]	455
Equivalent acceleration	[N.g]	125
Inflow rate (Avg)	[mlh]	1.8
Time until outflow	[hs]	78

12.3.2.2 Model optimization

The inverse solver from Hydrus package was implemented to predict the best set of parameters for each soil section. Only the time variable information from the two top GTDR nodes (top and middle) was used to calibrate the model in order to avoid the boundary effects. The model seeks to represent the flow process in the column in order to

derive the hydraulic properties, not to reproduce all the features of the experiment. A set of initial values for all the parameters on each model is indicated in Table 23.

Table 23. Initial values for Hydrus model optimization on centrifuge testing.

Test	Model	Section		Parameter					
		Material	e	θ_r	θ_s	α^*	n	k_{sat}	l
		[-]	[-]	[-]	[-]	[cm^{-1}]	[-]	[cm/s]	[-]
#EF1	1	Uniform	-	0.01	0.547	0.03	1.11	5.10^{-5}	0.50
	2	1(Top)	1.210	0.01	0.547	0.01	1.20	0.0001	0.50
		2(Mid)	0.964	0.01	0.55	0.01	1.50	5.10^{-5}	0.50
		3(Bot)	0.768	0.01	0.50	0.01	1.50	5.10^{-4}	0.50
Fitted		-	-	no	yes	yes	yes	yes	no

12.3.2.3 Model results

The best set of the parameters for each section obtained through the inversion process with the Hydrus 1-D model are summarized in Table 24. The best fit was obtained following a non-linear least-squares analysis.

The regression coefficient was 0.917 for Model 1 and 0.98 for Model 2. According to this metrics the second model allowed a better fit of the observations in the GTDR nodes. The results presented in Table 24 show that including the three materials gives the model the freedom to slightly change the α and n parameters of each layer to obtain a better fit. On the other hand, the saturated hydraulic conductivity and the saturated volumetric water content are very similar among the three layers.

Like in the analysis presented in Chapter 9 for RMA soil, the hydraulic conductivity obtained with the model is higher than the values measured for Eagle Ford clay using flexible wall permeameter tests.

Table 24. Best set of parameters after model optimization

Test	Model	Section		Parameter					
		Material	e	θ_r	θ_s	α^*	n	k_{sat}	l
		[-]	[-]	[-]	[-]	[cm^{-1}]	[-]	[cm/s]	[-]
#EF1	1	Uniform	-	5.10^{-4}	0.507	0.055	1.31	5.10^{-5}	0.50
	2	1(Top)	-	0.01	0.47	0.006	1.21	$1.6.10^{-5}$	0.50
		2(Mid)	-	0.01	0.55	0.041	3.47	$9.2.10^{-6}$	0.50
		3(Bot)	-	0.01	0.547	0.055	3.37	$1.3.10^{-5}$	0.50
Fitted	Fitted	-	-	yes	yes	yes	yes	yes	no

In the second model, the solutions obtained with the inverse solver was more influenced by the initial parameters. Estimation of the initial values using the SWRS did not provide good results. In this case, not having experimental data for the third material made the inversion problem more sensitive to the input parameters, and the resulting values for this layer should be taken as approximate.

Figure 140 shows a comparison between the response of Model 1 and the readings at the observation points. Although a similar behavior between the model response and the readings can be observed, the model with one soil layer does not capture correctly the volumetric water content increment observed at each sensor. Figure 141 illustrates the advance of the water content in the soil sample. The waterfront is represented as a comparatively steep plug flow. Also, the profiles are found to be smooth and continuous along the sample.

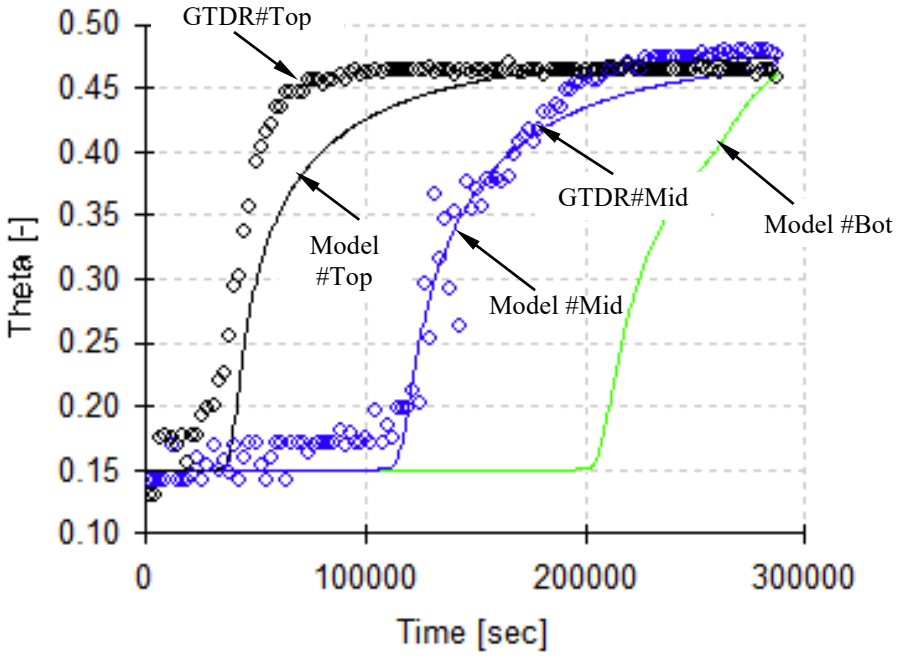

Figure 140. Comparison between the predicted behavior in Hydrus for a uniform soil model and the measured water contents at GTDR #Top and #Mid nodes during the infiltration stage of Test #EF1.

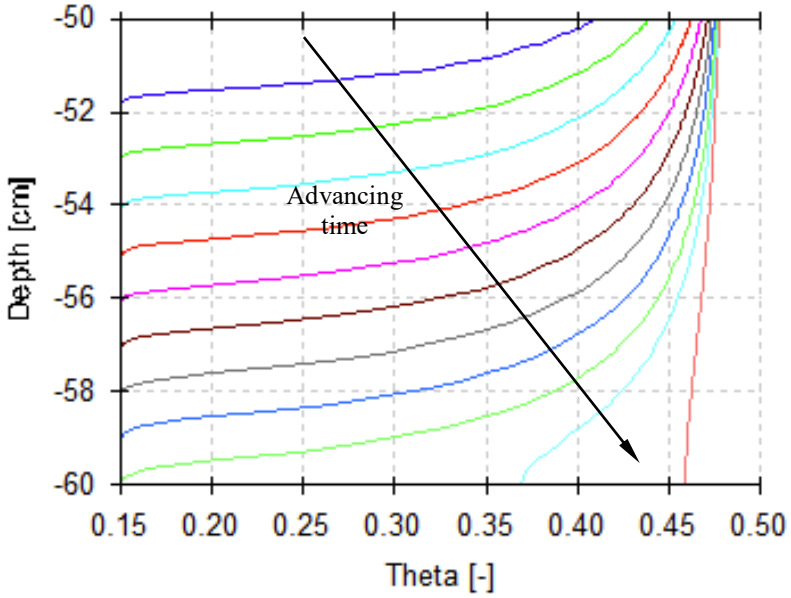

Figure 141. Water content profiles along the sample at different times predicted by Hydrus model 1 during the infiltration stage of Test #EF1.

Figure 142 illustrates the response of model 2 after the inversion procedure is completed and the volumetric water content readings at each GTDR node. In this model different transient behaviors are observed at each node. The increments in water content took comparatively less time in the top section in comparison to the middle section. This behavior agrees better with the measure results than the response predicted by Model 1.

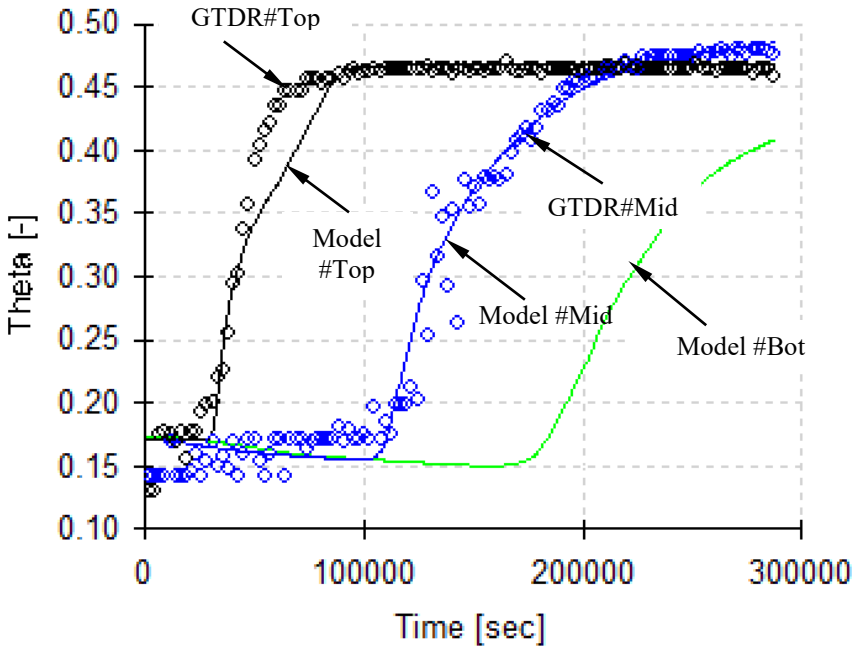

Figure 142. Comparison between the response of the Hydrus model 2 (including three soil layers) and the measured water contents at GTDR #Top and #Mid nodes during the infiltration stage of Test #EF1.

Figure 143 shows the water content profiles in the soil sample at different times. In this case, due to the different properties of the soil layers, the profiles are not smooth and in some cases water accumulation occurs at a given layer before a breakthrough occurs and water flows into the next layer.

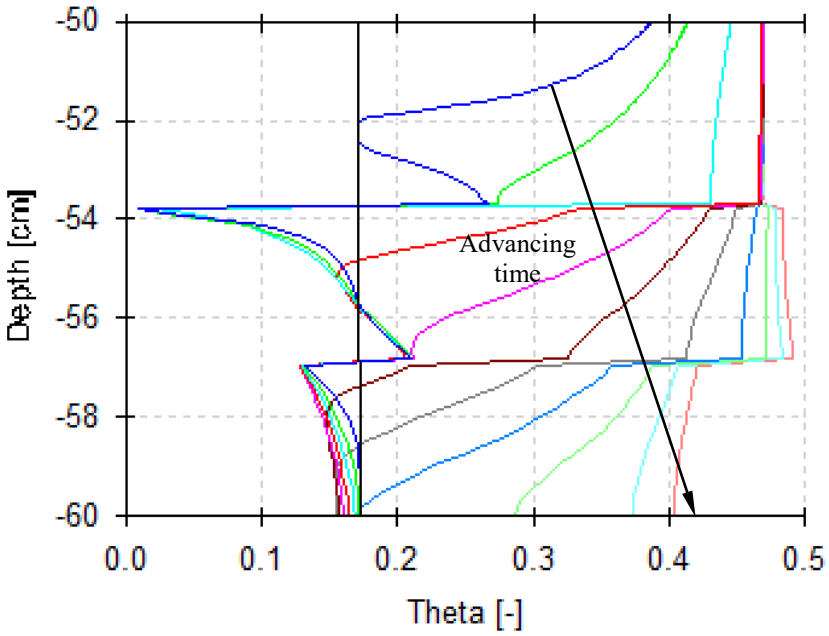

Figure 143. Water content profiles along the sample at different times predicted by Hydrus model 2 during the infiltration stage of Test #EF1.

Figure 144 shows the back analyzed unsaturated hydraulic conductivity obtained using the van Genuchten-Mualem k-function model with the values derived from Test #EF1 using Hydrus for Model 2 (Table 24). This figure also includes the unsaturated hydraulic conductivity values obtained in test #EF3 under steady state conditions, and the results from the ATX Cell derivation from test #EFW3a using Gardner's method.

It can be observed that, in general, the VGM model predicts a faster reduction in the hydraulic conductivity with increasing suction. In such case, the saturated hydraulic conductivity required in the VGM model must be higher than what could be assumed for this clay in order to fit correctly the unsaturated hydraulic conductivity values in the range area of interest.

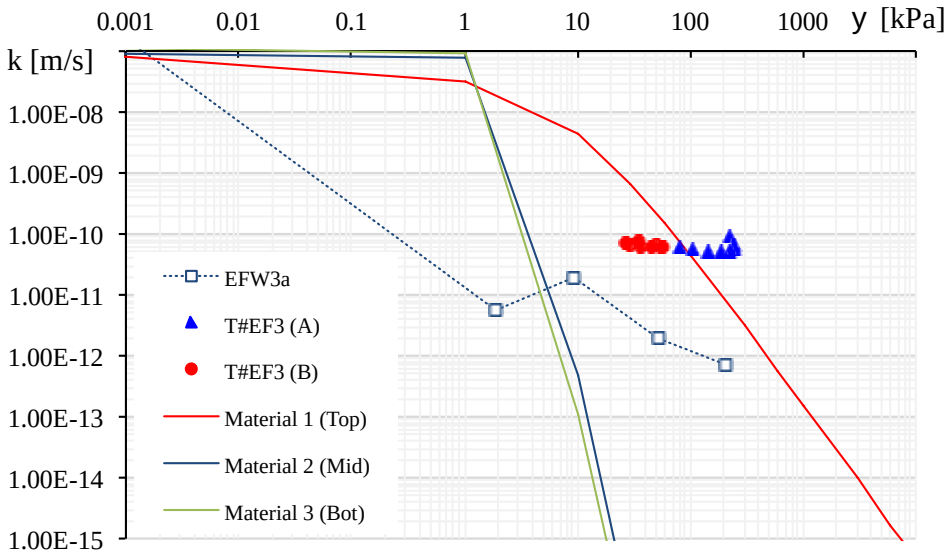

Figure 144. Comparison between the derived k-function model using Hydrus on test #EF1 (model 2), the hydraulic conductivity measurement performed in Test #EF3 under unsaturated steady state flow conditions, and the hydraulic conductivity values derived from test #EFW3a.

12.4 SUMMARY AND CONCLUSIONS

The objectives of this research component include the determination of the SWRS and the unsaturated hydraulic conductivity for Eagle Ford clay incorporating the results from Chapter 10 and Chapter 11. The analysis of the experimental data showed that:

- The SWRS model allowed incorporating experimental data generated for expansive clays with different experimental techniques (standard -1.g- or centrifuge -N.g-).
- In general, the errors (residuals) measured between the experimental data and the SWRS model were lower than 12%, with most of the errors being within 8%.
- As observed in Chapter 9, the availability of experimental data below 1 kPa has a significant effect on the shape of the SWRS, particularly at defining the relationship between the saturated volumetric water content and the void ratio.

- It was observed that the scarcity of data at low suctions values made the b_1 parameter (used to define θs) to be more influenced by the imposed lower limit constrains.
- Although the best set of parameters were similar for both experimental data sets, a comparison between surfaces allows evaluating the hysteresis effect between wetting and drying testing paths.
- The performance of the SWRS model for Eagle Ford clay was evaluated using various metrics. R-square values above 0.90 were obtained showing a similar performance to the results obtained for RMA soil.
- However, it was found that the SSE reported for the Eagle Ford SWRS (0.17) were higher than the SSE values measured for the RMA SWRS (0.035). This difference could be attributed to a higher scatter in the experimental measurements associated to the determination of the volume at each testing stage.
- A validation procedure showed that the equilibrium points [θ,ψ,e] measured from a test not included in the derivation of the surface, followed the SWRS, despite of the imposed stresses (different from any of those used in the construction of the SWRS).
- A comparison between the SWRS from set 1 (only 1.g test results) with centrifuge testing results showed a difference of up to 16% for suction values higher than 100 kPa. This difference was found to be higher than the hysteresis estimated between SWRS

Transient analyses were conducted in order to estimate the unsaturated hydraulic conductivity of Eagle Ford Clay. The results showed obtained with Gardner's (1956) multi-step outflow method and the numerical model Hydrus (Simmunek and Nimmo, 2005) showed that:

- Despite of the volume changes Gardner's method was be applied to the inflow readings obtained with the ATX Cell in order to obtain an approximate value of the unsaturated hydraulic conductivity.
- For RMA soil the unsaturated hydraulic conductivity measured in the range from 0.6 kPa to 200 kPa was found to range between 2.10^{-11} m/s to 7.10^{-13} m/s, for a sample compacted at 100% relative compaction and optimum water content.
- Comparison of the values estimated with Gardner's method against the prediction obtained with the van-Genuchten Mualem (1976) model shows that the assumed saturated hydraulic conductivity has a significant impact on the predicted values.
- A value of k_{sat} =1.10^{-8} m/s was found necessary to approximate VGM with the results derived with Gardner's method. This result is higher than the values measured using flexible wall permeameter tests.
- It was possible to estimate the unsaturated hydraulic conductivity by back-analyzing transient data obtained from centrifuge with the code Hydrus 1-D (Simmunek et al., 1998b).
- The effect of the void ratio could be taken into account using different material properties along the column. However, this model was found not to be suitable to evaluate the mechanical response under imposed loads or the soil expansion due to wetting.
- The VGM model used within Hydrus code predicts a much faster reduction in the hydraulic conductivity with the increasing suction. Consequently, higher saturated hydraulic conductivity values were required to fit the unsaturated hydraulic conductivity values correctly in the range of interest (suction values) to simulate the transient flow in the soil column correctly.

Chapter 13: Analysis of Soil Swelling using Centrifuge Technology

13.1 INTRODUCTION

The goal of this research component is provided insight on the hydro-mechanical behavior of unsaturated expansive clays in response to wetting process during swelling tests in the centrifuge environment.

The testing approach presented in this chapter to evaluate the swelling of Eagle Ford clay incorporates the non-intrusive sensors in order to illustrate the evolution of the global testing variables: soil volume, water content, degree of saturation and outflow during the wetting process.

A series of markers were included within the soil samples in order to evaluate the deformation profile along the sample. These results provide additional information to define the swell-stress relationship.

The results obtained during the swelling tests were represented in the [θ, e] plane in order to observe the coupled evolution of volume and water content changes. These curves could provide a method to evaluate the expansion in a soil profile under partial wetting conditions. It must be noticed that the correlation between volume changes and water content corresponds to an imposed vertical stress.

Also, it was observed that the swelling test data could be compared with the results obtained in the ATX Cell (at 1.g) if both tests were performed under the same constant overburden.

13.2 BACKGROUND REVIEW

The presence of expansive clays is usual in the subsurface profile of Central and Eastern Texas. These clays undergo major volumetric changes in response to wetting and drying cycles; as result, structures are often subjected to significant differential

settlements. In the case of Texas roadways, the soil movement creates damages that have been reported to cost millions of dollars (Holtz, 1973; Olson, 2009).

Centrifuge testing has been evaluated as an alternative methodology to evaluate the swelling behavior of highly plastic clays in an expeditious fashion (Plaisted, 2009; Kuhn, 2010; Armstrong, 2014). The framework consists on measuring the soil swelling at different stress levels rather than relying on indirect measurements such as soil plasticity index (McDowell, 1956). This information can then be used for design purposes, such as deciding if soil treatment is necessary.

This methodology has been also used to understand the influence of different initial conditions like density and compaction water content, as well as other external variables such as overburden pressure and time. Figure 145(a) shows the time response of four samples prepared at the same initial conditions and different total stresses. Figure 145(b) summarizes the swelling values at the end of these tests to form the Swell-stress curve.

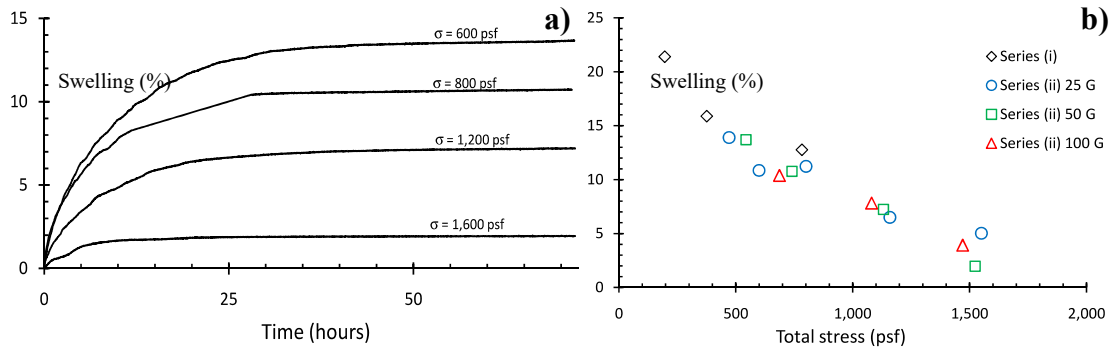

Figure 145. Information from swelling test performed in the CPUS (Kuhn 2010): (a) swelling vs. time and (b) swelling vs. total vertical stress curve.

Kuhn (2010) and Plaisted (2009) studied the expansive behavior of Eagle Ford clay. The conclusions of interest for this research are summarized below.

- The magnitude of swelling decreases with increasing total stress.
- The swell-stress curves obtained using centrifuge tests matched those found from free swell tests. This indicates that the final swelling is independent of the testing technique.
- Secondary swelling was found to be higher in free-swell tests in comparison with centrifuge testing.
- The primary swelling rate increases with the increasing total swell, and the rate of secondary swelling decreases with total swell.

13.3 TESTING PROGRAM

13.3.1 Testing procedures and measurement techniques

The current set up at the CPUS allows carrying out swelling tests under two possible configurations: a) ponded water on top of the sample at a constant level, or b) constant infiltration rate without ponding. In both cases water is provided through the rotary joint. The height of the sample, infiltration rate and elevation of ponded water can be modified in order to target different total stresses.

In all tests a linear displacement sensor was used in each bucket to monitor the overall vertical displacement of the soil column and an outflow chamber, located below the column, was used to measure the outflow rate using a pressure transducer.

Enhancement were incorporated in the swelling tests conducted in this research correspond. This includes the use of non-intrusive sensors, which minimize the soil-sensor interaction so that volume changes were not constrained by the sensors. Although the volumetric water content profile is not uniform, the average measurement of the water content provided by the GTDR in a 30 mm height soil sample was found to provide useful information.

In addition, the soil samples were compacted in three layers and a marker was placed at each interface (Figure 146). The image analysis system was used to track the deformation on each soil layer and define additional points in the swell-stress curve.

The vertical total stresses were estimated for each layer at the end of the tests. Also, the vertical equivalent stress representing the average expansion of the overall sample was calculated following the procedures described by Plaisted (2009).

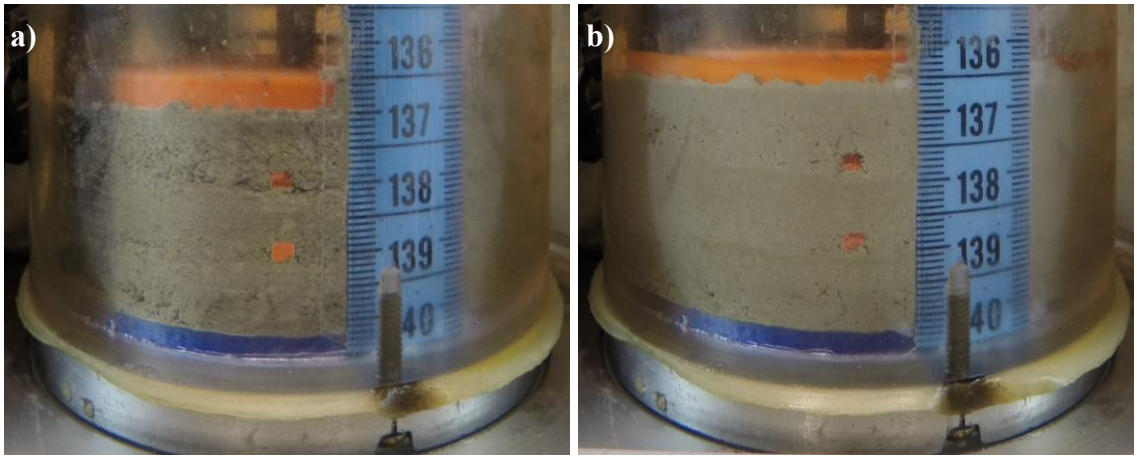

Figure 146. Sample in swelling test: a) at the beginning, and b) end of the test.

13.3.2 Scope of the testing program

A summary of the tests conducted in this research component, including the initial compaction conditions, centrifuge speed, wetting process, equivalent vertical stress imposed and measurement performed is provided in Table 25.

Table 25. Swelling tests performed using Eagle Ford clay samples

Test [#]	Date [-]	Initial RC [%]	Initial w_c [%]	Sample height [mm]	Centrifuge speed [rpm]	Equivalent g-level [N]	Water infiltration [mlh]
ES3	09/08/16	100	17.0	30	378	95	0.5-1
ES4	08/22/16	100	24.0	30	378	95	0.5-1

13.4 EXPERIMENTAL RESULTS

13.4.1 General swelling behavior

Results from test #ES3 are presented in this section to describe the partial information and stages that can be observed during the swelling test, as well as the hypothesis required to present the results. The results from Sample A and Sample B are presented in this section.

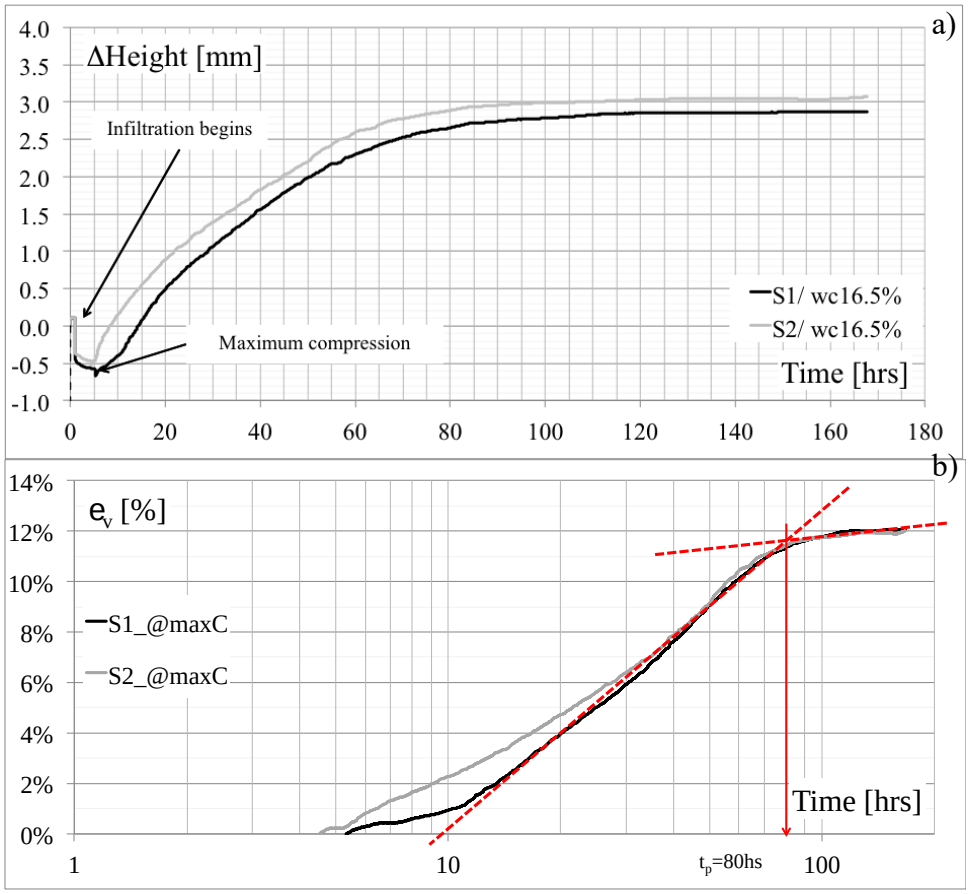

Figure 147. Expansion in swelling test #ES3 expressed in terms of: a) vertical displacement and b) vertical strain.

Different variables can be used to describe volume changes in the soil sample. Figure 147(a) shows the total change in height in millimeters, where an initial period is

observed where the sample was compressed due to the increased gravitational field. Once the sample leveled out under this loading condition, water was incorporated. Volumetric strain can be defined using different starting points, for example: a) when the water inflow started, or b) from the point of maximum compression. Although this arbitrary reference changes the final value of total swelling it does not change the correlation of swelling vs. time.

Figure 147(b) illustrates the volumetric strain vs time (logarithmic scale). A typical behavior can be observed with an initial "primary swelling" period of rapid increase in height and a subsequent "secondary swelling" period of a comparatively smaller constant swelling rate. The swelling process could be defined using two log-linear functions. The threshold between primary and secondary swelling portions (tp) was found to be 72 hs to 80 hs. At this point 90% of the total swelling was achieved.

Similar results can be obtained if void ratio is used as a dependent variable instead of volumetric swelling. Figure 148 illustrates the changes in void ratio in comparison with the changes in volumetric water content and degree of saturation. Figure 148(a) shows that the water content increased rapidly during the primary swelling stage. After reaching tp small changes in water content were measured. During this initial portion of the test degree of saturation increases as a result of the increasing water content.

Also, using the void ratio to represent the volume changes allows deriving the percentage of swelling using any reference point (e.g. initial void ratio, or maximum compression). For example, in test #ES3 using the maximum compression as reference (e=0.76), and the expansion achieved (e=0.97), the percentage of swelling (12%) can be directly calculated matching the results from Figure 147(b).

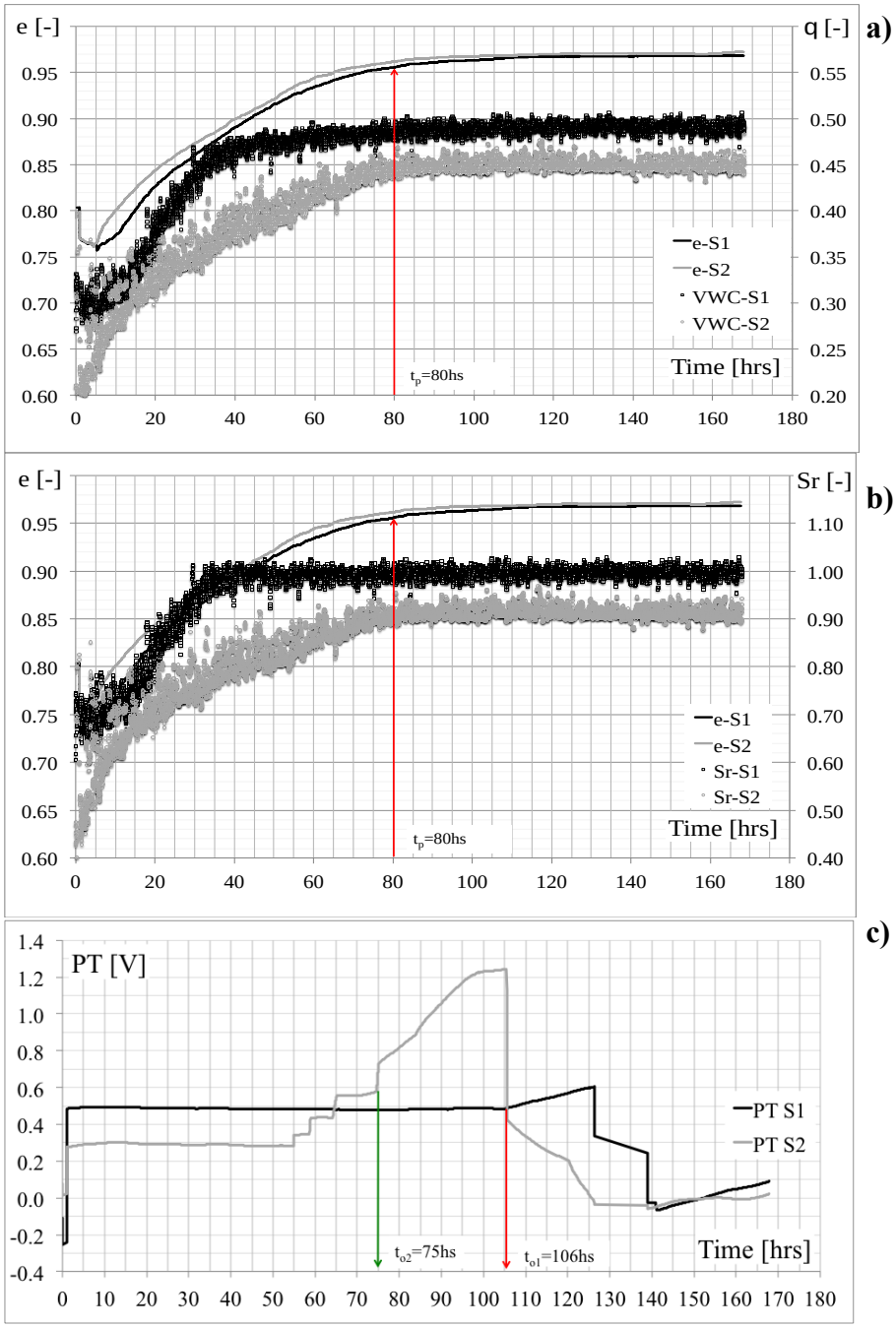

Figure 148. Changes in the global variables in swelling test #ES3: a) void ratio and volumetric water content vs. time; b) void ratio and degree of saturation vs. time; and c) voltage in pressure transducer vs. time.

Figure 148(b) shows that after 80 hs to 90 hs of testing volume changes (during secondary swelling) occurs at a constant degree of saturation. The testing time when saturation became constant correlates with the time when constant outflow was detected (Figure 148c).

In general it can be observed that after filtering the readings from the GTDRs the error in the volumetric water content was about +/-2%. It can be expected the values near saturation to have a higher error since the sensitivity in the calibration is lower for water contents between 0.4 and 0.5. Yet, the error measured in the degree of saturation after combining volumetric and water content measurements was about +/-3%.

13.4.2 Deformation profile and Swell-stress curve

The image analysis system was implemented to evaluate the displacement of the markers as well as the top disc. Figure 149 illustrates the displacements of each of the markers and the top disc after reaching maximum compression. In this way the expansion calculated using this information is consistent with the values presented in Figure 147(b).

The displacement of each rigid body (Disc, Top marker and Bottom marker) was measured using four different types of analysis in order to compare the accuracy of the results and the effects of the clay masking over the marker's face: a) upper edge detection (Up.E) with a reduced set of pictures, b) upper edge detection including the full set of pictures, c) lower edge detection (Lo.E), and d) template matching (PM).

It can be observed that there is good agreement between the different references used to calculate the displacements. However, it is recommended that the user visually inspects the pictures when deciding if any of the edges was covered by the clay. Also, this analysis shows that acceptable results could be obtained even with a reduced set of pictures.

The measurements performed with the LVDT from the top of the sample included in Figure 149 show a good agreement with the values measured with the image analysis tool when the upper edge of the disc is used as reference. In particular this edge was no interaction with the clay.

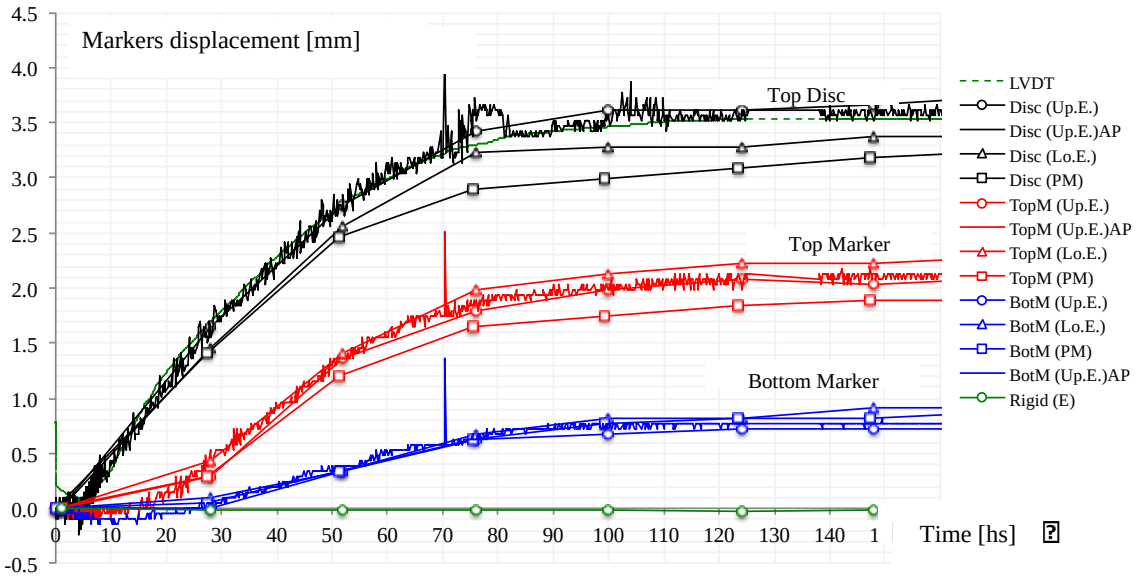

Figure 149. Top disc and markers displacement of swelling test #ES3 (Sample A).

Physically, the displacement of each marker represents the deformation of all the soil mas located below the marker. While centrifugation may compress the soil, and the markers could move down, the clay will swell upon the contact with water and the markers will move up.

Figure 150(a) shows a comparison between the swelling calculated for each soil layer using the non-intrusive image analysis tool and the average expansion measured using the LVDT. As expected the upper layer (under lower stress) showed higher expansion than the average.

The swelling measured after full wetting is presented in Figure 150(b) against the average total vertical stress for each layer. The inclusion of the markers allows defining three data points in the swell-stress curve (at three different stresses) from the same centrifuge test.

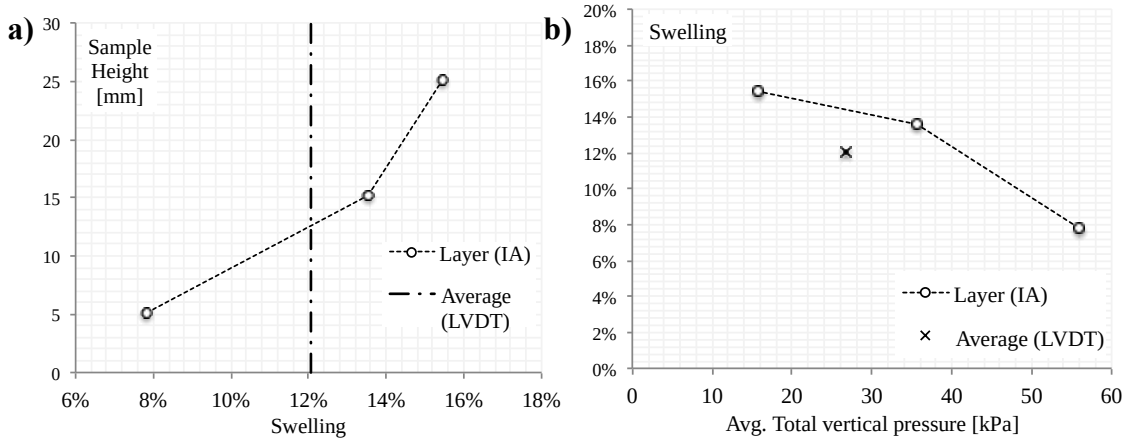

Figure 150. Summary of expansion at the end of the test #ES3 (Sample A): a) Swelling vs. sample height, and b) Swelling vs avg. total vertical stress per layer.

The swelling tests carried out with 30 mm high-specimens at 100 g's, represent the range of stresses of a 3.0m–deep soil profile (approx. 10 ft). This is the range of values typically used to analyze the design of structures over expansive clays.

13.4.3 Partial wetting analysis

The information presented in Figure 148(a) and (b) for test #ES3 was compiled in Figure 151 to correlate volume changes with changes in the volumetric water content (Figure 151a) and degree of saturation (Figure 151b). Although some differences were observed between Sample A and Sample B, as a result of the experimental procedure and the accuracy of the sensors, comparatively similar trends in the changes of the void ratio can be defined for both samples of the same test.

It can be observed in Figure 151(a) that the difference in primary and secondary swelling is also represented by a change in the slope of the increasing water content with respect to the void ratio. In Figure 151(b) the slope turns almost horizontal indicating changes in the void ratio at constant degree of saturation (secondary swelling).

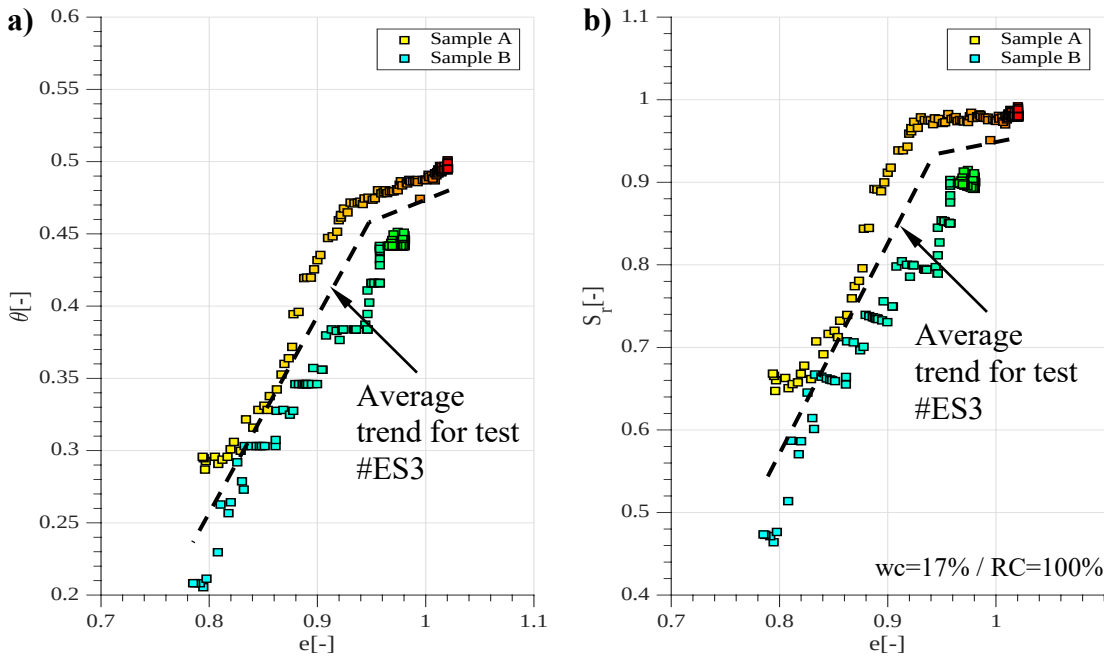

Figure 151. Correlation between volume change (void ratio) and: a) volumetric water content, b) degree of saturation during swelling test #ES3.

The time scale in Figure 151 was incorporated using colors (light to dark) and only data points every one-hour were represented. The higher spacing in between the first data points also indicates that most of the volume changes occur in a shorter period of time, and a comparatively high number of measurements are condensed in the last stage of the test.

The overall analysis was repeated for swelling test #ES4 with a soil sample compacted at optimum water content. In consequence the changes in water content and

volume were smaller in comparison to test #ES3. Figure 152(a) illustrates the changes in water content vs. void ratio and Figure 152(b) the corresponding changes in the degree of saturation vs. void ratio.

Yet a bi-linear trend could be approximated using the experimental results from both samples. Also, as a result of this representation a larger amount of data is superimposed at the highest void ratio values. These values correspond to the deformations measurements obtained during secondary swelling.

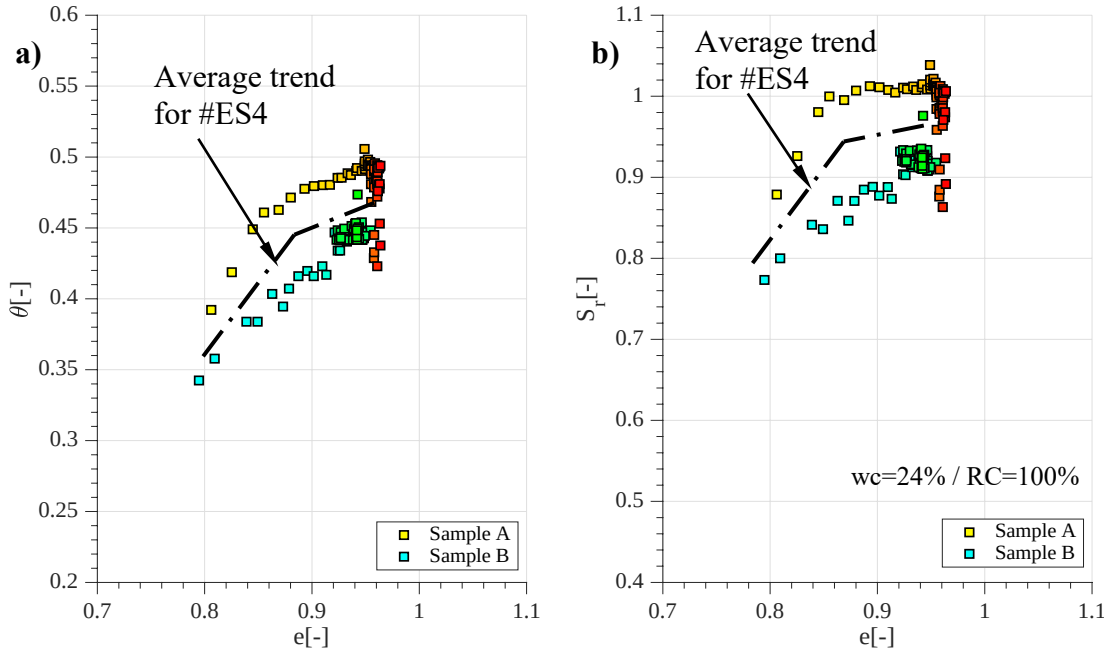

Figure 152. Correlation between volume change (void ratio) and: a) volumetric water content, b) degree of saturation, during swelling test #ES4.

Figure 153 shows a comparison of the results previously presented between in Figure 151 and Figure 152 for test #ES3 and #ES4 respectively. It can be observed that despite of the different initial compaction conditions, the final equilibrium condition of

both tests after fully wetting is similar, considering that both tests were performed under the same imposed stresses.

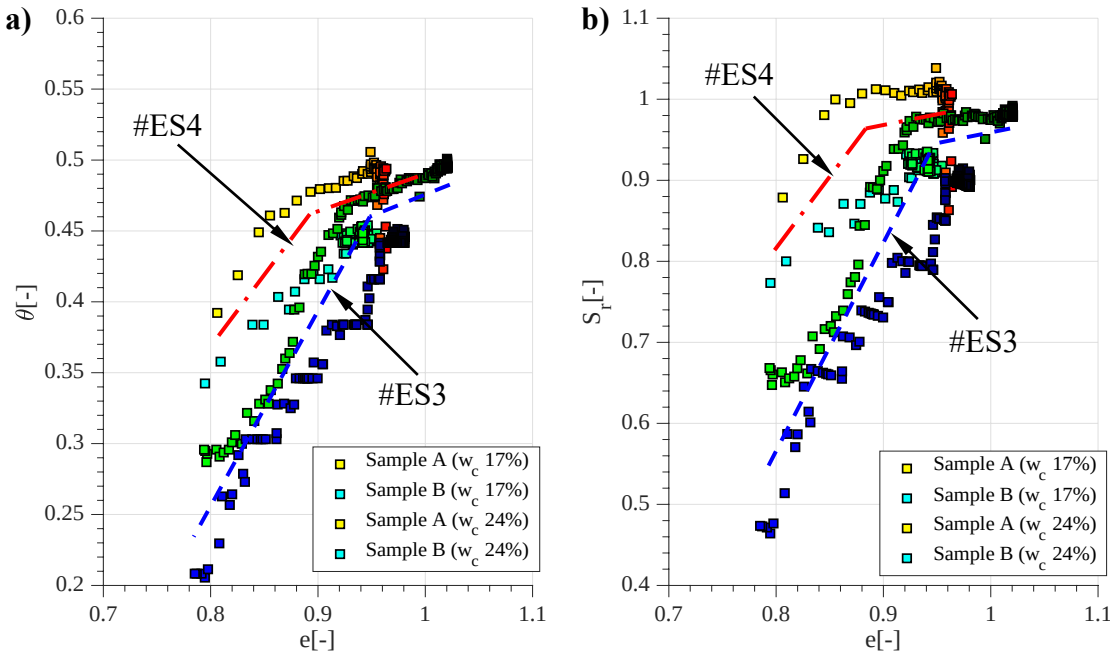

Figure 153. Comparison of the experimental results for test #ES3 and #ES4 including the correlation between volume changes and: a) volumetric water content, and b) degree of saturation changes.

Figure 154 illustrates a comparison between the results from the swelling test #ES4 and the measurements obtained in the ATX cell in test #EFW2a. In both test the soil samples were compacted at the optimum water content and 100% relative compaction (proctor standard). Also, both tests were carried under a similar vertical imposed overburden of 25 kPa.

It was observed that independently of the testing methodology the measured water content and void ratio values matched during the wetting process. The difference is that for test #EFW2a, each experimental point also represents the equilibrium values under an imposed matric suction value.

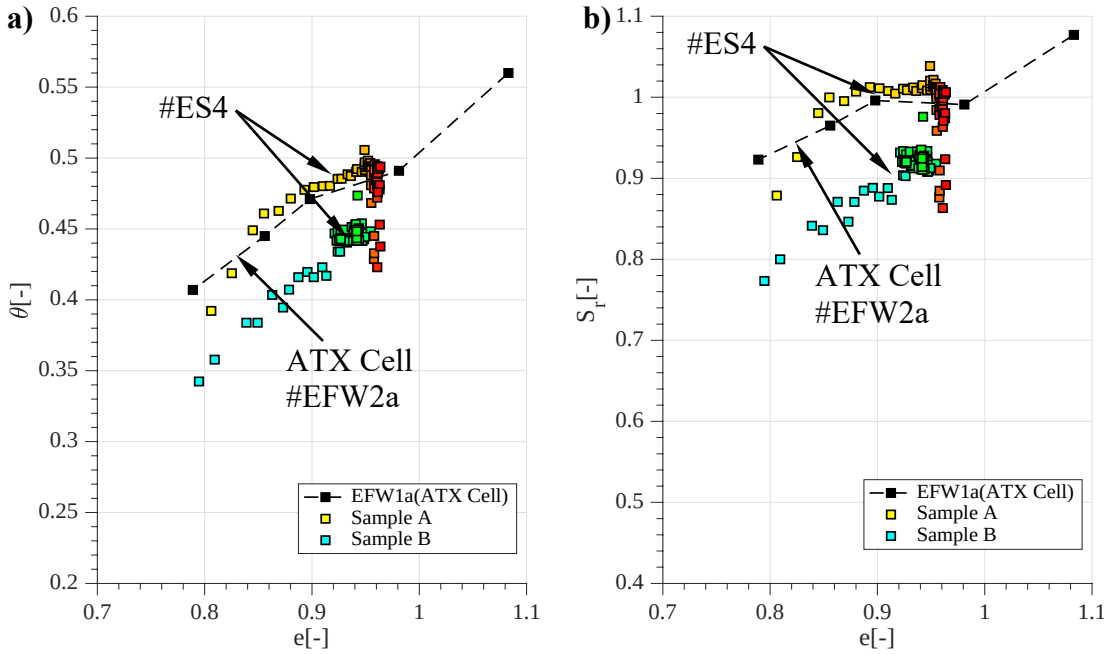

Figure 154. Comparison of the experimental results between swelling test #ES4 and ATX cell test EFW2a for Eagle Ford clay samples compacted at optimum water content and teste at

Overall, the curves presented between Figure 151 to Figure 154 illustrated the expansion process using the same variables typically used to describe the hydraulic properties of the unsaturated soils. Particularly Figure 154 showed that the experimental information from the swelling test stage could be observed as equilibrium points of a SWRS test.

Also, these curves could be implemented to evaluate the expansion in a soil profile under partial wetting conditions instead of assuming always that the clay has reached complete saturation. As it was previously mentioned, the correlation between the water content and volume changes depends on the vertical pressure imposed.

13.5 SUMMARY AND CONCLUSIONS

Centrifugation is an efficient methodology to characterize the swelling potential of clays in an expeditious way. The goal of this research component was to carry out enhanced swelling in the CPUS to provide additional information about the coupled hydro-mechanical behavior of the Eagle Ford clay. The results presented in this chapter showed that:

- It was found that although different variables (volumetric strain or void ratio) it did not change the correlation of swelling vs. time, particularly the threshold between primary and secondary swelling.
- It was observed that using the void ratio to represent the soil volume changes allows defining the percentage swelling from any testing stage without requiring a pre-defined reference (e.g. maximum compression).
- It was found that the volumetric water content measured with the GTDR increased rapidly during the primary swelling stage.
- During secondary swelling small changes in void ratio and water content could be observed. Also, these changes were found to occur under an approximately constant degree of saturation.
- Continuous outflow was observed around the same time as the primary swelling was completed.
- The inclusion of markers and the implementation of the image analysis tools allowed defining volumetric changes for all the layers in the soil sample, and it was possible to determine three additional data point in the swell-stress curve.
- The comparison in the [θ, e] (or [Sr, e]) plane of swelling tests performed at the same vertical stress in samples compacted at different water contents revealed that the final equilibrium achieved by both samples after fully wetting are similar.

- A comparison between the results from ATX Cell test and Swelling test performed in samples compacted at optimum water content showed that the water content and volumetric changes agree independently of the testing procedure.
- The representation of the swelling test in the θ-e (or Sr-e) plane could provide a method to evaluate the expansion in a soil profile under partial wetting conditions

Chapter 14: Conclusions and Recommendations

14.1 INTRODUCTION

Research was conducted at the University of Texas at Austin to characterize the hydro-mechanical behavior of unsaturated clays, with focus on their hydraulic properties. While several standard (1.g) experimental techniques were implemented, emphasis was placed on the use of centrifuge (N.g) techniques. Non-intrusive sensors were developed as part of this research, which were incorporated in the centrifuge permeameter to determine in-flight the volumetric water content and volumetric changes of unsaturated soils.

A series of tests were performed to characterize the soil-water retention surface (SWRS) and unsaturated hydraulic conductivity function of both low and high plasticity clays. Testing procedures and analysis tools explicitly incorporated four key variables: moisture content, suction, void ratio (or volumetric changes), and hydraulic conductivity.

General conclusions of this research are presented next. They are followed by specific conclusions derived from each Section of this dissertation. Recommendations for future research work are also provided.

14.2 OVERALL CONCLUSIONS

General conclusions regarding behavior of unsaturated clays, a about centrifuge testing are presented.

GENERAL BEHAVIOR OF CLAYS

- The hydro-mechanical characterization of clays requires incorporating the void ratio as an explicit variable. Volume changes should be taken into account in the

testing procedures as well as in the analytical methods when describing the water retention properties of unsaturated clays.

- Although volume changes are typically associated with high plasticity clays, in response to the physicochemical interaction of clay particles with water, they may also occur in low plasticity clays due to externally imposed stresses.
- The soil-water retention surface (SWRS) in the [θ,ψ,e] space is a useful representation of the retention capabilities of unsaturated clays, both low and high plasticity.
- The SWRS can be generated by incorporating experimental results from different testing techniques, performed at different void ratios, and under different loading conditions.
- Volume and water content changes show a clear correlation in response to wetting processes. This correlation can be observed using different testing techniques such as the ATX cell and the Centrifuge techniques used in this research.

CENTRIFUGE TESTING

- Destructive measurement techniques may impact the experimental measurements, making necessary the implementation of non-intrusive sensors to measure in-flight the volumetric changes and water content of clays.
- Centrifuge testing procedures and semi-destructive and non-destructive measurement techniques are useful to determine the SWRS and the hydraulic conductivity of both low and high plasticity clays.
- Centrifuge testing (N.g) allowed reducing the time required to generate experimental data in comparison to standard (1.g) testing techniques.

- The increased gravitational field was found to impose stresses and consequently deformations in the soil that should be accounted for in the interpretation of results.
- While steady-state centrifuge testing methods were found to be the preferred approach to expedite the generation of results for low plasticity clays, transient methods were identified as a useful approach for expansive clays to balance accuracy and time requirements.
- Centrifuge testing using non-intrusive measurements was found to provide valuable information about the transient flow processes to derive the unsaturated hydraulic conductivity function of clays.

14.3 SPECIFIC CONCLUSIONS

14.3.1 Conclusions Section 1

The purpose of the research components presented in Section 1 of this dissertation was to develop new tools to characterize the hydro-mechanical behavior of unsaturated clays. The main conclusions of Section 1 are summarized below. Detailed conclusions are presented at the end of each Chapter of Section 1 (Chapter 4 to 6).

- The newly developed ATX Cell was able to monitor continuously the changes in volume and water content of clay samples following the described hydro-mechanical paths for the imposed suction stages.
- The experimental data generated in individual tests conducted to determine the water retention properties of clays could be represented in the [θ,ψ,e] space to define the clay SWRS.

- The ATX cell good quantification of the advective-diffusive transport phenomenon. This information was interpreted to determine the unsaturated hydraulic conductivity of the soil.
- A non-intrusive volumetric water content sensor, the GTDR, was successfully developed by modifying 3-rod TDR sensors and embedding them in acrylic tubes.
- Two-point probe calibrations performed using PC-TDR from CSI was found to simplify the development of the GTDR.
- The correlation between the apparent dielectric permittivity and the volumetric water content obtained using the GTDR with the probe-fitting parameters previously calibrated with PC-TDR, resulted similar to Topp's universal equation.
- AWIGF code was implemented to determine the VWC of clays using the waveforms recorded with TDR100. In general, AWIGF provided outcomes with considerable less scatter than CSI algorithm
- The implementation of the AWIGF code required a probe calibration to determine the probe-fitting parameters, which accounts for the presence of the acrylic, as well as a an additional soil specific calibration.
- An image analysis system, including in-flight cameras and analysis algorithms, was implemented in the centrifuge to detect the movement of rigid bodies. The results were found to expose the deformation of clays during testing.
- Edge detection algorithm, which requires a user interaction to define the analysis parameters (searching window, channel, threshold, and selected edge), was found to provide accurate results reducing the computing time.

14.3.2 Conclusions from Section 2: Hydraulic characterization of unsaturated low plasticity clays

The objective of the research components presented in Section 2 of this dissertation was to evaluate the performance of the new equipment and sensors and to characterize the hydraulic properties of an unsaturated low plasticity clay (RMA soil). The main conclusions of Section 2 are summarized below. Detailed conclusions are presented at the end of each Chapter of Section 2 (Chapter 7 to 9).

- The ATX Cell was found to facilitate the hydro-mechanical characterization of RMA soil. Although changes in void ratio were negligible the goal of monitoring the three variables was achieved for void ratio values ranging from 0.50 to 0.95.
- The initial void ratio of the soil was found to affect the slope of the hydro-mechanical path of soil samples used to describe the correlation between the water content and matric suction.
- The total suction vs. soil moisture relationship for RMA soil was determined for suction values ranging from 300 kPa to 100 MPa using filter paper and chilled mirror hygrometer techniques. For water content values ranging from 0.20 and 0.35, the total suction was found to remain essentially constant.
- The osmotic suction for the RMA soil used in this research was estimated to be 600 kPa as a combination of the results from ATX Cell and WP4C.
- Deformation in RMA soil samples was measured during centrifuge testing. The level of deformation was found to depend on the combination of both the initial conditions and stresses imposed during testing.
- The results from centrifuge testing were represented in the $[\theta,\psi,e]$ space to account for the changes in void ratio during testing. These results were used to define the soil SWRS of RMA soil.

- The use of destructive measurements affected the volumetric water content and degree of saturation. Incorporating non-intrusive sensors was found to solve this problem allowing an adequate definition of the SWRS.
- In addition to a non-linearity of the SWRS in relation to suction, the SWRS was also found to be non-linear in relation to the void ratio axis.
- SWRS were defined using experimental data generated with different experimental technique (standard -1.g- or centrifuge -N.g-). It was found that the range of suction values tested influences the shape of the SWRS, in particular the experimental data obtained below 1.0 kPa.
- Comparison of SWRS defined using data generated following wetting and drying path tests revealed that hysteresis is a function not only of suction but also of void ratio. For the case of RMA the hysteresis was estimated to be as high as 0.07.
- RMA hydraulic conductivity was derived applying Gardner's outflow method to the transient information of the ATX Cell. RMA hydraulic conductivity was estimated ranging from 2.0 10^{-10} m/s to 1.3 10^{-12} m/s, for suction values ranging from 0.1 kPa to 100 kPa, at a constant void ratio of 0.504.
- Non-intrusive sensors provided valuable information about transient response of RMA soil during centrifuge testing. Hydrus 1-D code was implemented to back-analyze this transient information. The k-function derived for RMA was found to range from 1.0 10^{-6} m/s to 1.0 10^{-12} m/s, for suction values ranging from 0.01 kPa to 100 kPa (for a void ratio of 0.607).
- While Hydrus-1D was found to overestimate the saturated hydraulic conductivity, the k-function was found to show good agreement with the hydraulic conductivity values obtained at high suction values using steady-state (imposed flow) approach in the centrifuge.

14.3.3 Conclusions from Section 3: Hydro-mechanical characterization of unsaturated low plasticity clays

The main goal of the research components of Section 3 of this dissertation was to provide the hydro-mechanical characterization of an unsaturated expansive clay. The main conclusions of Section 3 are summarized below. Detailed conclusions are presented at the end of each Chapter of Section 3 (Chapter 10 to Chapter 13)

- The ATX Cell was found to facilitate the hydro-mechanical characterization of Eagle Ford clay. The void ratio was found to change throughout the wetting path tests. The volumetric changes and the associated changes in water content were found to depend on the initial void ratio and the imposed stresses.
- A coupled behavior was identified to govern the changes in volume and water content in each testing stage. The swelling rates and the inflow rates were found to follow the same pattern.
- A clear correlation could be defined between water content and matric suction using filter paper technique, but the correlation with total suction was defined using chilled mirror hygrometer (WP4C) tests.
- The osmotic suction for Eagle Ford was estimated to be 630 kPa as a combination of the results from ATX Cell, filter paper and WP4C tests.
- The use of image analysis techniques was found to successfully detect the swelling and contraction of the soil during centrifuge testing.
- The volumetric water content values measured using the GTDR's were found to be in good agreement with the semi-destructive results from hydrostatic tests.
- Increasing the centrifuge speed in hydrostatic tests resulted in a reduction in the void ratio due to the higher imposed stresses. In consequence, a larger section of the clay sample was saturated despite the higher suction values imposed

- The unsaturated hydraulic conductivity measured under steady-state condition (imposed inflow of 0.1 mlh) was found to range from 5.10^{-11} m/s to 1.10^{-10} m/s, for suction values ranging from 50 to 250 kPa.
- For Eagle Ford clay samples compacted at optimum water content, the equilibrium points (θ, ψ, e) measured in the ATX cell at each suction stage were found to belong to the same SWRS independently of the imposed stresses.
- The use of the void ratio was found to clear represent the volumetric changes from swelling tests performed in the centrifuge. Also, using the void ratio as it is possible to calculate the percentage of vertical swelling between two stages without pre-defining a reference point (e.g. maximum compression).
- Continuous outflow was found to initiate observed around the same time as the primary swelling was completed.
- Volumetric water content and degree of saturation in swelling tests were found to increase rapidly during primary swelling. Secondary swelling was observed to develop with low changes in the water content changes and at approximately constant degree of saturation.
- The image analysis tool allowed defining volumetric changes along the soil sample in addition to the overall measurement obtained with contact sensors.
- The comparison in the [θ, e] (or [Sr, e]) plane of swelling tests performed at the same vertical stress in samples compacted at different water contents revealed that the final equilibrium achieved by both samples after fully wetting are similar.
- The representation of the swelling test in the θ-e (or Sr-e) plane could provide a method to evaluate the expansion in a soil profile under partial wetting conditions

14.4 RECOMMENDATIONS FOR FUTURE WORK

The non-intrusive systems developed in this research showed a good performance to determine the volumetric water content and volumetric changes in-flight during centrifuge testing. However, the spatial resolution of the GTDR was limited by the size of the TDR sensors. It is recommended to update the GTDR sensors by replacing the 3-rod TDR sensors by coaxial lines. The coaxial lines could provide more localized measurements along the soil sample. Also, it is recommended to implement AWIGF as the default method to analyze the travel time of the waveforms recorded.

Although it could not be considered a fully non-intrusive method, the inclusion of psychrometer sensors, to determine the suction in high plasticity clays, is recommended due to their comparatively small size and wide range of application. In addition, these sensors could be monitored using the same datalogger implemented for the GTDR. Incorporating these sensors could allow determining the SWRS and k-function of the soil using a single test since all the relevant variables would be measured.

The analysis of transient information obtained from centrifuge testing showed to be a promising tool to determine the water retention capabilities as well as the hydraulic conductivity function of clays. However, the analytical and numerical methods implemented do not account for the imposed stresses and the associated volumetric changes. It is recommended to explore other analytical or numerical tools that incorporate the mechanical response of the soil in order to evaluate the impact of the volumetric changes in the hydraulic properties.

Implementing a complex tool that can model the coupled hydro-mechanical behavior of unsaturated clays may require evaluating additional mechanical parameters. Oedometer tests performed under selected suction conditions are typically used for this

purpose. It is recommended to use the ATX Cell to perform these tests, although the vertical stresses may remain limited for the current configuration.

APPENDICES

APPENDIX 1: Complementary information for the development of the GTDR sensor

1.1 INTRODUCTION

The development of the non-intrusive water content sensors GTDR required to run a series of soil and sensor calibrations in order to assess the accuracy of the TDR technique to determine the volumetric water content of soil and to evaluate the impact of the different modifications proposed during the construction of the sensor.

1.2 CALIBRATIONS

1.2.1 General calibration

G. C. Topp et al. (1980) presented a comprehensive work showing the correlation between the apparent dielectric permittivity (Ka) and the soil volumetric water content (VWC) for a wide variety of mineralogy, texture, density, salt content, and temperature.. As a result, a strong empirical correlation was found between this dielectric property and the soil volumetric water content for a wide range of water content (from air dry to saturation). Moreover, they indicate that this correlation is almost independent of the soil density, texture or salt content, and minimum temperature dependence. Since then, this polynomial calibration has been the default correlation for most TDR systems. Overall the level of error reported for this method is about 1 to 2% VWC. However, tests show that errors increase with increasing water contents.

This correlation was used in this research as a reference value for all the calibrations performed. Figure 155 shows the correlation between Ka and VWC for different soils together with the best fitting function obtained with a third degree polynomial equation.

$$\theta = -5.3 \cdot 10^{-2} + 2.92 \cdot 10^{-2} K_a - 5.5 \cdot 10^{-4} K_a^2 + 4.3 \cdot 10^{-6} K_a^3 \quad (36)$$

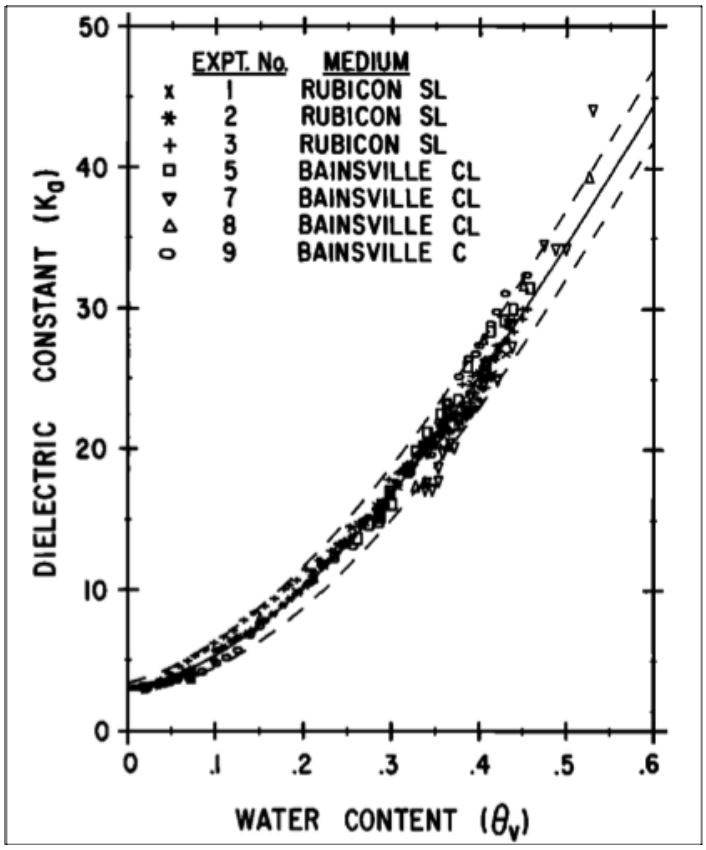

Figure 155. Relationship between VWC and Ka for a set of soils (Topp, 1980)

1.2.2 Soil specific calibration for Eagle Ford Clay

Although Topp's equation is widely used, a series of tests were performed to evaluate the correlation between apparent dielectric permittivity (Ka) and the volumetric water content of Eagle Ford Clay.

Figure 156(a) shows an acrylic column that was prepared with two TDR probes (CS645 L-33) to perform the calibration tests on Eagle Ford clay. The soil was compacted in three layers of 2.0 cm each, at a density of 1.24 g/cm3 (80% Relative

compaction of Proctor Standard) and several gravimetric water contents were used from 4.8% to 34.7%, equivalent to VWC between 0.06 and 0.43 (Figure 156).

Figure 156. Column set up for Eagle Ford calibration: a) lateral view before placing soil, and b) top view during compaction procedure.

Measurements were taken every 30 minutes during several hours. A permittivity value was calculated for each water content and for each probe ($Ka_{,pi}$). Figure 157 shows the values reported for the two different probes at different water contents.

The first observation that can be made is that measurements do not progress with time towards a stabilized value, but they alternate within a range that is independent of time. Also, the variation range values increases with the increasing water content. The soil specific calibration obtained with thiese results is presented in Figure 158. A polynomial fitting equation is reported for each probe, and Topp's equation is included for comparison purposes.

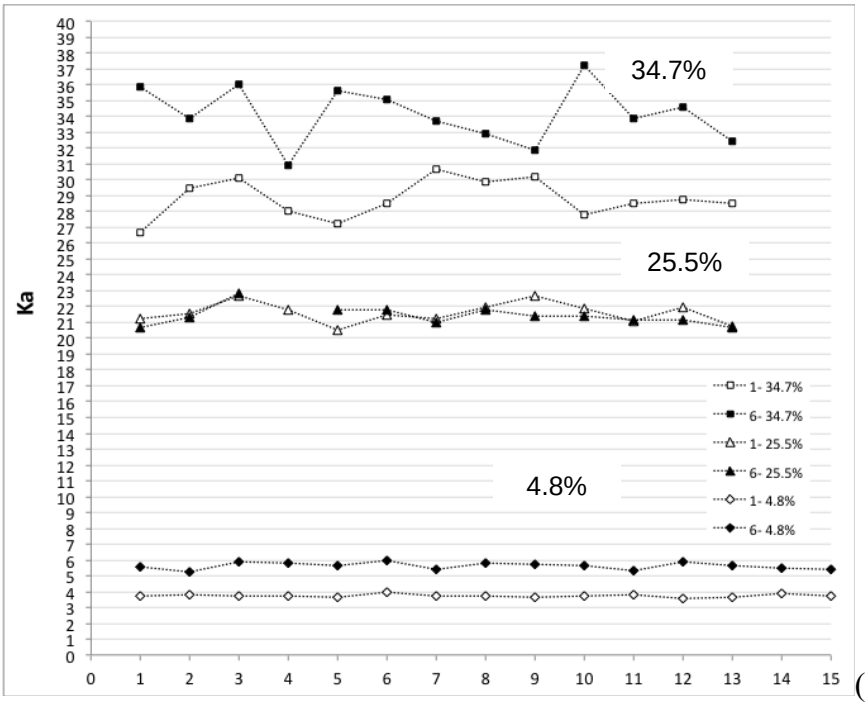

Figure 157. Ka values at different gravimetric water content.

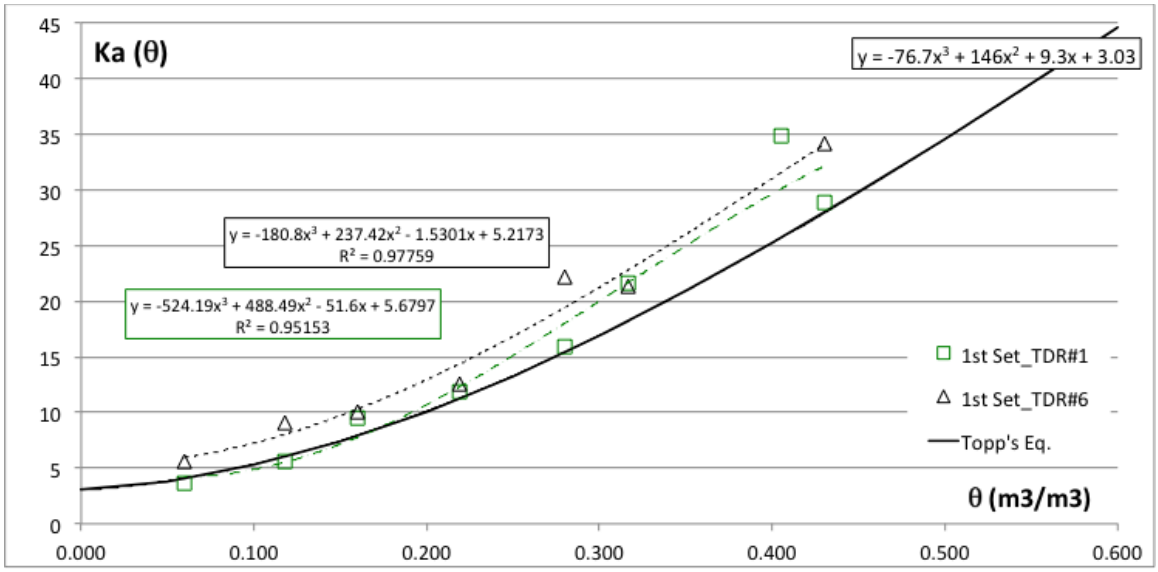

Figure 158. Eagle Ford Specific calibration (1st set).

Both fitting functions have a similar shape. They have slightly steeper increase in Ka with the increase of VWC with respect to Topp's equation. This trend is similar to what could be expected from Topp's raw data when only clays are analyzed (CL in Figure 155).

This difference between the calibrations can be also related to the use of standard probe parameters: CS645 probe length 7.5 cm and offset length 3.5 cm. The influence of these parameters will be addressed later in this chapter.

1.2.3 Preliminary analysis of errors

In order to quantify the inherent errors of the TDR system the following methodology was applied to the measurements showed in Figure 157. This analysis is based on a soil-specific calibration performed with standard TDR probes and standard parameters indicated by Campbell Scientific (CSI).

First, all measurements for each probe and for each test (selected water content and density) were separately arranged in frequency plots. From the frequency plots, particularly in those with the higher number of samples it could be inferred that the Ka values provided by the CSI analysis algorithm for given water content and density follow a normal distribution. From these distributions an average dielectric constant Ka (μ_{Ka}) and a standard deviation (σ_{Ka}) values were defined.

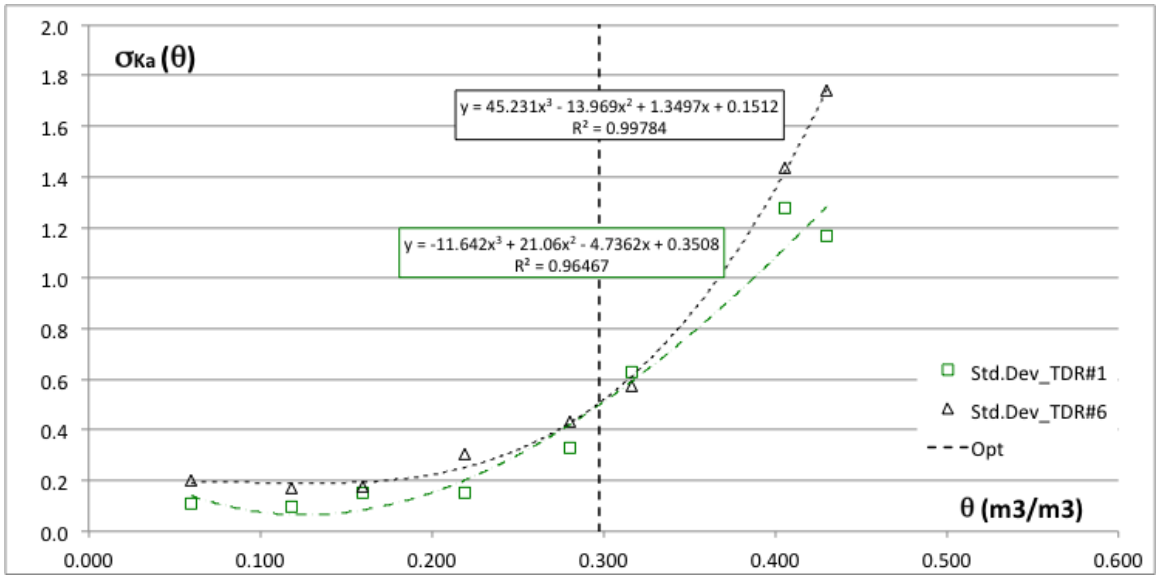

Figure 159. Standard deviation as function of VWC.

Figure 159 shows the standard deviation values obtained for each test (at constant VWC). The standard deviation remains fairly constant until a given VWC threshold A dotted line indicates the VWC that corresponds to the compaction optimum water content; σ_{Ka} increases rapidly after this value. Physically, this breakpoint corresponds to the change in structure and alignment of the clay particles.

Figure 160 shows the standard deviation values normalized by the mean (COV(Ka)) to have a better sense of the percentage of error that can be obtained from single data points. In average, the COV(Ka) is about 3%.

To complement this analysis, an error bar was added to each mean value in the calibration curves. A general plus/minus 9% from the mean is indicated on each average value. This error bar should cover any data point result from the TDR system on the 99.7% of the times. This result matches the same trend reported by Topp et al. (1980); where the error in the calibration is expected to increase with the increasing water content.

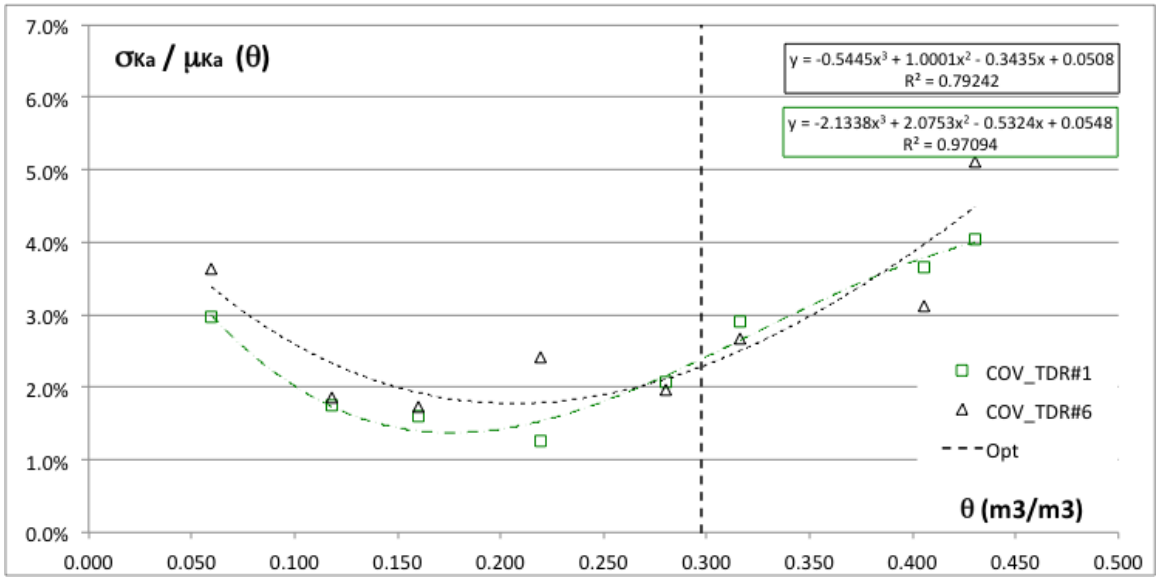

Figure 160. COV(Ka) – 1st set.

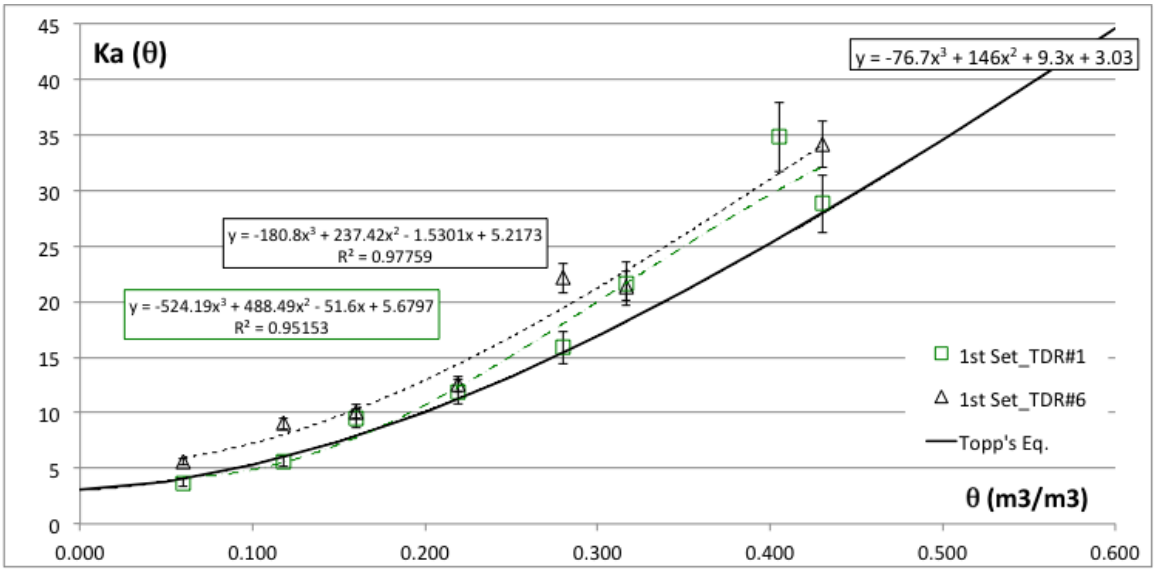

Figure 161. Calibration curve with range of measurements.

1.2.4 Calibration of curved TDR

The soil-specific calibration on Eagle Ford clay was repeated using a column, but using one straight TDR and one curved TDR. In order to ensure that both sensors are embedded in the same layer they were placed sideways (Figure 162).

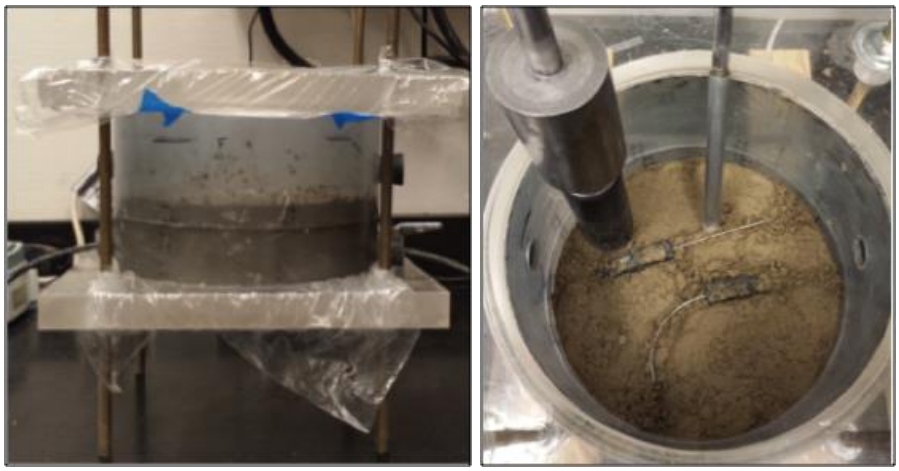

Figure 162. Compaction for procedure soil-specific calibration using curved TDR.

The soil was compacted in three layers of 2 cm at a dry density of 1.39 g/cm^3 (90% Relative Compaction of Proctor Standard Test). Several measurements were done at different gravimetric water content ranging from 4.5% to 34%, which corresponds to a VWC from 0.062 to 0.472. The results are compared with the first calibration (Figure 163).

The results of the second calibration lay almost on top showing that the same correlation between the dielectric permittivity and the VWC could be used despite the shape of the TDR.

It is important to clarify that both calibrations were done using the standard parameters provided for the CS645 (probe length 7.5 cm; offset length 3.5 cm). Further calibrations showed that even when using straight TDR, a specific probe-fitting calibration may be needed.

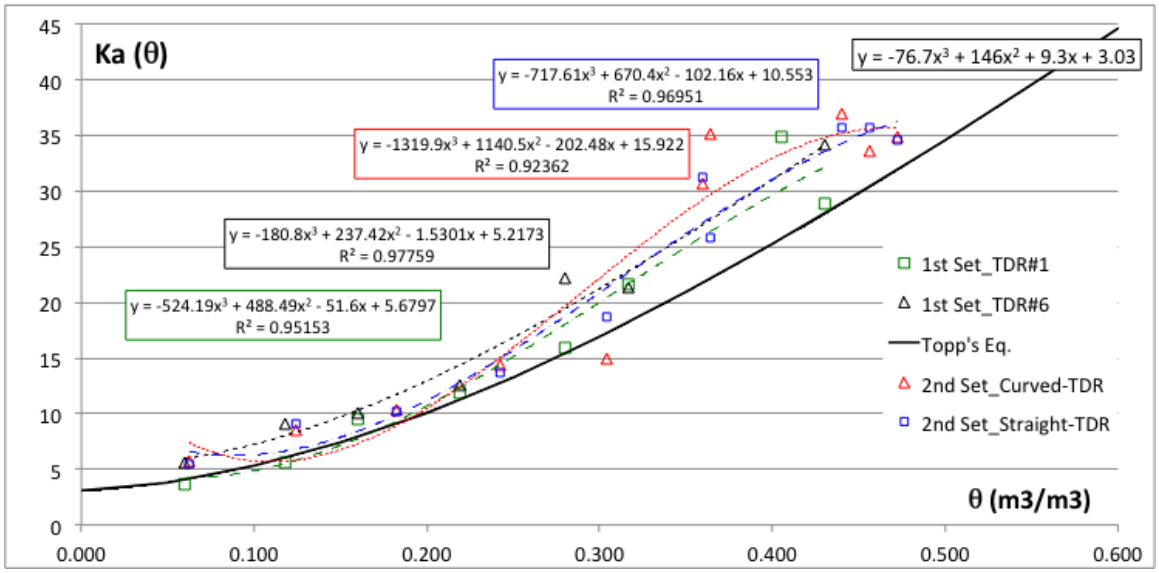

Figure 163. Soil-specific calibration for straight (1st set) and curved TDR (2nd set).

1.2.5 GTDR Calibration

A soil specific calibration was carried by compacting samples inside the acrylic permeameter and measuring the VWC with the GTDR. Figure 164 show the results from the calibration. Almost a linear response between the dielectric permittivity (Ka) and the VWC was observed. The values were restricted to the Ka range from 4 to 27.

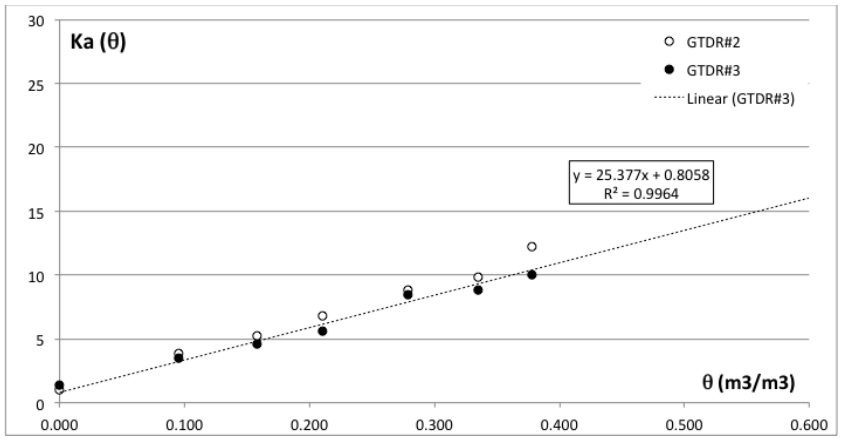

Figure 164. Calibration of Ka vs VWC.

The standard deviation values obtained from this calibration are presented in Figure 165. The scatter in the GTDR measurements represented by the standard deviation show a similar trend that the one reported by the regular TDR.

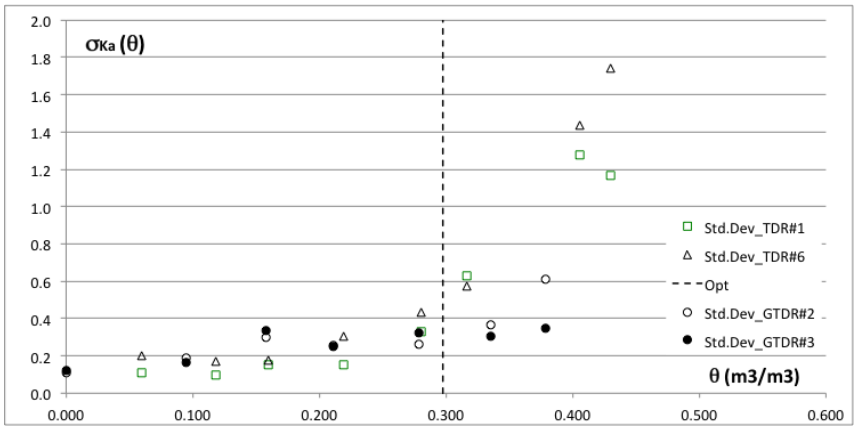

Figure 165. Standar deviation as function of VWC for GTDR and TDR.

1.3 Analysis of Wave Forms and other sources of error

In all soil calibration permittivity measurements showed to oscillate within a range of values for any constant volumetric water content imposed. If we consider two measurements performed at the same time (with a difference of 5 seconds) with the same GTDR then, it can be state that two measurements are taken under the exact same conditions in space and time, they could be indicated as replicate measurements.

Figure 166 shows the results of replicate measurements at different water contents. It can be seen that calculating the average value for these two consecutive identical measurements reduces the scatter. In all these cases, the same cable length, window length, and probe parameters were used. Therefore the oscillation in the Ka values cannot be attributed to them.

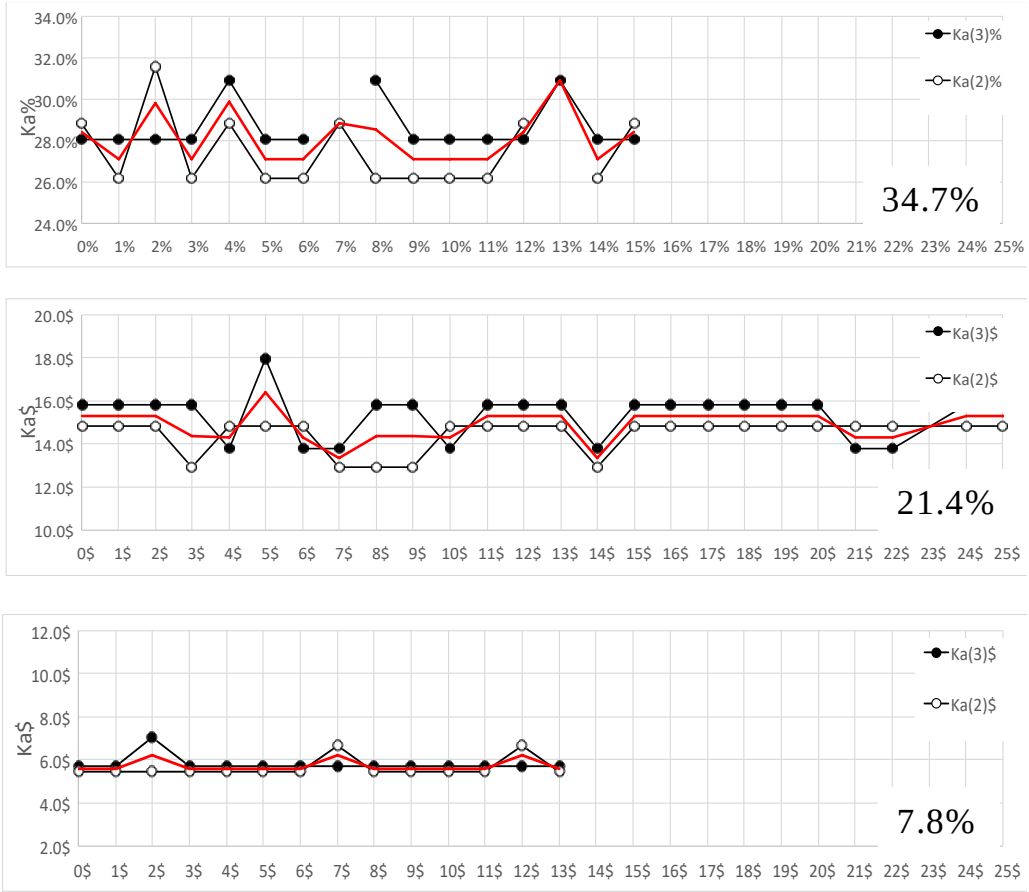

Figure 166. Average Ka for GTDR#2.

In order to analyze this inherent error of the TDR system a set of three Ka measurements were selected. Figure 167 illustrates the number of the measurement selected, the waveforms and first derivatives of the waveforms related to these values.

The Ka values are 9.5, 8 and 11, and correspond to the waveforms (WF) identified as number 19, 22, and 52. The WF and derivatives recorded are very similar and a minimum difference can be appreciated in the derivatives. Although no significant variation is observed between measurements, the algorithms reported a Ka of 9.5 with a variation of +/- 1.5. This oscillation in the measurements could be attributed to a

combination of the quality of the data recorded and the algorithm used. This error is indicated will be assumed in this research as the inherent error of the TDR system.

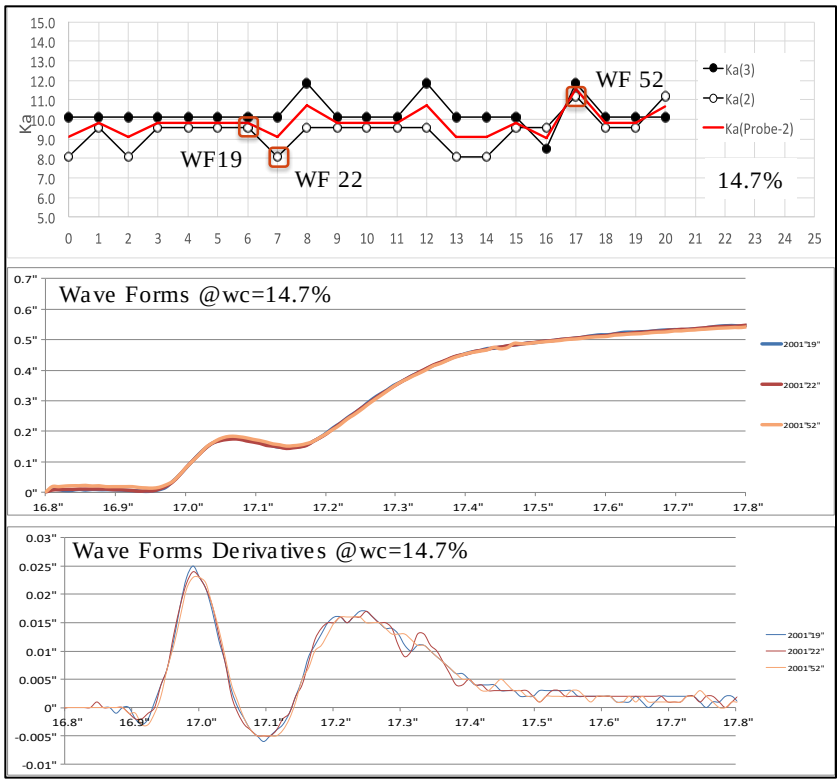

Figure 167. Analysis of the inherent error of the GTDR.

APPENDIX 2: Analysis of Results and Construction of SWRS

2.1 INTRODUCTION

In this Appendix, the results from a series of test carried out in the ATX-Cell (Quaglia et al. 2015) are presented in order to describe the hydro-mechanical behavior of unsaturated soils. A typical SWRC fitting procedure was carried out to evaluate the correlation in the fitting parameters in order to transform the isolated SWRC into a soil-water retention surface (SWRS).

2.2 MODELING AND CONSTRUCTION OF SWRS

In order to complete further calculations or numerical simulations, it is useful to obtain a continuous representation of the hydro-mechanical response of the soil. There are several continuous functions available to fit the retention data from soils for example: Van Genuchten (1968), Brooks & Corey (1964), Fredlund and Xing (1994). However, all these functions assume a constant void ratio and cannot be used to fit properly the data obtained from different tests were the void ratio varies during the testing procedure.

The approach proposed to incorporate the discontinuous data points into a retention surface is described as follows: a SWRS can be constructed as a succession of retention curves at a constant void ratio. The SWRS mathematical model incorporates the same set of parameters than SWRC, but each parameter is a function of the void ratio. Plaisted (2014) showed this approach to be successful using the van-Genuchten (1980) SWRC model with parameters that vary linearly with the void ratio. The SWRS was fitted to experimental data obtained with the CPUS. The main drawback of this work is that low suctions could not be reached, and the description of the SWRS was limited.

2.2.1 Parameterization analysis

In order to support this approach, a series of SWRC were fitted to experimental data obtained in the ATX Cell (Table 1). These results help to evaluate the hypothesis about the linearization of the fitting parameters, the possible limitations, and other key features that must be taken into account when fitting a surface.

First, each test presented in Figure 52 was fitted individually and the SWRC was assigned to an average void ratio. All possible fittings were carried out minimizing an objective function, in this case the sum of square error (SSE). No correlation between the successive curves was forced. In order to obtain each SWRC some individual restrictions were imposed to the fitting parameters:

- θs (saturated volumetric water content) was bounded between the minimum value measured and the porosity value for the specific void ratio.
- θr (residual volumetric water content) was bounded using three different scenarios and, therefore, three data sets (θs, θr, α, n) were obtained:

  i) Default condition: inclusion of a data point with a suction value of 105 MPa measured at a 3% gravimetric water content (air-dry condition).

  ii) the residual water content must be greater that air dry condition: $\theta r > \theta r_{min}$ = 3% gwc times γ (dry unit weight).

  iii) no limitation for θr.
- α a must be greater than or equal to zero
- n must be greater than one
- m is equal to 1-1/n

The data sets and their corresponding fittings are presented in Figure 168. All these curves correspond to the default case (i).

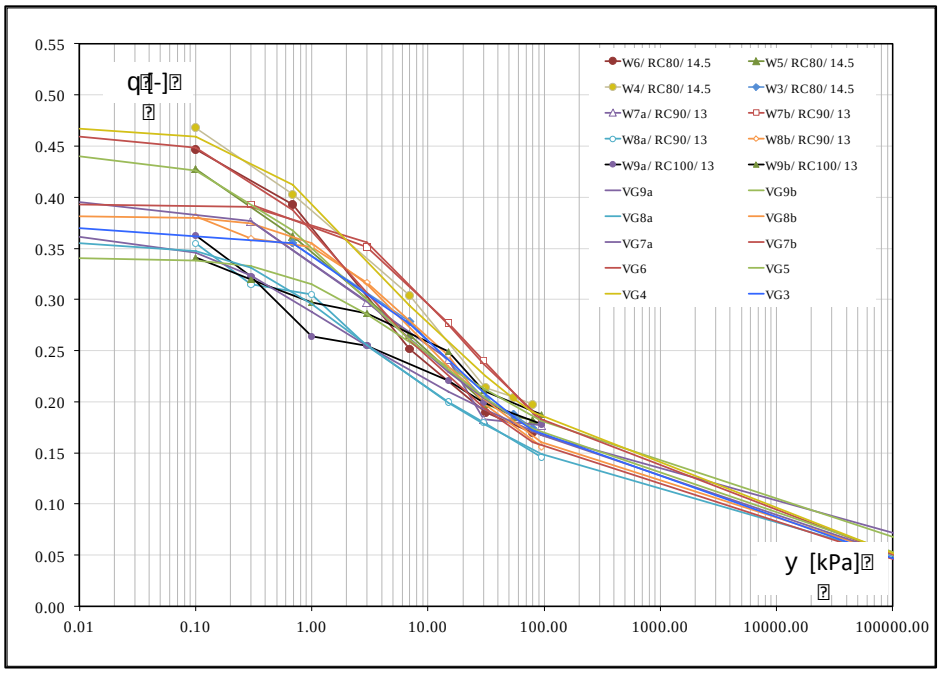

Figure 168. Analytical fitting of the SWRC.

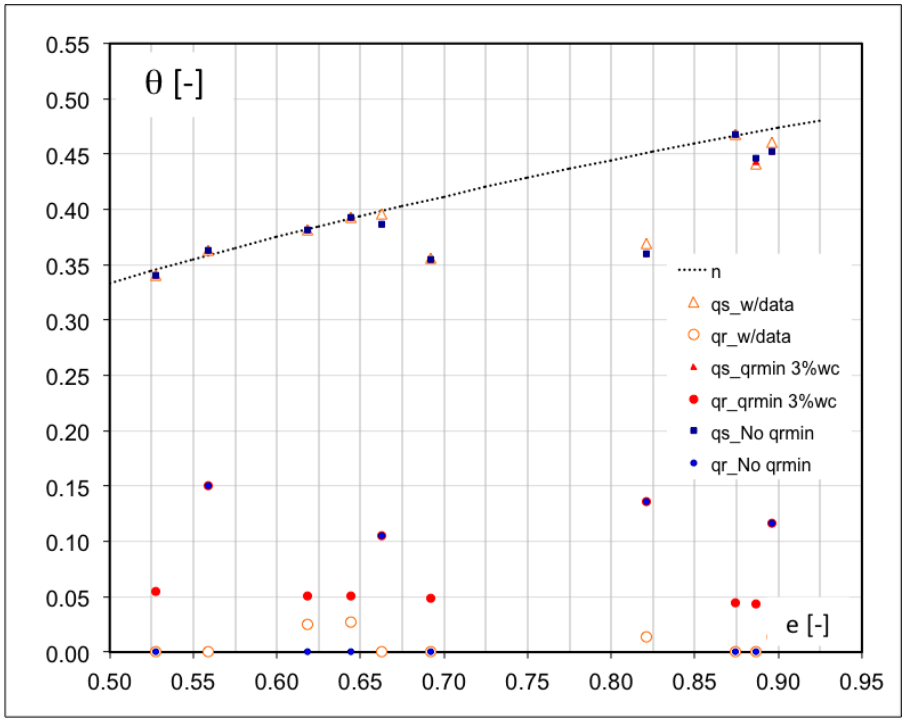

Figure 169. θs, and θr evolution with void ratio.

The variation with void ratio of the saturation and residual volumetric water content is presented in Figure 169. The saturated water content increases up to the sample porosity value in most cases, except in test W3 where the test was finished at 1 kPa. This shorter testing range has a significant effect on the maximum water content reached. Also, all saturated volumetric water content is mostly independent of the assumptions made for θr.

The residual water content (θr) is related to the vapor phase potential of the soil and, therefore, the soil structure has less influence over it. The impact of the three different scenarios proposed show that:

- Case (i): The addition of experimental data at high suction values reduces the scatter in the residual water content, and the parameter take values from 0 to 0.025.

- Case (ii): The lower limit imposed as a "physical" achievable condition where the soil is not expected to go under the air-dry water content ($\theta r > \theta r_{min}$), forces the fitting parameter to be from 0.044 to 0.150.
- Case (iii): If no restrictions are imposed, the fitted parameter ranges from 0.0 to 0.150.

From all these results, it can be derived that including a few measurements at high suction values may be the best option for the definition of the SWRS.

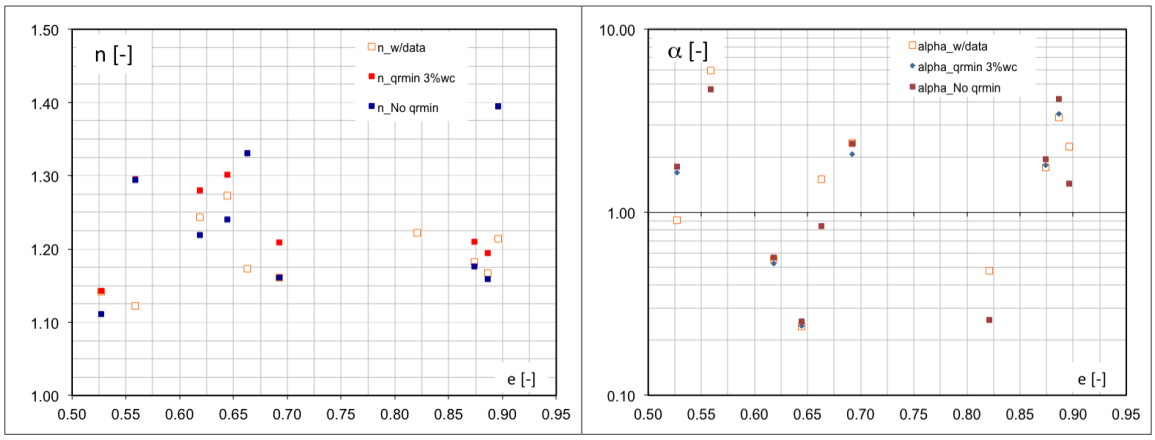

Figure 170. Variation of n (a) and α (b) fitting parameters with the void ratio.

Figure 170a shows that "n" increases with the increasing void ratio. This is consistent with the results presented in Figure 168 where the lower relative compaction (higher void ratio) has a steeper curve, then a bigger "n". Although these results have a considerable scatter, a linear trend could be considered as reasonable.

On the other hand, Figure 170b does not show any consistent trend. According to the model itself, when "α" increases the suction at the inflection point decreases this corresponds to a lower air entry pressure. Then it could be expected that "α" increase as

the void ratio increases too. A linear increase of "α" with void ratio may be suitable for the SWRS model, although this trend is not fully supported by this data set.

Overall, the sets of fitting parameters presented in Figure 169 and Figure 170 follow a similar trend that the ones presented by Tinjum & Benson (1997) for lime and sandy soils. The hypothesis that the fitting parameters follow linear trends in relationship with the void ratio based on experimental data are appropriate to develop a continuous SWRS based on van-Genuchten SWRC model.

APPENDIX 3: Discussion about experimental measurements from filter paper and chilled mirror hygrometer on Eagle Ford clay

3.1 INTRODUCTION

In this research the soil-water retention capabilities of Eagle Ford Clay was measured using several testing techniques, in particular the chilled mirror hygrometer (WP4C) and filter paper test were used to obtain experimental data over a broad range of suction values. In this Appendix some of the results obtained with these techinques are presented and the outcomes are discussed in order to complement the analysis presented in Chapter 10.

3.2 CHILLED MIRROR HYGROMETER TEST

Eagle Ford clay was tested using the WP4C equipment. A series of samples were prepared at different gravimetric water contents (6% to 30%) and void ratios.

In order to study the influence of the void ratio, samples were prepared at different densities. Three main groups were identified: i) Loose samples (65% relative compaction), in this case the soil was placed into the cup with no compaction at all and this was the lowest density measurable; ii) Barely Compacted (85% RC), and iii) Heavily Compacted (95% RC). Although the change in density between groups “ii” and “iii” is low, the energy required to reduce the voids is considerable. Samples were compacted with a kneading compactor inside the plastic cups. Each group has a deviation of +/-2% in relative compaction of the samples.

Figure 171 shows a linear correlation between the gravimetric water content and the suction (in logarithmic scale) is shown. It can be seen that when results are presented using gravimetric water content there is little or almost no effect of the void ratio.

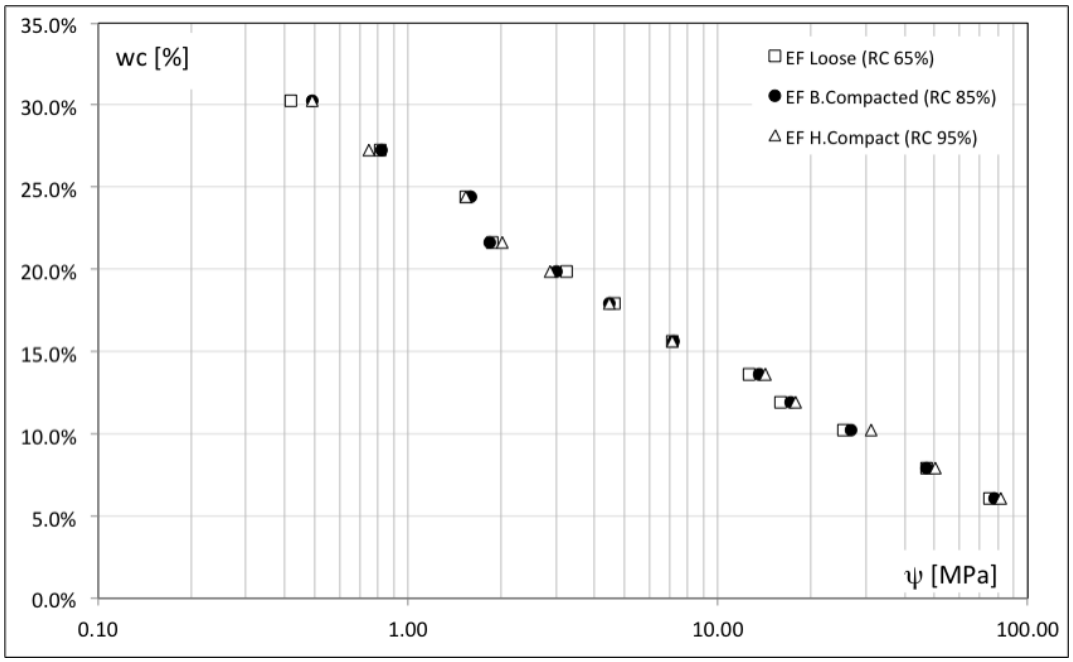

Figure 171. Correlation between gravimetric water content.

Results presented in Figure 171 show that the total suction values for this highly plastic clay ranges between 0.3 MPa to 80 MPa for broad range of water content that goes from the air-dry water content to an almost saturated condition.

Figure 172 illustrates the correlation between the volumetric water content and suction for the three series of tests. All three curves have similar trends, the correlation between total suction and water content is very well defined, and the residual water content is about 0.05 to 0.1.

However, there is an important feature to be addressed. The curve corresponding to the lower density (65% RC) is the lowest one, this suggest that to follow the typical response of these curves it should have a fast rise in water content at lower suctions, determining then a crossing point with the other curves.

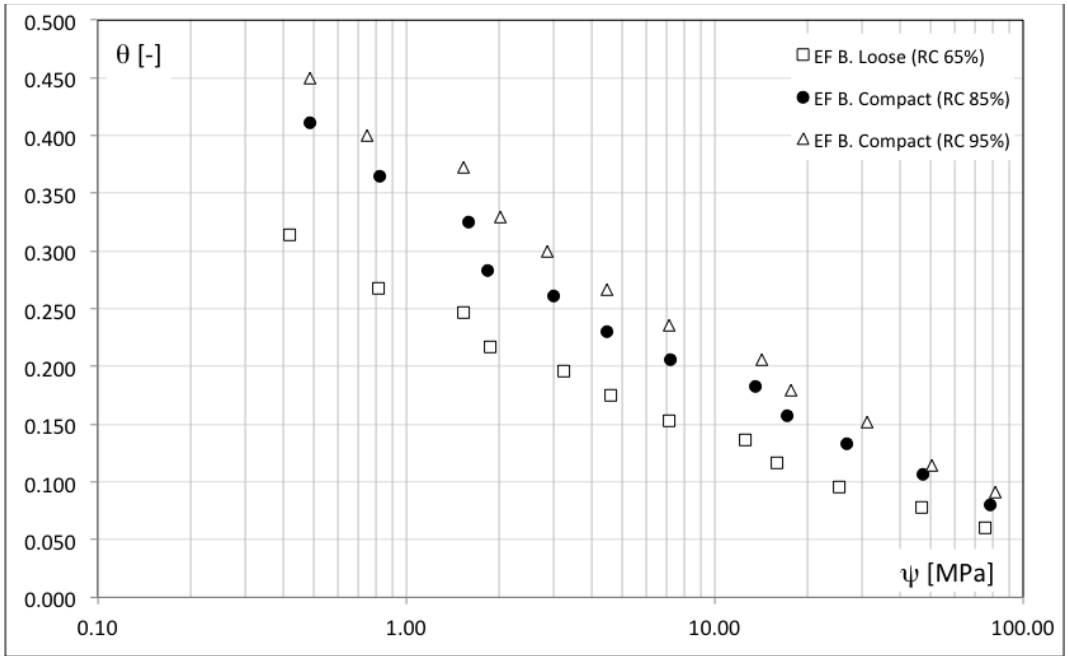

Figure 172. Eagle Ford clay SWRC at high suctions.

3.3 FILTER PAPER TEST

The Filter paper methodology allows determining the total suction and matric suction of the soil. A set of samples were prepared using Eagle Ford Clay in order to determine the soil-water retention characteristics and to compare the accuracy and scatter of this method with the Chilled Mirror Hygrometer test (WP4C). Strictly, only the total suction measurements are comparable between methods.

Soil samples were compacted at the maximum dry density (100% RC Standard Proctor Test) through a range of gravimetric water content from 6% to 30%. Each sample consisted of two discs of 7 cm diameter and 3 cm height. Soil discs were placed into a glass container with the two filter papers and storage at constant temperature for more than 14 days. The results of the filter paper test for both total and matric suction are presented in Figure 173.

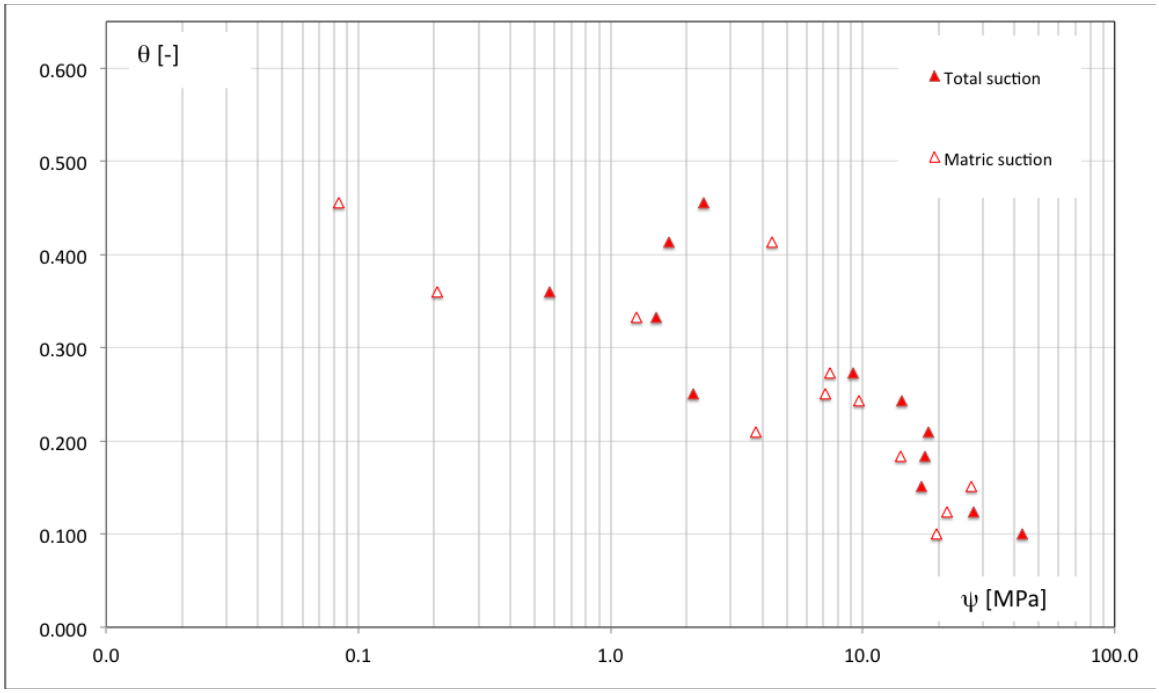

Figure 173. SWRC - Filter Paper & Chilled mirror results.

It can be seen that at low water contents the total and matric suction values are very similar. With the increase of the VWC, the matric suction should transition to lower values in comparison to the total suction (Marinho et al. 2010). However, this difference is not obvious in this case.

Figure 174 shows a comparison of the total suction values obtained with both testing techniques. It can be observed that the filter paper results show a similar average trend, but the scatter in the data points is much higher. The chilled mirror hygrometer shows a clear defined trend between the VWC and suction.

This scatter can be attributed to many factors in the filter paper test: the calibration curves, the filter paper water content measurement, or even the analytical methodology used to interpret the data from the precision scale.

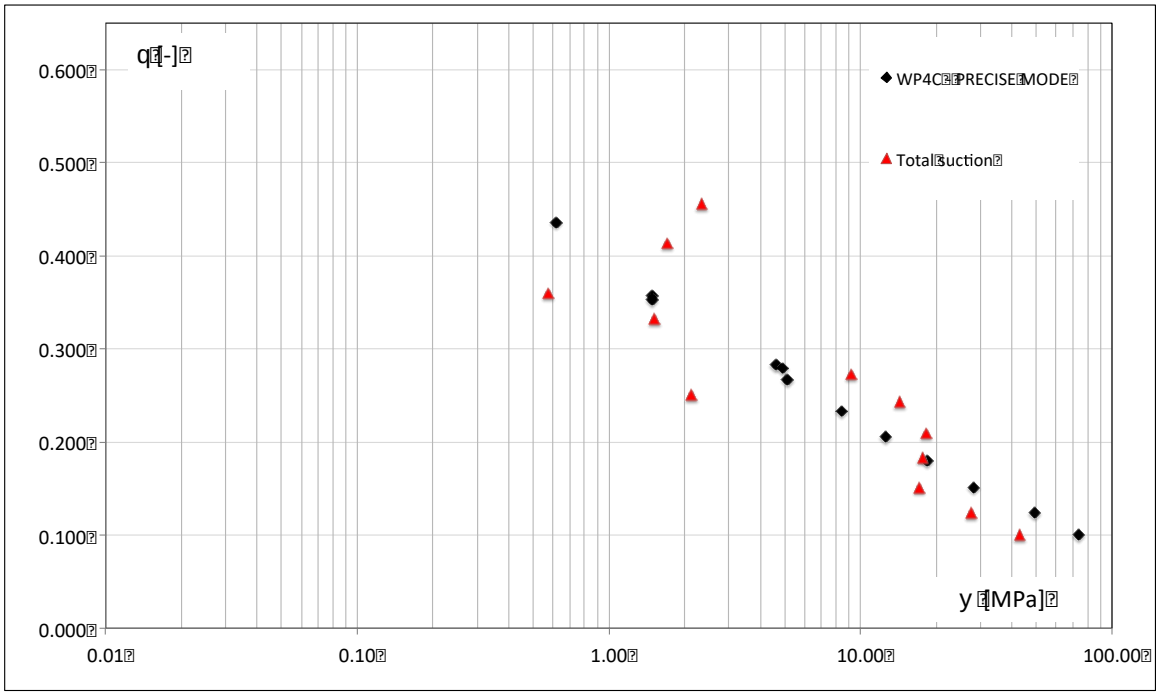

Figure 174. Comparison of Filter paper test and WP4C.

In particular, the laboratory procedure to measure the change in weight of the filter papers with time and the data analysis used to determine the to determine the wet and dry weights of the filter paper at time zero, are the ones that have most influence in the reported.

Figure 175 shows a series of different mathematical functions that could be used to extrapolate the weight of the filter paper at time zero. The selection of the number of data points and the function fitted has an impact in the weight of the paper predicted.

Any “error” in the estimation of the filter paper weight is then translated into errors in the gravimetric water content, and finally into the suction value reported for the soil.

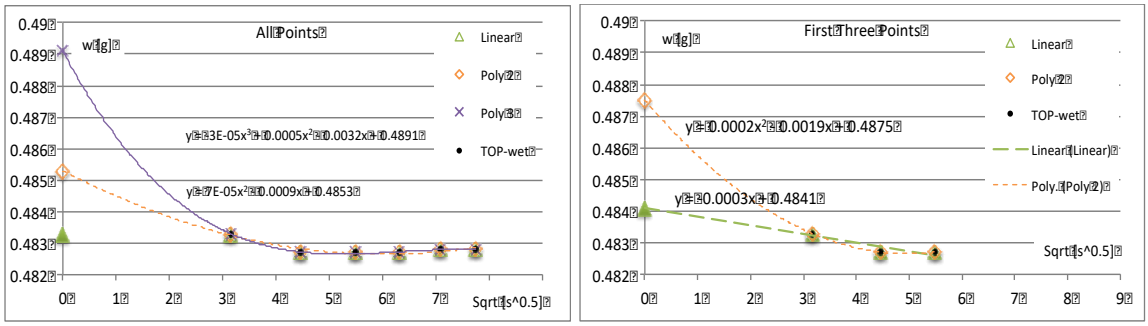

Figure 175. Extrapolation of "wet" weight using different number of data points.

An example can be used to quantify the errors that can be transferred from the weight of the papers to the suction measurements using this procedure. In this case, a sample compacted at a VWC 0.100 (6% gwc) had a reported matric suction of 43.2MPa. However, if we observe the raw data some interpretations can be done:

- Depending on the number of data points used (3, 4 or all 6) and the function fitted (linear, cuadratic or cubic) both the wet and dry weights vary between +/- 0.002 to 0.004 g from the average value. This amount represents a variation of +/-1% to 2% in the wet and dry weights of the actual filter paper.
- When the water content is calculated using a different combination of this wet and dry weights, the water content has an average of 9%, it can be as low as 7.3% and as high as 10.7%. This range means a variation of almost +/- a 20%.
- Once the filter paper water content is used altogether with the calibration curves the average suction measured is 43.2 MPa.
- The range of suction obtained with the minimum and maximum water content are 56.3 MPa and 31.4 MPa respectively. Now, the deviation from the average suction is about +/-30%.

It can be appreciated how a small percentage of errors at early steps of the tests can be propagated and become a significant error in the suction measurements.

3.4 DISCUSSION ABOUT THE DIFFERENCE BETWEEN TOTAL SUCTION AND MATRIC SUCTION RESULTS

Figure 176 illustrates the difference between total and matric suction values for Eagle Ford clay samples compacted at 90% relative compaction (proctor standard) including: i) difference between total and matric values derived using only the results from filter paper test, and ii) difference between total and matric values using WP4C test for total suction, and filter paper for matric suction.

The second set provides a more defined trend as result of the lower scatter in the total suction measurements. A power law fitting function was included in order to characterize the correlation between the derived suction values and the volumetric water content.

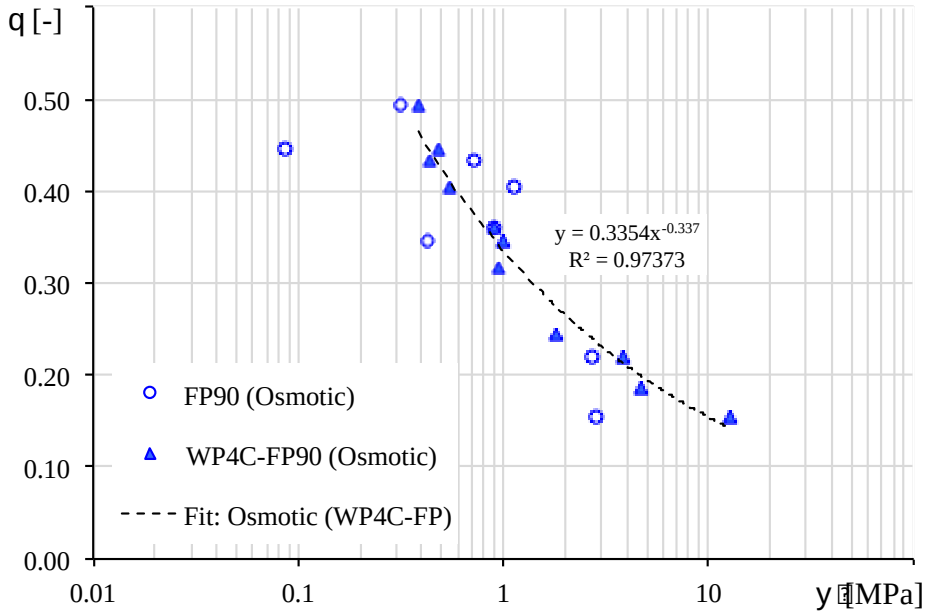

Figure 176. Osmotic suction derived for Eagle Ford clay samples compacted at 90% relative compaction (proctor standard) using Filter Paper and WP4C test experimental data.

This analysis was repeated for the three data sets presented in Figure 110 in order to evaluate the suction values at different void ratio. Figure 177 shows the correlation between the osmotic suction and the volumetric water content (obtained with the second method) for three different void ratio values. In all cases the results follow a power law with a small influence of the void ratio.

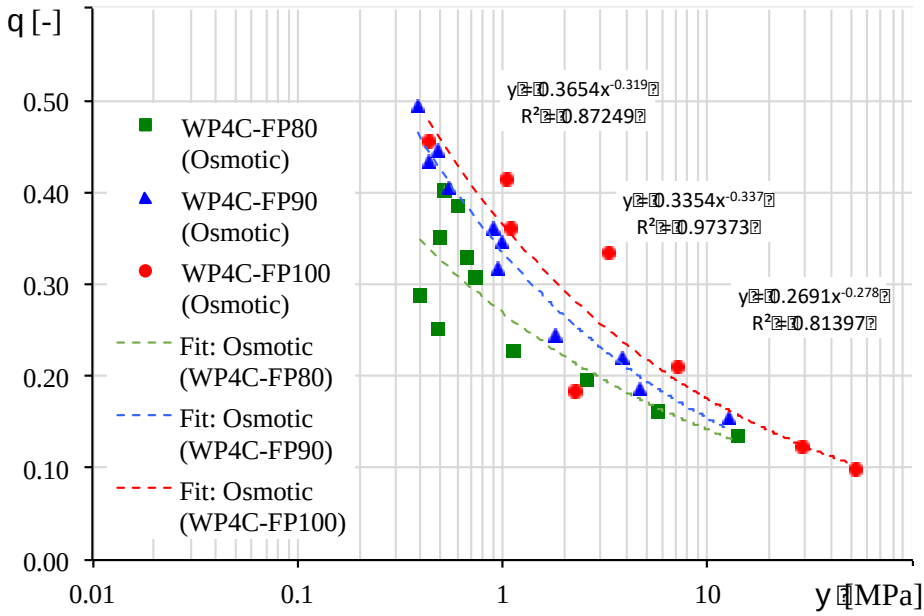

Figure 177. Osmotic suction derived using WP4C (total suction) and Filter Paper (matric suction) for Eagle Ford clay samples compacted at three different relative compactions (proctor standard).

Following the results presented in Figure 177 the following fitting equation was proposed to predict the osmotic suction as function of the volumetric water content

$$\psi_{total} - \psi_{matric} = \left(\theta / a\right)^{\left(-1/b\right)} + c \qquad (37)$$

The fitting parameters (a, b, and c) were calibrated by comparing the derived matric suction values against the matric suction values from the filter paper test. In order

to simplify the procedure only one set of parameters was derived independent of the void ratio. The best set of fitting parameters is shown in the following equation:

$$\left(\psi_{total} - \psi_{matric}\right)\left[MPa\right] = \left(\theta / 0.2358\right)^{\left(-1/0.255\right)} + 0.428 \quad (38)$$

These values are the difference between total and osmotic suctions, and typically they represent the osmotic suction component. However, this may not be true for high plasticity clays (Arifin & Schanz, 2009)

References

A.C. Bovik, The Essential Guides to Image and Video Processing, Academic Press; 1 edition (June 10, 2009).

Adams, A. G., Dukes, O. M., Tabet, W., Cerato, A. B., & Miller, G. A. (2008). Sulfate induced heave in Oklahoma soils due to lime stabilization. *Geotechnical Special Publication*, (179), 444-451.

Anne-Marie, W., Sandra, L. H., & William, N. H. (1994). Laboratory filter paper suction measurements.

Arifin, Y. F., & Schanz, T. (2009). Osmotic suction of highly plastic clays. *Acta Geotechnica*, *4*(3), 177-191.

Armstrong, C. P. (2014). Effect of fabric on the swelling of highly plastic clays.

Artur, B. R., Cláudio, R. M., Fernando, S., Rodrigo, M. R., Rubens, R. S., Sergio, T., & Wagner, N. S. (2011). Determination of the Soil-Water Retention Curve and the Hydraulic Conductivity Function Using a Small Centrifuge.

ASTM D5298-94. (1994). Standard test method for measure- ment of soil potential (suction) using filter paper. In *1994 Annual book of ASTM standards*. Philadelphia: ASTM.

ASTM D6836 (2008). Test Methods for Determination of the Soil Water Characteristic Curve for Desorption Using Hanging Column, Pressure Extractor, Chilled Mirror Hygrometer, or Centrifuge. *ASTM International, 2008*.

Baker, J. M., & Allmaras, R. R. (1990). System for automating and multiplexing soil moisture measurement by time-domain reflectometry. *Soil Science Society of America Journal*, *54*(1), 1-6.

Benny, M., Maria-Cristina, C., Herman, P., & Pavol, K. (2015). Unsaturated Permeability and Retention Curve Determination From In-Flight Weight Measurements in a Bench-Scale Centrifuge

Benson, C. H., & Gribb, M. M. (1997). Measuring unsaturated hydraulic conductivity in the laboratory and field. *Reprinted from Unsaturated Soil Engineering Practice Proceedings of Sessions on Unsaturated Soils at Geo-Logan '97 Sponsored by The Geo-Institute/ASCE Held*.

Bicalho, K. V., Cupertino, K. F., & Bertolde, A. I. (2013). Evaluation of the suction calibration curves for Whatman 42 filter paper. In *Proceedings of the 1st Pan-American Conference on Unsaturated Soils* (pp. 225–230).

Blatz, J. A., & Graham, J. (2003). Elastic-plastic modelling of unsaturated soil using results from a new triaxial test with controlled suction. *Géotechnique*, *53*(1), 113–122.

Branch, M. A., & Grace, A. (1996). MATLAB: optimization toolbox: user's guide version 1.5. The MathWorks.

Brooks, R. H., & Corey, A. T. (1964). Hydraulic properties of porous media and their relation to drainage design. *Transactions of the ASAE*, *7*(1), 26-0028.

Buckingham, E. (1907). Studies on the movement of soil moisture.

Bulut, R., & Mantri, S. (2014). Evaluating Performance of a Chilled Mirror Device for Soil Total Suction Measurements.

Bulut, R., & Wray, W. K. (2005). Free energy of water-suction-in filter papers. *Geotech Test Journal*, *28*(4), 355–364.

Bulut, R., Hineidi, S. M., & Bailey, B. (2002). Suction measurements—filter paper and chilled mirror psychrometer. In *Proceedings of the Texas Section of the American Society of Civil Engineers Fall Meeting*. Waco.

Bulut, R., Lytton, R. L., & Wray, W. K. (2001). Soil suction measurements by filter paper. In *Expansive clay soils and vegetative influence on shallow foundations* (Vol. 115, pp. 243–261). ASCE geotechnical special publication.

Bulut, R., Park, S. W., & Lytton, R. L. (2000). Comparison of total suction values from psychrometer and filter paper methods. In *Unsaturated soils for Asia. Proceedings of the Asian Conference on Unsaturated Soils, UNSAT-Asia 2000* (pp. 269–273). Singapore: AA Balkema.

Campbell Scientific (2015). CSI TDR 100 Instruction Manual. Revision, May 2015.

Canny, John, "A Computational Approach to Edge Detection," *IEEE Transactions on Pattern Analysis and Machine Intelligence,*Vol. PAMI-8, No. 6, 1986, pp. 679-698.

Casanova, J.J., R.C. Schwartz and S.R. Evett. 2014. Design and field tests of a directly coupled waveguide-on-access-tube soil water sensor. Appl. Engr. Agric. 30(1):105-112.)

Conca, J. L., & Wright, J. (1992). Diffusion and flow in gravel, soil, and whole rock. *Applied Hydrogeology*, *1*(1), 5-24.

Cui, Y., Ta, A. N., Tang, A. M., & Lu, Y. (2010). Investigation of the hydro-mechanical behaviour of compacted expansive clay. *Frontiers of Architecture and Civil Engineering in China*, *4*(2), 154-164.

D.J. White, W. Take, and M. Bolton, " Soil deformation measurement using Particle Image Velocimetry (PIV) and photogrammetry", Géotechnique, 53(7): 619–631, 2003.

Darcy, H. (1856). *Les fontaines publiques de la ville de Dijon: exposition et application...* Victor Dalmont.

Dell'Aavanzi, E. D., Zornberg, J. G., & Cabral, A. R. (2004). Suction profiles and scale factors for unsaturated flow under increased gravitational field. *Soils and Foundations*, *44*(3), 79-89.

Dirksen, C. (1991). Unsaturated hydraulic conductivity. *Soil Analysis*, 209–269.

Eching, S, Hopmans, J., & Wendroth, O. (1994). Unsaturated hydraulic conductivity from transient multi-step outflow and soil water pressure data. *Soil Science Society of America Journal*, *58*, 687–695.

Evett, S. R. (2000). The TACQ computer program for automatic time domain reflectometry measurements: I. Design and operating characteristics. *Transactions of the ASAE*, *43*(6), 1939.

Evett, S. R. (2000b). The TACQ computer program for automatic time domain reflectometry measurements: II. Waveform interpretation methods. *Transactions of the ASAE*, *43*(6), 1947.

Fredlund, D. G., & Xing, A. (1994). Equations for the soil-water characteristic curve. *Canadian geotechnical journal*, *31*(4), 521-532.

Gardner, W. (1956). Calculation of capillary conductivity from pressure plate outflow data. *Soil Science Society of America Proceedings*, *20*, 317–320.

Gardner, W. R. (1958). Some steady-state solutions of the unsaturated moisture flow equation with application to evaporation from a water table. *Soil science*, *85*(4), 228-232.

Heimovaara, T. J. (1993). Design of triple-wire time domain reflectometry probes in practice and theory. *Soil Science Society of America Journal*, *57*(6), 1410-1417.

Holtz W. G & Jones D. E. & (1973). Expansive soils - the hidden disaster. *Civil Engineering*, 43.8:49–51, 1973

Jones, S. B., Wraith, J. M., & Or, D. (2002). Time domain reflectometry measurement principles and applications. *Hydrological Processes*, *16*(1), 141–153.

Klute, A. (1972). The determination of the hydraulic conductivity and diffusivity of unsaturated soils. *Soil Science*, *113(4)*, 264–276.

Klute, A. (1986). Water retention: laboratory methods. *Methods of Soil Analysis: Part 1—Physical and Mineralogical Methods*, (methodsofsoilan1), 635-662.

Klute, A., & Dirksen, C. (1986). Hydraulic conductivity and diffusivity: Laboratory methods. *Methods of Soil Analysis: Part 1—Physical and Mineralogical Methods*, (methodsofsoilan1), 687-734.

Kuhn, J. (2005). Effect of cracking on the hydraulic properties of unsaturated highly plastic clays. *The University of Texas at Austin*.

Kuhn, J. A. (2010). Characterization of the swelling potential of expansive clays using centrifuge technology.

Marinho, F. A., & da Silva Gomes, J. A. (2012). The effect of contract on the filter paper method for measuring soil suction. *Geothecnical Testing Journal*, *35*, 1–10.

Masrouri, F., Bicalho, K. V., & Kawai, K. (2008). Laboratory hydraulic testing in unsaturated soils. In *Laboratory and Field Testing of Unsaturated Soils* (pp. 79-92). Springer Netherlands.

Matyas, E. L., & H. S. Radhakrishna. (1968). Géotechnique, *18*, 432–448.

McCarter, W. J. (1984). The electrical resistivity characteristics of compacted clays. *Geotechnique*, *34*(2), 263-267.

McCartney, J. S. (2007). Determination of the hydraulic characteristics of unsaturated soils using a centrifuge permeameter. (Doctoral dissertation).

McCartney, J. S., & Zornberg, J. G. (2010). Centrifuge permeameter for unsaturated soils. II: Measurement of the hydraulic characteristics of an unsaturated clay. *Journal of geotechnical and geoenvironmental engineering*, *136*(8), 1064-1076.

McCartney, J.S. & Zornberg, J.G. (2006). *TDR System for Hydraulic Characterization of Unsaturated Soils in the Centrifuge.* TDR 2006. Purdue University, West Lafayette, Indiana. September 18-20, 2006.

McDowell, C., Herner, R. C., & Wooltorton, F. L. (1956). Interrelationship of Load, Volume Change, and Layer Thicknesses of Soils to the Behavior of Engineering Structures. In *Highway Research Board Proceedings* (Vol. 35).

Meerdink, J. S., Benson, C. H., & Khire, M. V. (1996). Unsaturated hydraulic conductivity of two compacted barrier soils. *Journal of geotechnical engineering*, *122*(7), 565-576.

Moré, J.J. and D.C. Sorensen, "Computing a Trust Region Step," *SIAM Journal on Scientific and Statistical Computing*, Vol. 3, pp 553–572, 1983.

Mualem, Y. (1976). A new model for predicting the hydraulic conductivity of unsaturated porous media. *Water resources research*, *12*(3), 513-522.

Mualem, Y. (1978). Hydraulic conductivity of unsaturated porous media: generalized macroscopic approach. *Water Resources Research*, *14*(2), 325-334.

Munoz-Castelblanco, J., Pereira, J. M., Delage, P., & Cui, Y. J. (2013). The influence of changes in water content on the electrical resistivity of a natural unsaturated loess.

Nimmo, J. R. (1990). Experimental Testing of Transient Unsaturated Flow Theory at Low Water Content in. *Water Resources Research*, *26*(9), 1951-1960.

Nimmo, J. R., & Akstin, K. C. (1988). Hydraulic conductivity of a sandy soil at low water content after compaction by various methods. *Soil Science Society of America Journal*, *52*(2), 303-310.

Nimmo, J. R., Akstin, K. C., & Mello, K. A. (1992). Improved apparatus for measuring hydraulic conductivity at low water content. *Soil Science Society of America Journal*, *56*(6), 1758-1761.

Nimmo, J. R., Rubin, J., & Hammermeister, D. P. (1987). Unsaturated flow in a centrifugal field: Measurement of hydraulic conductivity and testing of Darcy's law. *Water Resour. Res*, *23*(1), 124-134.

Olson, R., & Daniel, D. (1979). Measurement of the hydraulic conductivity of fine-grained soils. In Zimmie, T. & Riggs, C. (Eds.), *Permeability and Groundwater Contaminant Transport* (pp. 169–181). Philadelphia: STP 746, ASTM.

Or, D., Tuller, M., & Wraith, J. M. (2010). Vadose Zone Hydrology/ Environmental Soil Physics

Plaisted, M. D. (2009). Centrifuge testing of an expansive clay. University of Texas.

Plaisted, M. D. (2014). Characterization of soil unsaturated flow properties using steady state centrifuge methods. (Doctoral dissertation).

Puppala, A. J., & Cerato, A. (2009). Heave distress problems in chemically-treated sulfate-laden materials. *Geo-Strata—Geo Institute of ASCE*, *10*(2), 28-30.

R.J. Adrian, "Particle-imaging techniques for experimental fluid mechanics", Annual Review of Fluid Mechanics, 23: 261–304, 1991.

Rahardjo, H., He, L., & Leong, E. C. (2002). Factors affecting the filter paper method for total and matric suction measurements. *Geotech Test Journal*, *25*(3), 322–333.

Rendon-Herrero, O. (2011). Special issue on construction on expansive soils. *Journal of Performance of Constructed Facilities*, *25*(1), 2-4.

Robinson, D. A., Jones, S. B., Wraith, J. M., Or, D., & Friedman, S. P. (2003). A review of advances in dielectric and electrical conductivity measurement in soils using time domain reflectometry. *Vadose Zone Journal*, *2*(4), 444–475.

S.A. Stanier, and D.J. White, "Improved Image-Based deformation measurement in the centrifuge environment," Geotechnical Testing Journal, Vol.36, No.6, pp.1–14, 2013.

S.-C. Hsu and P. P. Nelson. Characterization of eagle ford shale. *Engineering Geology*, 67: 169–183, 2002.

Salager, S., El Youssoufi, M. S., & Saix, C. (2007). Experimental study of the water retention curve as a function of void ratio. *Computer Applications In Geotechnical Engineering: Proceedings of Sessions of GeoDenver, Denver, Colo*, 18-21.

Salager, S., El Youssoufi, M. S., & Saix, C. (2010). Definition and experimental determination of a soil-water retention surface. *Canadian Geotechnical Journal*, *47*(6), 609-622.

Schindler, U., & Müller, L. (2006). Simplifying the evaporation method for quantifying soil hydraulic properties. *Journal of Plant Nutrition and Soil Science*, *169 (4)*, 623–629.

Schindler, U., Bohne, K., & Sauerbrey, R. (1985). Comparison of different measuring and calculating methods to quantify the hydraulic conductivity of unsaturated soil. *Zeitschrift Für Pflanzenernährung Und Bodenkunde*, *148*(6), 607–617.

Schwartz, R. C., Casanova, J. J., Bell, J. M., & Evett, S. R. (2014). A reevaluation of time domain reflectometry propagation time determination in soils. *Vadose Zone Journal*, *13*(1).

Simunek, J., M. Sejna, and M. T. van Genuchten (1998b), The HYDRUS- 1D software package for simulating the one-dimensional movement of water, heat, and multiple solutes in variably-saturated media, version 2.0, Rep. IGWMC-TPS-70, 202 pp., Int. Ground Water Model. Cent., Colo. Sch. of Mines, Golden, Colo.

Stephens, D. (1994). Hydraulic conductivity assessment of unsaturated soil. In Daniel, D. & Trautwein, S. (Eds.), *Hydraulic Conductivity and Waste Contaminant Transport in Soil* (pp. 169–181). Philadelphia: STP 1142, ASTM.

Tarantino, A., Ridley, A. M., & Toll, D. G. (2008). Field measurement of suction, water content, and water permeability. In *Laboratory and Field Testing of Unsaturated Soils* (pp. 139–170). Springer.

Tarantino, A., Romero, E., & Cui, Y.-J. (2008b). Laboratory and Field Testing of Unsaturated Soils. *Geotechnical and Geological Engineering*, *26*(6), 613–614.

Tinjum, J., C. Benson, & L. Blotz (1997). *Soil-Water Characteristic Curves for Compacted Clays*. Journal of Geotechnical and Geoenvironmental Engineering 123, no. 11: 1060–69.

Topp, G. C. (1980). Electromagnetic determination of soil water content: measurements in coaxial transmission lines. *Water Resources Research*, *16*(3), 574–582.

Topp, G. C., Davis, J. L., & Annan, A. P. (1982). Electromagnetic determination of soil water content using TDR: I. Applications to wetting fronts and steep gradients. *Soil Science Society of America Journal*, *46*(4), 672-678.

van Genuchten, M. T. (1980). A closed-form equation for predicting the hydraulic conductivity of unsaturated soils. *Soil Science Society of America Journal*, *44*(5), 892–898.

Vereecken, H., Huisman, J. A., Bogena, H., Vanderborght, J., Vrugt, J. A., & Hopmans, J. W. (2008). On the value of soil moisture measurements in vadose zone hydrology: A review. *Water Resources Research*, *44*(4).

Walker, S. C., Gallipoli, D., & Toll, D. G. (2005). The effect of structure on the water retention of soil tested using different methods of suction measurement. In

International Symposium on Advanced Experimental Unsaturated Soil Mechanics (pp. 33–39). Trento.

Walker, T. M. (2012). Quantifying using centrifuge of variables governing the swelling of clays.

Wendroth, O., Ehlers, W., Kage, H., Hopmans, J. W., Halbertsma, J., & Wösten, J. H. M. (1993). Reevaluation of the evaporation method for determining hydraulic functions in unsaturated soils. *Soil Science Society of America Journal*, *57*(6), 1436-1443.

Wind, G. (1968). *Capillary conductivity data estimated by a simple method*. Water in the Unsaturated Zone. Vol. 1, Proc. Wageningen Symp. June 1966. IASH. UNESCO, Paris. Ritjema, P. and Wassnik, H. eds. 181-191.

Xu, Z., Fujiyasu, Y., & Pierce, C. E. (2003). Performance of time domain reflectometers installed on a centrifuge. *International Journal of Physical Modelling in Geotechnics*, *3*(3), 01–08.

Vita

This dissertation was typed by Gastón Quaglia.

email: gastonquaglia@gmail.com